

# UAH/NASA Workshop On

# Fluids Experiment System

(NASA-TM-82492) UAH/NASA WORKSHOP ON FLUIDS  
EXPERIMENT SYSTEM (Alabama Univ.,  
Huntsville.) 261 p HC A12/MF A01 CSCI 20L

N82-32058  
THRU  
N82-32079  
Unclas  
28745

G3/70



**The University  
Of Alabama  
In Huntsville**

The summary of the panel reports from  
The University of Alabama in Huntsville/  
NASA Workshop conducted July 11-12,  
1979, at the Noojin House, Huntsville,  
Alabama

Edited by

John Hendricks  
School of Science and Engineering  
The University of Alabama in Huntsville  
Huntsville, Alabama 35807

and

Barbara Askins  
NASA/Marshall Space Flight Center  
Huntsville, Alabama 35812



UAH/NASA WORKSHOP ON FLUIDS EXPERIMENT SYSTEM

THE SUMMARY OF THE PANEL REPORTS FROM  
THE UNIVERSITY OF ALABAMA IN HUNTSVILLE/NASA  
WORKSHOP CONDUCTED JULY 11-12, 1979, AT  
THE NOOJIN HOUSE, HUNTSVILLE, ALABAMA

EDITED BY

JOHN HENDRICKS

SCHOOL OF SCIENCE AND ENGINEERING

THE UNIVERSITY OF ALABAMA IN HUNTSVILLE

HUNTSVILLE, ALABAMA 35807

AND

BARBARA ASKINS

NASA/MARSHALL SPACE FLIGHT CENTER

HUNTSVILLE, ALABAMA 35812

ORIGINAL PAGE IS  
OF POOR QUALITY

## PREFACE

The Fluids Experiment System (FES) Workshop was held at the Noojin House, a conference center operated by the University of Alabama in Huntsville. We would like to thank the University for their assistance and hospitality.

Special thanks go to the Institutional and Research Support Services Department and the Audio-Visual Department for their direct help. At the risk of leaving some important individual contributions unrecognized, we would like to acknowledge the special help of Virginia Tomme, Contracts and Grants administrator, Trudy King, manager of Noojin House, Eugenia Adams, caterer, and Heidi Holmes, workshop administrative coordinator.

We would like to thank all the participants at the FES Workshop for their assistance; and, in particular, we thank all the participants who submitted papers for the proceedings.

John Hendricks

Barbara Askins

## TABLE OF CONTENTS

	<u>Page</u>
PREFACE	ii
INTRODUCTION R.J. Naumann	vi
<u>SECTION A - GENERAL FLUID DYNAMICS</u>	1
PHASE SEPARATION IN TRANSPARENT LIQUID-LIQUID MISCIBILITY GAP SYSTEMS S.H. Gelles, B.N. Bhat & R.J. Laub	2
MEASUREMENT OF DIFFUSION COEFFICIENTS FROM SOLUTION RATES OF BUBBLES I.M. Krieger	18
INVESTIGATIONS ON TRANSPARENT LIQUID-MISCIBILITY GAP SYSTEMS L.L. Lacy, G. Nishioka & S. Ross	21
MEASUREMENT OF SURFACE VELOCITY FIELDS J.A. Mann, Jr.	36
SURFACE TENSION DRIVEN CONVECTION S. Ostrach	43
DEPLOYMENT OF SOLID PARTICLES ON LIQUID DROPLET SURFACES A.M. Schwartz	52
THE MIGRATION OF FLUID DROPLETS AND THEIR INTERACTIONS IN A THERMAL GRADIENT R.S. Subramanian & W.R. Wilcox	53
<u>SECTION B - CHEMICAL PROCESSES</u>	58
EXPERIMENTAL STUDIES IN OSTWALD RIPENING G.C. Kuczynski & C.B. Alcock	59
FORMATION OF METALLIC AND METAL HYDROUS OXIDE DISPERSIONS E. Matijevic & R.S. Sapiieszko	63
FLOCCULATION OF COLLOIDAL SUSPENSIONS WITH POLYMERIC FLOCCULANTS J.W. Vanderhoff	95

	<u>Page</u>
<u>SECTION C - BIOLOGICAL PROCESSES</u>	103
CELL PARTITION IN TWO PHASE POLYMER SYSTEMS D.E. Brooks	104
SOME POTENTIAL BLOOD FLOW EXPERIMENTS FOR SPACE G.R. Cokelet, H.J. Meiselman & H.L. Goldsmith	116
GEOMETRICAL CONSIDERATIONS IN THE SEPARATION OF BIOLOGICAL PARTICLES BY AFFINITY PARTITIONING S.D. Flannagan	124
CRYSTALLIZATION OF BIOLOGICAL MACROMOLECULES IN A REDUCED GRAVITY ENVIRONMENT E.J. Meehan, Jr.	130
FLOW AND THERMAL EFFECTS IN CONTINUOUS FLOW ELECTROPHORESIS D.A. Saville, P.H. Rhodes & R.S. Snyder	136
<u>SECTION D - CRYSTAL GROWTH EXPERIMENTS</u>	146
CRYSTAL GROWTH BY PRECIPITATION UNDER MICROGRAVITY A. Authier, F. Lefauchaux & M.C. Robert	147
MORPHOLOGICAL STABILITY OF A CRYSTAL GROWING IN SOLUTION D. Elwell	154
ANOMALOUS GROWTH OF SINGLE CRYSTALS IN SOLUTION W.N. Gill	160
CONVECTIVE FLOW DURING DENDRITIC GROWTH M.E. Glicksman & S.C. Huang	170
LOW DIMENSIONAL MAGNETIC SOLIDS AND SINGLE CRYSTAL ELPASOLITES: NEED FOR IMPROVED CRYSTAL GROWING TECHNIQUES M.L. Good, S. Watkins & R.W. Schwartz	191
INFLUENCE OF CONVECTION ON FREE GROWTH OF DENDRITE CRYSTALS FROM SOLUTION J. Hallett & E. Wedum	211
CONVECTIVE AND MORPHOLOGICAL INSTABILITY IN VAPOR CRYSTAL GROWTH F. Rosenberger	225
CRYSTAL GROWTH OF SULFIDE MATERIALS FROM ALKALI POLYSULFIDE LIQUIDS W.B. White	233

	<u>Page</u>
FLUID EXPERIMENT SYSTEM (FES) - OUTLINE OF CAPABILITIES J. Kropp	241
APPENDIX A Participant List for FES Workshop	A-1
APPENDIX B FES Workshop Agenda	A-6

## INTRODUCTION

The purpose of this Fluids and Chemistry Workshop is to acquaint researchers with the possibility of using the low gravity environment of space to extend various aspects of their research in ways that cannot be done in the terrestrial laboratory.

One objective of such research is understanding the role of gravity in processes involving fluid flows, particularly where there may be complicated coupling between gravity-driven flows and nongravity-driven flows. The complexities in many systems involving fluids and chemical reactions due to thermal and solutal convection often make it difficult to determine the relative importance of various effects and may confuse the measurements. This is especially true in the measurements of diffusion coefficients, solubility rates, thermal conductivities of fluids, and other parameters affected by convective transport. In many cases some of the more subtle nongravity-driven flows resulting from volume change, capillarity, soret diffusion, thermo-acoustic effect, etc., are overwhelmed, masked, or suppressed by the more dominant gravity-driven flows in the ground-based laboratory. Sometimes it is important to recognize and account for these flows in order to be able to control various processes. In many cases it is advantageous to perform idealized experiments that are simple enough to compare with a tractable model. Consider how difficult it would have been to deduce Newton's laws of motion had it not been possible to experiment with systems in which drag forces could be made negligible compared to inertial forces. Once the gravity forces are properly accounted for, the models can be extended reliably to include the gravity effects present in terrestrial processes, just as drag can be incorporated into Newton's laws of motion

once the basic principles are understood.

An excellent example of the use of low gravity experimentation to study various transport mechanisms was the series of closed-tube crystal growth experiments by chemical vapor transport developed by Prof. Heribert Wiedemeier and flown on the Skylab and Apollo-Soyuz missions. The observed transport rates in the space experiment were a factor of 2 to 8 times larger than expected based on extrapolation along the diffusion branch determined by laboratory experiments at low pressures. This indicates that either there is an unexpected nongravity-driven transport mechanism that acts at the higher pressures, or that what was thought to be diffusion-controlled transport in the laboratory was, in fact, confused by some unexpected gravity effect. In either case, the result indicates a fundamental deficiency in our understanding of the transport mechanisms in closed-tube chemical vapor transport.

Other motivations for doing research in a low gravity environment may include the elimination of density sedimentation, buoyancy-driven convection, and hydrostatic pressure which adds a new dimension in process control. It is anticipated that suitably designed low gravity experiments could take advantage of this unique research environment in a variety of ways. For example, the lack of sedimentation allows multicomponent systems with variable densities to be held in suspension more or less indefinitely. This is useful for the investigation of the nucleation, growth, and coalescence of bubbles, flocculants, colloids, and hydrosols and of their behavior in thermal gradients and acoustic fields. Apart from fundamental interest, such studies have important applications in many industrial processes.

For example, the kinetics of Ostwald ripening, although a classical

topic, is still not well understood. One of the experimental difficulties in the study of Ostwald ripening is maintaining a suspension without stirring, which affects the transport in a complicated manner. Since this is important in many precipitation processes, including precipitation and dispersion hardening of superalloys used to fabricate high-temperature gas turbine blades, there is an impetus to understand it in more detail. A low-g experiment could keep such particles in suspension long enough to study the change in size distribution as a function of time and concentration in a diffusion-controlled environment which can provide the experimental data required to evaluate the kinetics.

Another example is the use of seeded polymerization to grow larger sized monodispersed latex spheres. Very precise monodispersed spheres can be prepared by this technique in sizes up to 2 microns, where they are kept in suspension by Brownian motion. The agitation required to keep larger size particles in suspension often results in coagulation. Attempts will be made on early Shuttle flights to produce quantities of monodispersed spheres between 2 and 40 microns in diameter. Such particles are useful as calibration standards and may actually have commercial value greater than the cost to produce them in space.

The convective and sedimentation problems associated with continuous flow electrophoresis and other electrokinetic separation processes greatly limit the performance of such devices on the ground. It has been estimated that a 5-fold improvement in resolution and as much as a 400-fold improvement in throughput could be achieved by performing such processes in space. Some early experiments will be done on Shuttle to verify these concepts. Also, the improved understanding of the role of gravity in the flow may suggest

various improvements in the design of laboratory separation devices.

The quiescent environment of an orbiting vehicle provides a unique opportunity to study crystal growth environment. A Fluids Experiment System (FES) is being developed to fit into a Spacelab rack. This facility will provide precision temperature control in a test cell as well as a sophisticated holographic optical system that can obtain shadowgraph, Schlieren, and interferometric data. A more detailed description of this facility is given in the workshop proceedings. Let me just say here that the FES was designed as a general purpose facility to accommodate a variety of fluid and chemical experiments. The test cell is modular and could be configured to fit the experimenter's needs as long as the external envelope is maintained. It is hoped that this facility will provide an easy means of accomplishing a number of fluid and chemical experiments that we envision.

The invited participants at this workshop are a cross section of active researchers involved in a variety of disciplines that have in common the need to provide better understanding or control of fluid and chemical processes and, therefore, have a rationale for extending their research into a low-g environment to eliminate or drastically reduce gravity effects. It is hoped that these presentations will produce cross stimulation among the presenters and will suggest possible flight experiments to other workers in the field.

Robert J. Naumann  
Chief Scientist, Materials Processing in Space  
Marshall Space Flight Center

SECTION A  
GENERAL FLUID DYNAMICS

**Page intentionally left blank**

**Page intentionally left blank**

# PHASE SEPARATION IN TRANSPARENT LIQUID-LIQUID MISCIBILITY GAP SYSTEMS

by

S. H. Gelles, B. N. Bhat<sup>(a)</sup> and R. J. Laub<sup>(b)</sup>

## INTRODUCTION

The field of processing materials in space has provided a renewed incentive to study materials systems containing a liquid phase miscibility gap, i.e., a field in the phase diagram representing the equilibrium between two liquid phases. These studies have concentrated on understanding the development of both the macro- and microstructures of these materials during thermal processing and have also taken advantage of the low-gravity environment afforded by sounding rockets and orbiting spacecraft to minimize the effects of buoyancy and fluid flow. The programs have generally concentrated on opaque metallic systems and have been primarily concerned with the separation process wherein a single phase liquid transforms into two liquid phases and with the accompanying coalescence processes. Since solidification can affect the macro- and microstructures, this transformation has been studied as well.

As will be delineated in what follows, the studies of the metallic systems at low-g have led to unexpected results, and have prompted the analysis of mechanisms which might have disturbed the transformation and led to the unusual results observed. These disturbing effects are generally difficult to analyze even if they occur alone. They are all the more complicated when more than one mechanism is involved. Moreover, other processes that as yet have not been conceptualized may also occur. It is with these factors in mind that we have outlined a program to be carried out on transparent liquid-phase miscibility gap materials for the purpose of acquiring additional insight into

---

(a) S. H. Gelles Associates, Columbus, OH 43204

(b) Department of Chemistry, Ohio State University, Columbus, OH 43201

the separation process occurring in these systems. The transparency feature allows the reaction to be viewed directly through light scattering and holographic methods.

#### BACKGROUND

A number of opaque miscibility gap metallic systems have been made the subject of ground base and flight studies.<sup>(1-8)</sup> We have been studying aluminum-indium alloys<sup>(1,2)</sup> in terrestrial and SPAR rocket experiments. In a typical experiment, an alloy of composition within the extremes of the miscibility gap is heated into the single phase liquid field above the miscibility gap (See Figure 1)<sup>(2,9)</sup> held for a time sufficient to homogenize the alloy and then cooled through the gap at a controlled cooling rate. It was expected that the structure resulting from conducting this heat treatment at low-g would consist of a uniform precipitate contained within a host phase. In the aluminum-rich end of the miscibility gap the dispersed phase would be rich in indium while indium-rich alloys would produce aluminum-rich precipitates in an indium-rich phase. The Al-In alloys processed at 1-g would consist of a layered structure with the indium-rich phase at the bottom and the aluminum-rich phase floating on the top.

Samples of various compositions of aluminum-indium alloys have been processed on both the SPAR II and SPAR V sounding rocket flights. An example of the results obtained is shown in Figure 2 where the macrostructures of an Al-40 and -70 wt. Pct. In alloy processed on SPAR II are compared with their ground base counterparts. The ground base samples possess the expected layered structures but those processed in space did not produce the anticipated uniform dispersions. Instead, as may be seen in Figure 2a, the structure

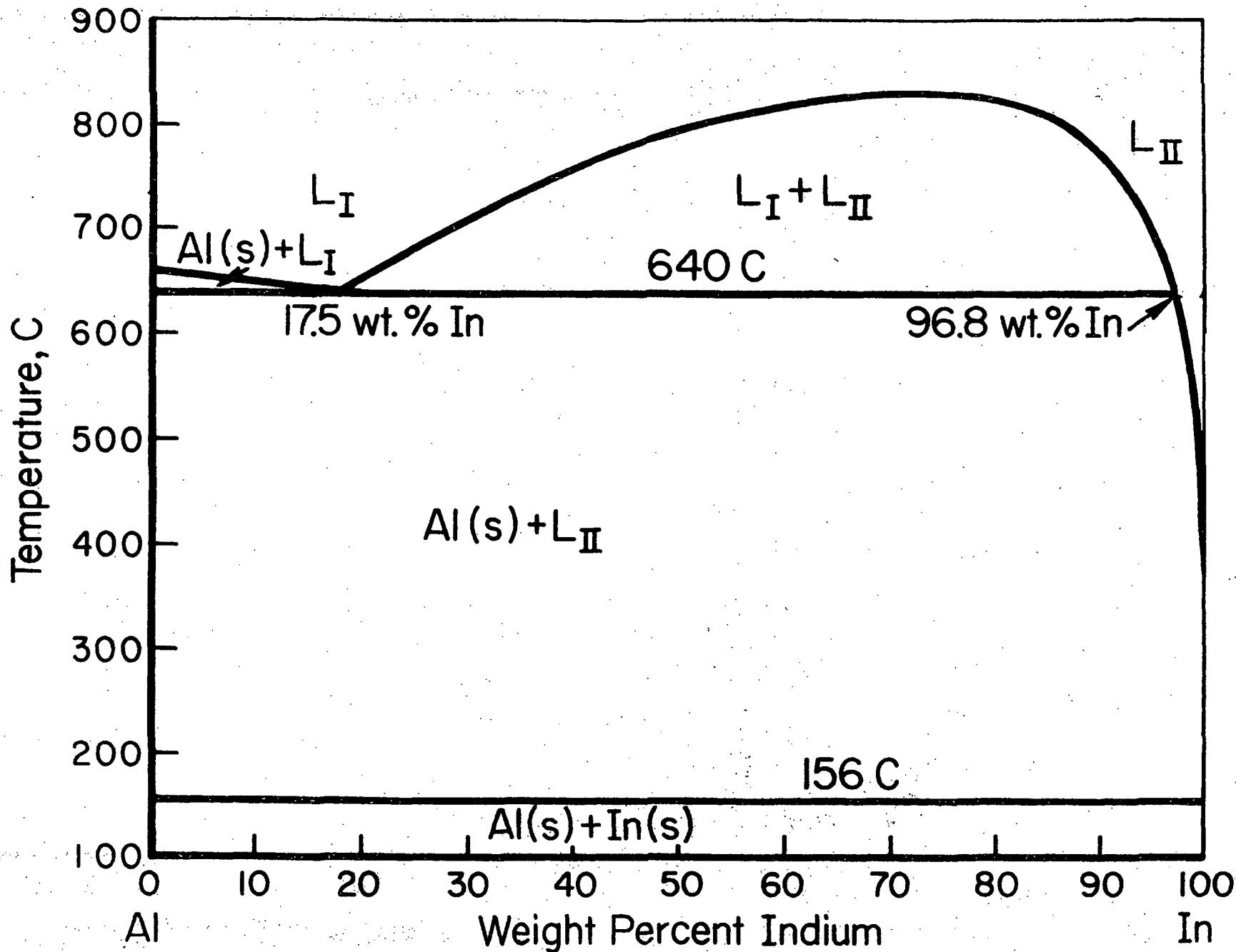
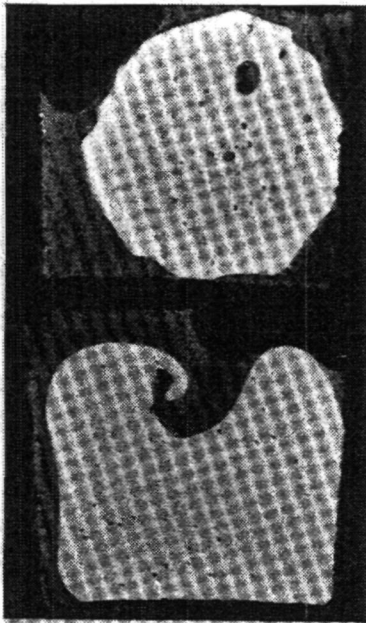


FIGURE 1. THE ALUMINUM-INDIUM EQUILIBRIUM DIAGRAM<sup>(2,9)</sup>

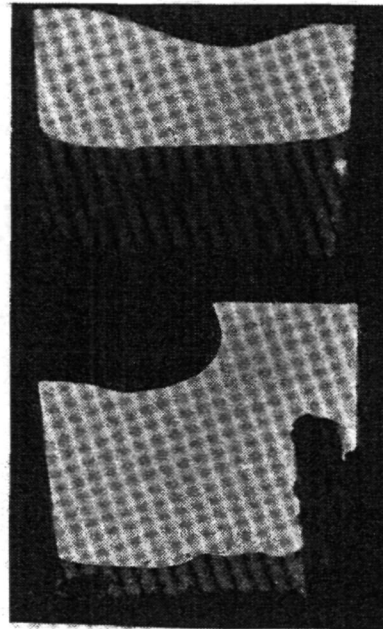
5 ORIGINAL PAGE IS OF POOR QUALITY

ORIGINAL PAGE IS  
OF POOR QUALITY



Flight

(a)



Ground Base

(b)

Al-70 wt. % In

Al-40 wt. % In

FIGURE 2. MACROSTRUCTURE OF SPAR II Al-In ALLOYS  
AND THEIR GROUND-BASE COUNTERPARTS

consists of a massively separated aluminum-rich core surrounded by indium-rich material. Observations similar to these have been made in other metallic miscibility gap systems processed at low-g (See for example References 3-5).

Various mechanisms generally involving fluid flow have been proposed to explain the structures of the miscibility gap alloys processed in space. A listing of these mechanisms is presented in Table 1. Some of them have been considered in detail from a theoretical standpoint while others have as yet not been analyzed. For example, detailed calculations have been made on the residual fluid motion present after spin-up and despin in the SPAR rocket experiments with the conclusion that this potential source of fluid motion did not significantly contribute to the development of the observed structures. Similarly, inhomogeneities in the starting Al-In alloys have been ruled out as being contributory after extensive measurements of liquid phase diffusion had been made and after long homogenization times had been applied to the experimental procedure with no discernable difference in results.

Evidence has been obtained that surface tension driven fluid motion has influenced the structure of the Al-In alloys processed in SPAR II and SPAR V. In support of this model, wave-like structures have been observed at the liquid-liquid interfaces and in addition evidence of droplet migration driven by surface tension forces has been presented as shown in Figure 3<sup>(2)</sup>. The alloy illustrated in this figure is an Al-90 wt. pct. In alloy processed aboard SPAR V. The macrostructure consists of two massive aluminum-rich regions surrounded by indium-rich material. Adjacent to the larger aluminum-rich region is an annular area that consists of agglomerating aluminum-rich spheres (See Figure 3b). Further away from the aluminum-rich metal, there

ORIGINAL PAGE IS  
OF POOR QUALITY

TABLE 1. POSSIBLE MECHANISMS FOR MASSIVE PHASE SEPARATION

---

---

Residual Fluid Motion

Surface Tension Drive Flow (Marangoni Effect)

Conventional Convection

Capillarity (Spreading)

Transformation Segregation

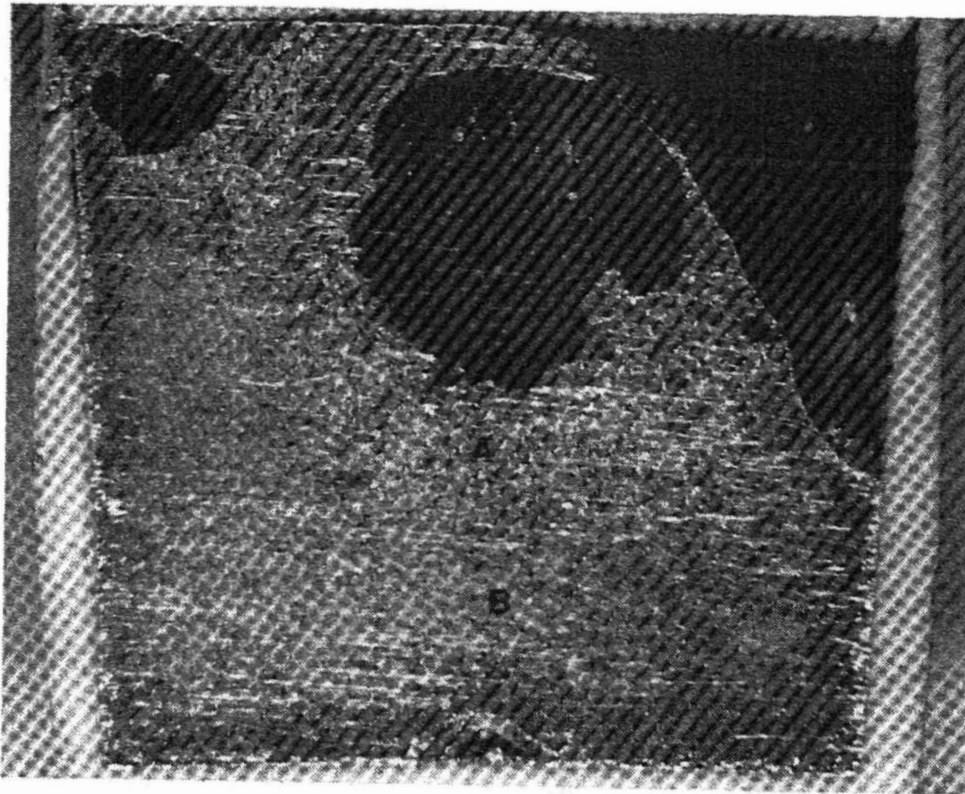
Transformation Volume Changes

Nonuniform Starting Composition

---

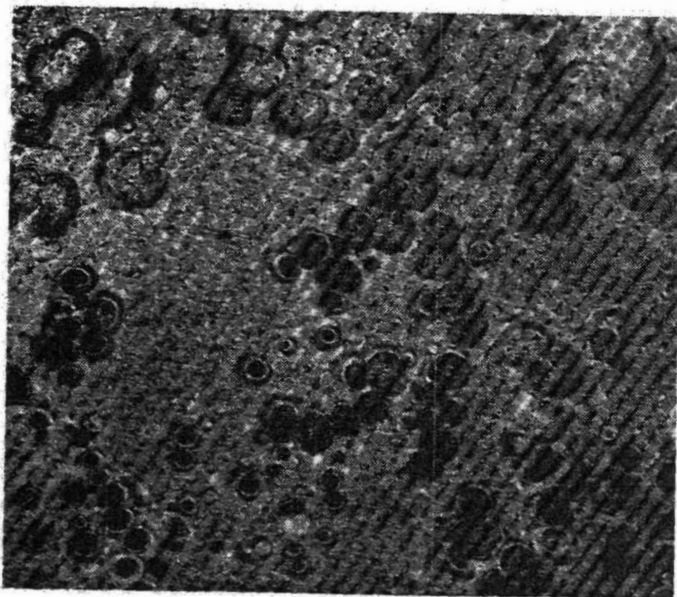
---

ORIGINAL PAGE  
BLACK AND WHITE PHOTOGRAPH



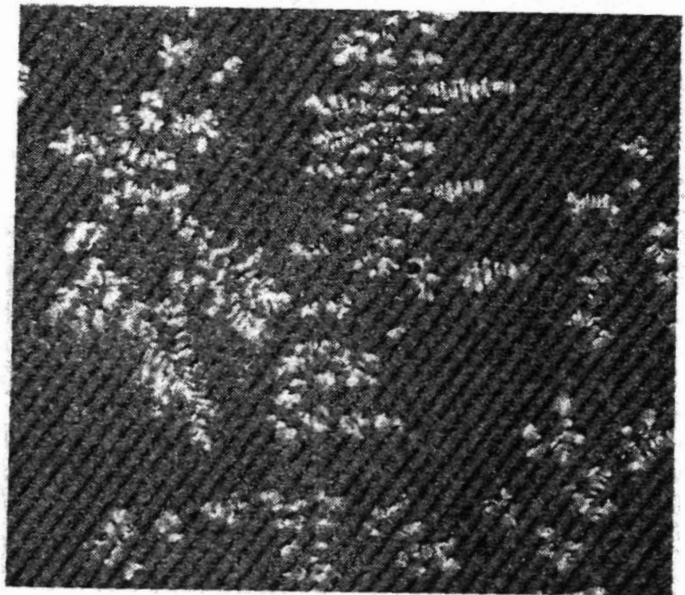
(a)

10x



(b)

100x



(c)

100x

FIGURE 3. STRUCTURE OF Al-90 WT. PCT. IN ALLOY PROCESSED ON SPAR V.  
(a) Macro View of Longitudinal Cross-Section. (b) Micro-  
structure of Region A in (a) and (c) Microstructure of  
Region B in (a).

in an area that is relatively free of the aluminum-rich spheres (Figure 3 c). These structural observations can be explained by a model consisting of the aluminum-rich spheres migrating to the warmer regions of the molten alloy during cooling through the miscibility gap. Quantitative support for this model has also been obtained. (2)

It is rather difficult to sort out the various phenomena that are contributing to the structural evolution of the liquid-phase miscibility materials. This is especially difficult in opaque systems where generally only the final structure is available for analysis of the mechanisms which might have contributed to its formation. Studies in transparent analogue systems would offer two distinct benefits. First of all, they would allow direct observations of the fluids during transformation and secondly, they would provide systems with a wider range of physical properties so that the importance of various physical parameters can be assessed in terms of phase separation kinetics and emulsion stability. In the following section we outline an experimental program dealing with transparent liquid phase miscibility gap systems which would supplement the present research activities on the metallic systems.

#### SUGGESTED RESEARCH PROGRAM ON LIQUID PHASE MISCIBILITY GAP SYSTEMS

A study of transparent liquid phase miscibility gap systems would have as its objectives:

1. To view phase-separation in situ in an attempt to determine the mechanism of massive separation previously seen in metallic systems.

**ORIGINAL PAGE IS  
OF POOR QUALITY**

2. To determine the effect of material properties on the kinetics of phase separation, on the occurrence of various fluid flow mechanisms and on emulsion stability.

To accomplish these objectives, we are suggesting the following program which can be organized into the following phases.

Phase 1. System Selection

Phase 2. Ground Base Experiments

Phase 3. Flight Experiments

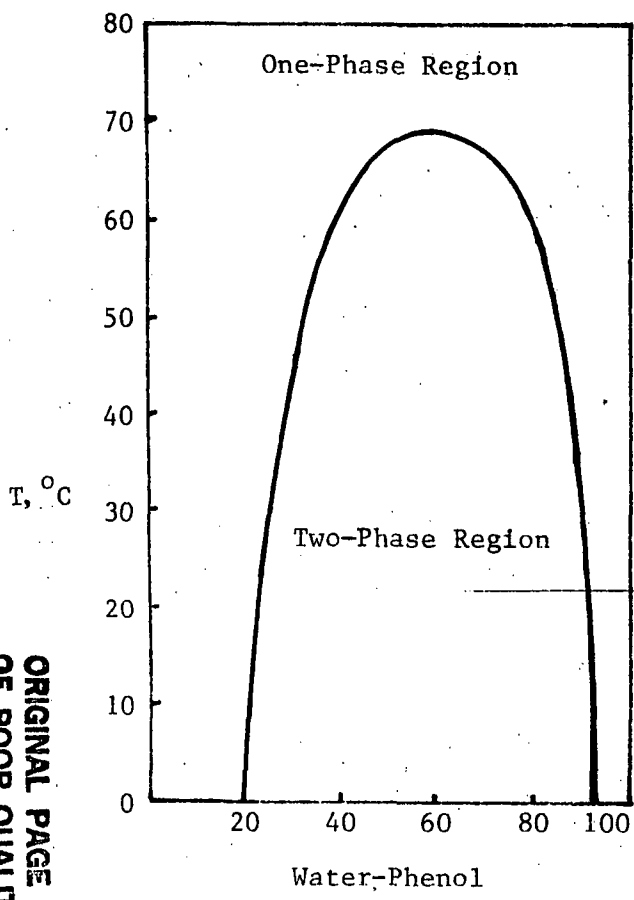
#### System Selection

This part of the program would be devoted to the very important task of selecting the proper systems for study. In the selection process the most important parameters are the physical properties such as the surface energies and interfacial energies between the two coexisting liquids and their variation with composition and temperature. In addition, fluid flow properties such as viscosities are of importance. Aside from these basic physical properties, it is important to select systems that are convenient to work with, i.e. that have convenient consolute temperatures, miscibility gap widths and heights and which will not create excessive handling problems, due to extreme toxicity, for example, or to a requirement for ultra-purification. Examples of three types of transparent liquid phase miscibility gap systems are shown in Figure 4. Figure 4a shows the more common type with an upper critical temperature, whereas Figure 4b shows one with a lower critical temperature. Figure 4c has both upper and lower critical temperatures.

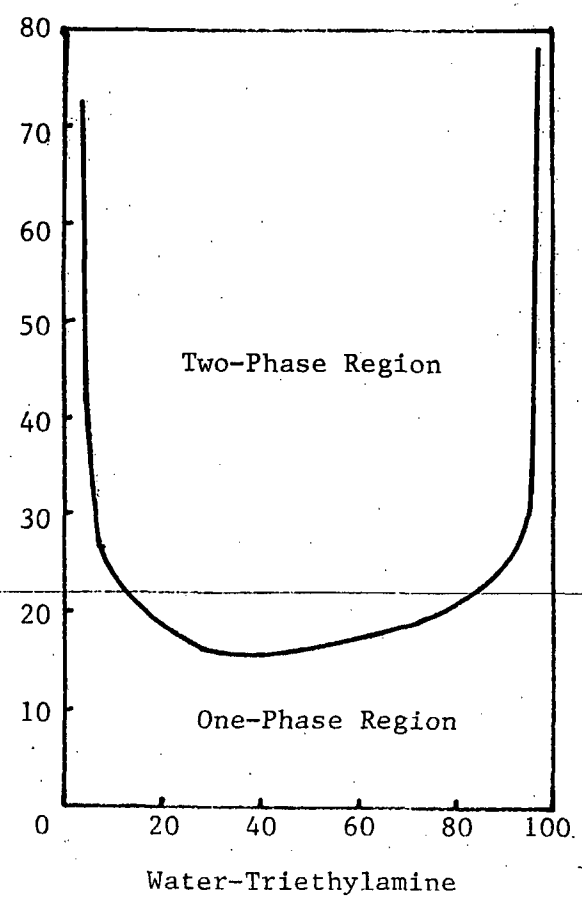
#### Ground Base Experiments

It is envisioned that the ground base research would be in three areas.

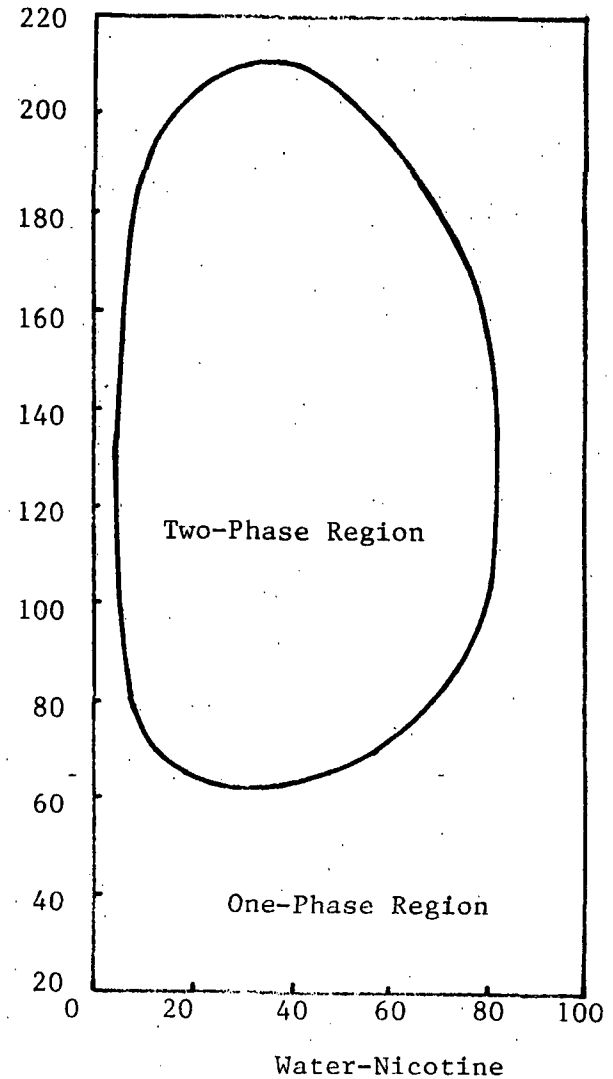
ORIGINAL PAGE IS  
OF POOR QUALITY



(a)



(b)



(c)

FIGURE 4. EXAMPLES OF TRANSPARENT MISCIBILITY GAP SYSTEMS. (a) Shows an upper critical temperature. (b) A lower critical temperature and (c) both lower and upper critical temperature.

1. System property evaluation.
2. Phase separation kinetics and emulsion stability.
3. Fluid flow mechanisms.

#### System Property Evaluation

In this portion of the program, the literature dealing with the physical parameters listed in Table 2 would be reviewed for the selected systems and the reliability of pertinent published data would be assessed. In those cases where the data are missing or unreliable, supplementary measurements would be made.

#### Phase Separation Kinetics

Phase separation kinetics and emulsion stability of various transparent systems having a wide range of material properties would be evaluated by means of light scattering and holographic techniques. The effect of composition within the miscibility gap would be determined in both isothermal and controlled cooling rate experiments. In the isothermal experiments, a chemical mixture making up the transparent system would be cooled or heated from a single phase liquid field into the two phase liquid field where it would be held and monitored as a function of time by such techniques as light scattering. In the cooling rate experiments, the samples would be cooled at controlled rates through the miscibility gap again while monitoring the particle size distribution as a function of time. The results of these experiments would be compared to theoretical models dealing with nucleation, droplet collisions, coalescence and emulsion stability.

#### Fluid-Flow Mechanisms

Transparency in the systems of interest will provide the opportunity to carry out experiments on the mechanisms of fluid flow which affect the stability and structure of liquid phase miscibility gap systems. Such mechanisms include droplet migration under the driving force of surface tension, thermo-

TABLE 2. PHYSICAL PROPERTIES OF INTEREST IN STUDIES ON  
TRANSPARENT MISCIBILITY GAP MATERIALS

---

---

Phase Equilibria

Viscosities

Interfacial Energies

Thermal Properties

Diffusional Characteristics

Transformation Volume Changes

---

---

ORIGINAL PAGE IS  
OF POOR QUALITY

capillary and solutalcapillary convection, spreading, fluid motion due to volume changes associated with transformations and fluid motion due to coalescence mechanisms. The experimental approach would be supplemented with theoretical modeling.

LOW GRAVITY EXPERIMENTS

Experiments dealing with transparent liquid phase miscibility gap systems at low gravity will be designed with the objective of determining the effect of gravity on the separation kinetics, emulsion stability and fluid flow phenomena associated with the phase separation. The Fluids Experiment System (FES) now being designed would appear to be a suitable apparatus in which to carry out these experiments. Specific experiments dealing with the pertinent mechanisms of fluid flow would probably develop from the ground base studies.

The rationale for conducting these studies at low gravity is to reduce the complications associated with buoyancy effects, conventional convection and their associated contributions to droplet collisions.

ANTICIPATED BENEFITS

The extension of the research on liquid phase miscibility gap systems into studies on transparent systems should provide insight into the mechanisms causing massive separation in metallic miscibility gap alloys. The research should also provide a better understanding of the effect of material parameters on phase separation kinetics, droplet size distribution, and emulsion stability. Since the experiments on transparent systems would allow measurements of the separation process to be made while the reaction is occurring these systems would also be ideal for studying spinodal decomposition.

The research would also provide insight into the fluid flow mechanisms which are active in these systems and which may be accentuated in an acceleration-free environment. With the attaining of an understanding of the material parameters of importance in the phase separation, it will be far easier to select systems of potential technical importance.

## REFERENCES

1. S. H. Gelles and A. J. Markworth, "Microgravity Studies in the Liquid Phase Immiscible System: Aluminum-Indium," AIAA Journal, 16 (1978) 431.
2. S. H. Gelles and A. J. Markworth, "Final Post-Flight Report on SPAR V Experiment 74-30, Agglomeration in Immiscible Liquids," Final Report to NASA-MSFC on Contract NAS8-31542, October, 1979.
3. L. L. Lacy and C. Y. Ang, "Monotectic and Syntectic Alloys Experiment MA-044," Apollo-Soyuz Test Project Summary Science Report, Vol. 1, NASA SP-412, 1977.
4. H. U. Walter, "Stability of Multi-Component Mixtures Under Microgravity Conditions," Presented at the Third European Symposium on Materials Science in Space, Grenoble, France, April 24-27, 1979.
5. T. Carlberg and H. Fredriksson, "The Influence of Microgravity on the Structure of Bismuth-Zinc Immiscible Alloys," Presented at the Third European Symposium on Materials Sciences in Space, Grenoble, France, April 24-27, 1979.
6. J. L. Reger, "Experimental Development of Processes to Produce Homogenized Alloys of Immiscible Materials," Final Report, III, Prepared Under Contract NASA-27805, to NASA-MSFC, TRW Report 18677-6019-RU-00, Jan., 1973.
7. C. Potard, "Directional Solidification of Aluminum-Indium Alloys at Micro-Gravity: Results of Basic Preparatory Investigations," Paper Presented at the 17th Aerospace Meeting, AIAA, New Orleans, La., Jan. 15-17, 1979.
8. H. Ahlborn and K. Lohberg, "Aluminum-Indium Experiment SOLUOG - a Sounding Rocket Experiment on Immiscible Alloys," Paper 790172 Presented at the 17th Aerospace Sciences Meeting, AIAA New Orleans, La., Jan. 15-17, 1979.
9. B. Predel, "Beitrag zur Konstitution und Thermodynamik von Entmischungssystemen," Zeitschrift fur Metallkunde, 56 (1965) 791.

32 34/ N82 32060

## MEASUREMENT OF DIFFUSION COEFFICIENTS FROM SOLUTION RATES OF BUBBLES

Irvin M. Krieger<sup>(a)</sup>

The rate of solution of a stationary bubble is limited by the diffusion of dissolved gas molecules away from the bubble surface. Diffusion coefficients computed from measured rates of solution give mean values higher than accepted literature values, with standard errors as high as 10% for a single observation. Better accuracy is achieved with sparingly soluble gases, small bubbles, and highly viscous liquids. Accuracy correlates with the Grashof number, indicating that free convection is the major source of error. Accuracy should, therefore, be greatly increased in a gravity-free environment. The fact that the bubble will need no support is an additional important advantage of Spacelab for this measurement.

---

<sup>(a)</sup> Case Western Reserve University

# MEASUREMENT OF DIFFUSION COEFFICIENTS FROM SOLUTION RATES OF BUBBLES

by

Irvin M. Krieger<sup>(a)</sup>

A stationary gas bubble immersed in a liquid will dissolve at a rate limited by the outward transport of solute molecules from the bubble surface. In the absence of convection, the rate of transport is controlled by diffusion, and can readily be calculated from Fick's law. A closed-form solution for the rate of disappearance of the bubble is available for the isothermal case with concentration-independent diffusion coefficient and spherical symmetry. Diffusion coefficients can be calculated by fitting the theoretical equation to the experimental data. If the experiment can be conducted under conditions where the assumptions are valid, one should obtain better reproducibility and accuracy in the measured diffusion coefficients than is achievable by the best methods currently available. Given accurate diffusion coefficients for probe molecules of various sizes in pure liquids and solutions, valuable inferences can be drawn about the structures of the liquids and the mechanisms of mass transport.

Due to buoyancy effects, a stationary free bubble can not be achieved in a gravitational field. Various artifices have been invoked to hold the bubble....attachment to flat plates or fibers, even confinement by a centrifugal field. Use of a flat plate destroys the spherical symmetry, so that either approximate integrations or empirical calibrations are needed. Attachment of the bubble to a single fiber, of diameter far less than that of the bubble, was achieved in the author's laboratory (J. Phys. Chem. 71, 1173 (1967); 78, 2516 (1974)). Statistical analysis of a large body of data showed that

---

<sup>(a)</sup>Departments of Chemistry and Macromolecular Science, Case Western Reserve University, Cleveland, Ohio

average diffusion coefficients obtained by this method were consistently higher than those obtained by such accepted methods as the liquid jet technique. The relative standard deviations of the measurements in pure liquids were typically from 5 to 9%; only for measurements in viscous polymer solutions were the relative standard deviations appreciably below 5%. The standard deviations correlated with the dimensionless Grashof Number

$$Gr = \frac{\rho_l g d^3 \Delta C \frac{\partial p}{\partial c}}{\eta^2},$$

where  $\rho_l$  is the density of the liquid,  $g$  the gravitational acceleration,  $d$  the bubble diameter,  $c$  the solute concentration,  $\Delta C$  the difference between concentrations at the bubble surface and in the bulk, and  $\eta$  the liquid's viscosity.

What is proposed, then, is a Spacelab experiment in which a small bubble is injected into a liquid, and its rate of solution followed by time-lapse photography. The gravity-free environment would confer two very important benefits: (1) absence of appreciable buoyancy would allow the free bubble to remain stationary; and (2) the very low  $g$ -value would effectively eliminate gravity-driven convection. The accurate diffusion coefficients that should be obtainable from these data should permit determination of the effects of such variables as solute concentration, temperature and size of probe molecules.

Ground-based experiments in preparation for those in Spacelab should concentrate on reducing the Grashof number. The most sensitive variables are bubble diameter and liquid viscosity. Use of small bubbles and viscous polymer solutions should allow reductions in the Grashof number equivalent to reduction of  $g$  by two or three orders of magnitude. With liquids of sufficiently high viscosity, it should be possible to slow the bubble's rise to such an extent as to achieve an effectively stationary bubble without a supporting fiber.

INVESTIGATIONS ON TRANSPARENT LIQUID-MISCIBILITY GAP SYSTEMS

L.L. Lacy and G. Nishioka  
 Space Sciences Laboratory  
 NASA, G. C. Marshall Space Flight Center  
 Huntsville, Alabama 35812

and

S. Ross  
 Chemistry Department  
 Rensselaer Polytechnic Institute  
 Troy, New York 12181

ABSTRACT

Sedimentation and phase separation is a well known occurrence in monotectic or miscibility gap alloys. Previous investigations indicate that it may be possible to prepare such alloys in a low-gravity space environment but recent experiments indicate that there may be non-gravity dependent phase separation processes which can hinder the formation of such alloys. We are studying such phase separation processes using transparent liquid systems and holography. Holography has advantages over conventional microscopy since large numbers ( $10^3 - 10^4 \text{ cm}^{-3}$ ) of particles can be accurately recorded in a single exposure. By reconstructing such holograms into a commercial-particle-analysis system, real time computer analysis can be performed on emulsions with diameters in the range of  $5\mu\text{m}$  or greater. Thus dynamic effects associated with particle migration and coalescence can be studied. Characterization studies on two selected immiscible systems including an accurate determination of phase diagrams, surface and interfacial tension measurements, surface excess and wetting behavior near critical solution temperatures have also been completed. It was found that surface activity of the component of lower surface tension increases as solutions approach the consolute point. These findings agree well with predictions based on the two surface layer model of Defay and Prigogine. Experiments that measure the influence of large values of surface excess on surface tension driven flow are underway.

Values of contact angle against glass in the heterogeneous region of two systems are also reported. The behavior is opposite to that predicted by Cahn. The influence of this behavior on heterogeneous nucleation is now being studied.

ORIGINAL PAGE IS  
OF POOR QUALITY

INVESTIGATIONS ON TRANSPARENT LIQUID-MISCIBILITY GAP SYSTEMS

L. L. Lacy and G. Nishioka  
Space Sciences Laboratory  
NASA, G. C. Marshall Space Flight Center  
Huntsville, Alabama 35812

and

S. Ross  
Chemistry Department  
Rensselaer Polytechnic Institute  
Troy, New York 12181

INTRODUCTION

The low-gravity environment of space has prompted interest in the formation of unique monotectic or miscibility gap alloys. Previous experiments using the MSFC drop tower [1,2] have demonstrated that fine dispersions of a Ga-rich phase could be achieved in a Bi-rich matrix. The elimination of buoyancy driven separation has been demonstrated on a Skylab experiment [3] using isothermal dispersions of krytox oil and water. The Skylab dispersions were completely stable for all compositions and for a long period of time (10 hours) even though the spacecraft experienced transient accelerations in the range of  $10^{-3}$  to  $10^{-2}$  g. More recent experiments on metallic systems have, however, provided confusing results.

An experiment [4] performed on the Apollo-Soyuz Test Project in 1975 dealt with an alloy of Pb-Zn slowly (cooling rate  $\approx 0.03^\circ$  C/s) and isothermally (thermal gradient  $< 2^\circ$  C/cm) cooled through the consolute temperature and then solidified at the monotectic temperature. The Pb-Zn samples consisted of fine dispersions of a Pb-rich phase in a Zn-rich matrix with the Pb-particles showing an aligned structure in much of the sample. The occurrence of major macroscopic regions of Pb-rich and Zn-rich regions in the sample, which corresponded to

the initial location of the pure metals, and the appearance of a diffusion-type gradient away from the interface led to the conclusion that the samples were not homogeneous at the beginning of the cooling period. The appearance of a relatively large Zn-rich particle on the Pb-rich side of the sample provided evidence that major coalescence was probably taking place within the material.

Similar results have also been obtained on Al-In alloys flown on a suborbital rocker flight [5]. In this case, the alloys were cooled at a faster rate ( $\approx 15^\circ \text{C/s}$ ) and contained compositions on both sides of the consolute temperature. The Al-In samples showed almost complete separation of the phases into a lower-surface-tension In-rich phase surrounding a higher-surface-tension Al-rich phase. Unlike the Pb-Zn samples, there was a distribution of particle sizes from micron size to millimeter size. A later analysis of the experiment indicated that this experiment may have been influenced by the lack of a homogeneous starting liquid and a subsequent experiment was reflowed on SPAR V. Since the results of the second flight are similar to the first flight, this provides strong experimental evidence of massive non-gravity dependent phase-separation processes.

The processes in low-gravity which may affect the ultimate structure of miscibility gap alloys include:

1. Nucleation of a dispersed phase or spinodal decomposition of congruent phases.
2. Rapid diffusional growth and Brownian coalescence of the phases during the early stages of phase separation.
3. Coalescence processes of the dispersed phase which are influenced by surface and interfacial forces or by residual spacecraft accelerations.
4. Thermocapillary particle motion due to thermal gradients as has been observed for bubbles in liquids (ref 6).
5. Non-gravity dependent convective fluid motion caused by volume changes occurring during phase changes or differential surface tension gradients.
6. Coalescence processes caused by the interaction of the dispersed phase with the solidification interface.

These processes involve complex kinetic mechanisms which are often interrelated in a given experiment and which are worthy of detailed study.

We have chosen to study these processes in transparent model organic systems because of their obvious advantages. We have proposed the study of growth kinetics in model systems in space because these processes are strongly affected by convection and buoyancy. It should be noted that although three component neutrally buoyant emulsions can be formed at a given temperature, there exists no two component partially miscible system that is neutrally buoyant over range of temperatures [7]. To study the phase separation processes in model materials, we have proposed [8,9] to use holography since it has advantages over conventional microscopy in maintaining good resolution and superior depth of field that allow the recording of  $10^3$  to  $10^5$  particles in a single exposure.

#### EXPERIMENTAL TECHNIQUES AND CHARACTERIZATION STUDIES

Holography has been previously used to measure small particles in meteorology [10] and crystal growth experiments [11]. We have experimentally investigated an in-line system for use with dispersions and emulsions [8,9,12].

Figure 1 is a schematic of the holographic construction system and Figure 2 is a schematic of the reconstruction system. This holographic arrangement allows overall system magnification in the range of 800 to 1200 X. Typical reconstructed holograms of calibrated test squares can be seen in Figure 3 which demonstrates the overall system capability to accurately measure particle diameters for particle sizes  $5\mu\text{m}$  or greater. The measured particle size in Figure 3 are shown by the display in the upper left hand corner of each picture. This system is capable of accurately recording up to  $10^4$  particles/cm<sup>3</sup> on a single hologram for later analysis.

In order to determine the system capability to measure particle distributions, holograms were taken of a known distribution of glass

beads dispersed in a clear oil. The holograms were then reconstructed and the particle size measured using the Omnicon computer system. The results are shown in Figure 4 which compares the particle distribution in the dispersed system to the distribution as measured by the Omnicon system using conventional microscopy.

Two binary systems were chosen for ground based characterization study. Both the ethyl salicylate-diethylene glycol system and the cyclohexane-methanol system are relatively nontoxic and have a large miscibility gap region. These systems are almost completely characterized with respect to many important properties, such as the phase diagram, surface and interfacial tensions, density, viscosity, and refractive index.

Because many important processes in space are influenced by surface activity, the quantitative measurement of surface activity (the Gibbs excess) in our miscibility gap systems was undertaken. Figure 5 describes some results, the solid line is the binodal curve and the dotted lines represent lines of equal surface activity, called cosorption lines. The cosorption lines are calculated from surface tension and activity coefficient measurements. Figure 5 reads as a contour map and shows a rise in surface activity of solutions whose temperature and composition approach a point near the active component. In this system ethyl salicylate is the surface active component. Solutions near the critical solution point have high surface activity and display all the phenomena of a soap solution, i.e.: they foam [13,14], they contain micelles [15], and they are probably less responsive to surface tension driven flows than a non-surface active solution, or pure liquid. The last conclusion is a hypothesis we are currently testing.

Figure 6 shows similar behavior in the hexane-aniline system. This plot is derived from data published by Campbell and coworkers [16,17]. Figure 7 shows reduced surface activity for a regular solution using the two layer surface model of Defay and Prigogine [18,19]. Component 1 was assumed to have the higher surface tension, in all three diagrams the maximum in surface activity is shifted towards the component of

higher surface tension.

Heterogeneous nucleation is an important effect as solutions are cooled into the two phase region. The contact angle between the two conjugate phases on a solid substrate is a parameter we have studied since it greatly influences heterogeneous nucleation. Figure 8 summarizes measurements we have made of the cyclohexane-methanol system on glass. Curve b represents behavior for a system of reagent grade methanol-cyclohexane; the methanol contains 0.20% water by weight. Curve a shows behavior of a highly purified system; the methanol contains less than 0.02% water by weight. Although small amounts of water can drastically affect the consolute temperature, the wetting behavior remains essentially the same. One conjugate solution preferentially wets the glass within five degrees of the critical solution point. The contact angle rises very rapidly with rising temperature and becomes  $90^\circ$  close to the critical solution temperature. As temperature then rises to the critical temperature, the meniscus thickens and finally disappears. Similar behavior was observed with the ethyl salicylate-diethylene glycol system.

It is interesting that our observations show that  $\cos \theta$  is proportional to  $(T_c - T)^{-1}$ , in agreement with Cahn's prediction [20]. However, the contact angle approaches  $90^\circ$  near the critical solution point, rather than  $0^\circ$  as predicted by Cahn. This should not be surprising, since as the consolute point is approached, the conjugate phases approach each other in chemical composition and the contact angle should approach the symmetric angle of  $90^\circ$ . Therefore, the two phase region near the critical solution point is better described by the term "critical point dewetting" rather than "perfect wetting" as formerly suggested [20]. We are now examining the influence of different contact angles on heterogeneous nucleation in both of our systems.

### Legends for Figures

- Figure 1. In-line holographic construction system for studying emulsions and dispersions.
- Figure 2. Holographic reconstruction and Omnicon particle analysis system.
- Figure 3. Calibration squares measured by Omnicon. The true particle sizes are (a) 100 $\mu\text{m}$ , (b) 37.5 $\mu\text{m}$ , and (c) 5 $\mu\text{m}$ . The measured particle sizes are displayed in the upper left hand corner.
- Figure 4. Comparison of measured particle distribution using ordinary microscopy of the particles placed on glass slides and holograms of the particles dispersed in clear oil.
- Figure 5. Phase diagram and surface activity in the ethyl salicylate-diethylene glycol system. Cosorption lines represent surface excess  $\Gamma^{(G)}$  of ethyl salicylate ( $\times 10^{10}$  moles/cm<sup>2</sup>).
- Figure 6. Phase diagram and surface activity in the hexane-aniline system. Cosorption lines represent surface excess  $\Gamma^{(G)}$  of hexane ( $\times 10^{10}$  moles/cm<sup>2</sup>).
- Figure 7. Phase diagram and surface activity for a two layer regular solution. Component 1 has the higher surface tension.
- Figure 8. Contact angle vs. temperature in the cyclohexane-methanol system. Curve a represents a system containing less than 0.02% water. Curve b represents a system containing less than 0.20% water.

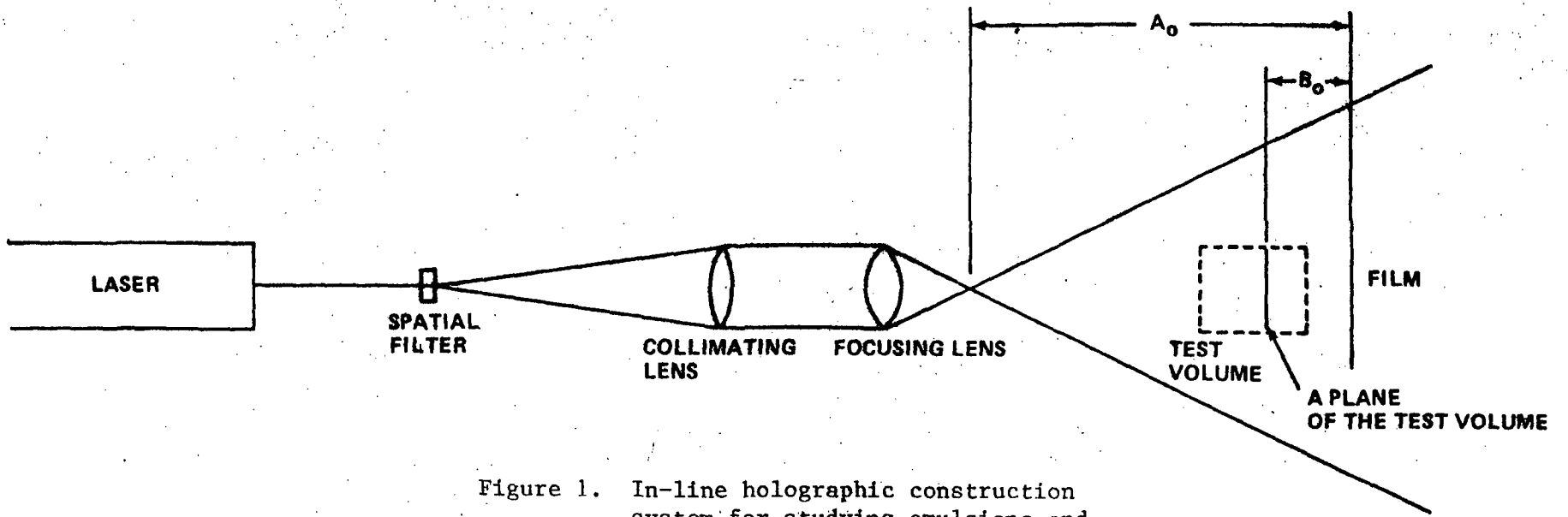


Figure 1. In-line holographic construction system for studying emulsions and dispersions.

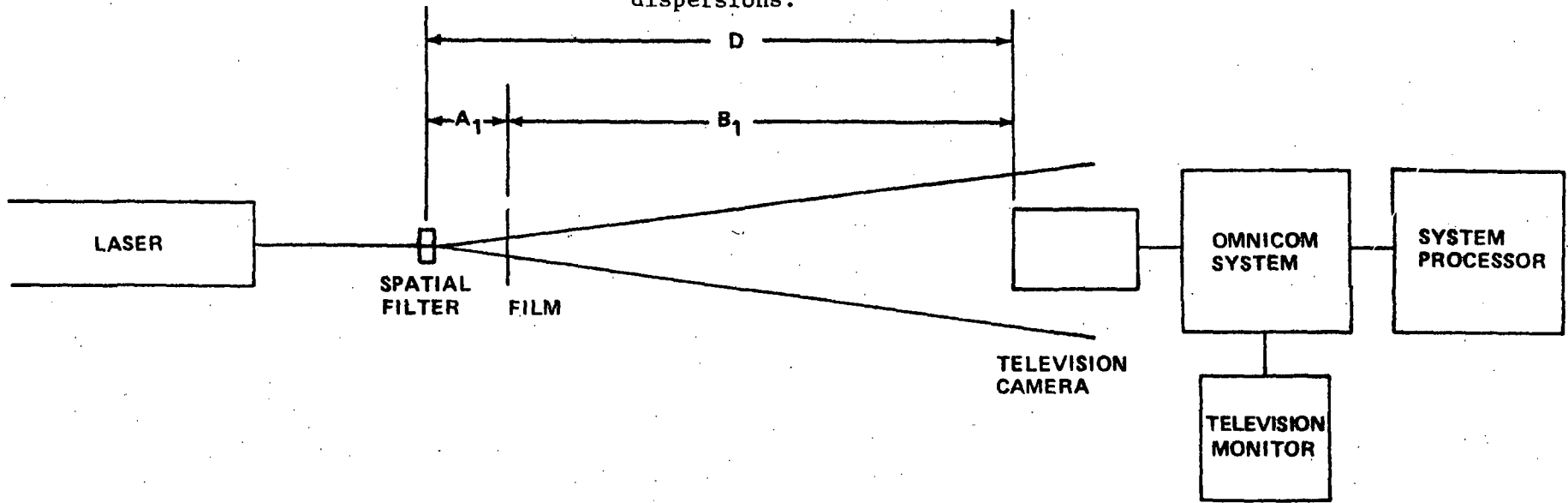


Figure 2. Holographic reconstruction and Omnicon particle analysis system.

ORIGINAL PAGE  
BLACK AND WHITE PHOTOGRAPH

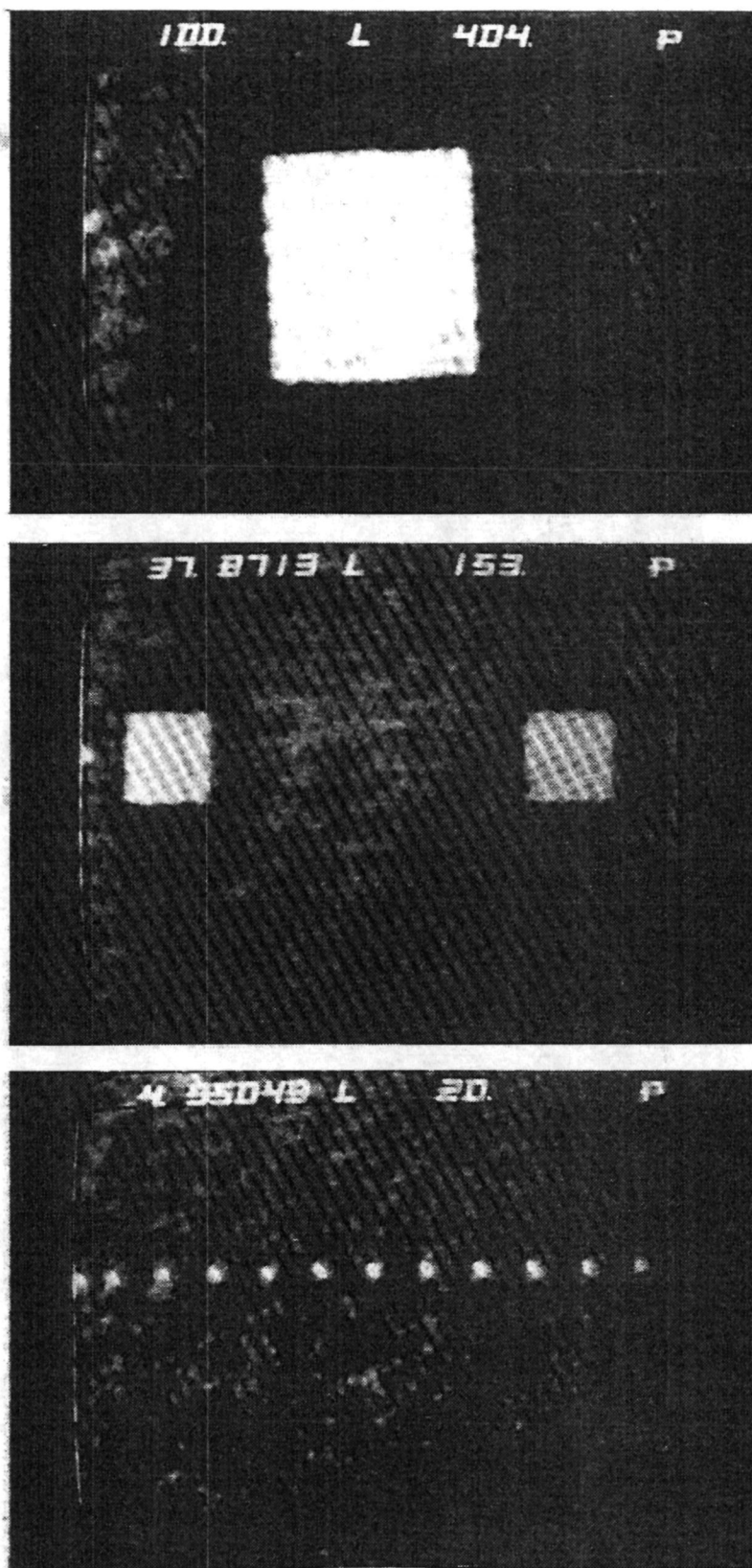


Figure 3. Calibration squares measured by Omnicon. The true particle sizes are (a)  $100\mu\text{m}$ , (b)  $37.5\mu\text{m}$ , (c)  $5\mu\text{m}$ . The measured particle sizes are displayed in the upper left hand corner.

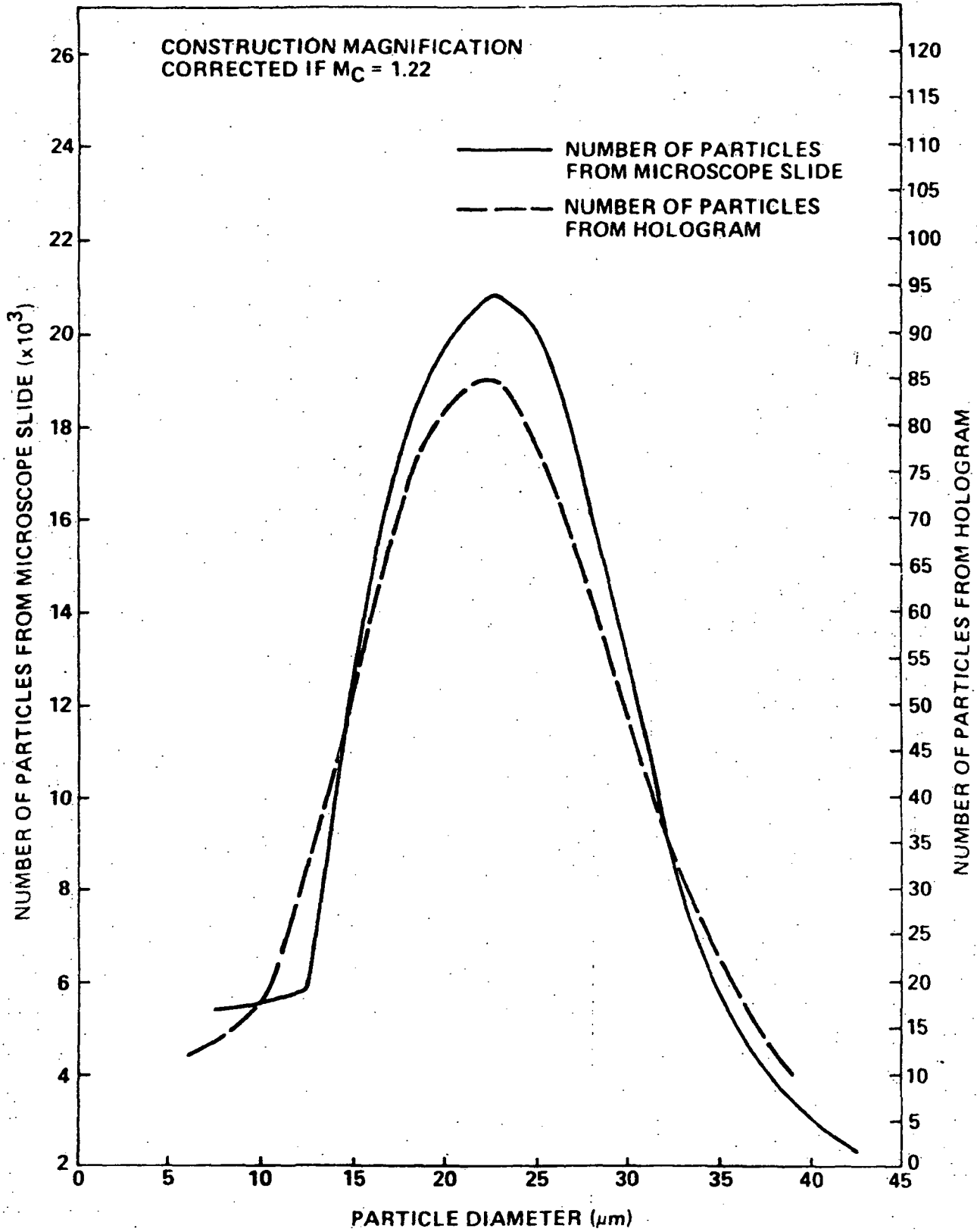


Figure 4. Comparison of measured particle distribution using ordinary microscopy of the particles placed on glass slides and holograms of the particles dispersed in clear oil.

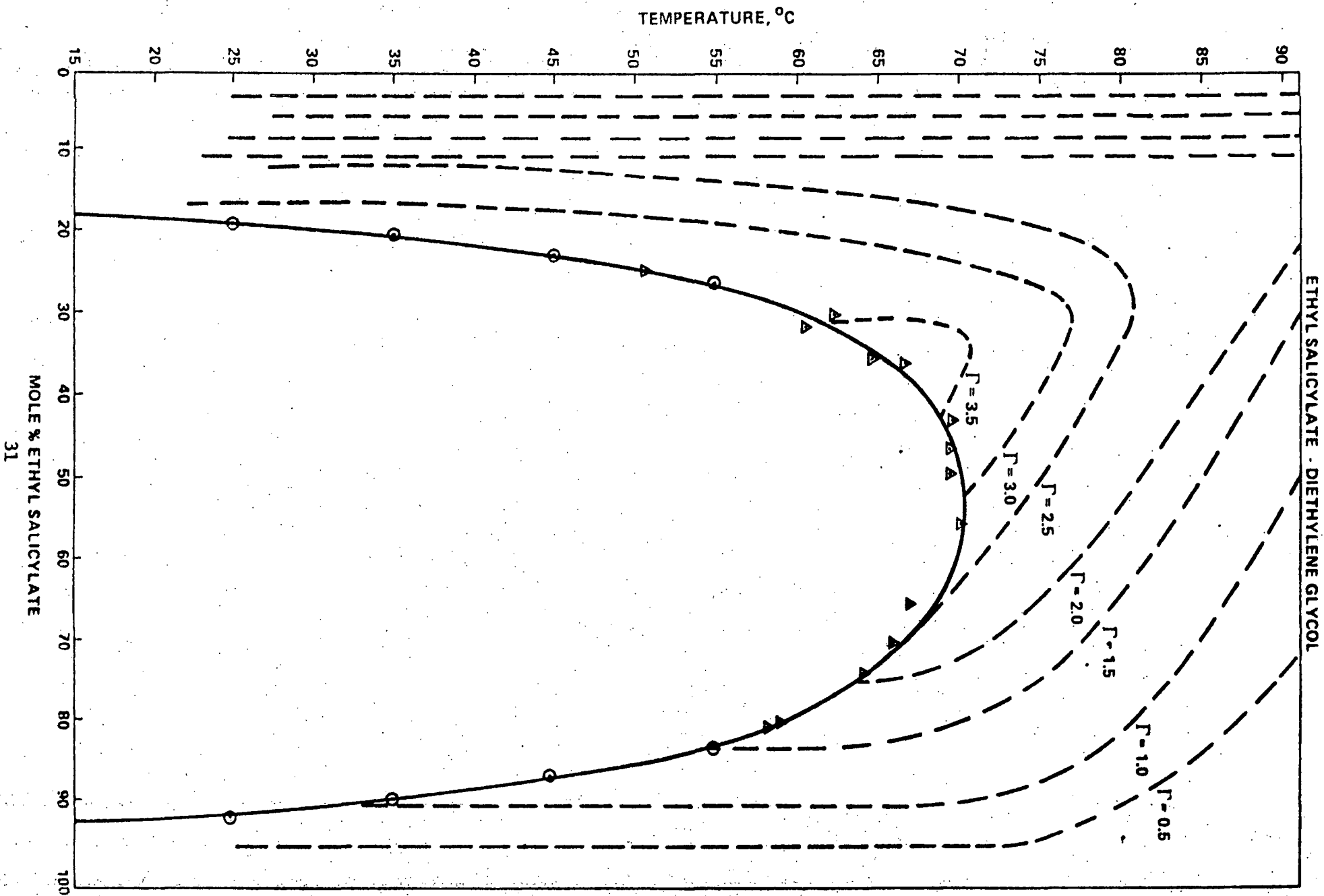


Figure 5. Phase diagram and surface activity in the ethyl salicylate-diethylene glycol system. Cosorption lines represent surface excess  $\Gamma^{(G)}$  OF ethyl salicylate ( $\times 10^{10}$  moles/cm<sup>2</sup>).

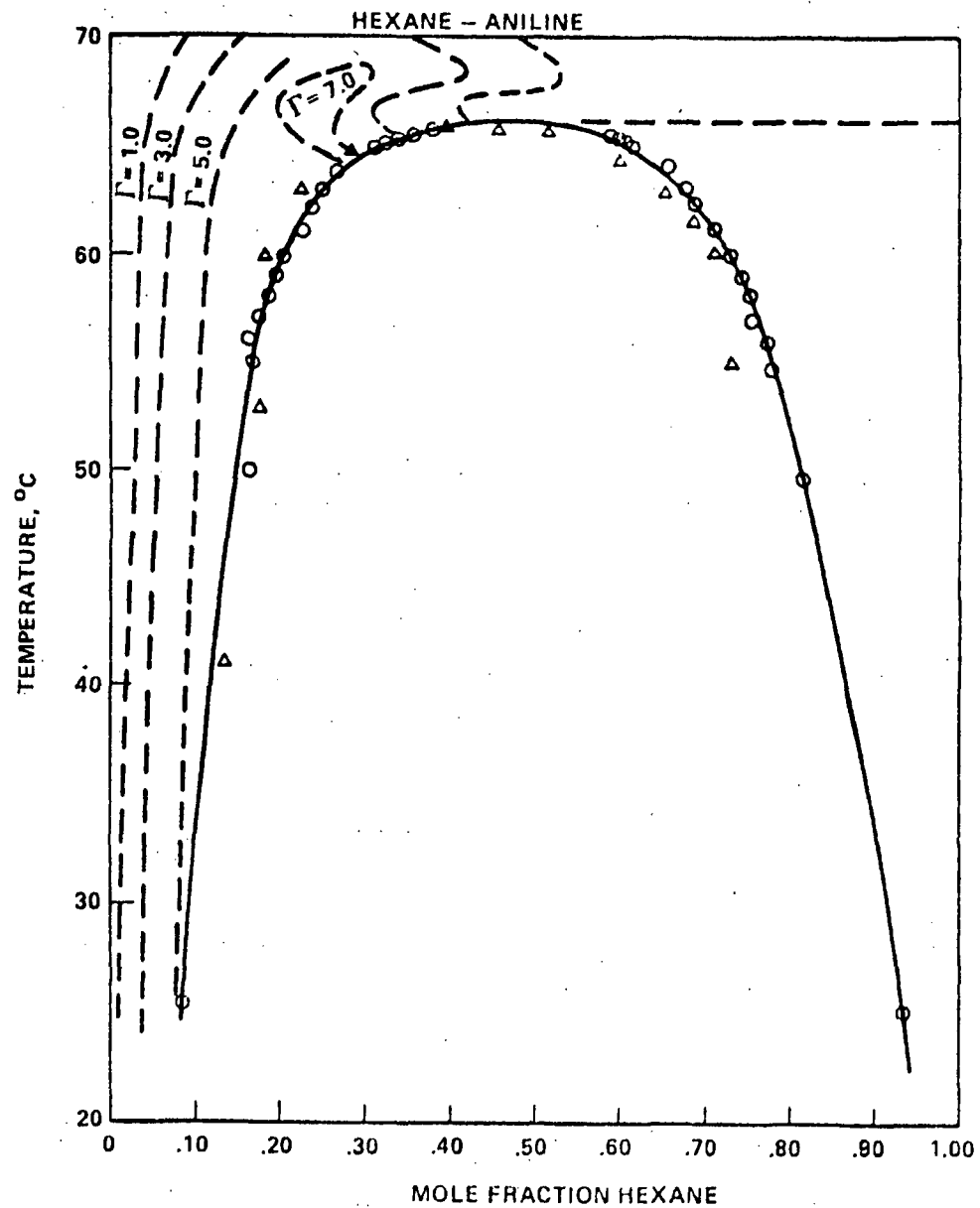


Figure 6

Phase diagram and surface activity in the hexane-aniline system. Cosorption lines represent surface excess  $\Gamma(G)$  of hexane ( $\times 10^{10}$  moles/cm<sup>2</sup>).

ORIGINAL PAGE IS  
OF POOR QUALITY

ORIGINAL PAGE IS  
OF POOR QUALITY

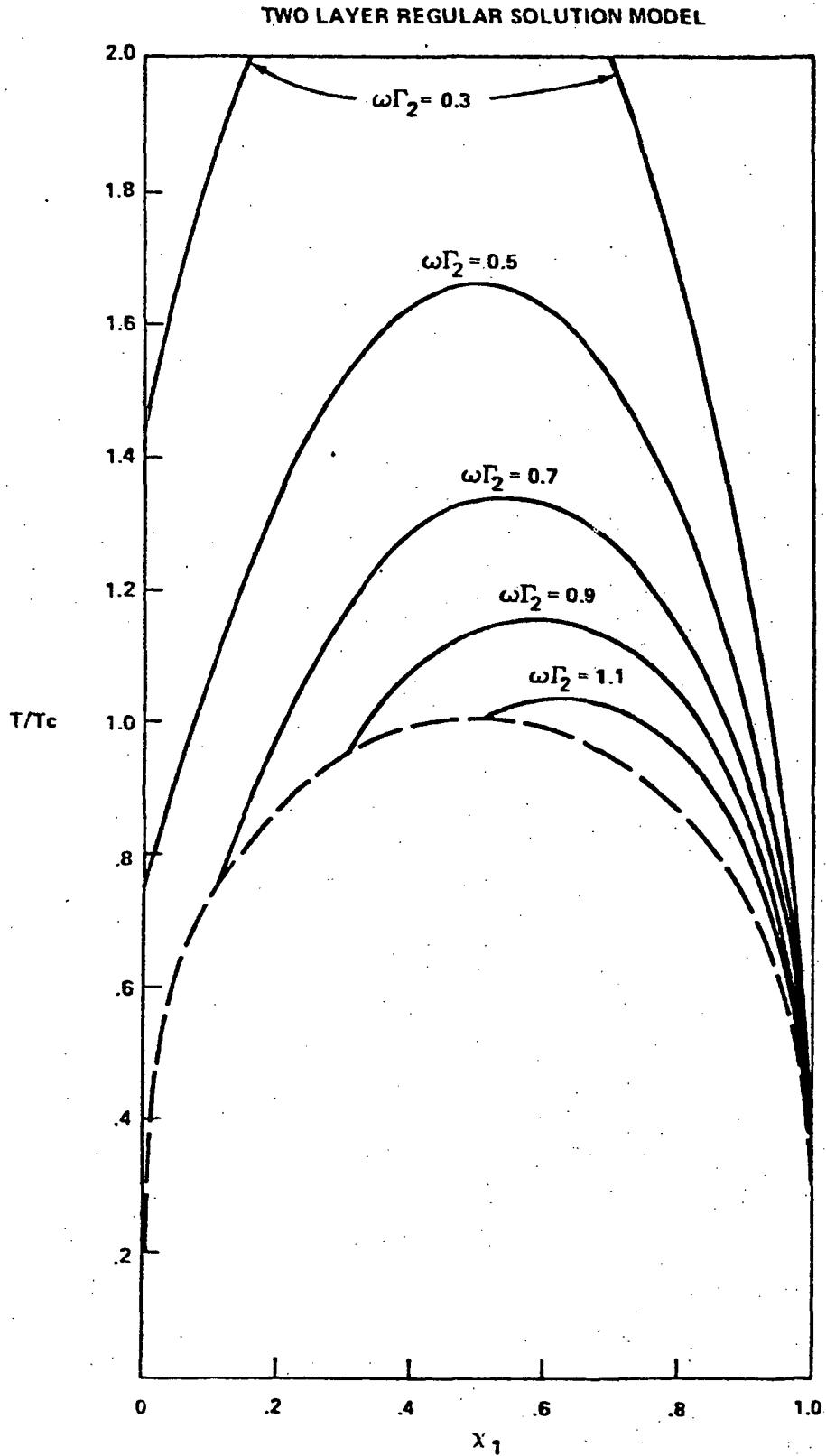


Figure 7. Phase diagram and surface activity for a two layer regular solution. Component 1 has the higher surface tension.

ORIGINAL PAGE IS  
OF POOR QUALITY

References

- [1] G.H. Otto and L.L. Lacy, Proceedings of the Third Space Processing Symposium on Skylab Results, vol 12, NASA TMX-70253 (1974); p. 1031.
- [2] L.L. Lacy and G.H. Otto, AIAA Journal 13, 219 (1975).
- [3] L.L. Lacy and G.H. Otto, Materials Sciences in Space with Applications to Space Processing, ed. L. Steg, pp. 495-507, AIAA Progress in Astronautics and Aeronautics, vol 52 (1977).
- [4] L.L. Lacy and C.Y. Ang, Apollo-Soyuz Test Project Summary Sciences Report, vol I, NASA SP-412 (1977).
- [5] S.H. Gelles and A.J. Markworth, Space Processing Applications Rocket Project, SPAR II Final Report, p. VI-1, NASA TMX-78125 (1977).
- [6] S.C. Hardy, J. of Colloid and Interface Sci. 69, 157 (1979).
- [7] A.W. Frances, Adv. Chem. Sci., no 31 (1961).
- [8] L.L. Lacy, S. Ross and G. Nishioka "Nucleation and Growth of Immiscible Phases" Investigation Proposal submitted to NASA in response to Announcement of Opportunity AO-77-3 (1977).
- [9] L.L. Lacy, G. Nishioka and B. Facemire "Studies of Model Immiscible System" Investigation Proposal submitted by NASA in response to Application Notice AN: OSTA-78-A (1978).
- [10] B.A. Silverman, B.J. Thompson and J.H. Ward, J. of Applied Meteorology 3, 792 (1967).
- [11] J.A. Blodgett, R.J. Schaefer and M.E. Glickman, Metallography 1, 753 (1977).
- [12] W.K. Witherow, J. Society of Photo Optical Inst. Eng. 18, 249 (1979).
- [13] S. Ross and G. Nishioka, J. Phys. Chem. 79, 1561 (1975).
- [14] S. Ross and G. Nishioka in "Foams, An International Conference" Brunel V., September 1975 (Butterworth 1976) p. 15-30.
- [15] L.A. Kochanova, et.al., Colloid J. of the USSR 779 (1973).
- [16] A.N. Campbell, et.al., Can. J. Chem. 46, 2399 (1968).
- [17] A.N. Campbell and E.M. Kartzmark, Can. J. Chem. 45, 2433 (1967).
- [18] R. Defay and I. Prigogine, Trans. Far. Soc. 46, 199 (1950).
- [19] R. Defay, et.al., "Surface Tension and Adsorption" Wiley, New York, (1966), chapter 12.
- [20] J. Cahn, J. Chem. Phys. 66, 3667 (1977).

24  
34  
N82 32062

## Measurement of Surface Velocity Fields

J. Adin Mann, Jr.  
Dept. of Chemical Engineering  
Case Western Reserve University  
Cleveland, Ohio 44106

Several preliminary remarks may be helpful before describing briefly a new technique for measuring surface velocity fields. All will appreciate that non-zero velocity fields at a free surface can be caused by bulk flows coupling to the surface. It is less well appreciated that surface velocity fields can be generated by other mechanisms so that bulk flows will result. In this case surface tension gradients provide the driving force for the velocity fields. Surface curvature can complicate the measurement as well as the calculation of velocity fields from first principles.

So far as we can determine  $\nabla\sigma$  ( $\sigma$  is the surface tension or perhaps the surface tension tensor) is zero for 1 component systems kept at constant temperature. Since  $\sigma$  depends on temperature, a temperature gradient parallel to the surface will generally cause the development of a surface velocity field. Those trained in fluid mechanics tend to emphasize the effects of temperature gradients on surface flows.

The surface tension or interfacial tension of most any liquid-fluid system depends on composition in ways that are often very sensitive to concentration levels of certain components called surfactants. Long chain fatty acids, alcohols, amines and "soaps" in general are very effective in producing large excesses of these components at the surface. As a result the surface tension lowers. At equilibrium, the "Gibbs equation" holds

$$\Gamma = -\frac{1}{kT} \frac{\partial\sigma}{\partial \log c}$$

where  $\Gamma$  is the surface excess (sometimes takes in units of molecules/cm<sup>2</sup>),  $k$  is the Boltzmann constant and  $c$  the bulk concentration level of the surface active agent. From a molecular viewpoint,  $\Gamma$  is an excess defined across a sharp surface by the integral

$$\Gamma = \int_{-\infty}^{+\infty} (\rho(z) - \rho^{\pm}) dz$$

where  $z$  is taken along the normal to the interface and  $\rho^{\pm}$  is the density of the fluid far into the fluid on either side of a "dividing surface" and  $\rho(z)$  the local density through the interface. A discussion of important details such as the choice of the surface is not appropriate here.

For most systems far from the critical temperature, the distance over which  $(\rho(z) - \rho^{\pm}) \neq 0$  holds is of molecular dimensions, viz. ca 10 Å - 40 Å. This characteristic range of thickness is that which surface chemists usually think about in studies of adsorption and desorption and catalysis as well as surface flows. Other characteristic distances are often involved depending on the nature of the flows being analyzed. Unfortunately this can be misleading.

A striking example where intuition may lead to serious error occurs when certain surfactant molecules are allowed to spread at the air-water interface. A close packed monolayer of a long chain fatty acid will have  $\Gamma \sim 5 \times 10^{14}$  molecules/cm<sup>2</sup>. Since such materials are relatively insoluble in the substrate the concentration amounts to about 10<sup>-9</sup> molar which is a very dilute solution. However, the surface tension will have gone from about 72 mN/m for pure water to less than 30 mN/m. Further since the "Gibbs elasticity"  $-\Gamma \frac{\partial \sigma}{\partial \Gamma}$  is large, there can be large surface tension gradients with only small dilations,  $\frac{\sigma - \sigma_0}{\sigma_0}$ .

These fundamental notions from the field of surface chemistry<sup>1</sup> can be easily demonstrated. Partially fill a petri dish with water, sprinkle a small amount of clean, dry talcum powder over the surface and then touch the tip of your finger

to the surface of the water. A monolayer will start to spread on the surface pushing the talcum away from the finger. The effect is rapid and obviously involves substantial surface tension gradients.

Since such a small amount of material can cause substantial surface flows, it is obvious that contamination will be an important factor to control whenever such flows are important. This factor should be kept in mind when developing designs for the floating zone process in zero gravity. Unfortunately, it may well be that surface contamination factors are not well enough controlled in many crystal growth situations. For example, note well that so called "deionized distilled water" can be sufficiently contaminated with amine surfactants so as to lower  $\sigma$  by a few mN/m and develop a non-trivial excess at the surface.<sup>1</sup>

The velocity fields confined to the surface can be measured by techniques that are rather similar to them used for bulk measurements. For example, seed particles can be floated at the air-water interface that will provide trajectories from which the velocity field can be determined at least approximately. Laser doppler methods can be used. However, the particles are large compared to the thickness of the interfacial region so that bulk effects are averaged in with the surface fields. This may be satisfactory depending on the characteristic length scales.

My group is developing new methodology based on the fluctuations intrinsic to any fluid surface. Even at equilibrium, liquid systems are agitated on the microscale as molecules move and collide on very short time scales ( $10^{-14}$  sec or less). The effects of these collisions average in cooperative ways producing small amplitude fluctuations observable on a liquid-fluid surface in macroscopic time and length scales by various techniques. The appropriate measurements can be made by various scattering methods<sup>2</sup> including laser light scattering spectroscopy.

Surface fluctuations develop into either propagating or non-propagating waves of very small amplitude. The situation can be modeled accurately by the conventional methods of hydrodynamics. The theory is too long and complicated to discuss here<sup>3</sup> other than to point out a starting place.

The surface elevation from a fixed plane is taken to be a summation of decoupled, harmonic surface waves

$$\zeta(\vec{x}^s, t) = \sum_{\vec{q}} A(\vec{q}) e^{i(\vec{q} \cdot \vec{x}^s - \hat{\omega}_{\vec{q}} t)}$$

where  $\vec{q}$  is the surface wave number, and  $\hat{\omega}_{\vec{q}} (= \omega'_{\vec{q}} + i\omega''_{\vec{q}})$  is the complex frequency. The light scattering technique picks out a particular  $\vec{q}$  for analysis so that the spectrum (or the equivalent autocorrelation function) of the surface waves is determined. The spectrum can be analyzed to produce the frequency ( $\omega'_{\vec{q}}$ ) and damping factor ( $\omega''_{\vec{q}}$ ) associated with waves characterized by the wave number  $\vec{q}$ . The wave number,  $q$ , is  $\frac{2\pi}{\lambda_{rip}} \hat{e}$  where  $\lambda_{rip}$  is the wave length of the surface waves and  $\hat{e}$  the direction of propagation. Light scattering techniques allow one to select both  $\lambda_{rip}$  and  $\hat{e}$ .

The sensitivity of the light scattering measurement to surface profile fluctuations is incredible in that  $\sqrt{\langle A(\vec{q}) A(\vec{q}) \rangle}$  is on the order of  $1 \text{ \AA} (10^{-8} \text{ cm})$  for a good signal/noise ratio to obtain.

The dispersion relations ( $\hat{\omega}_{\vec{q}} = \hat{\omega}_{\vec{q}}(\vec{q}, \dots)$ ) required for analysis are generated from the hydrodynamical field equations by a rather tedious calculation<sup>4</sup> when all of the details of the surface response is included. I note only that  $|A(\vec{q})|/\lambda_{rip}$  ratios are always small enough so that all of the field equations can be linearized; linear response function techniques can be applied easily. When the viscosity of the medium is zero, the dispersion equation is simply

ORIGINAL PAGE IS  
OF POOR QUALITY

$$\frac{\rho \omega'^2}{\sigma q^3} = 1 \quad (1)$$

with  $\omega'' = 0$ .

In a typical light scattering experiment,  $100 \text{ cm}^{-1} < q < 2000 \text{ cm}^{-1}$  so that  $\omega' \sim 500 \text{ kHz}$  (Note  $\omega' = 2\pi\nu$ ). This is a convenient frequency range for measurement. Further, the scattering region only needs to be large enough so that the required averages can be done properly. A careful design of the lens system used to focus light onto the surface does allow spacial discrimination ranging from ca  $50 \mu\text{m}$  as the minimum characteristic distance. In fact, we have designed such a system in order to determine local values of  $\sigma$  and the velocity fields over a fluid surface of about  $100 \text{ cm}^2$  area. With the incident beam focused on a given location in the surface, the scattered light is analyzed for  $\hat{\omega}$  from which the local  $\sigma$  and the velocity information can be determined. The geometrical factors can be controlled experimentally so that  $\vec{q}$  is specified and not just  $|\vec{q}|$ . As a result, velocity information is available and not just the speed.

The model invoked so as to determine the surface velocity includes the substrate velocity field as a part of the potential function used in solving the relevant field equations:  $\phi = -Ux + \phi'$  where  $U$  is the speed of the fluid flow in direction  $x$  and  $x$  is the direction of wave propagation. The jump conditions at the surface,  $\Sigma$ , include

$$\frac{\partial \zeta}{\partial t} + U \frac{\partial \zeta}{\partial x^s} = - \left. \frac{\partial \phi}{\partial z} \right|_{\Sigma} + \left. \frac{\partial \Psi}{\partial x} \right|_{\Sigma}$$

where  $\Psi$  is the stream function. The resulting dispersion equation is of the form

$$f(q, \omega', \omega'', \sigma, U, \dots) = 0$$

where  $q = |\vec{q}|$  and  $\dots$  implies that there are other parameters that must

be included (viscosity, etc.). The experiment can be run for different  $q$  values so that it is possible to determine both  $\sigma$  and  $U$  independently. Clearly it will be more convenient to know  $\sigma$  by an independent experiment so that only  $U$  need be determined during one observation.

Work is in progress directed toward the development of an apparatus to measure this surface laser doppler velocity (SLDV) effect quantitatively. The first experiments will be done in collaboration with Dr. Fowle (Arthur D. Little) who has developed an apparatus for the study of temperature gradient effects in thin liquid films. We will attempt to resolve in time and space velocity fields on the slowly flowing surfaces of pure liquids (water, mercury, etc.) using our SLDV techniques. If our estimations of precision, accuracy and discrimination are verified, we will design a SLDV system for the float zone experiment that we hope will be flown in about five years.

It is also possible to generate waves on the surface of a liquid. The methodology has been developed by a number of workers<sup>3</sup> so that  $\omega$  is fixed and  $\hat{q}$  ( $= q' + iq''$ ) is determined very accurately. This approach can also be used to determine  $\sigma$  and  $U$  and the sensitivity, precision and accuracy will be of a higher order than that obtained by the use of fluctuations as described in this paper. Unfortunately, the use of wave generators provides a complication that makes the simplicity of the light scattering method very attractive. Nevertheless, we are experimenting with new pulsing techniques that may lead to a superior instrument for determining velocity fields on the surface of a liquid.

#### Summary

I have emphasized the need to consider the effects of very small concentrations of impurities on the surface properties of liquids. I have described a new methodology for determining the surface velocity vector

as a function of location and time by the analysis of thermal fluctuations of the surface profile in a small domain around the point of interest. These fluctuations turn out to be waves so that the method amounts to the analysis of the local phase and group velocities of the waves as modified by a flow field. The apparatus now being constructed will be used in a series of experiments involving flow fields established by temperature gradients imposed along a surface. The SLDV methodology is difficult at this stage of development and may turn out to be impractical if the expected signal to noise ratio of the spectrum is not observed. With this in mind we are experimenting with driven wave arrangements that will provide the appropriate information but with a more awkward experimental arrangement.

#### References

1. Adamson, A.W., "Physical Chemistry of Surfaces," (3rd ed.), Wiley-Interscience (1977). Also see Hiemenz, P.C., "Principles of Colloid and Surface Chemistry," Marcel Dekker, Inc., New York (1977).
2. Chen, S. and Yip, S., "Spectroscopy in Biology and Chemistry: Neutron, X-Ray, Laser," Academic Press, Inc., New York (1974). Also see Chu, B., "Laser Light Scattering," Academic Press, New York (1974).
3. Mann, J.A., Porzio, K., "Capillarity: The Physical Nature of Fluid-Fluid Interfaces Including the Problem of Biomembrane Structure," in "International Review of Science: Surface Chemistry and Colloids," Physical Chemistry Series Two, Volume 7, ed. by Kerker, M., Butterworths, London (1975).
4. Hansen, R.S. and Mann, J.A., J. Appl. Phys. 35, 158 (1964).

## SURFACE TENSION DRIVEN CONVECTION

Simon Ostrach<sup>(a)</sup>

In a normal gravitational environment, the free surface of a liquid in a container plays a passive role in the transport processes. However, at microgravity, the free surface can become the dominant factor. A simple but meaningful spaceflight experiment is proposed to investigate the nature and extent of flows induced by surface-tension gradients along the free surface. The influences of container geometry, wettability, contamination, and imposed heating modes will be investigated.

---

<sup>(a)</sup> Department of Mechanical and Aerospace Engineering, Case Western Reserve University

SURFACE TENSION DRIVEN CONVECTION

by

Simon Ostrach<sup>(a)</sup>

INTRODUCTION

At reduced gravity, surface-tension gradients on the free surface of liquids or molten metals become a dominant driving force for fluid flows. The nature and extent of such flows over ranges of conditions must be known both for the intrinsic scientific interest and for possible technological applications as, for example, in the containerless processing of the materials.

Theoretical analysis of such problems are extremely complex because the surface shape must be determined from the solution and the boundary conditions are not well defined. (The contact angle and its variation are not well known.) Furthermore, complete ground-based simulation is not possible because the interface shape and damping on earth are different from what they would be in a micro-gravity environment. Also, it is not possible to achieve the proper parametric ranges on earth. Thus, spaceflight experiments are required.

STATE OF EXISTING KNOWLEDGE

The distinction among physical mechanisms involved in such flows is unclear. For example, there exist two distinct basic modes of flow depending on whether the temperature and/or concentration gradients are along or normal to the free surface. Although this was indicated by Scriven (Proc. Internat'l Colloquim on Drops and Bubbles, Vol. 1, Caltech & TPL, Aug. 1974), the major emphasis has been placed on the latter configuration. Furthermore, the relevant dimensionless parameters are either incomplete or misunderstood. It is

---

<sup>(a)</sup>Department of Mechanical and Aerospace Engineering, Case Western Reserve University, Cleveland, Ohio 44106

essential that these be explicitly known in order to make proper simplification of analyses, appropriate experimental simulations, the number of experiments minimal, and meaningful data correlations.

The existing analyses are based on ad hoc models in which there are inconsistent assumptions, the configurations are overly idealized and the boundary conditions are inappropriate in that surface shapes and temperatures are specified. Furthermore, the studies deal with restricted ranges of the parameters. Surface-tension gradient driven flows involve the solution of free-boundary problems, and therefore, the position and shape of the interface cannot be specified a priori but must emerge as part of the solution. Likewise, the surface-temperature distribution cannot be specified.

#### PROBLEM DESCRIPTION

The configuration to be studied is shown in Fig. 1. A liquid in a container will be subjected to a temperature variation along its free surface. Flow patterns, velocity and temperature profiles, free surface shapes, and transient phenomena will be observed and measured. The effects on those quantities of different heating modes (e.g., radiant or side wall), initial interface shape (contact angle), fluid properties, container shape, and liquid volume (aspect ratio) will be investigated.

#### PROGRAM BACKGROUND AND STRUCTURE

This experimental program was first proposed in 1974 to the Physics and Chemistry Experiments Working Group (PACE) where it was reviewed by a committee of scientists who strongly recommended such experiments. Funding for analytical and experimental justification of the program was given by OAST under the direction of PACE for 1975-76. A survey of the state of the art and some exploratory drop-tower experiments were made and that work received a peer review. In

1977-79 feasibility studies were funded. During that period, theoretical modeling and analysis and laboratory tests were done.

### RESULTS OF GROUND-BASED RESEARCH

#### Theoretical

Since no general and formal derivation of the relevant dimensionless parameters was available, such a derivation was made (Ref. 1 and 2). It was found that the flow depends on a surface-tension Reynolds number  $R\sigma = \sigma_T \Delta T h / \mu \nu$ , the relative effects of buoyancy to surface tension is given by a dynamic Bond number,  $Bo = \rho \beta g L^2 / \sigma_T$ , and the transport depends on the Marangoni number,  $Ma = Pr R\sigma$  where  $\sigma_T$  is the change of surface tension with temperature,  $\Delta T$  is the imposed temperature difference,  $h$  and  $L$  are characteristic lengths,  $\mu$  and  $\nu$  are the absolute and kinematic viscosities, respectively,  $\rho$  is the fluid density,  $\beta$  the volumetric expansion coefficient,  $g$  the acceleration of gravity, and  $Pr$  is the Prandtl number.

An analysis was made of the developing flow in a thin layer due to various imposed bell-shape surface temperature distributions. No ad hoc assumptions were made and the proper basic equations were obtained by formal ordering procedures. It was found that for a short time interval the free surface remains flat and the velocity monotonically approaches the Couette profile. Thereafter, the surface shape changes with time. The flow undergoes a development which results in a secondary cell and fluid recirculation. The nature and extent of such flows depend on the imposed surface temperature distribution. The results are given in Ref. 3.

An attempt was made in the laboratory to induce surface-tension driven flows in deep water layers by heating the surface from above so that a stabilizing temperature gradient would reduce buoyancy effects. This is contrary to

LABORATORY TEST APPARATUS

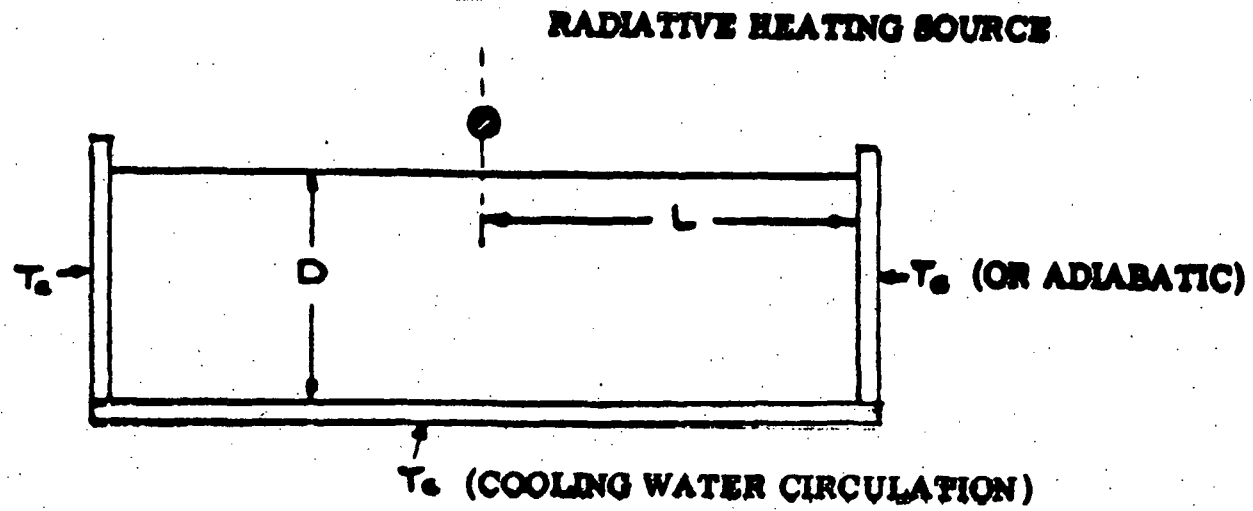


FIGURE 1

ORIGINAL PAGE IS  
OF POOR QUALITY

the usual concept that such flows could only be achieved in thin layers. The test indicated that the new concept is valid but surface contamination obviated any quantitative data. Therefore, liquids other than water will be used in subsequent tests.

A series of tests was conducted in the NASA Lewis Research Center drop tower in which reduced-gravity conditions prevailed for about 5 seconds. The objectives of these tests were to generate flows driven by surface-tension gradients, to establish the time required for steady flow, and to obtain some qualitative measure of the flow. It was found that surface-tension gradients at micro-gravity cause measurable transient flows to occur. Surface velocities as large as 3 cm/sec were experimentally observed. The results of this phase of the research program are presented in Ref. 4.

#### SPACELAB RESEARCH PROGRAM OBJECTIVES

The experimental apparatus will be similar to that used in the laboratory and the schematic set-up is shown in Fig. 2. The aspects to be investigated in the spacecraft are:

- (a) The extent and nature of the flows
- (b) The effects of container material (wettability, contact angles)
- (c) Configuration effects (circular and rectangular)
- (d) Heating rate and distribution (surface or sidewalls)
- (e) Effects of surface absorption on thermocapillary flows (contamination)
- (f) Stability criteria (turbulence, secondary flows)

#### SPACELAB EXPERIMENT REQUIREMENTS

##### 1. Measurements:

Free-surface shapes

**SPACELAB APPARATUS**

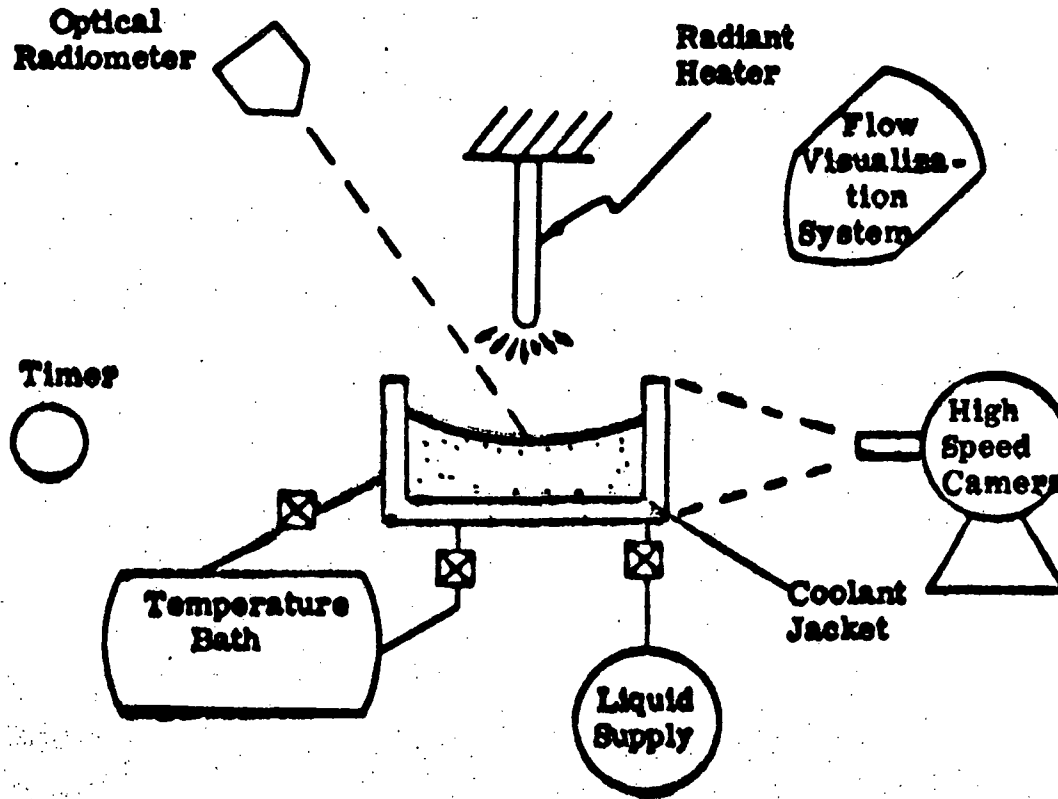


FIGURE 2

Fluid velocity and flow visualization (accuracy  $\pm 10\%$ ; velocity range 0-2 cm/sec)

Temperature (thermocouple accuracy  $\pm 0.1^{\circ}\text{C}$ , radiation thermometer accuracy  $\pm 0.5^{\circ}\text{C}$ )

2. Spacelab Support:

Environment (1 atm,  $20^{\circ}\text{C}$ )

Power (200w)

SUMMARY

The objectives of the research program are to determine the basic fluid mechanics and heat transfer phenomena of reduced-gravity surface-tension gradient driven convection. Analytical and experimental bases for this research have been established and considerable feasibility work has been conducted. The proposed experiment is simple to conduct and the measurement techniques are essentially state of the art.

## REFERENCES

- (1) Ostrach, S., Motion Induced by Capillarity, Physicochemical Hydrodynamics, Advance Publications Ltd., Vol. 1, 1977.
- (2) Ostrach, S., Convection Due to Surface Tension Gradients, Proc. COSPAR Space Research, Vol. VIII, Innsbruck, Austria, 1978.
- (3) Pimputkar, S. M. and Ostrach, S., Transient Thermocapillary Flow in Thin Liquid Layers, Presented at the 31st Meeting of the American Physical Society, 1978 (to be published in Physics of Fluids).
- (4) Ostrach, S. and Pradhan, A., Surface-Tension Induced Convection at Reduced Gravity, AIAA Jour., Vol. 16, No. 5, May 1978.

## DEPLOYMENT OF SOLID PARTICLES ON LIQUID DROPLET SURFACES

by

Anthony M. Schwartz<sup>(a)</sup>

Attachment of solid particles to suspended liquid droplets is of practical importance in operations such as dust abatement in coal mines and stack gas purification. The number and total mass of particles that can be stably accommodated on the surface of a single fixed size droplet depends on the size and shape of each particle and on the equilibrium contact angle of the system. Except for trivially simple values of these parameters the accommodation cannot be calculated. The proposed experiment consists in suspending a sizeable drop of liquid; then sequentially touching to its surface solid particles of various well-defined and commonly encountered shapes, sizes and contact angles. The positions they assume, influenced solely by the system's surface forces, will be recorded and systematized. The first liquid used will be pure water. Aqueous solutions and other liquids of varying surface and rheological properties will also be used. The empirical data so derived will be of inductive theoretical value as well as immediately applicable practical value.

---

<sup>(a)</sup>Consultant in Chemistry

The Migration of Fluid Droplets and Their Interactions  
in a Thermal Gradient

R. S. Subramanian\* and W. R. Wilcox

Department of Chemical Engineering

Clarkson College of Technology

Potsdam, New York 13676

When materials are processed in free fall, buoyant forces will be substantially reduced. Thus, the buoyant migration of droplets and bubbles which normally occurs on earth is expected to be overshadowed by migration due to other mechanisms in space processing. In particular, capillary forces on droplets due to the variation of interfacial tension around their periphery will play a significant role in governing their motion in space. While such interfacial tension gradients can be caused by thermal, compositional, and/or electrical gradients in the continuous phase, thermal gradients are convenient to use in controlled experimentation. On earth, due to interference from buoyant effects, it is difficult to study thermocapillary migration in sufficient detail. Also, the effects of a thermal gradient on the interactions among droplets are hard to study on earth. Thus, an orbital facility for conducting experiments on the migration and interactions of fluid droplets in a continuous phase due to the action of a thermal gradient appears attractive.

\*Currently on sabbatical leave at Jet Propulsion Laboratory, Pasadena, CA 91103.

ORIGINAL PAGE IS  
OF POOR QUALITY

The Migration of Fluid Droplets and Their Interactions  
in a Thermal Gradient

R. S. Subramanian\* and W. R. Wilcox

Department of Chemical Engineering

Clarkson College of Technology

Potsdam, New York 13676

In the space processing of materials, it is expected that many occasions will arise where liquid bodies containing droplets of a second fluid (liquid or gaseous) will be encountered. An example would be in the manufacture of space-processed glasses. In the glass production process, gas bubbles are formed due to chemical reactions as well as from gaseous pockets trapped in the interstitial spaces in the grains of the raw material. These bubbles have to be eliminated to produce usable glasses. Due to the reduction of the buoyant effect in orbiting spacecraft, the usual buoyant migration of such droplets or bubbles observed on earth will be reduced correspondingly, and their movement due to other forces will become important. Such movement will also have a significant effect on heat/mass transfer from/or to the droplet phase, and therefore needs to be characterized. It also is anticipated that in systems containing many droplets of a second phase, interactions among these droplets would be of great importance.

There are several mechanisms which would generate a force on a fluid droplet present in another fluid. There could be effects due to electric and magnetic fields. More subtle are the effects of a thermal or compositional gradient in the continuous phase. Such gradients on the droplet - fluid interface will usually result in interfacial tension gradients. An imbalance in the interfacial tension around the periphery of the droplet will result in traction being exerted on the neighboring fluids, the result of which is a net force on the droplet. The direction of this force is toward decreasing interfacial tension. Thus, gas bubbles in a temperature gradient in a pure single-component liquid will migrate toward the hot end in the absence of other forces.

The fact that thermal gradients can cause the motion of gas bubbles has been quite well-known, and is illustrated in a film on the role of "Surface Tension in Fluid Mechanics" by Trefethan. An experimental demonstration as well as an approximate theory were provided by Young et al. (1959). These investigators held a small quantity of silicone oil between the anvils of a micrometer in which the lower anvil surface could be heated to different temperatures. The resulting vertical gradient of temperature

\*currently on sabbatical at the Jet Propulsion Laboratory, Pasadena, CA 91103

exerted a force opposing the buoyant rise of gas bubbles in the column of silicone oil. By generating a sufficiently large thermal gradient in the liquid, Young et al. were able to arrest the buoyant motion of the bubbles and move them downward. They compared their experimental observations on the temperature gradient needed to keep a bubble stationary against buoyant forces with their theory, and noted reasonable agreement in spite of the scatter of the data. The thermocapillary force on a gas bubble in a thermal gradient was measured by McGrew et al. (1973) who used gas bubbles attached to a fine cantilever wire. Good agreement with the theory of Young et al. was found in ethanol while bubbles in methanol experienced a stronger force than that predicted by Young et al. This was attributed by McGrew et al. to the effects of volatilization and condensation at the opposite ends of the bubble. Recently, Hardy (1979) has performed careful experiments on bubble migration in a vertical temperature gradient. These experiments were conducted in a closed rectangular cell which eliminates the problems associated with the optical distortion through the cylindrical free liquid surface in the Young experiments. Perhaps more importantly, the absence of a free liquid surface avoids the thermocapillary convection which probably caused considerable scatter in the data of Young et al. Hardy's results for the vertical temperature gradient needed to arrest buoyant motion were in agreement with the theory of Young et al. The velocities observed were, however, somewhat lower than the theoretical predictions.

The types of experiments that can be performed on the migration of individual droplets or bubbles in a temperature gradient on earth are necessarily limited because of the presence of buoyant forces. The imposed thermal gradient has to be parallel or anti-parallel to the gravity vector. Any other thermal gradient (with a non-vanishing component in a direction normal to the gravity vector) always will result in buoyant convection in the fluid. This would strongly interfere with the interpretation of experimental data. Moreover, the theoretical problems of migration under the combined action of buoyancy and a temperature gradient in such situations becomes quite complex due to the loss of axisymmetry.

Even when a temperature gradient in the direction of the gravity vector is employed, there are severe constraints on the experiments that would be feasible on earth. If the temperature increases with height, the thermocapillary force would assist buoyancy and result in larger velocities, and hence, relatively small experiment durations. On the other hand, this situation usually results in a stable density gradient in the continuous phase far away from the droplet. It must be mentioned that in the vicinity of the droplet, lateral gradients of temperature cannot be avoided even though the fluid far away from the droplet is stably stratified. Because of the resulting lateral density gradients, it would be difficult to avoid buoyant convection contributions in the vicinity of the droplet.

The other alternative which still preserves axisymmetry and permits longer experimental times is the one used by Young et al. (1959) and by Hardy (1979). In these systems, the temperature decreases with height resulting in a thermocapillary force which opposes buoyancy. Thus, situations where

droplets/bubbles are slowed down in their rise, and even stopped and reversed can be achieved. However, in these experiments, there is an unfavorable density gradient in the continuous phase, and buoyant convection will set in when the Rayleigh number exceeds a critical value. Thus, there are severe upper bounds on the thickness of the fluid layer and the adverse temperature gradient which can be used since both of these quantities appear in the Rayleigh Number.

As indicated above, the presence of buoyant forces places serious constraints on the types of experiments that can be performed on earth on the migration of single bubbles or droplets in a thermal gradient. The problems are more severe when it is desired to study interactions between two or more such droplets in a thermal gradient on earth. Recent qualitative experiments (Mattox et al. 1978) indicate that such interactions may play a dramatic role in enhancing coalescence.

It would be desirable to have an orbital experimental facility available to study the motion of bubbles and/or droplets and their interactions in a continuous phase wherein a known thermal gradient can be imposed and maintained. While it is expected that compositional gradients in multicomponent systems will probably result in stronger capillarity-induced effects, a known steady thermal gradient can be established and maintained in a liquid with more ease than an analogous compositional gradient. The above facility would make it possible to study phenomena which are either difficult or impossible to study on earth. Due to the large reduction in buoyant forces, thermocapillary effects on larger droplets can be studied (without interference from buoyancy) than is possible on earth.

The experimental facility should provide for the convenient introduction of bubbles and/or droplets of various fluids of a variety of sizes in specific locations inside a continuous liquid phase. There should be arrangements for maintaining and measuring thermal gradients in the liquid. Also, provisions should be available for recording the positions and sizes of the bubbles and/or droplets through the duration of the experiments. It would also be desirable to be able to measure the temperature fields in the vicinity of the migrating droplets so that more detailed comparisons with theory can be made. It is quite possible that a specialized version of the "Fluids Experiment System" would be an appropriate apparatus for performing these experiments.

#### ACKNOWLEDGEMENT

This work was supported by contracts from  
the National Aeronautics and Space Administration.

ORIGINAL PAGE IS  
OF POOR QUALITY

References

1. Hardy, S.C., J. Colloid Interface Sci. 69, No. 1 157 (1979).
2. Mattox, D.M., Smith, H.D., Wilcox, W.R., and Subramanian, R.S., "The Migration of Bubbles in Molten Glass due to Thermal Gradients", presented at the American Ceramic Society Spring Meeting, Detroit, MI, May 1978.
3. McGrew, J.L., Rehm, T.L., and Griskey, R.G., Appl. Sci. Res. 29, 195 (1974).
4. Trefethan, L.M., "Surface Tension in Fluid Mechanics", a color film by Encyclopaedia Britannica Education Corporation.
5. Young, N.O., Goldstein, J.S., and Block, M.J., J. Fluid Mech. 6, 350 (1959).

SECRET  
NOV 1952

SECTION B  
CHEMICAL PROCESSES

ORIGINAL PAGE IS  
OF POOR QUALITY

Experimental Studies in Ostwald Ripening

G. C. Kuczynski

Dept. of Metallurgical Engineering and Materials Science

University of Notre Dame

Notre Dame, IN 46556

C. B. Alcock

Dept. of Metallurgy and Materials Science

University of Toronto

Toronto, Canada

Introduction

The phenomenon of coarsening of a dispersion of particles in a solid or liquid medium was first reported by Ostwald<sup>1</sup> in 1900. In this process the matter is transferred from small to large particles, reducing the free energy associated with the particle/matrix interface area. The process is controlled either by the rate of diffusion in the matrix or the rate of the reactions occurring at the interface. Theoretically it is a formidable problem, going deeply into physical meaning of the second law of thermodynamics and of assymetry of time. The attempts of predicting the steady state distribution function of particle sizes as a function of time was tackled by Lifshitz and Slyozov<sup>2</sup> and C. Wagner.<sup>3</sup> Their theories, usually called L.S.W. theory, arrive at essentially the same solution characterized by a sharp cutoff of the population densities at large particle radii. However, the experimental determinations yield the distribution functions with the exponential tails. Recently another theory based on the

fundamental principle of the minimum entropy production rate, predicts clearly this exponential tail. Therefore, from the purely fundamental point of view, it is important to test these theories experimentally.

The problem has practical importance as well. The degradation of the catalytic systems is one of the practical examples. Finely dispersed metallic particles on the oxide substrate lose their area very fast at the reaction temperatures, thus decreasing the catalyst activity.

In metallurgy the good examples are thoria dispersion-strengthened Ni/Cr alloys for jet aircraft applications. In ceramics, calcia stabilized zirconia is toughened by the presence of a dispersed phase of monoclinic zirconia. In these materials the coarsening of the dispersed phase through the disappearance of the small particles and the growth of the larger particles leads to a loss of the desirable properties.

### Experimental

The problem at hand is a fundamental one. What is the mechanism of Ostwald ripening? There were several attempts to determine the distribution function of particle size experimentally. Here we shall limit our discussion to two such attempts.

Footner and Alcock<sup>5</sup> studied the ripening of the ThO<sub>2</sub> particles in Ni/Cr alloys. The particles were of the order of 10 - 100 A and temperature of annealing, 1300°C. They observed the increase of the average particle size over 100 hours of heating. However, to measure the disperse phase particle size distribution required very laborious sample preparation and analysis using an electron microscope, a problem with all solid state studies. The final analysis of the results was

made ambiguous due to the strain fields at the particle/matrix interface. To avoid these difficulties, it was decided to measure the Ostwald ripening in a system in which the matrix was liquid, in this case NaCl - KCl lowest melting point composition with PbS particles as a dispersed phase.<sup>6</sup> The advantages of this dispersed phase system are that diffusion in the liquid matrix is very much more rapid than in the corresponding solid systems and hence, bigger particles could be employed. The matrix was transparent and thus dispersed phase, PbS particles, could in principle be studied during ripening. In addition the matrix was water soluble, and hence it could be easily separated from the insoluble PbS particles.

The studies showed reaction controlled growth, but the particle size distribution did not correspond with that predicted and commonly adopted L.S.W. theory.<sup>2,3</sup> There is a tail in the distribution at the large particle size end which is predicted by the Kuczynski theory.<sup>4</sup> Because of the non-negligible effects of sedimentation and coagulation which could lead to the observed "tail" in the distribution curve, it is not at present clear if the effect is real or not, and this, as we have seen above is fundamental to our understanding of the Ostwald ripening phenomenon. Thus, the solid-liquid or liquid-liquid systems, although very convenient from the experimental point of view and seemingly a most straightforward method to study the process, suffer from the effects of the gravitational field on the dispersed phase of the matrix. It does not seem to be easy to find a dispersed phase system in which dispersoid and matrix would have the same density.

It is now obvious that the experiments in the microgravity environment are at present the only ones which could lead us to the

solution of the problem, by practically eliminating the sedimentation and coagulation effects.

It is realized that in a space laboratory the power is at the premium; therefore, a convenient system NaCl - KCl - PbS which requires the temperatures in excess of 600°C is out of the question. However, there are numerous organic systems or aqueous salt solutions which can be experimented with near the room temperature. Because the dispersed particles do not have to be too small, the laser optical system developed at NASA could probably be used in this study to observe the particles in situ.

#### References

1. W. Ostwald Z. Phys. Chem 34 495 (1900)
2. I. M. Lifshitz and V. V. Slyozov. J. Phys. Chem Solids 19 35 (1961)
3. C. Wagner Z electrochem. 65 581 (1961)
4. G. C. Kuczynski to appear in Proc. 5th Int. Conference on Sintering and related Phenomena. Notre Dame June 1979
5. P. K. Footner and C. B. Alcock Met. Trans. 3 2633 (1972)
6. R. D. McKellar and C. B. Alcock "Sintering and Catalysis" Materials Sc. Res. Vol 10 Plenum Press. Ed. by G. C. Kuczuyski p. 409 (1975)

## FORMATION OF METALLIC AND METAL HYDROUS OXIDE DISPERSIONS

Egon Matijevic and R. S. Sapiieszko<sup>(a)</sup>

The formation, via hydrothermally induced precipitation from homogenous solution, of a variety of well-defined dispersions of metallic and hydrous metal in the conditions under which the particles are produced (e.g. pH and composition of the growth medium, aging temperature, rate of heating, or degree of agitation) can be readily discerned by following changes in the mass, composition, and morphology of the final solid phase. The generation of colloidal dispersions in the absence of gravity convection or sedimentation effects may result in the appearance of morphological modifications not previously observed in terrestrially formed hydrosols.

---

<sup>(a)</sup> Institute of Colloid and Surface Science and Department of Chemistry, Clarkson College of Technology

**ORIGINAL PAGE IS  
OF POOR QUALITY**

FORMATION OF METALLIC AND METAL HYDROUS OXIDE DISPERSIONS

by

Egon Matijevic<sup>1</sup> and R. S. Sapiieszko<sup>(a)</sup>

INTRODUCTION

Few families of inorganic compounds are as significant as metal (hydrous) oxides\*. These materials appear in nature as different minerals and ores and they are produced by hydrolytic corrosion of metals. In addition, metal hydrous oxides in various forms find numerous uses, such as pigments, catalysts, catalyst carriers, fillers, coatings, etc. Thus, it comes as no surprise that much work has been done on these compounds, both in terms of their preparation and characterization; nevertheless, relatively little is still known about the mechanism of formation of any of the metal oxides or hydroxides. This lack of knowledge is easily understood if one recognizes the complexity of the processes involved in the precipitation of such solids. For example, a minor change in pH can result in the formation of entirely different species in terms of chemical composition as well as of morphology. Equally important are the roles of other parameters, primarily of the temperature and of the nature of the anions in the solution in which the precipitation takes place. The latter can exercise a profound effect on the solid phase formed, even though the respective anions may not appear as constituent species of the precipitate. All the factors mentioned above (pH, temperature, anions) affect the complexation of the solutes which act as precursors to the nucleation of the metal hydrous oxides and which later determine their growth.

---

(a) Institute of Colloid and Surface Science and Department of Chemistry, Clarkson College of Technology, Potsdam, New York 13676

\* Metal (hydrous) oxide designation is taken here in a rather general way; it includes oxides, hydroxides, hydrated oxides, oxyhydroxides, etc.

The sensitivity of the described precipitation processes explains the poor reproducibility usually encountered in the studies of metal hydrous oxide formation. It also accounts for the finding that the resulting solids are mostly ill defined in shape and polydisperse.

Over the past few years we have succeeded in the preparation of colloidal dispersions of a number of metal hydrous oxides consisting of particles exceedingly uniform in size and shape (1). Such sols can be repeatedly obtained by relatively simple procedures and, as one would expect, the morphology, chemical composition, and other characteristics of the precipitates depend strongly on the experimental conditions. The reproducibility in the generation of well defined suspensions makes the elucidation of the chemical formation mechanisms possible. In order to accomplish the latter aim, the knowledge of the composition of all species in solution, in which the solid phase is formed, and particularly of the complexes containing the metal ion which is the major constituent of the precipitate, is implied. The task in obtaining this information is by no means easy. The monodispersed sols can also be employed in studies of various phenomena, such as in adsorption, adhesion, heterocoagulation, color determination, to mention a few.

In this presentation, an overview of the author's program in metal hydrous oxides will be offered with examples in the following areas of research:

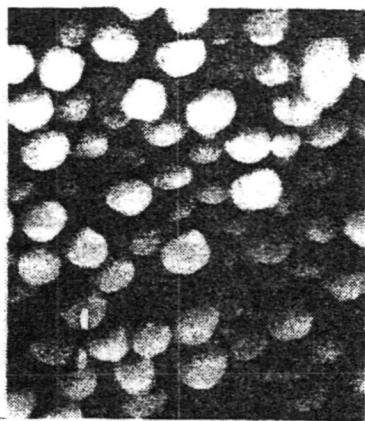
- a. Preparation of monodispersed sols.
- b. Mechanism for formation.
- c. Characterization of the particulate matter.
- d. Interactions with solutes.
- e. Interactions with other particles.
- f. Adhesion.

PREPARATION OF MONODISPERSED SOLS OF METAL HYDROUS OXIDES

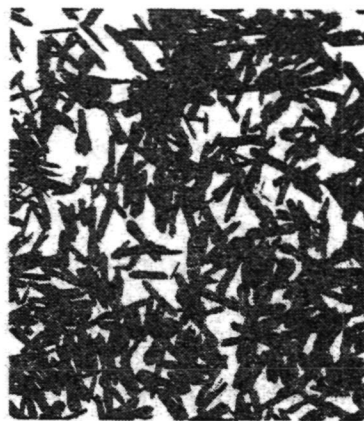
If uniform particles are to be obtained from a solution in which the precipitating components are continuously generated, secondary nucleation must be avoided. This condition implies that, upon reaching the critical supersaturation leading to the burst of nuclei, the rate of crystal growth must exceed the rate of nuclei formation. In the case of systems studied in this work, complexes of metal ions with hydroxyls, and often with other anions, are the precursors to the solid phase separation. Thus, hydroxylation is the controlling step, which will determine the nature of the final product. The usual procedure of adding base leads to local supersaturations and, consequently, to poorly defined stages of nucleation and particle growth. As a result the produced solids are irregular in shape and of broad size distributions.

Hydroxylation is greatly accelerated with temperature, depending on the metal and on the temperature of aging, hydrolyzed metal ion complexes may form in solutions of various degrees of acidity. Thus, it is possible to regulate the rate of complex formation in an aqueous solution of metal salts by proper adjustment of pH and temperature. Once the solution becomes supersaturated in the constituent species of a given metal hydrous oxide, the nucleation occurs. Further aging at a convenient temperature will continue to produce the precipitating complexes which, assuming a proper rate of their generation, are consumed in particle growth. Consequently, no secondary nucleation will take place, and a uniform uptake of the constituent species by the existing primary particles yields a monodispersed sol.

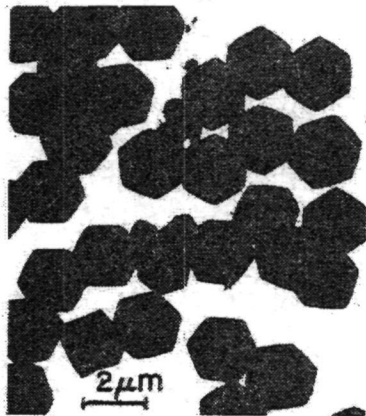
The chemical composition of the solid will strongly depend on the nature of the complex solutes produced on aging. In this respect the anions play a dominant role. In some cases well defined stoichiometric species form which include one or more hydroxyl and negatively charged ions, whereas in other cases the anions may cause condensation of hydrolysis products into polynuclear solutes of different



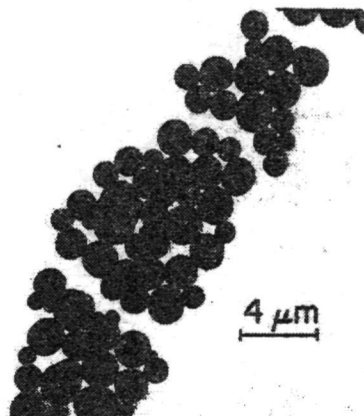
a



b



c



d

Fig. 1. Scanning and transmission electron micrographs of particles precipitated from various ferric salt solutions. (a) Hematite,  $\alpha\text{-Fe}_2\text{O}_3$  (solution 0.0315 M in  $\text{FeCl}_3$  and 0.005 M in  $\text{HCl}$  aged for 2 weeks at  $100^\circ\text{C}$ ). (b)  $\beta\text{-FeOOH}$  (solution 0.27 M in  $\text{FeCl}_3$  and 0.01 M in  $\text{HCl}$  aged for 24 hr at  $100^\circ\text{C}$ ). (c) Ferric basic sulfate  $\text{Fe}_3(\text{OH})_5(\text{SO}_4)_2 \cdot 2\text{H}_2\text{O}$  (solution 0.18 M in  $\text{Fe}(\text{NO}_3)_3$  and 0.32 M in  $\text{Na}_2\text{SO}_4$  aged for 2 hr at  $98^\circ\text{C}$ ). (d) Ferric phosphate,  $\text{FePO}_4$  (solution 0.0038 M in  $\text{FeCl}_3$  and 0.24 M in  $\text{H}_3\text{PO}_4$  at pH 1.86 aged for 20 min at  $100^\circ\text{C}$ ).

degrees of complexity. As a result the precipitated particles from solutions of different salts of the same metal ion may have different composition and structure.

To illustrate the above described situations in Figure 1 are given electron micrographs of four different systems, all precipitated by aging acidified ferric salt solutions. The scanning electron micrograph 1a shows spherical particles of hematite ( $\alpha\text{-Fe}_2\text{O}_3$ ) obtained by aging a solution 0.0315 M in  $\text{FeCl}_3$  and 0.005 M in HCl for 2 weeks at  $100^\circ\text{C}$  (2), whereas 1b is a transmission electron micrograph of  $\beta\text{-FeOOH}$  particles generated in solution 0.27 M in  $\text{FeCl}_3$  and 0.01 M in HCl heated at  $100^\circ\text{C}$  for 24 hr. Figure 1c represents submicron alunite type crystals of the composition  $\text{Fe}_3(\text{OH})_5(\text{SO}_4)_2 \cdot 2 \text{H}_2\text{O}$  which formed on aging at  $98^\circ\text{C}$  for 2 hr a solution 0.18 M in  $\text{Fe}(\text{NO}_3)_3$  and 0.32 M in  $\text{Na}_2\text{SO}_4$  (3). Finally, Figure 1d shows particles obtained on heating for 20 min at  $100^\circ\text{C}$  a solution which was 0.0038 M in  $\text{FeCl}_3$ , 0.24 M in  $\text{H}_3\text{PO}_4$  with NaOH added to adjust the pH to 1.86. The chemical analysis of these particles gave a composition consistent with  $\text{FePO}_4$ .

The four examples show that in the presence of chloride ions, under rather similar conditions, two entirely different sols are generated in terms of chemical composition and particle morphology (Figures 1a and b). The solid  $\beta\text{-FeOOH}$  contained considerable amounts of chloride ions when freshly prepared, but these anions could be removed by repeated washing with water without any apparent change in particle size or shape. On the other hand, solids formed on heating ferric salt solutions in the presence of sulfate ions consist of stoichiometrically stable and structurally well defined basic ferric sulfates. Finally, no detectable amounts of hydroxyl ligands are found in the systems precipitated as described above from aged solutions in the presence of phosphate ions. The resulting ferric phosphate redissolves on cooling.

The four different dispersions shown in Figure 2 were obtained by aging acidified aluminum salt solutions. Again the anions play an essential role.

The perfect spheres (Figure 2a) were generated on heating aluminum sulfate solutions ( $2 \times 10^{-3}$  M) for 48 hr at  $97^{\circ}\text{C}$  (initial pH 4.0). The precipitate contained a considerable amount of sulfate ions, but these anions were readily leached out by rinsing the solids with water yielding pure amorphous aluminum hydroxide particles without change in shape (4). Heating at the same temperature for 20 hr a solution which was 0.050 M each in  $\text{Al}(\text{NO}_3)_3$  and  $\text{Na}_2\text{HPO}_4$  and 0.035 M in  $\text{HNO}_3$  (initial pH of the mixture being 2.0) gave also spherical particles (Figure 2b) but the X-ray and chemical analysis identified the solids to be consistent with the composition of the mineral variscite,  $\text{AlPO}_4$ . Scanning electron micrographs (2c and d) show two unusual morphologies of boehmite, obtained by aging of aluminum chloride (0.0050 M  $\text{AlCl}_3$ ) and aluminum perchlorate (0.0030 M  $\text{Al}(\text{ClO}_4)_3$ ) solutions, respectively, at  $125^{\circ}\text{C}$  for 12 hr (5).

Again, it is clearly demonstrated that rather different, yet quite uniform colloidal metal oxide dispersions, can be prepared by homogeneous precipitation of different salt solutions in which different anions have a profound effect on the properties of the solid formed.

As a last example, Figure 3 gives a transmission electron micrograph and a replica of  $\text{Co}_3\text{O}_4$  particles which have a spinel structure. The significant finding is that such systems are formed on heating at  $100^{\circ}\text{C}$  of cobalt(II) salt solutions in oxygen or air only in the presence of acetate ions. No precipitate was obtained when, under otherwise identical conditions, the sulfate, chloride, perchlorate, or nitrate salts of cobalt(II) were aged.

Many more monodispersed sols of different hydrous metal oxides, involving those of chromium (6,7) copper (8), titanium (9), and other metals, have now been prepared following similar procedures.

ORIGINAL PAGE  
BLACK AND WHITE PHOTOGRAPH

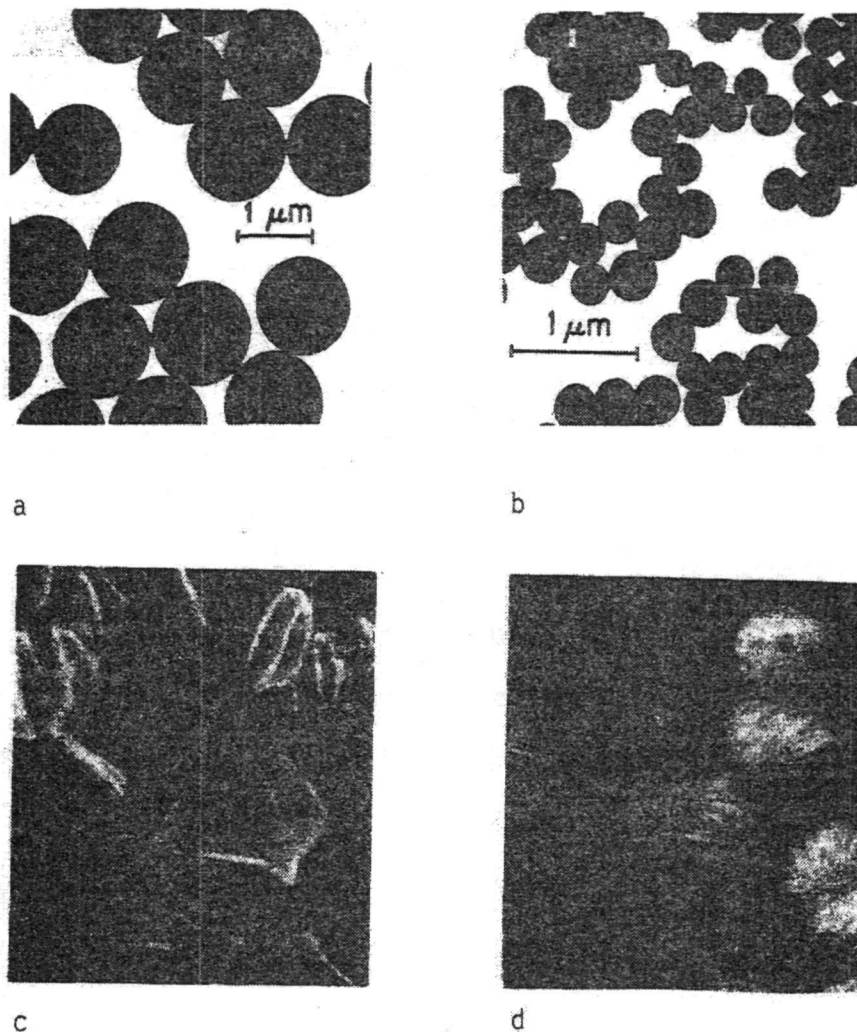


Fig. 2. Transmission and scanning electron micrographs of particles precipitated from various aluminum salt solutions. (a) Amorphous aluminum hydroxide (solution 0.0020 M in  $\text{Al}_2(\text{SO}_4)_3$ , pH 4.0 aged for 48 hr at  $97^\circ\text{C}$ ). (b) Variscite,  $\text{AlPO}_4$  (solution 0.050 M in  $\text{Al}(\text{NO}_3)_3$  and  $\text{Na}_2\text{HPO}_4$  and 0.035 M in  $\text{HNO}_3$  aged for 20 hr at  $97^\circ\text{C}$ ). (c) and (d) Boehmite,  $\alpha\text{-AlOOH}$  (solutions of 0.0050 M in  $\text{AlCl}_3$  and 0.0030 M in  $\text{Al}(\text{ClO}_4)_3$ , respectively, aged for 12 hr at  $125^\circ\text{C}$ ).

## MECHANISM OF METAL HYDROUS OXIDE FORMATION

The examples in the preceding section clearly show that it is necessary to know the composition of the solution in terms of the nature and of the concentration of all complexes if one is to explain the chemical processes in homogeneous precipitation of metal hydroxides. Unfortunately, such information is not always available, particularly for solutions at higher temperatures. Thus, one has no choice but to determine the composition of the different solutes under the actual conditions of the solid phase formation.

Until recently no substantiated mechanisms on metal hydroxide formation have been available (10). Using the monodispersed sols it was possible to develop a better understanding of the essential processes in the generation of chromium hydroxide (11,12), titanium dioxide (9), and ferric basic sulfates (13). In all these cases the particles formed in the presence of sulfate ions, but the role of these anions was quite different in each system.

Thus, in solutions containing chromium and sulfate ions solid chromium basic sulfate precursor precipitates first, which acts as a heterogeneous nucleating material for the amorphous chromium hydroxide (11). An application of the Nielsen's chromal analysis showed that the particles grow via surface reaction which involves polynuclear layer growth (12).

In the highly acidic solutions of titanium salts, sulfate ions bind the titanium(IV) ions into solute complexes, which on prolonged aging at elevated temperatures slowly decompose. These species act as a reservoir for the titanium ions; on decomplexation they hydrolyze and precipitate.

Finally, in solutions containing ferric and sulfate ions at low pH, well defined monomeric and dimeric solute hydroxy and sulfato complexes of iron(III) form, giving crystals of fixed stoichiometric composition (13).

ORIGINAL PAGE  
BLACK AND WHITE PHOTOGRAPH

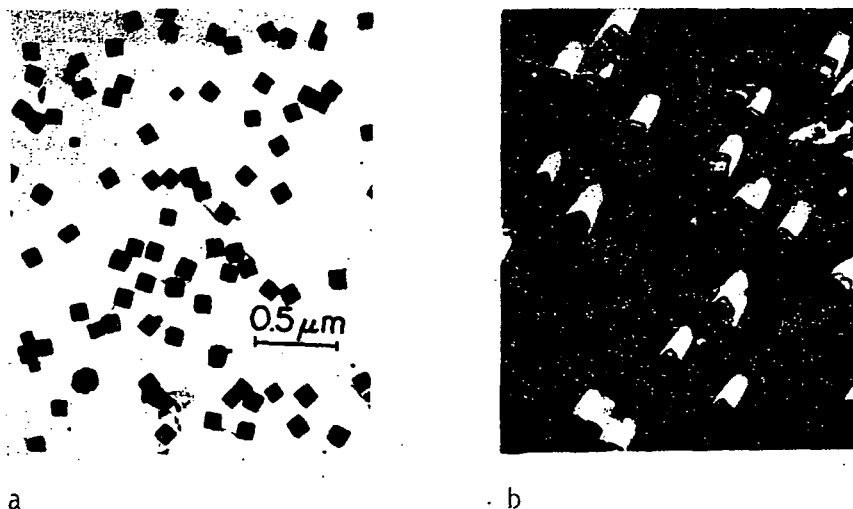


Fig. 3. Electron micrograph and a replica of  $\text{Co}_3\text{O}_4$  spinel particles obtained by heating a 0.010 M Co(II)-acetate solution for 4 hr at 100 C.

The role of chloride ions in the precipitation of different ferric hydroxous oxides has not been explained yet, but the work on the chloro-ferric complexes in acidic solutions, which is presently carried out in our laboratory, may shed light on the findings that a relatively small variation in conditions not only yield particles of different morphologies, but also of entirely different chemical compositions.

#### CHARACTERIZATION OF MONODISPersed METAL HYDROUS OXIDE SOLS

Depending on application, the characterization of colloidal particles may take many forms. In this review, only two properties will be discussed: surface charge and magnetism.

##### Surface Charge

Owing to the nature of the stabilizing species ( $\text{OH}^-$ ,  $\text{H}^+$ ) the surface charge of any metal hydroxous oxide is strongly pH dependent. Furthermore, the

electrokinetic point of zero charge (isoelectric point, i.e.p.) varies not only with the constituent metal, but also with the composition of its hydrous oxides. As a matter of fact, the reported values for the i.e.p. for apparently the same materials differed by several units in pH (14). For example, the literature data for the i.e.p. of synthetic titanium dioxide range from pH 2.6 to 7.3, whereas for a very pure sample of  $TiO_2$  it was found to be between 4.5 and 5.2 (15). In another example, the cubic  $Co_3O_4$  particles illustrated in Figure 3 show an i.e.p. at pH 5.4 (16); a considerably higher value of 11.4 was reported for a Co(II,III) oxide by Tewari and Campbell (17).

Since the isoelectric point defines the pH below which the particles are positively charged and above which they are negatively charged, this property of a metal hydrous oxide is essential in considering the sol stability, particle adhesion, heterocoagulation with other particles, and interactions with different solutes.

Figure 4 gives the electrokinetic mobility data of four aluminum hydroxide sols as a function of pH. Three of these curves refer to systems illustrated in Figure 2. The interesting finding is that the largest difference in the mobility curves is for two amorphous spherical particles prepared by aging aluminum sulfate solutions. The lower values of the i.e.p. is for the sol, as directly generated (diamonds), whereas the higher value is for the same sol from which the sulfate ions were removed by repeated rinsing with water (triangles). This example shows that anionic "impurities" have a pronounced effect on the surface charge characteristics of metal hydrous oxides. Obviously, the discrepancies in many reported data may be due to similar causes.

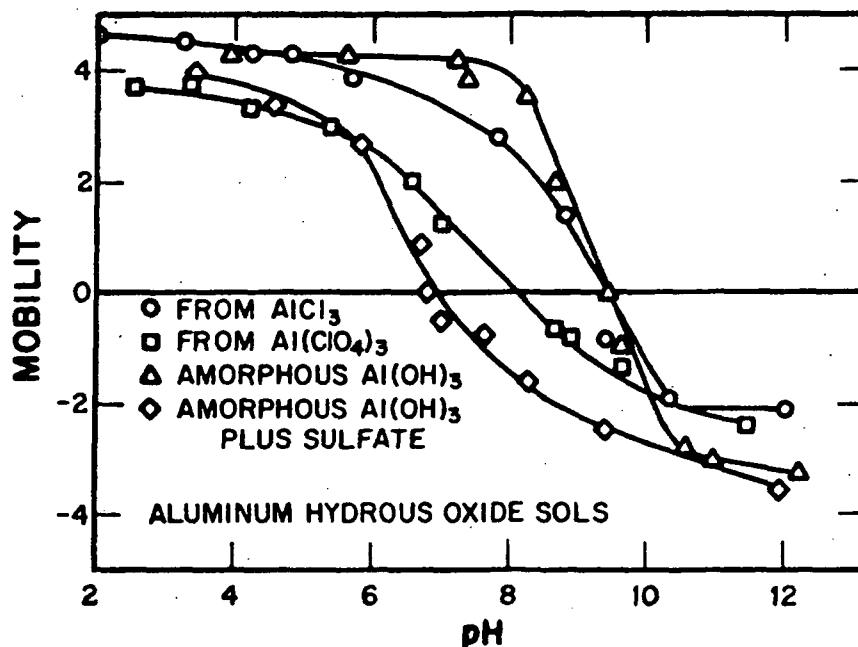


Fig. 4. Electrokinetic mobilities ( $\mu\text{m}/\text{sec}/\text{V}/\text{cm}$ ) as a function of pH of four different colloidal aluminum hydroxide oxides as illustrated in Figure 1c (○), 1d (□), 1a (△), and the same particles as shown in 1a from which sulfate ions were removed by leaching (◇).

### Magnetism

It is well known that magnetic properties of different (hydrated) oxides of a given metal strongly depend on their composition. Much less well understood is the relationship between various types of magnetism and the shape of the particles of the same chemical composition or of the materials having the same chemical composition and shape but different particle size. The monodispersed metal hydroxide oxides lend themselves exceedingly well for the investigation of magnetic properties as a function of various parameters.

Figure 5 shows the magnetization as a function of applied magnetic field for nearly spherical  $\alpha\text{-Fe}_2\text{O}_3$  particles (30-40 nm modal diameter at 298<sup>0</sup>K). It was suggested that hematite particles of this size should be in the antiferro-

ORIGINAL PAGE IS  
OF POOR QUALITY

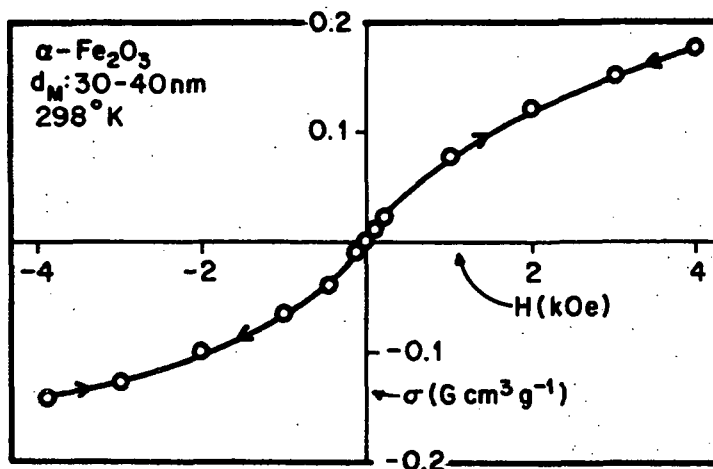


Fig. 5. Magnetization at  $298^\circ\text{K}$  as a function of applied field of spherical  $\alpha\text{-Fe}_2\text{O}_3$  particles having modal diameters of 30-40 nm.

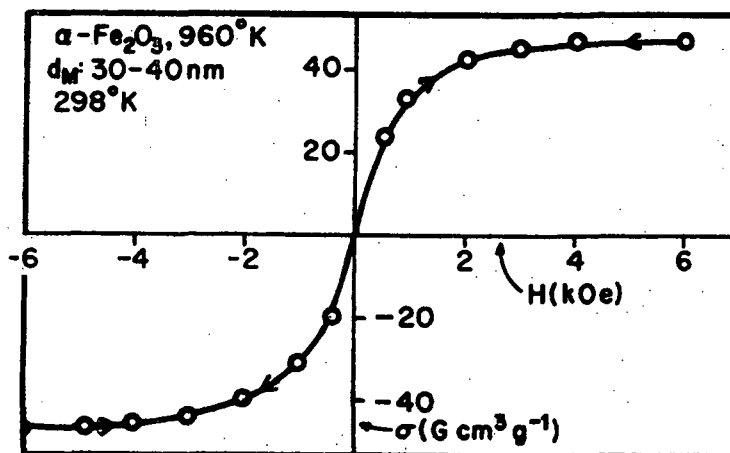


Fig. 6. Magnetization at  $298^\circ\text{K}$  as a function of applied magnetic field of spherical  $\alpha\text{-Fe}_2\text{O}_3$  particles having modal diameters of 30-40 nm after heat treatment at  $960^\circ\text{K}$  in a He atmosphere of 500 torr.

magnetic state (18). Thus, the  $\sigma$  vs H plot should exhibit some hysteresis. Within the experimental error no hysteresis is seen and the curve is typically S-shaped, characteristic of pure superparamagnetism (possibly in coexistence with weak ferromagnetism). This observation would suggest that the proposed relationship of the magnetic states to particle size (18) for  $\text{Fe}_2\text{O}_3$  systems may not be correct.

Heating the same hematite particles at high temperatures ( $960^\circ\text{K}$ ) in the helium atmosphere of 500 torr drastically alters the magnetic properties of  $\alpha\text{-Fe}_2\text{O}_3$  (Figure 6), although little change could be observed with respect to particle size and shape. The high  $\sigma$  values indicate the presence of ferromagnetic components, presumably  $\text{Fe}_3\text{O}_4$  or  $\gamma\text{-Fe}_2\text{O}_3$ , in these particles. Obviously, the crystallinity of the solids must have been affected by the heat treatment.

#### INTERACTIONS WITH SOLUTES

It is well known that the surfaces of hydrous metal oxides are rather reactive, i.e. various molecular or ionic species adsorb on such solids from aqueous solutions. The interfacial processes depend on the pH, since the latter is the factor controlling the surface charge. It is important to note that the opposite charge between the adsorbent and the adsorbate is not a sufficient condition for adsorption. The electrostatic attraction will only facilitate the approach of the solute species to the particle surface; other forces are needed to keep them at the interface. These forces may be hydrogen bond or other types of bindings (such as chelation), surface precipitation, etc. It is the ability of the constituent metal ions and of the potential determining species to interact with a variety of solutes that make metal hydrous oxide surfaces so reactive.

Two examples to be given here deal with the interaction of monodispersed, spherical, amorphous chromium hydroxide particles with aspartic acid and of crystalline rod-like  $\beta\text{-FeOOH}$  particles with ethylenediamine tetraacetic acid (EDTA).

ORIGINAL PAGE IS  
OF POOR QUALITY

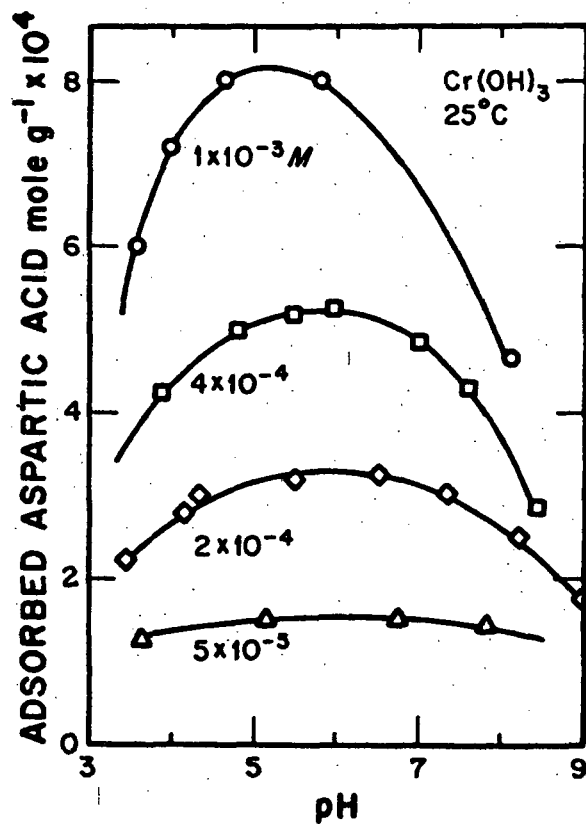


Fig. 7. The total amount of aspartic acid sorbed on spherical chromium hydroxide particles (modal diameter 350 nm) as a function of pH using different initial concentrations of aqueous solutions of the amino acid.

Figure 7 gives the total amount of aspartic acid sorbed on a chromium hydroxide sol having particles of a modal diameter of 350 nm as a function of pH using different initial concentrations of the solute. Analogous measurements showed that at 90°C the adsorbed amounts are considerably higher (19). The pH effect is obviously due to the charge on the solid. The i.e.p. of the used sol is at pH ~ 8.5 and little uptake of aspartic acid was observed above this pH value. It is evident that opposite charges of the adsorbent and adsorbate are needed to bring about the interaction.

The significant finding is that the amounts of the amino acid taken up by the metal hydroxide are approximately four orders of magnitude higher than the quantities calculated on the basis of monolayer adsorption assuming geometric surface areas of the spherical adsorbent particles. The obvious conclusion is that the major fraction of the aspartic acid molecules is absorbed in the interior of the adsorbent, which presumes that the amorphous chromium hydroxide is permeable to this amino acid. The absorption seems to be due either to chelation or to coordination of chromium ions with aspartic acid molecules. The much stronger uptake of these solute species at higher temperature supports the suggested chemisorption mechanism.

Contrary to the findings with aspartic acid, the same chromium hydroxide sol did not adsorb any measurable quantities of tryptophan. The latter is a larger molecule with a stronger aromatic (hydrophobic) character; its monocarboxylate nature (as distinguished from the dicarboxylic aspartic acid) precludes chelate formation by the carboxyl groups only.

The amount of EDTA adsorbed on  $\beta$ -FeOOH is also pH dependent and the uptake decreases strongly with increasing pH (Figure 8). The area per Fe atom in  $\beta$ -FeOOH, calculated from the crystal structure of this solid, is  $27 \text{ \AA}^2$ , and the

ORIGINAL PAGE IS  
OF POOR QUALITY

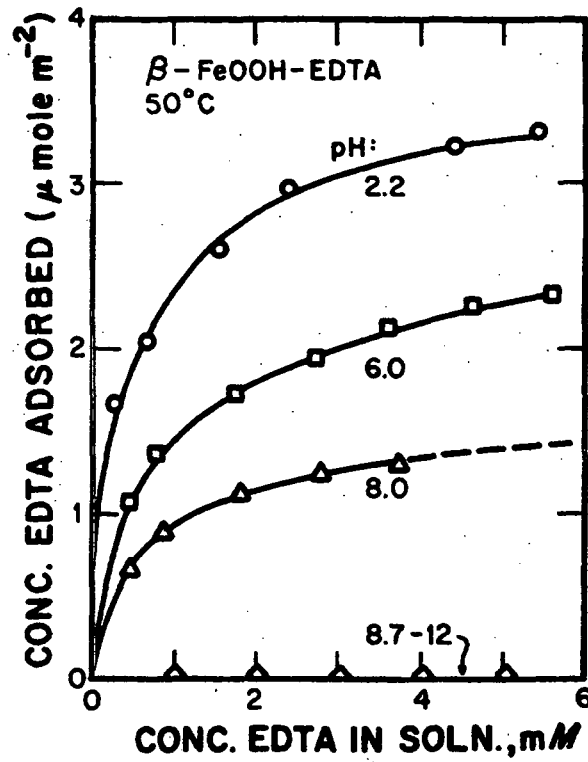


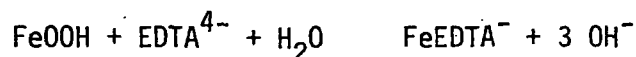
Fig. 8. Adsorption isotherms at 50°C for EDTA on  $\beta$ -FeOOH consisting of rod-like particles with an average length of 1  $\mu$ m and a width of 0.3  $\mu$ m. Each curve is for a different pH value.

area per ligand molecule at the condition of maximum adsorption at pH 2.8 (at 25°C), as calculated from the corresponding adsorption isotherm and the BET specific surface area of the ferricoxyhydroxide, is  $33 \text{ \AA}^2$ . The latter value is in reasonable agreement with the estimated cross-sectional area of the EDTA molecule, which indicates that at saturation a monomolecular layer is formed based on a Fe:EDTA interfacial complex of 1:1. The surface complexation is further supported by the value of the free energy of adsorption, which was found to be  $\Delta G_{\text{ads}}^0 = -9 \text{ kcal/mole}$  (20).

It was of special interest to investigate if the interaction of EDTA with the same  $\beta\text{-FeOOH}$  was accompanied by dissolution of some of the oxyhydroxide. Figure 9 is a plot of the amount of ferric ions released as a function of pH in the absence of EDTA and in the presence of three different concentrations of this chelating agent. A very pronounced maximum is observed. At lower pH values, at which considerable adsorption takes place, the release of ferric ions is rather small; the dissolution is inhibited by the surface complexation of lattice ferric ions with the organic ligand.

The maximum dissolution of ferric ions is over the pH range 8-10. Under these conditions no adsorption takes place. Partial dissolution of particles yields positively charged ferric hydrolysis products ( $\text{Fe}(\text{OH})_2^+$ ,  $\text{FeOH}^{2+}$ ,  $\text{Fe}_2(\text{OH})_2^{4+}$ ) which react with EDTA anions and, thus, enhance further release of ferric ions from the solid  $\beta\text{-FeOOH}$ .

Finally, at the highest pH values ( $> 12$ ), the complete inhibition of the dissolution can be understood, if one considers that the reaction



is strongly shifted to the left.

The two examples offered clearly illustrate the important role of specific interactions between a solid and a solute resulting in entirely different behavior of different systems.

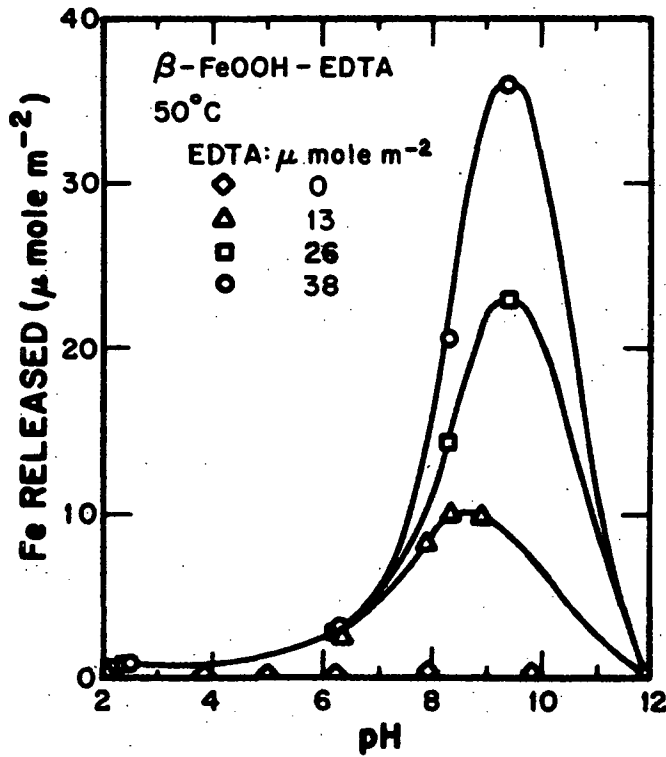


Fig. 9. Solubility of  $\beta$ -FeOOH (expressed as released iron) in the absence and in the presence of EDTA in different concentrations as a function of pH at 50°C.

## INTERACTIONS OF METAL HYDROUS OXIDES WITH OTHER PARTICULATE MATTER

### Heterocoagulation

Most of the colloid stability studies have been carried out with single systems, preferably monodispersed sols, such as polymer latexes. Yet, by far a majority of the naturally occurring dispersions, or those used in various applications, consists of mixed type particles, which may vary in composition, size, shape, and other phenomena, which implies stability of systems containing dissimilar suspended solids.

In order to apply the theoretical analysis it is necessary to work with spherical particles of known size, potential, and specific attraction characteristics. In addition, the stability of such mixed systems depends on the ratio of the particle number concentrations as well as on the ionic composition of the suspending media.

Monodispersed spherical metal hydroxide sols are particularly suitable for the study of interactions between unlike particles, because the necessary parameters can be experimentally determined. A comprehensive investigation was carried out with a binary system consisting of a polymer (polyvinyl chloride, PVC) latex stabilized with sulfate ions and spherical chromium hydroxide particles (21). The advantage of such a combination is that changing pH affects little the surface potential of the latex, whereas the metal hydroxide particles not only undergo a change in this quantity, but the sign of the charge can be reversed. The obtained data showed that excellent qualitative agreement existed between the experimental results and the theoretical calculations for dispersions of these two colloids.

To illustrate the effects of interactions in a mixed system, the stability ratios of sols consisting of spherical aluminum hydroxide particles (4) having a modal diameter of 570 nm and of a polystyrene latex (PSL, modal diameter 380 nm)

stabilized by sulfate ions will be given. The rate of coagulation was followed by means of laser light scattering at a low angle ( $\theta = 5^\circ$ ). Figure 10 is a plot of the total stability ratio,  $W_T$ , defined as

$$1/W_T = (n_1^2/W_{11}) + (n_2^2/W_{22}) + (2n_1n_2/W_{12}) \quad (1)$$

where  $W_{11}$  and  $W_{22}$  are the homocoagulation stability ratios for aluminum hydroxide and the latex, respectively, and  $W_{12}$  is the heterocoagulation stability ratio.  $n_1$  and  $n_2$  are the primary particle number fractions of the two dissimilar particles.

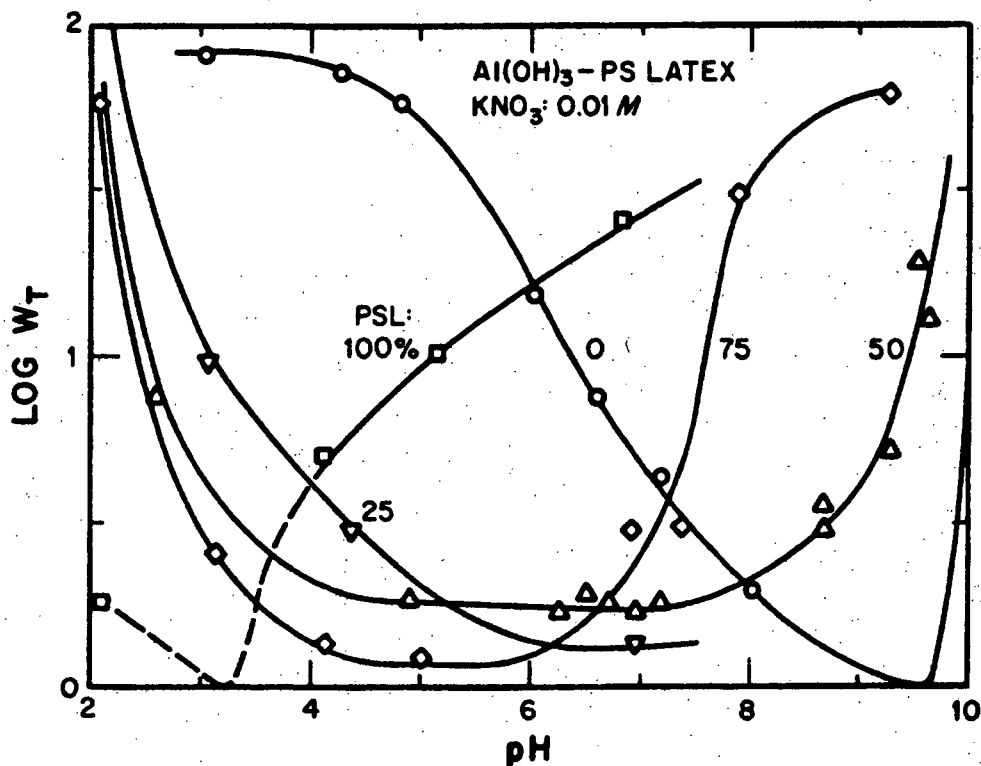


Fig. 10. Total stability ratio,  $W_T$ , as a function of pH for a pure aluminum hydroxide sol (Modal diameter 570 nm) (○), a pure polystyrene latex (PSL, modal diameter 380 nm) (□), and for mixtures of the two sols containing 25% (▽), 50% (△) and 75% (◇) PSL particles (in terms of number concentration).

C-2

As seen in Figure 10, the latex is least stable at low pH ( $\sim 3$ ) whereas pure aluminum hydroxide is unstable at high pH ( $\sim 9.5$ ). These pH values are close to the isoelectric points of the two colloidal systems. Depending on the particle number ratio and pH the binary systems may be either less or more stable than individual sols. For example, at pH 6 all mixed dispersions are less stable than the single systems. This is understood if one considers that the particles of PSL and of aluminum hydroxide carry opposite charges. At pH 8 the system containing 25% aluminum hydroxide particles is more stable than the pure aluminum hydroxide sol. In the studied case, aluminum hydroxide sol was carefully washed to eliminate all sulfate ions which are present in the particles as they are prepared (4).

Figure 11 gives an analogous plot to the previous one except that the aluminum hydroxide particles still contained some sulfate ions. The difference in the behavior of the purified and unpurified aluminum hydroxide sol is quite dramatic. In addition, the reproducibility of the results in the latter case is rather poor. This study exemplifies the sensitivity of such systems to anionic contaminations which often tend to be disregarded.

#### Particle Adsorption

Mixed systems which contain particles greatly divergent in size cannot be analyzed in the same manner as those having particles of comparable size. In the former case, the more finely dispersed systems may coagulate selectively, a heterofloc may form, or the small particles may adsorb on the larger ones, causing a change in the properties of the latter. All of these phenomena were observed in a binary system containing negatively charged polyvinyl chloride (PVC) latex (particle diameter 1020 nm) and silica (diameter  $\sim 14$ nm). It was shown that under certain conditions silica adsorbs on latex enhancing its stability toward electrolytes (22).

ORIGINAL PAGE IS  
OF POOR QUALITY.

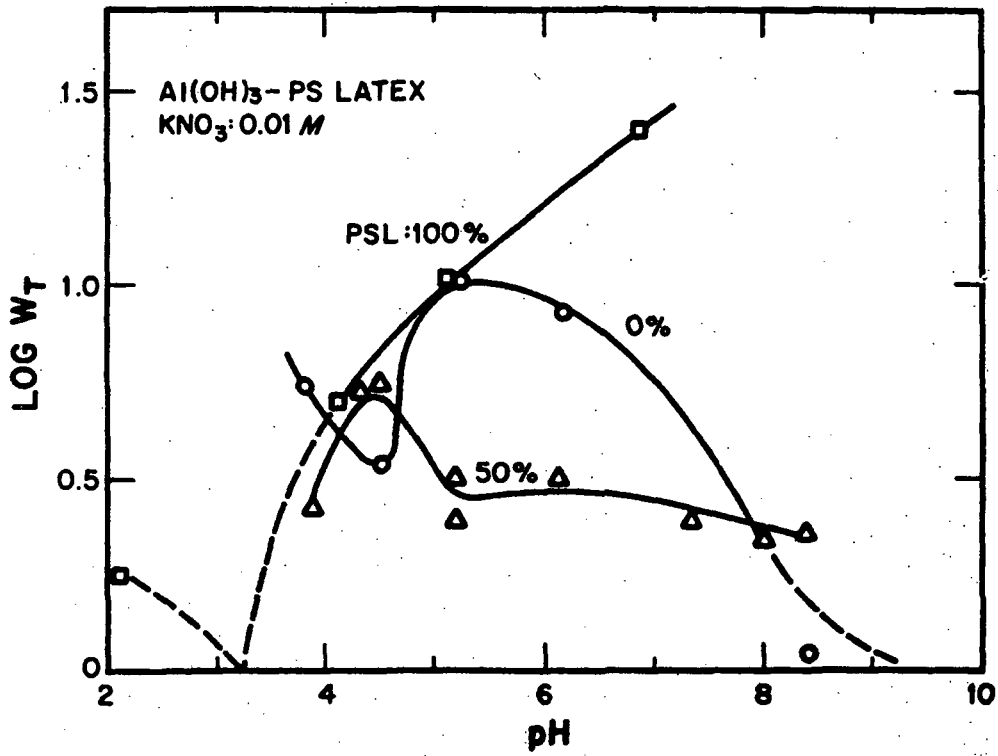


Fig. 11. Analogous plot as Figure 10 except that the aluminum hydroxide particles contained some sulfate ions.

The adsorption of small particles on larger ones is of particular interest, as other properties - in addition to stability - can be altered, such as the surface charge, reactivity, wettability, adhesivity, pigment characteristics, etc.

Figure 12 shows the mobility of a (PVC) latex as a function of pH and of the same latex in the presence of four different concentrations of  $\text{Fe}(\text{NO}_3)_3$ . In all cases the addition of the ferric salt had a strong effect on the particle charge causing the charge reversal from negative to positive at appropriate pH values. Independent measurements showed that the sharp change in the electrokinetic mobility was associated with the precipitation of ferric hydroxide. Consequently, the modification of the latex surface was due to the deposition of the metal hydrous oxide on the polymer particles. Needless to say the so coated latex showed different stability, adhesion characteristics, etc. than the untreated material.

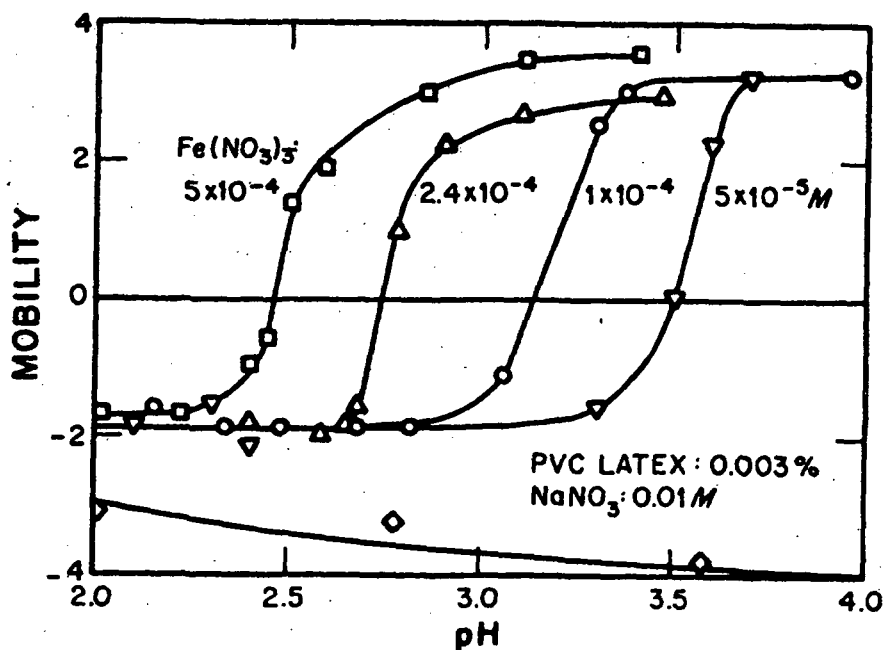


Fig. 12. Electrokinetic mobilities ( $\mu\text{m}/\text{sec}/\text{V}/\text{cm}$ ) as a function of pH of PVC latex (0.003% by wt, modal particle diameter 320 nm) in the absence ( $\diamond$ ) and in the presence of  $\text{Fe}(\text{NO}_3)_3$ :  $5 \times 10^{-5}$  ( $\nabla$ ),  $1 \times 10^{-4}$  (O),  $2.4 \times 10^{-4}$  ( $\Delta$ ), and  $5 \times 10^{-4} \text{ M}$  ( $\square$ ).

It is expected that reactants which affect the precipitation of ferric hydroxide would also influence its interaction with the latex. This is clearly evident in Figure 13, which gives the mobility data of the same latex in the presence of  $\text{Fe}(\text{NO}_3)_3$  to which NaF was added in different concentrations. Fluoride ions are known to complex with the ferric ion and, as a result, the precipitation phenomena as well as the surface charge groups of ferric hydroxide are altered by these anions. Indeed, with increasing fluoride concentration the charge reversal occurs at higher pH values and the magnitude of the positive charge decreases.

Acidification of the sols containing particles with adsorbed metal oxides should bring about dissolution of the coating and, consequently, a change in the surface charge to less positive, or even negative. Figure 14 shows that in the presence of  $\text{HNO}_3$  and HCl very long times are needed to dissolve, at least in part, the metal oxide coating. However, even after one month the charge is not reversed back to negative; obviously, the metal hydrous oxide must be polymerized at the surface to which it adheres tightly. Addition of only 0.0010 M NaF greatly accelerates the removal of the oxide layer and the particles eventually become uncharged. The latter observation implies that the negatively charged potential determining groups of the original latex surface are neutralized by the metal counterion complexes. Apparently, the bonds formed between the stabilizing sulfate ions and the adsorbed ferric species are not broken by acidification even in the presence of  $\text{F}^-$ .

#### PARTICLE ADHESION

The deposition of colloidal particles on other solids and their removal from these substrates depend on the chemical and physical forces acting between the adhering surfaces. In the absence of chemical bonds the adhesion can be treated as heterocoagulation of dissimilar particles, taking the radius of one

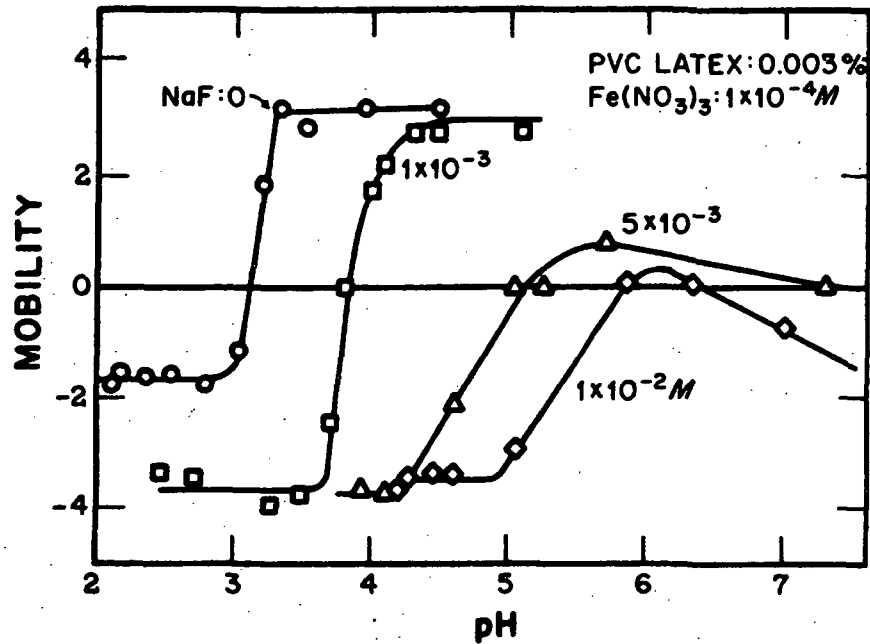


Fig. 13. Electrokinetic mobilities as a function of pH of the same PVC latex as in Figure 12 in the presence of  $1 \times 10^{-4}$  M  $\text{Fe}(\text{NO}_3)_3$  (○) to which  $1 \times 10^{-3}$  (□),  $5 \times 10^{-3}$  (Δ), and  $1 \times 10^{-2}$  M (◇) NaF was added, respectively.

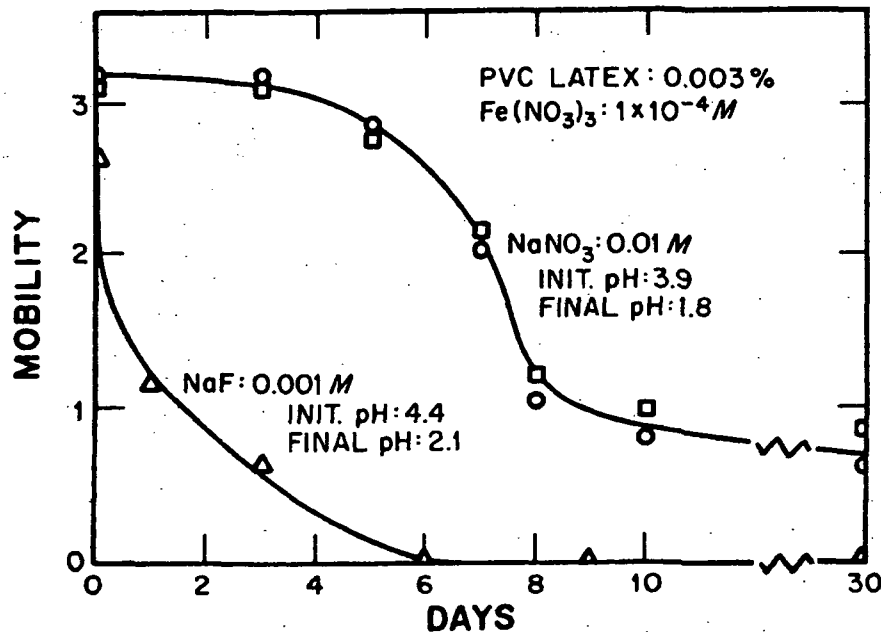


Fig. 14. The change of electrokinetic mobilities ( $\mu\text{m}/\text{sec}/\text{V}/\text{cm}$ ) as a function of time (days) of the same PVC latex as in Fig. 12 on acidification of a sol containing  $1 \times 10^{-4}$  M  $\text{Fe}(\text{NO}_3)_3$ . Circles and squares represent systems to which HCl and  $\text{HNO}_3$ , respectively, were added to lower the pH in the presence of 0.01 M  $\text{NaNO}_3$ ; triangles represent systems the pH of which was lowered by  $\text{HNO}_3$  in the presence of 0.0010 M NaF prior to aging.

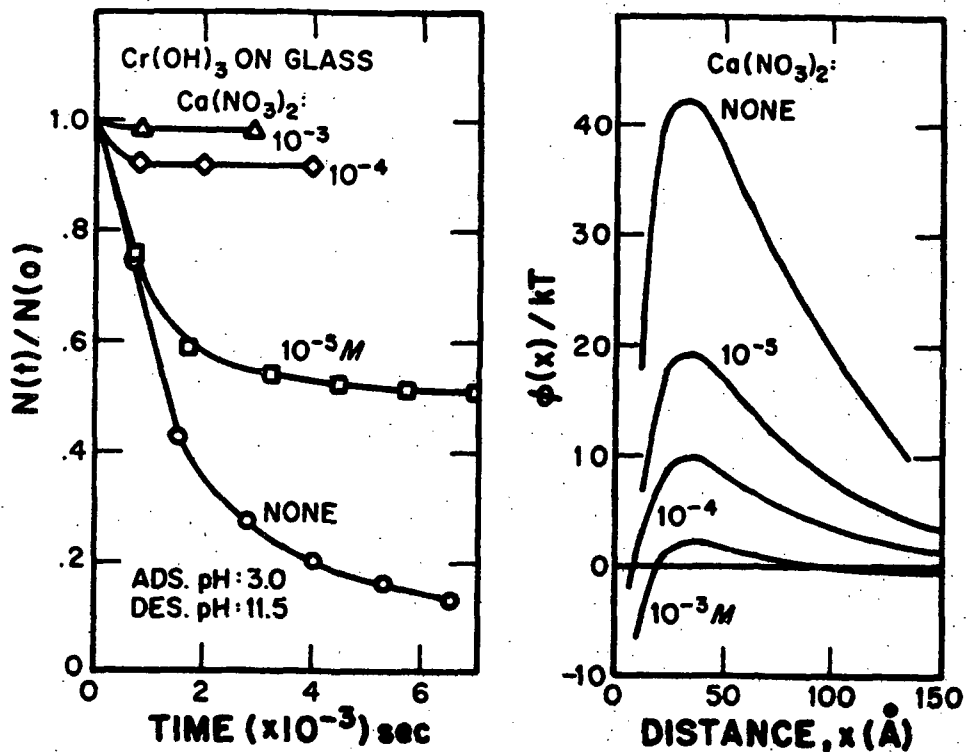


Fig. 15. Left: Fraction of monodispersed spherical chromium hydroxide particles (modal diameter 280 nm) desorbed from glass on repeated elution with rinse solutions of pH 11.5 in the absence (○) and in the presence of 10<sup>-5</sup> (◻), 10<sup>-4</sup> (◇), and 10<sup>-3</sup> M Ca(NO<sub>3</sub>)<sub>2</sub>. The particles were adsorbed on the glass from a sol at pH 3. Right: Calculated potential energy curves as a function of distance using the sphere-plate model (Eqs. 2 and 4) for the same systems shown left.

to go to infinity. In order to compare the theoretical predictions with experimental data it is necessary to have sufficiently well defined systems with known parameters. Again, monodispersed metal hydroxides, particularly those of spherical particles, can serve as excellent models for particle adhesion and removal studies. Using the packed column procedure (23), the interactions of such sols with glass and steel have been studied as a function of various conditions (pH, different electrolytes, temperature, etc.)

Figure 15 illustrates the results obtained with spherical chromium hydroxide particles (diameter 280 nm) on glass (24). At pH 3 glass beads placed in a column rapidly and quantitatively remove these metal hydroxide particles from an aqueous suspension by adhesion. Under these conditions the sol is positively charged and stable whereas the glass beads are negatively charged. Precautions are taken that no filtration takes place in the course of the deposition process. The subsequent removal of particles depends on the composition of the rinsing solution. At pH 11.5, at which both solids are negatively charged, rapid desorption of the particles is observed (Figure 15 left). However, if the rinse solution contains  $\text{Ca}(\text{NO}_3)_2$ , desorption can be reduced or completely inhibited depending on the concentration of the electrolyte. The higher the charge of the added cation, the lower is the concentration needed to prevent particle removal (24).

The results can be interpreted in terms of the total interaction energies. The attractive energy,  $\phi_A$ , as a function of distance ( $x$ ) was calculated using the equation:

$$\phi_A(x) = \frac{A_{132}}{6} \left[ \frac{2a(x+a)}{x(x+2a)} - \ln \frac{x+2a}{x} \right] \quad (2)$$

$A_{132}$  is the overall Hamaker constant for the system sphere-medium-plate, which can be approximated by:

$$A_{132} \approx (\sqrt{A_{11}} - \sqrt{A_{33}}) (\sqrt{A_{22}} - \sqrt{A_{33}}), \quad (3)$$

where subscript 1 applies to chromium hydroxide, 2 to glass, and 3 to water.

The value  $A_{11}$  for chromium hydroxide was taken as 14.9 kT,  $A_{22}$  for glass as 20.9 kT, and  $A_{33}$  for water as 10.3 kT.

For double layer repulsive energy,  $\phi_R$ , the plate/sphere expression of Hogg, Healy and Fuerstenau (25) was taken:

$$\phi_R(x) = \frac{\epsilon a}{4} \left[ (\psi_1 + \psi_2)^2 \ln(1 - e^{-\kappa x}) + (\psi_1 - \psi_2)^2 \ln(1 - e^{-\kappa x}) \right] \quad (4)$$

in which  $\psi_1$  and  $\psi_2$  are the surface potentials (equated with the corresponding  $\zeta$ -potentials), for the plate and the particles, respectively,  $\epsilon$  is the dielectric constant, and  $\kappa$  the reciprocal Debye-Hückel thickness.

The right side of Figure 15 gives the calculated total interaction energy curves,  $\phi(x) = \phi_A(x) + \phi_R(x)$ , as a function of distance of separation for the chromium hydroxide/glass systems in the absence and in the presence of the same concentrations of  $\text{Ca}(\text{NO}_3)_2$  as used in the desorption experiments. At the highest salt concentration essentially only attraction prevails and indeed no particle removal is observed. When no calcium nitrate is added, a number of particles appears to be at sufficient distance which enables them to overcome the energy barrier and desorb; however, particles which escaped cannot re-adsorb due to the high potential barrier. Thus, the double layer theory, albeit in its oversimplified form, explains at least semiquantitatively the adhesion phenomena in the described system.

Similar observations were made with chromium hydroxide on steel (Figure 16). The reproducibility of data is best shown by triangles and squares which represent two separate runs made with beds of steel beads on which the number of originally adsorbed particles differed by nearly one order of magnitude.

ORIGINAL PAGE IS  
OF POOR QUALITY

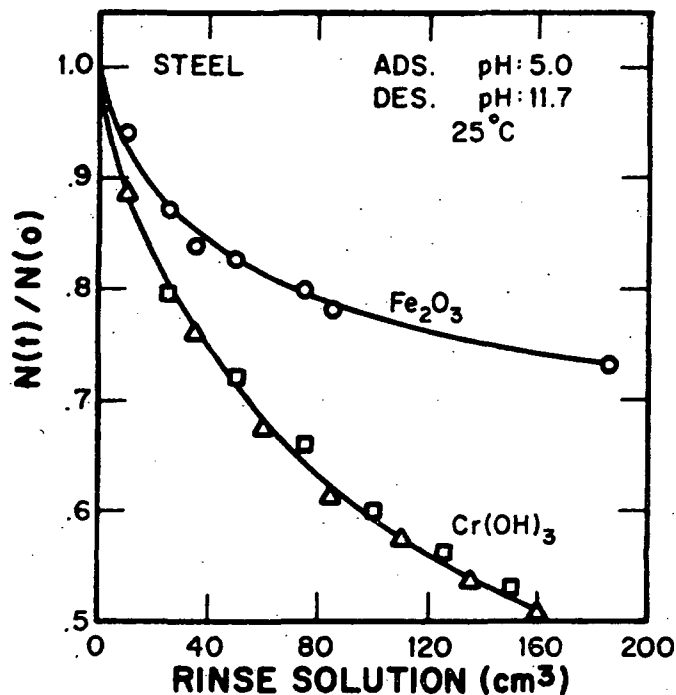


Fig. 16. Fraction of monodispersed spherical chromium hydroxide particles (modal diameter 280 nm) desorbed from steel on rinsing with an aqueous solution of pH 11.7. Number of particles originally deposited on 3 g of steel at pH 5.0 was  $2.9 \times 10^9$  ( $\square$ ) and  $1.8 \times 10^{10}$  ( $\Delta$ ). Circles give the analogous data for desorption of spherical hematite particles (modal diameter 140 nm) from the same steel. The number of originally deposited hematite particles:  $3.0 \times 10^9$ .

In the same diagram is also included the desorption curve of spherical hematite particles from the same steel under otherwise identical conditions. The large difference in the desorption rate is primarily due to the variation in the attractive forces, as determined by the Hamaker constants. This illustrates the sensitivity of the adhesion phenomena to the physical properties of the adsorbent/adsorbate system.

#### CONCLUDING REMARKS

It was not the intention of this review to give an in depth analysis of each problem discussed. Readers are referred to individually cited reports for more detailed information of the experimental techniques, the results obtained, and the theoretical analyses. However, it is hoped that the different cases described in this presentation clearly show the usefulness of the monodispersed metal hydrous oxide systems in the studies of various interfacial phenomena.

#### ACKNOWLEDGMENTS

This article is based on work done with the support of the NSF Grants CHE77 02185 and ENG 75-08403 as well as EPRI contract RP-966-1.

The author is greatly indebted to his many collaborators, and specifically to R. Brace, B. Gray, E. Katsanis, J. Kolakowski, H. Kumanomido, R. Kuo, J. Rubio, R. Sapiieszko, H. Sasaki, P. Scheiner, W. Scott, T. Sugimoto, and R. Wilhelmy, on whose contributions was based this presentation.

REFERENCES

1. E. Matijevic; Progr. Colloid Polymer Sci., 61 (1976) 24.
2. E. Matijevic and P. Scheiner, J. Colloid Interface Sci., 63 (1978) 509.
3. E. Matijevic; R. Sapiieszko and J. B. Melville, J. Colloid Interface Sci., 50 (1975) 567.
4. R. Brace and E. Matijevic; J. Inorg. Nucl. Chem., 35 (1973) 3691.
5. W. B. Scott and E. Matijevic; J. Colloid Interface Sci. (in press).
6. R. Demchak and E. Matijevic; J. Colloid Interface Sci., 31 (1969) 257.
7. E. Matijevic; A. D. Lindsay, S. Kratochvil, M. E. Jones, R. I. Larson and N. W. Cayey, J. Colloid Interface Sci., 36 (1971) 273.
8. P. McFadyen and E. Matijevic; J. Inorg. Nucl. Chem., 35 (1973) 1883.
9. E. Matijevic; M. Budnik and L. Meites, J. Colloid Interface Sci., 61 (1977) 302.
10. K. H. Lieser, Angew Chem., Int. Ed., 8 (1969) 188.
11. A. Bell and E. Matijevic; J. Inorg. Nucl. Chem., 37 (1975) 907.
12. A. Bell and E. Matijevic; J. Phys. Chem. 78 (1974) 2621.
13. R. S. Sapiieszko, R. C. Patel, and E. Matijevic; J. Phys. Chem., 81 (1977) 1061.
14. G. A. Parks, Chem. Rev., 65 (1965) 177.
15. M. Visca and E. Matijevic; J. Colloid Interface Sci. (in press).
16. T. Sugimoto and E. Matijevic; J. Inorg. Nucl. Chem. (in press).
17. P. H. Tewari and A. B. Campbell, J. Colloid Interface Sci., 55 (1976) 531.
18. Yu. F. Krupyanskii and I. P. Suzdalev, Sov. Phys.-JETP, 38 (1974) 859.
19. H. Kumanomido, R. C. Patel and E. Matijevic; J. Colloid Interface Sci. (in press).
20. J. Rubio and E. Matijevic; J. Colloid Interface Sci. (in press).
21. A. Bleier and E. Matijevic; J. Colloid Interface Sci., 55 (1976) 510.
22. A. Bleier and E. Matijevic; J. Chem. Soc., Faraday Trans. I, 74 (1978) 1346.
23. E. J. Clayfield and E. C. Lumb, Disc. Faraday Soc., 42 (1966) 285.
24. J. Kolakowski and E. Matijevic; J. Chem. Soc., Faraday Trans. I (in press).
25. R. Hogg, T. W. Healy and D. W. Fuerstenau, Trans. Faraday Soc., 62 (1966) 1638.

N82 32066 D8  
27

Flocculation of Colloidal Sols:  
Diffusion-Controlled vs. Agitation-Induced Flocculation

John W. Vanderhoff  
Center for Surface and Coatings Research  
Lehigh University  
Bethlehem, Pennsylvania 18015

Colloidal sols comprise dispersions of submicroscopic particles in water. The particles are stabilized by the combination of electrostatic repulsion arising from the charge on the particle surfaces and the London-van der Waals attraction arising from the difference in dielectric constant between the particles and the medium (1). Colloidal particles are also stabilized sterically by adsorption of uncharged polymer molecules, which with their water of hydration give a mechanical barrier to flocculation (2). The same uncharged polymer molecules may also cause flocculation of the colloidal sol by "bridging" i.e., the adsorption of a single polymer chain on more than one colloidal particle (see "Flocculation of Colloidal Suspensions by Polymeric Flocculants"). The resultant stability of a given colloidal sol depends upon the contributions of all these factors --- electrostatic and steric repulsion as well as London-van der Waals attraction and flocculation by adsorbed polymers.

The flocculation of colloidal sols has long been of scientific and industrial interest. The scientific interest arises, not only because of its practical implications, but also because there are theories of flocculation that can be tested experimentally. The industrial interest arises from the use of this process in reclaiming land from the sea, production of synthetic rubber, ABS resins, and latex foam, dewatering of sludges, water purification, waste water treatment, beater addition in paper production, and recycling of wastepaper. There is a gap between the scientific and industrial application of the principles of flocculation: the scientific theories are best tested in the beginning of the flocculation and are difficult to apply to the complete process from beginning to end; the industrial interest is in the completeness of the flocculation, the clarity of the supernatant phase, the form of the flocs, and the ease in their filtration and washing.

Theories have been developed for two types of flocculation: diffusion-controlled flocculation and agitation-induced flocculation. The diffusion-controlled flocculation theory (3) assumes that, for a stable colloidal sol comprised of uniform-size primary particles which is suddenly subjected to conditions that cause flocculation, each primary particle acts as a center to which other particles diffuse and flocculate and that all particle-particle collisions are effective in giving flocculation.

95+96

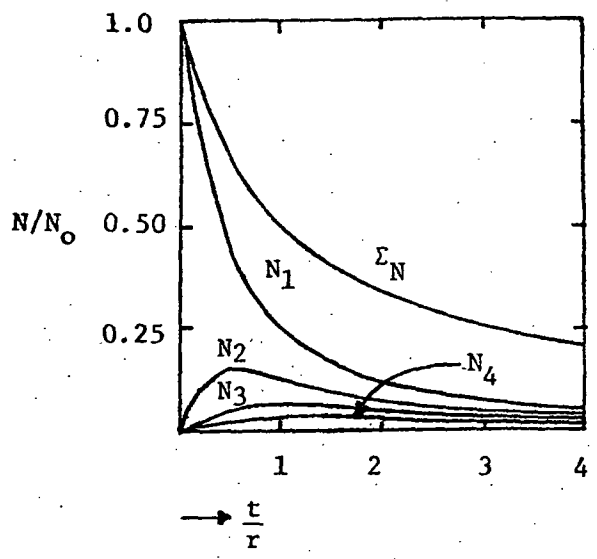
~~65-66~~

$$-dN/dt = 8\pi DRN^2$$

where  $N$  is the number of primary particles,  $D$  the diffusion constant, and  $R$  the collision radius. Equation 1 shows that the rate of flocculation is proportional to the square of the number of particles. However, this equation is applicable to the early stages of flocculation, since the flocculation produces aggregates of particles which also act as centers for flocculation. For aggregates of various sizes

$$-d \sum_{k=1}^{\infty} N_k / dt = 4D_1 R \left\{ N_0 / (1 + t/T) \right\} \quad (2)$$

where  $t$  is the time of flocculation, and  $T$  the time in which the number of particles is halved. Figure 1 shows the variation of the number of particles (expressed as  $N/N_0$  with time (expressed as  $t/T$ ). Typically, for water media at  $25^\circ$ , the value of  $T$  is about ca.  $2 \times 10^{11}/N_0$ .



The total number of particles as well as the number of singlets decreases monotonically throughout the flocculation; however, the number of doublets, triplets, and quartets increases to a maximum as the flocculation proceeds and then decreases as these aggregates flocculate to form larger particles.

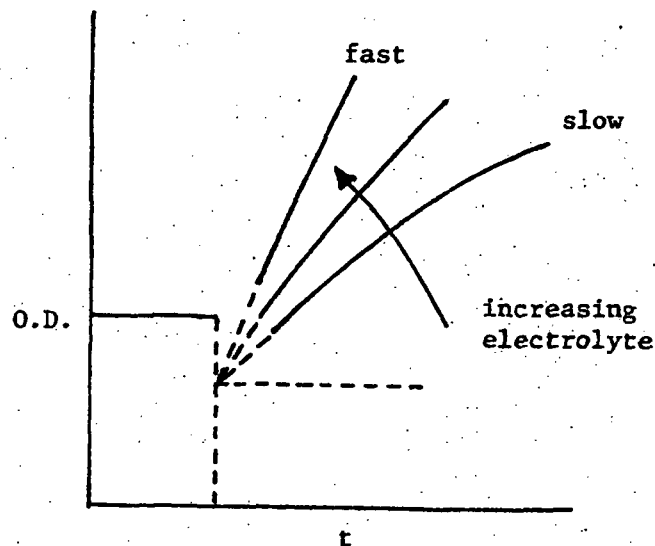
The foregoing treatment assumes that all particle-particle collisions are effective in causing flocculation. For most colloidal sols, there is a potential energy barrier which must be surmounted before flocculation can occur (4). This energy barrier means that only a certain proportion of particle-particle collisions are effective in causing flocculation. Therefore, the types of flocculation can be divided into fast flocculation in which all particle-particle collisions are effective and slow flocculation in which a certain proportion of collisions are effective.

$$\text{fast flocculation: } T = 1/4\pi D_1 R N_0 \quad (3)$$

$$\text{slow flocculation: } T = 1/4\pi D_1 R N_0^\alpha \quad (4)$$

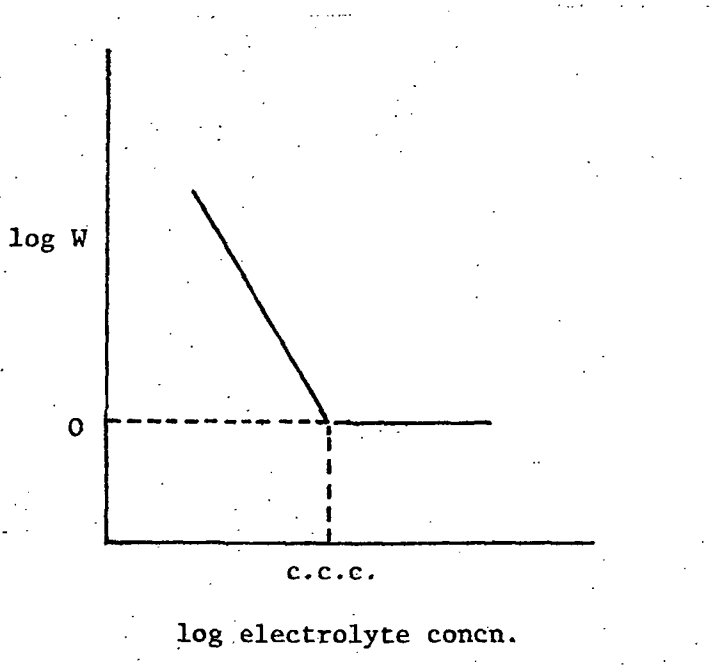
where  $\alpha$  is the proportion of collisions that are effective in causing flocculation.

Experimentally, the rates of flocculation are measured in different ways; however, one of the most widely used methods is to measure the optical density of the colloidal sol during the flocculation process. For example, for the flocculation of a colloidal sol by electrolyte, the sol is placed in the spectrophotometer cell and its optical density is read off from a chart recorder; at the desired time, the electrolyte solution is added and mixed with the sol; then, the variation of optical density with time gives a measure of the rate of flocculation, as shown in Figure 2.



The addition of electrolyte dilutes the sol slightly; this reduction in optical density can be calculated from Beer's law. The measured variation can then be extrapolated to zero time and zero degree of flocculation. The rate of flocculation is taken as the initial slope of the optical density-time curve. As can be seen in Figure 2, increasing electrolyte concentration gives an increasing slope of this curve until a limiting slope (fast flocculation) is reached.

The rates of flocculation (initial slopes) are plotted as the log reciprocal slope relative to that for fast flocculation (or stability factor  $W$ ) (4) versus log electrolyte concentration as shown in Figure 3.



It can be seen that  $\log W$  decreases linearly to a plateau value of 0, i.e., the fast flocculation region in which further increases in electrolyte concentration give no further increase in flocculation rate. The intersection of the descending straight line with the horizontal line gives the critical coagulation concentration or c.c.c., i.e., the electrolyte concentration that denotes the onset of fast flocculation. The literature contains many examples of measurement of rates of flocculation of colloidal sols of various types.

Agitation-induced flocculation has also been analyzed theoretically (5,6). The probability J of collision of a central particle i with particle j, of which there are N per cc, is

$$J = (4/3) N(R_{ij})^3(du/dz) \quad (5)$$

where  $R_{ij}$  is the collision radius and  $(du/dz)$  is the velocity gradient. This equation is difficult to test experimentally because the velocity gradient varies from one part of the sample to another. However, the probability of agitation-induced flocculation can be related to that of diffusion-controlled flocculation (6).

$$I = 4\pi D_{ij} R_{ij} N \quad (6)$$

where I is the probability of diffusion-controlled (Brownian) collisions. The ratio of these two probabilities is given by

$$J/I = \eta(R_{ij})^3(du/dz)2kT \quad (7)$$

where  $\eta$  is the viscosity of the medium and k the Boltzmann constant.

For a colloidal sol of 0.1 $\mu$ m initial particle size and a velocity of 1 sec<sup>-1</sup>, the ratio J/I is ca. 10<sup>-3</sup>, i.e., in the initial flocculation, agitation-induced flocculation is negligible compared with diffusion-controlled flocculation. However, as the flocculation proceeds and the size of the particle aggregates increases, the ratio J/I increases. For example, at an average diameter of ca. 1 $\mu$ m, J/I is ca. 1, i.e., the contributions of diffusion-controlled and agitation-induced flocculation are about the same. At an average particle diameter of ca. 10 $\mu$ m, J/I is much greater than unity, i.e., the agitation-induced flocculation is much more important than the diffusion-controlled flocculation.

The foregoing estimated J/I ratios show that, for an agitated industrial flocculation which proceeds from a small primary particle size to a large-size floc, the predominant mechanism of flocculation shifts from diffusion-controlled to agitation-induced as the flocculation proceeds from beginning to end. Furthermore, it shows that the growth of aggregates by agitation-induced flocculation is auto-accelerating.

Thus there are problems in correlating the theories of flocculation with the practical industrial examples. The initial rates of flocculation of a given colloidal sol can be measured spectrophotometrically, but these rates are those of the diffusion-controlled flocculation. Industrial flocculations always proceed past the initial stage of diffusion-controlled flocculation to the final stage of

agitation-induced flocculation. Moreover, industrial flocculations almost always involve agitation, e.g., in mixing the electrolyte or other flocculant with the colloidal sol. Thus the industrial flocculation begins in the diffusion-controlled range and ends in the agitation-induced range. Experimentally, it is difficult to separate the diffusion-controlled flocculation from the agitation-induced flocculation. The flocculation may be followed to the end spectrophotometrically, but the large flocs tend to settle and thus are not represented in the overall measurement of optical density. The settling can be obviated by faster agitation rates, but this affects the rate of flocculation and, in extreme cases, can break down aggregates as well as form them. The net result is that there are very few examples in the literature where the rate of industrial flocculations from the beginning to end have been correlated with the theories of flocculation.

Carrying out such flocculation experiments in microgravity would give several advantages that might allow such a correlation between theory and experiment. First, all particles, whether single primary particles or aggregates of primary particles, would not settle or cream at any agitation rate, or even in the absence of agitation. This failure to separate or cream would keep all aggregates "active", i.e., still serving as centers for diffusion-controlled flocculation. Keeping all particles suspended would allow the possibility of determining the total number of particles as a function of time from beginning to end of the flocculation (laser holography may enhance the possibility of such a determination). Finally, experiments in microgravity would allow a definite separation of diffusion-controlled and agitation-induced flocculation by studying diffusion-controlled flocculation with and without agitation.

#### References

1. E.J.W. Verwey and J.Th.G. Overbeek, "Theory of Stability of Lyophobic Colloids," Elsevier, New York, 1948.
2. W. Heller and T.L. Pugh, J. Chem. Phys. 22, 1778 (1954); R. H. Ottewill, in "Nonionic Surfactants", M. Schick, editor, Marcel Dekker, New York, 1967.
3. M. von Smoluchowski, Physik, Z. 17, 557, 585 (1916); ibid. Z. Physik. Chem. 92, 129 (1917).
4. N. Fuchs, Z. Physik 89, 736 (1934).
5. M. von Smoluchowski, Z. Physik. Chem. 92, 155 (1917); P. Tuorila, Kolloidchem. Beihefte 24, 1 (1927); H. Mueller, Kolloidchem. Beihefte 27, 223 (1928).
6. J. Th. G. Overbeek, in "Colloid Science Vol. 2", H. R. Kruyt, editor, Elsevier, New York, 1952, p. 290.

**S E C T I O N C**

**BIOLOGICAL PROCESSES**

21 [ N82 32067

CELL PARTITION IN TWO PHASE POLYMER SYSTEMS

D. E. Brooks<sup>(a)</sup>

Aqueous phase-separated polymer solutions can be used as support media for the partition of biological macromolecules, organelles and cells. Cell separations using this technique have proven to be extremely sensitive to cell surface properties but application of the systems are limited to cells or aggregates which do not sediment significantly while the phases are settling. Partition in zero g in principle removes this limitation but an external driving force must be applied to induce the phases to separate since their density difference disappears. We have recently shown that an applied electric field can supply the necessary driving force. We are proposing to utilize the NASA FES to study field-driven phase separation and cell partition on the ground and in zero g to help define the separation/partition process, with the ultimate goal being to develop partition as a zero g cell separation technique.

---

<sup>(a)</sup> Departments of Pathology & Chemistry, University of British Columbia, Vancouver, Canada V6T 1W5

## CELL PARTITION IN TWO PHASE POLYMER SYSTEMS

D.E. Brooks

Departments of Pathology and Chemistry

University of British Columbia

Vancouver, Canada

### INTRODUCTION

Much of modern biomedical research is directly aimed at defining and elucidating the normal and pathological activity of living systems. A problem in such work is frequently encountered when attempts are made to prepare the specific cell population of interest in a pure state. Non-specific preparation techniques based on cell size or density are seldom sufficiently sensitive, as the total range of these parameters encountered among biological organisms is relatively narrow. Separation methods based upon cell surface properties hold more promise, however, since a cell's function and its ability to interact with other cells in its immediate environment appear frequently to be reflected in characteristics of the cell membrane. One such characteristic which is being exploited for preparative purposes is cell surface charge as detected by electrophoresis. Free-flow electrophoresis is capable of spatially distributing a cell population on the basis of the net charge density located on the exterior of the cell membrane. An even more sensitive separation technique is available, however, which also depends partly on the surface charge but which has been shown to be capable of separating cell populations which are electrophoretically indistinguishable.

When aqueous solutions of two different polymers are mixed above certain concentrations they usually form immiscible, liquid, two-phase solutions. Each of these phases generally consists of more than 90 percent water and can be buffered and made isotonic by the addition of low molecular weight species. If a cell or particle suspension is added to such a system, then shaken, the cells--upon re-equilibration--are frequently found to have partitioned unequally between one of the phases and the interface. This preferential

ORIGINAL PAGE IS  
OF POOR QUALITY

partition behavior can be used as the basis of a separation procedure for differing cell populations since partition in these systems is determined directly by cell membrane properties (1,2).

Cell populations which have related, but not identical, surface properties seldom exhibit sufficiently different partition behavior to be separated in a single extraction. In such cases, sequential partitions are carried out via countercurrent distribution (CCD) to effect the separation. CCD in phase systems derived from dextran/polyethylene glycol (PEG) mixtures has proven to be an extremely sensitive and valuable preparation technique in cell biology. Erythrocyte populations can be separated on the basis of cell age by CCD, for instance (3). This separation cannot be accomplished by preparative electrophoresis (4). The leukocyte fractions from various mammalian species have been fractionated via CCD (5,6) as have mouse spleen cells (7) and a mouse leukemic cell line (8,9). Human lymphocytes can be sub-fractionated this way into sub-populations which vary dramatically in their T:B:null cell ratios and in their responses to various mitogens (10). Cells from other organs also distribute into sub-populations according to maturity after CCD. Rapidly regenerating rat liver cells, for instance, have a higher partition coefficient than normal liver cells (11). Similarly, the relative position of rat epithelial cells in a CCD curve depends strongly on cell age and location in the epithelium (crypt or villus) (12). CCD has therefore produced some very interesting and useful cell separations.

The effectiveness of CCD as a separation procedure resides in the fact that the partition coefficient,  $K$ , is sensitive to a variety of cell surface characteristics. Moreover,  $K$  should depend exponentially on the relevant surface properties, as may be seen from the approximate thermodynamic expression (13):

$$K = n^t/n^{if} = C \exp(1/kT(\Delta G_{el} - (\gamma_{cb} - \gamma_{ct} - \gamma_{tb})^2 A/4\gamma_{tb}))$$

where:  $n^t$  = number of cells in top phase  
 $n^{if}$  = number of cells adsorbed at interface

ORIGINAL PAGE IS  
OF POOR QUALITY

- $C$  = constant, independent of cell properties  
 $\Delta G_{el}$  = difference in electrostatic free energy of cell when  
adsorbed at interface and when in top phase  
 $\gamma_{cb}$  = interfacial free energy of cell in bottom phase  
 $\gamma_{ct}$  = interfacial free energy of cell in top phase  
 $\gamma_{tb}$  = interfacial tension between top and bottom phases  
 $A$  = cell surface area  
 $k$  = Boltzmann's constant  
 $T$  = absolute temperature

The electrostatic free energy term occurs because in the presence of some salts a stable Donnan potential exists between the bulk phases (vide infra) which affects the distribution of charged particles.  $\Delta G_{el}$  will in general be directly proportional to the cell surface charge density although its exact form will depend on the shape of the potential profile across the interface, which is complex. The partition coefficient therefore depends exponentially on the cell surface charge, in contrast to the linear dependence of electrophoretic mobility on charge density. This fact accounts in part for the relatively higher sensitivity of CCD over preparative cell electrophoresis.

The above expression also indicates that cell charge is not the only parameter determining  $K$ . The interfacial free energy of the cell/solution interface also can play a strong role. This free energy will be determined by the intrinsic nature of the interaction between the cell membrane and the phase polymers and the degree to which each of them adsorbs to the cell surface. This adsorption will lower the free energy between the polymer-coated cell and the phase in which that polymer predominates. The competitive adsorption of the two polymer species depends in turn on the chemical nature of the polymers and on a variety of cell membrane properties. Few of these membrane properties have been identified as yet, but in a PEG/dextran system having no phase potential difference there is good evidence that PEG-membrane interactions become stronger and partition into the PEG-rich phase higher as cells with a greater ratio of polyunsaturated to mono-unsaturated fatty acids in the membrane lipid are partitioned (2). The chemical composition and

structure of the membrane--independent of surface charge--can, therefore, determine partition behavior as well.

A strength of the partition approach to cell separation is that the conditions which determine the value of  $K$  are mainly under experimental control. Hence, the cell characteristic on which the separation is to be based can be made the dominant determinant of  $K$  by appropriate choice of operating conditions. The potential difference which appears between the two bulk phases, referred to earlier, is caused by the slight preference of some salts (sulfates, phosphates, citrates) for one phase over the other. By manipulating the ionic species and concentrations in the system, then, the magnitude of this potential difference can be controlled. Likewise, by varying the chemical character of the phase polymers themselves,  $\gamma_{ct}$ ,  $\gamma_{cb}$  and  $\gamma_{tb}$  can be changed and the interfacial free energy term made dominant. In particular, if appropriate polymers are used, affinity ligands such as antibodies or haptens can be covalently bonded to one of the phase polymers. Cells bearing the specific structure to which the affinity ligand is directed will be preferentially coated with the substituted polymer and the cells will partition into the phase rich in that species. The phase can, therefore, act as a support medium for the affinity ligand, one which has much greater access to the cell surface than the gel beads commonly used. Separation on the basis of an extremely wide variety of membrane characteristics is therefore possible depending on the choice of phase system.

#### LIMITATIONS OF PARTITION ON EARTH

Countercurrent distribution of cells has been applied with great success to relatively small biological cells, such as erythrocytes and lymphocytes. However, there are a variety of cell types such as megakaryocytes, many tumor cells and tissue culture lines which are too large and/or dense to be separated successfully on earth. Such cells do not remain in suspension long enough to allow the phases to separate and permit a transfer along the countercurrent train.

ORIGINAL PAGE IS  
OF POOR QUALITY

In a one g environment, the partition of cells in phase-separated aqueous polymer systems is not an equilibrium process. Although the phases themselves can readily be brought to equilibrium, the distribution of partitioned material is time dependent due to sedimentation. Only after all the cells have sedimented to the phase boundary or the bottom of the container will the distribution be stationary—and then of no use. The degree to which the non-stationary nature of the distribution affects the usefulness of partition depends on the sedimentation rate of the cells in the appropriate phase, that is, on the cell size, shape, and density and on the phase density and viscosity. Since cell partition usually occurs between the top, PEG-rich phase and the interface, large cells or cell clumps will sediment into the interface from the top phase during the time it takes for the phases to separate, distorting the true, equilibrium distribution. If CCD is performed on such suspensions, the material transferred as the top phase will not contain all the cells that belong in that phase and the bottom phase will contain the cells that have sedimented into the interfacial region as well as those that are truly adsorbed there. This gravity-driven accumulation has two related effects on the CCD. First, it reduces the resolution of separation for all cells with a finite sedimentation rate; the CCD curves obtained for most cell types will therefore represent only a fraction of the separation in principle possible. Secondly, it eliminates the use of this separation technique entirely for cells which are so large they sediment as rapidly as the phases settle. Nominally, the critical cell diameter for this effect is 24 microns. There is a variety of cell types of clinical and fundamental interest which are larger than this, however. Carrying out partition studies and CCD under low gravity conditions would eliminate the cell size constraint because sedimentation would be insignificant.

#### PHASE SEPARATION AND PARTITION IN A REDUCED GRAVITY ENVIRONMENT

Countercurrent distribution with two phase aqueous polymer systems can be successfully applied on earth because phase separation occurs sufficiently rapidly that the 60 to 120 transfers necessary for many separations can be accomplished in a reasonable length of time. Under the best conditions, using

a thin layer CCD apparatus to minimize the phase thickness, it takes about five minutes for dextran/PEG phases to separate, resulting in run times of up to 10 hours. Phase separation at one g is driven by two mechanisms:

1. convective forces caused by the density difference between the phases;
2. interfacial free energy which tends to minimize the interfacial area between the phases.

In a low g environment the convective forces will be too small to produce phase separation in an acceptable length of time. Moreover, it is known that the interfacial tensions developed in these systems are also too small ( $10^{-2}$ - $10^{-4}$  dyne  $\text{cm}^{-1}$ , (14)) to be effective in driving separation. This conclusion is based on the behavior of dextran/Ficoll phase systems which can be made with phases of equal density; such systems take many hours to separate after mixing. An external driving force must therefore be applied if partition experiments are to be carried out in zero g.

The approach we have taken to producing phase separation by an external force involves the application of a small electric field across the system. This technique was suggested by the observation (15) that droplets of one phase suspended in the other had an easily measurable electrophoretic mobility. Moreover, the mobility was found to be a linearly increasing function of droplet size, up to at least 15  $\mu\text{m}$  in diameter. The phase systems therefore follow to some extent the behavior predicted by Levich (16) and Levine's (17) theory of the electrophoresis of mercury drops in ionic solutions which predicts such a size dependence, although the mechanisms of charging must be different in the two systems. The sign of the mobility inverts depending on which of the two phases is dispersed (i.e., depending on which side of the interface is externalized).

The effect is illustrated in Figure 1 where a phase system made up of 5% dextran ( $M_w = 5 \times 10^5$ ) and 4% PEG ( $M_w = 6 \times 10^3$ ) in 0.2M  $\text{K}_2\text{SO}_4$  has been examined. The system was allowed to equilibrate then a small volume of top, PEG-rich phase was dispersed in a large volume of bottom phase. The

ORIGINAL PAGE IS  
OF POOR QUALITY

sizes of individual top phase drops were measured visually and their electrophoretic mobilities (T/B) determined at 25°C via analytical particle electrophoresis. The phase volume ratios were then reversed and the mobilities of bottom phase, dextran-rich drops suspended in top phase (B/T) also determined as a function of drop diameter. The results, plotted in Figure 1, show that the mobilities of both types of drops vary linearly with diameter. If the slopes of the mobility-diameter plots for T/B and B/T drops are compared their ratio is 1.28. If it is assumed that the magnitude of the surface potential is equal and opposite for each type, Levich's theory predicts this ratio ought to be given, under our conditions of relatively low conductivity, by:

$$(2\eta_t + 3\eta_b)/(2\eta_b + 3\eta_t)$$

where  $\eta_b$  = bottom phase viscosity

$\eta_t$  = top phase viscosity

Substituting in the appropriate values gives a value of 1.39, in reasonable agreement with experiment.

It should be clearly pointed out that the electrophoretic mobilities of T/B and B/T drops are of opposite sign. Application of an electric field across a phase system which has been mixed to form an emulsion ought to induce phase separation, therefore, since drops of the two phases will move in opposite directions.

The principle of electric field driven phase separation has recently been demonstrated. A phase separation chamber across which a known electric field can be applied was constructed by the Advanced Technology Operations Division of Beckman Instruments. The apparatus consists of two electrode chambers containing bright Pt electrodes separated from a phase chamber (5 cm L x 0.5 cm W x 0.2 cm deep) by two Amicon XM-100 membranes. Feeder ports give access to the chamber for filling and drainage. Electrode rinse buffer is circulated through the upper and lower electrode chambers to remove electrode reaction

products. The chamber and electrode assembly is made of poly(methyl methacrylate) lapped and polished to provide a good seal between the upper and lower halves. The optical system used to follow phase separation turbidimetrically consists of a small ruby laser whose beam diameter is limited to 0.03 cm by an entrance aperture. The beam traverses the width of the phase chamber at a vertical position which can be adjusted relative to the midline. The beam intensity is measured with a solid state detector and amplified after traversing the chamber and an 0.03 cm diameter exit aperture.

When a mixed turbid phase system is introduced into the chamber most of the light is scattered off the optical axis and the photodetector output is low. As the phases separate, the upper and lower phases clear, the scattering decreases and the detector output increases with time, reflecting the kinetics of separation. Experiments may be run in the presence or absence of the electric field and the kinetics readily compared.

Using this apparatus we have demonstrated field-driven phase separation in a system consisting of 7.5% dextran ( $M_w = 4 \times 10^4$ ), 4.5% PEG ( $M_w = 6 \times 10^3$ ) and 0.1M  $K_3$  citrate. The lower molecular weight dextran was used to reduce the phase viscosity and increase mobility. With an applied field of  $E = 0$ , at a phase volume ratio of 9:1 (top:bottom) the initial rate of clearing is about 0.12% per minute. With an applied field  $E = 6 \text{ V cm}^{-1}$  the rate increases to 1-2.5% per minute. Phase separation therefore takes place about an order of magnitude more rapidly in the presence of the field than in its absence at this ratio of bottom to top phase volume.

Applying an electric field to a system containing cells to produce phase separation in the absence of gravity will also result in motion of the cells, in this case by electrophoresis. In all the phase systems studied to date, including all those used in cell separation work, the sign of the phase drop mobilities are such that top phase drops bear a negative surface potential so the anode is placed at the top of the chamber. Since cells in physiological media all bear a net negative surface charge, they will also migrate upwards--away from the interface--when the field is applied. Cells will therefore tend

to move out of that region above the interface which is retained with the bottom phase when a CCD transfer is made. This motion will therefore have the opposite effect on the partition coefficient to that of cell sedimentation and, in principle, effective partition coefficients approaching the ideal values should be realized.

While most of the principles discussed above have been demonstrated in terrestrial experiments, examination of phase separation, electric field effects and cell partition in a reduced gravity environment has yet to be carried out. It is hoped that through the use of the Fluids Experiment System these concepts can be tested and developed sufficiently fully that low g partition separations of cell populations of biomedical interest will become feasible.

#### ACKNOWLEDGEMENTS

Financial support for this work from NASA is gratefully acknowledged.

#### REFERENCES

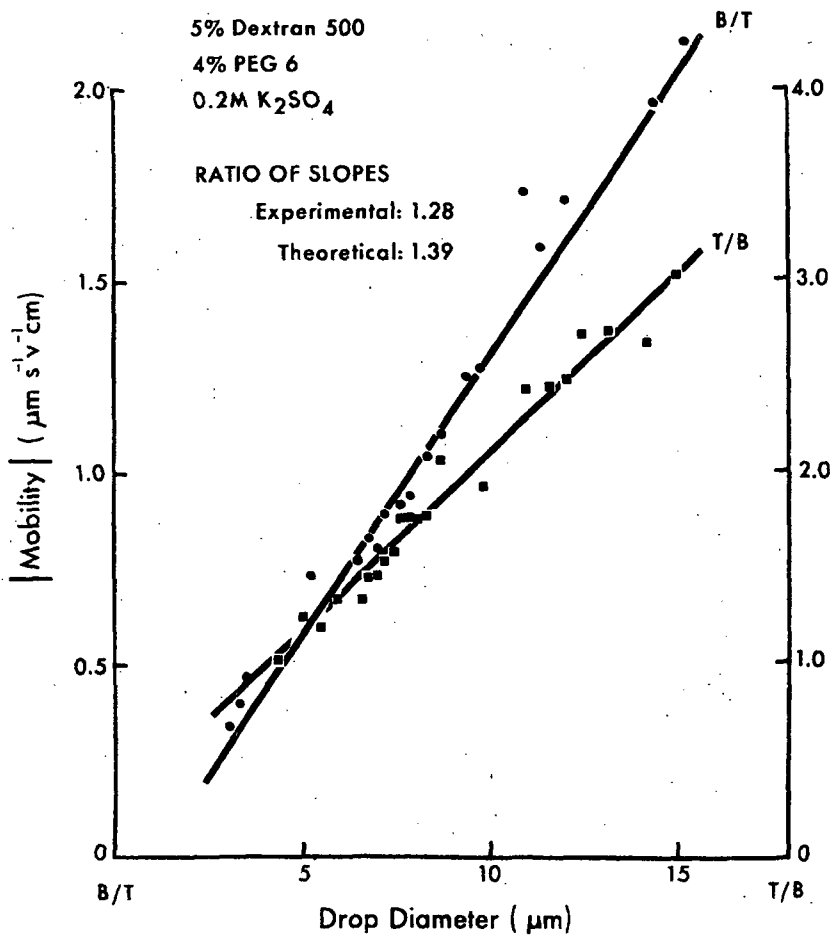
1. Walter, H. Partition of cells in two-polymer aqueous phases: a surface affinity method for cell separation. In: N. Catsimoolas (Ed.), *Methods of Cell Separation*, Vol. 1, Plenum Publishing Corp., New York (1977), p. 307.
2. Walter, H., Krob, E.J. and Brooks, D.E. Membrane surface properties other than charge involved in cell separation by partition in polymer, aqueous two-phase systems. *Biochemistry* 15:2959 (1976).
3. Walter, H. and Selby, F.W. Counter-current distribution of red blood cells of slightly different ages. *Biochem. Biophys. Acta* 112:146 (1966).
4. Luner, S.J., Szklarek, D., Knox, R.J., Seaman, G.V.F., Josefowicz, J.Y. and Ware, B.R. Red cell charge is not a function of cell age. *Nature* 269:719 (1977).
5. Walter, H., Krob, E.J. and Ascher, G.S. Separation of lymphocytes and polymorphonuclear leukocytes by counter-current distribution in aqueous two-polymer phase systems. *Exp. Cell Res.* 55:279 (1969).

ORIGINAL PAGE IS  
OF POOR QUALITY

6. Walter, H. and Nagaya, H. Separation of human rosette- and non-rosette-forming lymphoid cells by counter-current distribution in an aqueous two-phase system. *Cell. Immunol.* 19:158 (1975).
7. Brunette, D.M., McCulloch, E.A. and Till, J.E. Fractionation of suspensions of mouse spleen cells by counter current distribution. *Cell Tissue Kinet.* 1:319 (1968).
8. Gersten, D.M. and Bosmann, H.B. Behavior in two-phase aqueous polymer systems of L5178Y mouse leukemic cells in the stationary phase of growth. *Exp. Cell Res.* 87:73 (1974).
9. Gersten, D.M., and Bosmann, H.B. Behavior in two-phase aqueous polymer systems of L5178Y mouse leukemic cells. II. The lag and exponential phases of growth. *Exp. Cell Res.* 88:225 (1974).
10. Walter, H., Webber, T.J., Michalski, J.P., McCombs, C.C., Moncla, B.J., Krob, E.J. and Graham, L.L. Subfractionation of human peripheral blood lymphocytes on the basis of their surface properties by partitioning in two-polymer aqueous phase systems. *J. Immunol.* (In press).
11. Walter, H., Krob, E.J., Ascher, G.S. and Seaman, G.V.F. Partition of rat liver cells in aqueous dextran-polyethylene glycol phase systems. *Exp. Cell Res.* 82:15 (1973).
12. Walter, H. and Krob, E.J. Alterations in membrane surface properties during cell differentiation as measured by partition in aqueous two-polymer phase systems. Rat intestinal epithelial cells. *Exp. Cell Res.* 91:6 (1975).
13. Brooks, D.E. Manuscript in preparation.
14. Ryden, J. and Albertsson, P-A. Interfacial tension of dextran-polyethylene glycol-water two-phase systems. *J. Colloid Interface Sci.* 37:219 (1971).
15. Brooks, D.E., Seaman, G.V.F. and Walter, H. Potential distributions in phase-separated aqueous polymer solutions. In: M. Kerker (Ed.), *Colloid and Interface Science*, Vol. 4, Academic Press, New York (1976), p. 367.
16. Levich, V.G. *Physicochemical Hydrodynamics*, Prentice-Hall, Englewood Cliffs (1962), p. 493.
17. Levine, S. and O'Brien, R.N. A theory of electrophoresis of charged mercury drops in aqueous electrolyte solutions. *J. Colloid Interface Sci.* 43:616 (1973).

FIGURE LEGENDS

Figure 1. Absolute values of electrophoretic mobilities of phase drops as a function of drop size. See text for description of system. Mobilities of drops of top phase suspended in bottom phase (T/B) have a negative sign while those for bottom phase drops in top phase (B/T) are positive.  $T = 25.0^{\circ}\text{C}$ .



## SOME POTENTIAL BLOOD FLOW EXPERIMENTS FOR SPACE

Giles R. Cokelet  
Radiation Biology and Biophysics  
University of Rochester Medical Center  
Rochester, New York 14642

Herbert J. Meiselman  
Department of Physiology and Biophysics  
University of Southern California School of Medicine  
Los Angeles, California 90033

Harry L. Goldsmith  
University Medical Clinic  
Montreal General Hospital  
Montreal, Quebec H3G 1A4

## ABSTRACT

Blood is a colloidal suspension of cells, predominantly erythrocytes, (red cells) in an aqueous solution called plasma. Because the red cells are more dense than the plasma, and because they tend to aggregate, erythrocyte sedimentation can be significant when the shear stresses in flowing blood are small. This behavior, coupled with equipment restrictions, has prevented certain definitive fluid mechanical studies from being performed with blood in ground-based experiments. Among such experiments, which could be satisfactorily performed in a microgravity environment, are the following: (a) studies of blood flow in small tubes, to obtain pressure-flow rate relationships, to determine if increased red cell aggregation can be an aid to blood circulation, and to determine vessel entrance lengths, and (b) studies of blood flow through vessel junctions (bifurcations), to obtain information on cell distribution in downstream vessels of (arterial) bifurcations, and to test flow models of stratified convergent blood flows downstream from (venous) bifurcations.

## INTRODUCTION

Blood is a rather typical colloidal suspension, consisting of dispersed phases, called cells, and a continuous aqueous phase, known as plasma. The red cells (erythrocytes) are the most numerous of the cells, numbering about  $5 \times 10^9$  per  $\text{cm}^3$  and normally occupying about 42% of the blood by volume (the hematocrit). In contrast, the other types of cells occupy only about 1% of the blood. Consequently, the red cells dominate the flow behavior of the blood (except in vessels whose diameter is comparable to the cellular characteristic dimension).

Each erythrocyte is a flexible particle with a biconcave discoid shape when not deformed by stresses or crowding by other cells. It has a volume of about 90 cubic microns, a major diameter of about 8 microns and a maximum thickness of about 2 microns. Its density is about 4% larger than that of plasma. Consequently, an individual red cell at the earth's surface has a very small sedimentation rate - about 0.1 micron/sec.

However, when the local shear stress is less than about  $3 \text{ dyne/cm}^2$  in normal blood, the red cells aggregate. The primary aggregates are formed by the joining of erythrocytes face to face, to form stacks of disks, called rouleaux. In turn, these rouleaux aggregate into larger aggregates. The sizes of these rouleaux and secondary aggregates are a function primarily of shear stress, concentration of certain macromolecules (e.g., fibrinogen) and erythrocyte concentration. This aggregation results in two effects: (1) increased rate of red cell sedimentation, and (2) red cell syneresis.

On earth, because of this aggregation, the steady settling rate of erythrocytes in normal, quiescent blood is about 10 mm/hr, or 3 micron/sec. With increased aggregation, such as often found under pathological conditions, this sedimentation rate may increase by a factor of 10, or more. While sedimentation effects normally are not a factor in blood circulation in the body (except for slow flows in the veins), they are sufficient to interfere with or confound the analysis of some blood flow experiments. Syneresis on the other hand, not only confounds analysis of blood flows but also may have physiological significance, even in the small arteries and arterioles where the major resistance to blood flow generally occurs.

Syneresis is the attractive movement of red cells together, leaving an irregularly bounded, but well defined, layer of cell-free plasma next to solid boundaries, such as vessel walls and viscometer surfaces. In a concentric cylinder viscometer, for example, this results in a time-dependent response of the instrument as the plasma layer develops at the blood-instrument interfaces, and in the steady state results in a two-phase fluid flow with a torque less than what would be required if syneresis did not occur. This effect is seen for hematocrits between 10 and 70% with a maximum rate of plasma layer development for hematocrits of 30-35%. The effect of syneresis on blood flow in vessels is mentioned later.

## EXPERIMENTS

In this section, discussion will center on specific studies, for the most part already performed in ground-based experiments, that could be performed profitably in a microgravity environment.

### I. Single Tube Experiments

The simplest blood flow experiments involve steady flow of blood from a feed reservoir through a straight, circular-cylindrical tube into a discharge reservoir. The quantities measured are tube dimensions, pressure drops versus blood flow rates, blood hematocrits in the feed reservoir, and, for tubes with inside diameters below 300  $\mu\text{m}$ , hematocrits of the blood in the tube and of the blood flowing from the tube.

The preferred method of showing such pressure versus flow rate data is to plot the wall shear stress,  $\tau_w$ , against the average velocity divided by the tube diameter,  $\bar{U} = u/D$ . It can be shown that for any fluid for which the shear stress is only a function of the shear rate, a plot of  $\tau_w$  versus  $\bar{U}$  will define a universe curve valid for steady flow in any size tube. A typical set of data for blood of hematocrit equal to 20.1% is shown in Figure 1.

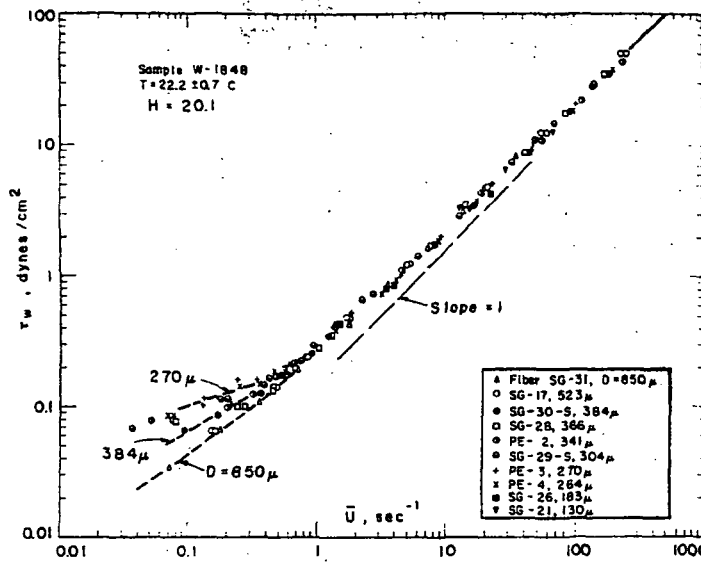


Figure 1.  $\tau_w - \bar{U}$  for blood in tubes of diameters from 130 to 850  $\mu\text{m}$ . (Reproduced with permission from [1]).

These data were gathered by Benis for tubes whose inside diameters ranged from 130  $\mu\text{m}$  to 850  $\mu\text{m}$ . For  $\bar{U} \geq 1 \text{ sec}^{-1}$ , all the data for a given blood fall on one curve, as expected, but for  $\bar{U} < 1 \text{ sec}^{-1}$ , the data show a dependence on tube diameter. The tubes were horizontal. Original speculation as to the cause of this data dispersion centered on the possibility of erythrocyte adhesion to the tube walls at low flow rates.

However, Meiselman [2] found by microscopic observation that when  $\bar{U} < 2 \text{ sec}^{-1}$ , the red cells flowed as aggregates and significant erythrocyte sedimentation occurred by the time blood flowed a few centimeters down the tubes. It therefore seems probable that the low  $\bar{U}$  dispersion of data in Figure 1 is due to erythrocyte sedimentation. (Red cell sedimentation rate data, for blood in horizontal tubes 102-888  $\mu\text{m}$  ID can be found in [2].)

It would be worthwhile to perform similar experiments in a microgravity environment so as to obtain  $\tau_w - \bar{U}$  data for low values of  $\bar{U}$ . But an even more important question could be answered by such experiments: When red cell aggregation increases (as it does in many pathological situations), does the resistance to blood flow, at a given flow rate, increase or decrease? On one hand, increasing aggregation increases viscosity and thereby flow resistance; on the other hand, the

increased aggregation (by syneresis) causes a larger marginal layer of plasma at the vessel wall, which would tend to decrease flow resistance. This question has not been answered, although it has both theoretical and clinical significance.

One study on this question, by Palmer and Jedrzejczyk [3], gives some information on this problem. Data obtained with flow of red cell suspensions through a vertical 400  $\mu\text{m}$  ID tube are shown in Figure 2: a plot on the ordinate of the ratio of the pressure drop for the cell suspension to the suspending medium pressure drop (same flow rate) versus  $8\bar{U}$ .

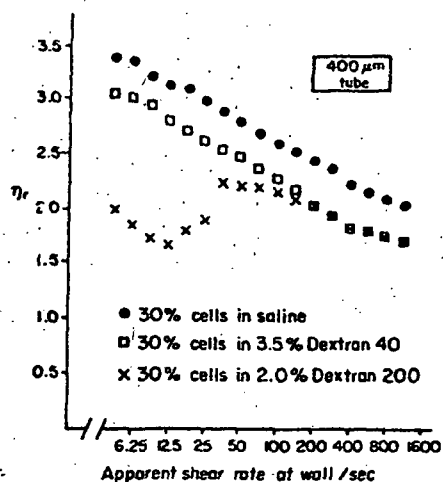


Figure 2: Relative flow resistance venous  $8\bar{U}$  (Reproduced with permission from [3].)

Two suspensions are of interest: cells in 3.5 Dextran 40 solution (where cell aggregation does not occur) and cells in 2% Dextran 200 solution (very strong aggregation); the suspending media have the same viscosities. At high flow rates ( $\bar{U} > 200 \text{ sec}^{-1}$ ) all cells are dispersed and the two suspensions show identical flow resistances; for  $\bar{U} < 200 \text{ sec}^{-1}$ , the aggregating suspension shows a lower flow resistance than the suspension of dispersed cells. Two comments need to be made about these experiments: (1) the red cell sedimentation velocity in the direction of flow is estimated to be significant compared to the fluid

flow velocity, and (2) this level of cell aggregation is probably at the high end of the range of pathological conditions. It would be worthwhile to repeat and extend this type of experimentation in a microgravity environment.

An additional question which needs investigation and which could be most easily studied in a microgravity environment is that of the extent of the entrance length in blood flow in vessels. Even in the absence of cell aggregation, radial redistribution of cells on entering a small vessel causes entrance lengths to be much longer than predicted on the basis of the behavior of continuum fluids, e.g., about 5000  $\mu\text{m}$  in a 25  $\mu\text{m}$  parallel plate channel [4]. Entrance lengths for blood flow, when stresses are low enough to permit red cell aggregation, can best be determined in the absence of sedimentation effects.

## II. Bifurcation Experiments

Hollow replicas of vascular bifurcations can be made in clear, rigid plastic blocks [5]. With these flow channels, one can then study blood flow through arterial and venous bifurcations.

In arterial bifurcations (blood flows into the junction through one vessel and leaves in two other vessels) in the microcirculation (vessel diameters less than about 100  $\mu\text{m}$ ), erythrocytes are not distributed between the downstream vessels in proportion to the blood flow rates. Since the Reynolds number is small (1-0.01), this is not due to inertial effects, but rather due to the nonuniform distribution of red cells across the feed vessel lumen and to cell-wall interactions. The physical laws governing red cell distribution at such bifurcations are not known. Investigation of this problem, for low flow rates where red cell aggregation occurs, could be best performed under microgravity conditions.

With the Reynolds number for microcirculatory blood flow so small, there is essentially no mixing between two convergent flows downstream from a venous bifurcation, even over an axial distance of a thousand vessel diameters. If the two convergent streams of blood have markedly different hematocrits, stratified flow persists downstream from the bifurcation. Bifurcations occur so frequently along a small vein,

that several layers could exist in the stratified flow. Some combinations of layers are unstable on earth, due to gravity; a few such flows could be studied in a low gravity field to establish the validity of theoretical models of such flows.

#### COMMENT

A natural question asks why such experiments should be performed under conditions which minimize sedimentation effects. After all, real circulatory systems operate in a one-g field. The answer is that usually sedimentation effects are not found in the body, except perhaps in slow venous flows. This is because an elementary volume of blood, as it flows, is continuously having its orientation in the gravitational field varied and the conditions under which it flows are continuously changing. The sedimentation effects, found in *in vitro* experiments, are therefore of our own making; this comes about for two reasons. First, the demands of experimental precision require us to make the flow channels long (e.g., long cylindrical tubes so that the pressure drops for physiologically relevant flow rates can be precisely measured with currently available instruments) with resultant blood residence times in the flow channels of the order of minutes, allowing significant cell sedimentation. Second, when performing experiments on systems composed of very small vessels (5-100  $\mu\text{m}$  ID), fluids must be brought into (and away from) the flow system through tubes which may be several inches long and in which the flow is very slow, again leading to complications due to sedimentation. These problems can be circumvented in a microgravity field.

#### ACKNOWLEDGEMENT

This paper is partly based on work performed under contract with the U.S. Department of Energy at the the University of Rochester Department of Radiation Biology and Biophysics and has been assigned Report No. UR-3490-1729 and under research grant HL-233355 from the National Heart, Lung and Blood Institute, NIH.

## REFERENCES

1. Merrill, E. W., A. M. Benis, E. R. Gilliland T. K. Sherwood and E. W. Salzman: J. Appl. Physiol., 20(5), 954-967 (1965).
2. Meiselman, H. J.: Ph.D. thesis, Dept. of Chem. Eng. Mass. Inst. Tech., Oct. 1965.
3. Palmer, A. A. and H. J. Jedrzejczyk: Biorheology, 12(5), 257-264 (1975).
4. Palmer, A. A. and W. H. Betts: Biorheology, 12(5), 283-292 (1975).
5. Meiselman, H. J. and G. R. Cokelet: Microvasc. Res. 9, 182-189 (1975).

GEOMETRICAL CONSIDERATIONS IN THE SEPARATION OF BIOLOGICAL PARTICLES  
BY AFFINITY PARTITIONING

Steven D. Flanagan  
Division of Neurosciences  
City of Hope National Medical Center  
Duarte, California

Highly specific and selective purification techniques are urgently needed in such diverse biological fields as immunology, the neurosciences, and cell biology. Often, only a very highly specific subpopulation of cell particles is required for a given clinical or basic research application. When purifying a specific particle population from an extremely heterogeneous mixture, only methods that are based upon the binding of specific ligands to membrane surface components are likely to yield the required selectivity. Affinity partitioning, a new separation technique, is based upon the distribution of biological particles between aqueous polymer phase systems (cf. D. Brooks) and has advantages over affinity chromatography in applications to the purification of cells and cell particles. In affinity partitioning separations, a specific ligand-polymer that binds to biospecific sites is added to the aqueous polymer phase systems. The binding of the ligand-polymer to a subpopulation of biological membranes changes the distribution of that subpopulation, thus effecting a selective change in distribution of the particles. Application of affinity partitioning to several interesting biological problems has been hindered by a lack of complete experimental and theoretical foundations for the technique. New ground-based and zero g experiments, designed to increase our experimental and theoretical understanding of affinity partitioning, are likely to yield new insights and will allow the application of affinity partitioning to a number of important biological problems. Geometrical considerations that may influence the distribution of biological membranes will be described.

ORIGINAL PAGE IS  
OF POOR QUALITY

GEOMETRICAL CONSIDERATIONS IN THE SEPARATION OF BIOLOGICAL PARTICLES  
BY AFFINITY PARTITIONING

Steven D. Flanagan  
Division of Neurosciences  
City of Hope National Medical Center  
Duarte, California

INTRODUCTION

Highly specific and selective purification techniques are urgently needed in such diverse biological fields as immunology, cell biology, and the neurosciences. Often, a highly specific subpopulation of cell or cell particles is required for clinical or basic research applications. When purifying a specific particle population from an extremely heterogeneous mixture, only methods that are based upon the binding of specific ligands to membrane surface components are likely to yield the required selectivity. Affinity partitioning (1-3) is a promising new affinity separation technique based upon the phase partition method for the distribution of biological particles between aqueous polymer phase systems (4). In affinity partitioning a specific ligand is covalently attached to one of the water soluble polymers that make up the phases. Binding of a ligand-polymer to biospecific binding sites selectively changes the distribution of particles that are rich in the binding sites. Affinity partitioning has advantages over affinity chromatography in applications to the purification of cells and cell particles. Often biological particles are bound irreversibly to the ligand matrices used in affinity chromatography. In affinity partitioning separations, the purified fractions are recovered from the phases by addition of sufficient water to break the phases, and concentrated by centrifugation. Unfortunately, application of affinity partitioning to several interesting biological problems has been hindered by a lack of adequate experimental and theoretical foundations for the technique.

THEORETICAL DESCRIPTION OF THE AFFINITY PARTITIONING EFFECT

The interfacial surface tension between the phases in typical poly(ethylene oxide)-dextran phase systems is from 0.001 to 0.1 dynes/cm. For cells and subcellular particles, the energy released by reduction of the interfacial surface area upon adsorption into the interface (surface tension X area of particle cross section) is many-fold  $3/2 kT$  (see figure). The energy transferred to cell particles by collisions with solvent molecules is on the order of  $3/2 kT$ . Therefore, cells and subcellular particles that distribute into the interfacial layer are not displaced by molecular collisions. In contrast, soluble proteins of molecular weight one million or less are not significantly bound in the interface because of their low cross sectional area. This considerably simplifies our task of developing a theory based upon thermodynamic considerations to describe the distribution of proteins containing biospecific binding sites. For a protein consisting of  $n$  binding sites, the distribution of the complex formed between the protein and  $n$  ligand-polymers is quantitatively described by the following expression (1):

$$K_{PL} = \left[ \frac{k_{aT}}{k_{aB}} \right]^n \cdot K_L^n \cdot K_o$$

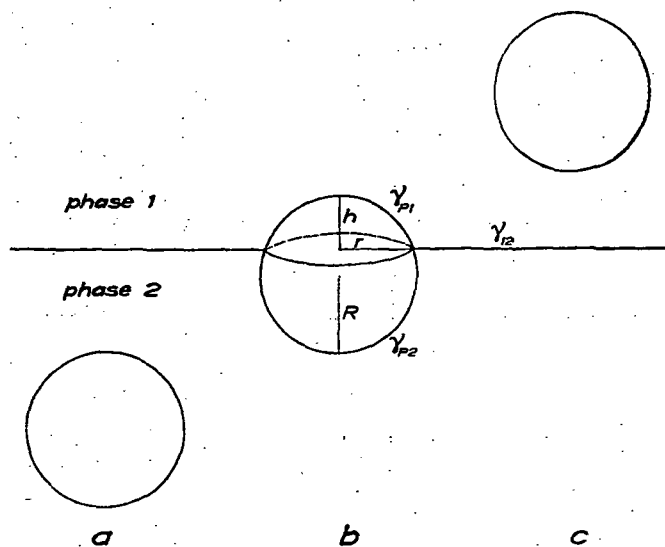
where  $K_{pL}$  is the partition coefficient of the complex,  $k_{aT}$  is the association constant of the complex in the top phase,  $k_{aB}$  the association constant in the bottom phase and  $K_L$  and  $K_O$  are the partition coefficients of the free ligand-polymer and protein, respectively. By substituting typical values into the

above expression ( $K_L=3$ ,  $K_O=1$ ,  $n=4$  and  $\frac{k_{aT}}{k_{aB}} \approx 1$ ), we find that  $K_{pL}=81$  and the

affinity partitioning effect is significant. This theory has been validated in a number of cases and appears to describe quantitatively the distribution of proteins containing biospecific binding sites.

Although affinity partitioning has proved useful in the purification of enzymes difficult to purify by affinity chromatography (5,6), its most promising applications are in the purification of intact cells and subcellular particles. Our efforts have been directed at the purification of membrane fragments enriched in cholinergic neurotransmitter receptors. Subcellular particles containing nicotinic cholinergic receptors from the electroplax of Torpedo californica are  $0.3\mu$  to  $0.4\mu$  in diameter, each containing 1,000 sites that bind cholinergic ligands or 30,000 per square  $\mu$ . If the above expression correctly approximates the affinity partitioning of subcellular particles, then even particles containing as few as ten binding sites should be easily separated from other particles by affinity partitioning.

Unfortunately, the above theory does not quantitatively describe the distribution of nicotinic cholinergic receptor-containing membranes. By blocking various fractions of the binding sites with  $\alpha$ -bungarotoxin, we have shown that at least 5,000 binding sites per square micron or 150 binding sites per particle are required for a significant affinity partitioning effect. Albertsson (4, pp 58-65)



A spherical particle at three different positions in a liquid two-phase system.  $\gamma_{12}$  is the interfacial tension between the two phases;  $\gamma_{P1}$  between the particle and phase 1; and  $\gamma_{P2}$  between the particle and phase 2.

From Albertsson (4).

ORIGINAL PAGE IS  
OF POOR QUALITY

concluded, based upon geometrical and thermodynamic grounds, that the distribution of particles between the interface and one of the phases is given by

$$\frac{C_{min}}{C_1} = \exp \left[ \frac{\pi R^2 (\gamma_{p2} - \gamma_{p1} - \gamma_{12})^2}{\gamma_{12} kT} \right],$$

where  $C_{min}$  is the number of particles per  $cm^3$  in a thin layer of the interface and  $C_1$  refers to the concentration of particles per ml in one of the phases. This formulation assumes that the surface tension energy released by a particle in the interface is on the order of  $3/2 \cdot kT$ , the translational energy of a molecule. Thus, in the limiting case, where the absolute value of  $\gamma_{p2} - \gamma_{p1}$  is much less than  $\gamma_{12}$ , the radius of a particle of 300 Å would release an interfacial energy on the order of  $3/2 \cdot kT$ . The radius 300 Å is calculated assuming a surface tension of 0.001 dyne/cm and a temperature (T) of 277 degrees Kelvin. Therefore, both  $\gamma_{12}$  and particle radius must be taken into account when evaluating the distribution of particles of radii larger than approximately 300 Å.

In affinity partitioning the value  $\gamma_{12}$  remains constant, but the value of  $\gamma_{p2} - \gamma_{p1} - \gamma_{12}$ , or  $\Delta\gamma$ , is changed upon the addition of the affinity partitioning reagents. The addition of the ligand-polymer produces a change which is equal to the density (d) of the binding sites times the energy ( $\epsilon$ ) contribution of each ligand-polymer bound to a specific site, i.e.,  $\Delta\gamma_f = \Delta\gamma_i + d\epsilon$ , where  $\Delta\gamma_i$  is the initial value in absence of affinity partitioning reagents and  $\Delta\gamma_f$  is the value in phase systems containing ligand-polymer. It is apparent that a substantial affinity partitioning effect is favored by the maintenance of  $\Delta\gamma_i$  as low in absolute magnitude as possible while striving to maintain  $\epsilon$  as large as possible. Since conditions have been achieved where particles as large as red blood cells partition between the phases and the interface, it was assumed that the value of  $\pi R^2 \cdot \Delta\gamma_i$  was on the order of  $kT$ . The value of  $\epsilon$  is estimated to be on the order of  $kT$  per binding site. Therefore, it was concluded that only a low density of binding sites should be required to achieve a significant affinity partitioning effect. That 10,000 per  $\mu^2$  is required indicates that one or more of the assumptions is not correct, and that nonideal considerations make a significant impact on the final result.

Possible explanations for the above discrepancy may be: 1) thermodynamic equilibrium is not achieved during the distribution of the particles among the phases and interface; 2) entropic effects on the binding of high densities of ligand-polymers to cell surface membranes are not considered; and 3) linear tension energies are not evaluated (7). Two experimental observations may help to resolve these points. First, microscopic observations indicate that the distribution of red blood cells in phase droplets is predominately into the droplet interface even when red blood cells ultimately are distributed into the top phase (8,9). This indicates that the final distribution of particles between the bulk phases and the microscopic distribution during phase separation are at variance. This may result in incomplete attainment of equilibrium during bulk phase separation. A second observation is that affinity partitioning separations are best achieved with systems near the critical point of the phase diagram, where the phases become almost equal in composition and isopycnic.

## EXPERIMENTS AT REDUCED AND ZERO X g

When phase systems near the critical point are compared with phase systems far from the critical point, two important parameters co-vary: the interfacial surface tension and the density difference between the phases. The density difference may be corrected by appropriate reduction of  $g$  forces. A further complication is the effect of phase droplet curvature on the microscopic distribution of biological particles. During phase separation driven by surface tension and gravitational forces the geometry of phase droplets is complex. Shortly after phase separation has begun at  $1 \times g$ , there is a large range in the distribution of droplet curvature at different depths in the tube. At the bottom of the tube, droplets of top phase are found surrounded by bulk bottom phase, while at the top of the tube the situation is reversed. The geometry is considerably simpler during phase separation at  $0 \times g$ , where phase separation is driven only by the reduction of interfacial surface area. The direction of the curvature at  $0 \times g$  is dependent on the overall ratio of the two phase volumes. As phase droplets collide, phase coalescence occurs. The average radius of phase droplets increases, and the biological particles interact with a relatively uniform population of phase droplets. Under these conditions we may expect the microscopic distribution of particles between the droplets to approach equilibrium as coalescence continues because, as the droplet radii increase, we approach a planar interface. Should the microscopic distribution depend on the curvature of the phase droplets, the distribution found after  $0 \times g$  incubation followed by  $1 \times g$  phase separation would be quite different from that observed when both processes occur at  $1 \times g$ . Further analysis of these interesting interfacial phenomena should lead to new theoretical insights which may be applied to  $1 \times g$  separation and help in the design of suitable phase systems for affinity partitioning of particles.

## REFERENCES

1. Flanagan SD & Barondes SH (1975) Affinity partitioning: A method for purification of proteins using specific polymer-ligands in aqueous polymer two-phase systems. *J. Biol. Chem.* 250, 1484-1489.
2. Flanagan SD, Taylor P & Barondes SH (1975) Affinity partitioning of acetylcholine receptor enriched membranes and their purification. *Nature* 254, 441-443.
3. Flanagan SD, Taylor P & Barondes SH (1976) Affinity partitioning of membranes: Cholinergic receptor-containing membranes from Torpedo californica. *J. Biol. Chem.* 251, 858-865.
4. Albertsson PA (1971) Partition of Cell Particles and Macromolecules, 2nd Ed., Almqvist and Wiksell, Stockholm.
5. Hubert P, Dellacherie E, Neel J & Baulieu E-E (1976) Affinity partitioning of steroid-binding proteins. *FEBS Lett.* 65, 169-182.
6. Chaabouni A & Dellacherie E (1979) Affinity partition of proteins in aqueous two-phase systems containing polyethylene glycol-bound ligand and charged dextran. *J. Chromatography* 171, 135-143.
7. Gershfeld NL & Good RJ (1967) Line tension and penetration of a cell membrane by an oil drop. *J. Theoret. Biol.* 17, 246-251.
8. Reitherman RW, Flanagan SD & Barondes SH (1973) Electromotive phenomena in partition of erythrocytes in aqueous polymer two-phase systems. *Biochim. Biophys. Acta* 297, 193-202.
9. Reitherman RW, Flanagan SD & Barondes SH (1973) Unpublished observations.

82 32070 76

CRYSTALLIZATION OF BIOLOGICAL MACROMOLECULES  
IN A REDUCED GRAVITY ENVIRONMENT

by

Edward J. Meehan, Jr. (a)

Application of the techniques of x-ray diffraction to crystal structures of biological macromolecules has been overwhelmingly successful. The three-dimensional molecular structure of over 70 proteins and the nucleic acid t-RNA<sup>phe</sup> have been determined (1). These structural studies, together with other biochemical techniques, have provided a molecular basis for understanding the biological activities of enzymes, hormones, antibodies, redox, and transport proteins.

There are, however, limitations associated with the use of x-ray diffraction studies that can be overcome using neutron radiation. The x-ray scattering factor of an atom is proportional to the number of electrons it contains, thus scatter from hydrogen is very weak. As a consequence, the positions of hydrogen atoms in macromolecules cannot be determined experimentally using x-ray radiation and can only be inferred from the locations of non-hydrogen atoms. Experimentally determined hydrogen positions would be valuable considering the importance of hydrogen bonding in maintaining protein and nucleic acid structures, and the putative roles of hydrogen atoms in the catalytic mechanisms of a number of enzymes. Neutrons, on the other hand, in non-magnetic materials are scattered by the nucleus and all atoms including light ones have significant scattering factors. Thus, the positions of hydrogen atoms in biological macromolecules could be determined using neutron diffraction techniques.

(a) Chemistry Department, The University of Alabama in Huntsville, Huntsville, Alabama 35807

There are other advantages offered by neutron radiation. Since it is non-ionizing, there is no radiation damage and the entire data set may be collected from a single crystal. X-ray induced radiation damage often necessitates the use of several crystals and data from individual crystals must be scaled together to obtain a complete data set. Absorption problems are minimized using neutron radiation, while useful anomalous dispersion effects are large. X-ray scattering factors also display a large dependence on scattering angle and fall off rapidly at high resolution, neutron scattering factors lack this strong angular dependence. More high resolution reflections should therefore be observable using neutrons, theoretically yielding more accurate results.

Despite all these advantages and the existence of excellent facilities for collecting neutron diffraction data, very few proteins have been examined using this technique. The difficulty and indeed the rate limiting step is the growth of single crystals of sufficient size. The neutron flux available at suitable wavelengths is approximately  $10^3$  times less than that available for x-rays. A high resolution x-ray study of a protein of approximately 50,000 molecular weight would require a crystal about 0.3 mm in all dimensions, while a neutron diffraction study would require a crystal in excess of 3 mm in all dimensions.

Methodologies need to be developed for growing large crystals required for neutron diffraction studies. The factors controlling nucleation and growth of simple systems such as crystals of metals and salts have received much attention, yet very little work has been done to understand these factors in protein systems. It is also difficult to extend the theoretical work obtained in these simple systems to biological macromolecules. The absence of a good theoretical model hinders efforts to obtain improved crystals; nevertheless, the importance of this class of molecules warrants their detailed study.

Current strategies for growing large protein crystals attempt to limit the number of nucleation sites and to very, very slowly approach the point of insufficient solvation. This is based on evidence demonstrating the correlation of crystal size and quality with the rate of growth. Amorphous precipitate or many small crystals are formed if the macromolecule is rapidly forced out of solution, while slower rates of growth result in larger, more perfectly formed crystals. The low gravity environment of space may have special advantages when trying to obtain low growth rates. In the absence of gravity driven convection and sedimentation, diffusion becomes the principle means of material transport. The rate of transport can then be controlled by the concentration of the diffusing substances and by the diffusion pathlength.

When attempting to crystallize a protein or nucleic acid, the crystallographer or biochemist must examine its solubility as a function of a number of parameters. These include the concentration of macromolecule, pH, temperature, ionic strength, choice of buffer, choice and concentration of "precipitating agent." Special cofactors, metal ions, or reducing agents may also be required.

The task then is to search this multiparameter space for solubility minima. The fact that proteins commonly grow in many different crystal forms demonstrates the possibility of many local minima (2,3). A battery of micro techniques have been developed which allow the screening of a large number of conditions using only a small amount of the macromolecule. Experience indicates that if a water soluble globular protein with molecular weight less than 100,000 can be isolated in sufficient quantity and purity, the chance of obtaining crystals are excellent. Once conditions that produce crystals have been determined, the task then is to grow them to sufficient size. Again, either micro or macro techniques can be used, and a wide variety of methods is available. These methods include diffusion techniques that could be readily adapted for flight experiments.

ORIGINAL PAGE IS  
OF POOR QUALITY

REFERENCES

- (1) T. L. Blundell and L. N. Johnson, Protein Crystallography, Academic Press, New York, N. Y. (1976).
- (2) R. Czok and T. Bucher, Av. in Prot. Chem. 15, 315 (1960).
- (3) J. T. Edsall, Proteins, Amino Acids and Peptides, E. J. Cohn and J. T. Edsall, eds., Reinhold, N. Y. (1950).
- (4) H. P. Avey, R. J. Poljak, G. Rossi and A. Nisonoff, Nature 220, 1248 (1968).
- (5) A. McPherson and A. Rich, Arch. Biochem. Biophys. 157, 23 (1973).
- (6) A. Jack, J. Weinzierl and A. J. Kalb, J. Mol. Biol. 58, 389 (1971).
- (7) J. B. Sumner, J. Biol. Chem. 37, 137 (1919).
- (8) S. Higashi and T. Ooi, J. Mol. Biol. 34, 699 (1968).
- (9) F. R. Salemme, Arch. Biochem. and Biophys. 151, 533 (1972).
- (10) J. Drenth and J. D. G. Smit, Biophys. Biochem. Res. Comm. 45, 1320 (1971).
- (11) C. H. Wei, J. Biol. Chem. 248, 3745 (1973).

PRECEDING PAGE BLANK NOT FILMED

3  
25  
N82 32071

FLOW AND THERMAL EFFECTS IN CONTINUOUS FLOW ELECTROPHORESIS

D. A. Saville  
Princeton University  
Princeton, N.J. 08544

P. H. Rhodes & R. S. Snyder  
George C. Marshall Space Flight Center  
Marshall Space Flight Center, Alabama

ABSTRACT

In continuous flow electrophoresis the axial flow structure changes from a fully developed rectilinear form to one characterized by meandering as power levels are increased. The origin of this meandering is postulated to lie in a hydrodynamic instability driven by axial (and possibly lateral) temperature gradients. Experiments done at MSFC show a noteworthy agreement with the theory.

## FLOW AND THERMAL EFFECTS IN CONTINUOUS FLOW ELECTROPHORESIS

D. A. Saville  
Department of Chemical Engineering  
Princeton University  
Princeton, New Jersey 08544

P. H. Rhodes and R. S. Snyder  
George C. Marshall Space Flight Center  
Marshall Space Flight Center, Alabama

### INTRODUCTION

In one application of continuous flow electrophoresis the objective is the *fractionation* of biological cell populations rather than separation. The problems encountered with cells arise from the fact that the mobility differences are very small and so large electric fields are required. In the chamber a buffer fluid is inserted at the top and the sample (which consists of a suspension of the biological cells in the buffer solution) enters just below the buffer inlet. As fluid moves through the chamber in a more or less laminar flow an electric field is applied across the flow. The purpose of the electric field is to move the particles laterally at a rate proportional to their mobility. Then, at the bottom of the chamber, a set of collection tubes picks up the various fractions. This technique has been highly developed for many purposes but relatively unsuccessful for the fractionation of cell populations.

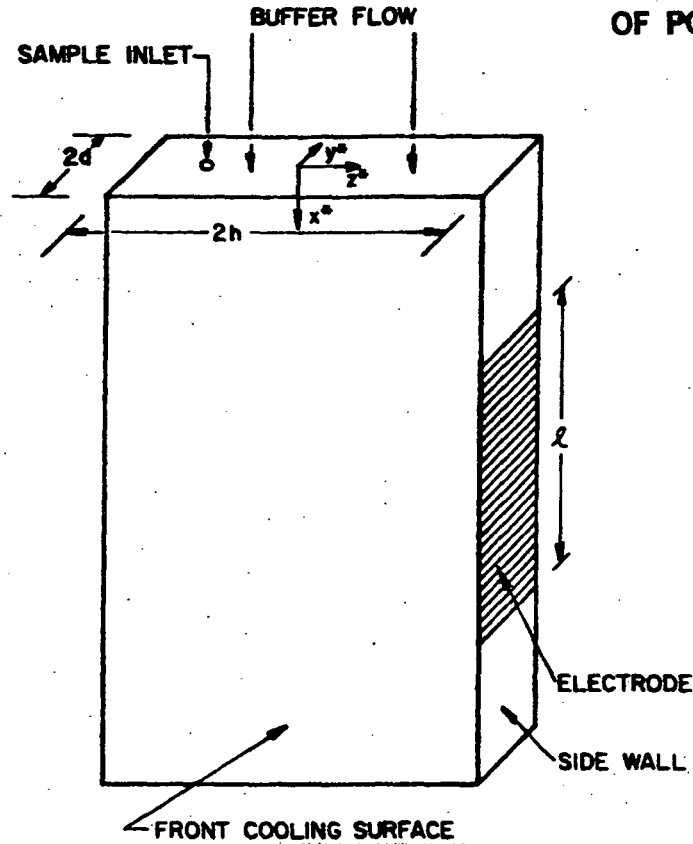


Figure 1. Chamber Schematic

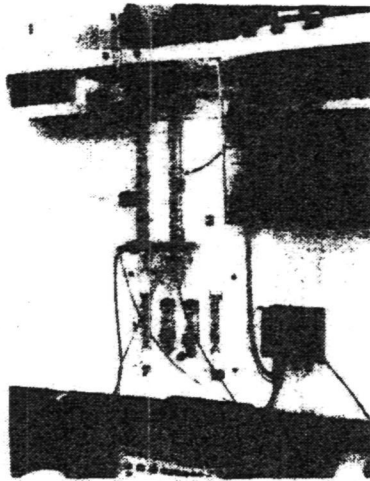
In the conventional device, one has the familiar parabolic velocity profile along with a similar temperature profile because of the applied electric field and the associated Joule heating. To restrict the temperature rise the thickness of the chamber is kept small with cooling on the front and rear faces. Difficulties arise from a phenomenon known as electro-osmosis. In the chamber cross-section the applied electric field acts on the diffuse charge along the front and rear surface to induce flow. Since the chamber is closed by electrode membranes at either end, there is a return flow down the center of the chamber. This flow deforms the sample cross-section and stretches it out into a crescent shape. The longer the sample stays in the device, the higher the electric field, and the larger the sample diameter compared to the chamber thickness, the more electro-osmosis works to thwart matters. Thus, when the fractions are collected at the bottom of the chamber, the fractionation is poorer than it might have been. To overcome this the chamber can be made thicker to decrease the electro-osmotic shear across the sample cross-section. This works up to a point but produces some severe scale-up problems.

Changing from the narrow gap device ( $\sim 1.5$  mm) to a wider one ( $\sim 5$  mm) increases the temperature rise by an order of magnitude. Thus a small increase of  $2-3^{\circ}\text{C}$  in the narrow gap device is raised to a value that is almost unsatisfactory from the standpoint of biological viability. More importantly, since the Grashof number is changed by the fifth power of the thickness ratio because of the Joule heating, buoyancy effects become very important. This changes the structure of the flow dramatically and makes it possible for the flow to be hydrodynamically unstable. Experiments show that as the power is increased, the sample stream begins to twist and meander. Eventually the performance is completely unsatisfactory for any sort of fractionation process.

#### HYDRODYNAMIC INSTABILITY

The instability seems to depend upon the orientation of the chamber and at one point it was argued as to whether this is a really an instability or related to some other phenomena associated with the hydrodynamics or characteristics of the chamber. A first order stability analysis was carried out wherein there is an *axial* temperature gradient [1]. Such gradients could arise from uneven heating or cooling or from entrance effects. It turns out, according to the analysis, that fluids confined laterally but un-confined above and below are very sensitive to hydrodynamic instabilities. Whereas the critical Rayleigh number for fluids confined between two horizontal plates is 1700, the critical Rayleigh number is 6 if the plates are vertical and the walls isothermal. If the walls are perfectly insulated, which means that any disturbance is reflected back into the chamber, the critical Rayleigh number becomes inversely proportional to the aspect ratio. For the chambers under study this ratio is  $10^{-2}$  and so the critical Rayleigh number is much smaller. Thus the temperature gradient required to produce the instability is only a fraction of a degree per centimeter.

ORIGINAL PAGE  
BLACK AND WHITE PHOTOGRAPH



(a) EQUIPMENT SET UP

- 1 BUFFER RESERVOIR
- 2 FLOW CHAMBER
- 3 BACK LIGHT
- 4 SYRINGE PUMP
- 5 DATA LOGGER (THERMISTOR VOLTAGE)
- 6 THERMISTOR SWITCH BOX
- 7 LEFT SIDE WALL COOLANT FLOW
- 8 REAR WALL COOLANT FLOW
- 9 FRONT WALL COOLANT FLOW
- 10 RIGHT SIDEWALL COOLANT FLOW

CHAMBER DIMENSIONS  
WIDTH 5.05 cm, HALFWIDTH, W - 2.53 cm  
ELECTRODE LENGTH, L 18.1 cm  
LENGTH 27 cm  
THICKNESS 5 mm  
ASPECT RATIO, 10:1

FIGURE 2. Experimental Apparatus

Experiments have been done at MSFC with the device shown schematically in Fig. 2. The dimensions of the chamber are 5 cm wide, 0.5 cm thick and 30 cm long. Neutrally buoyant colored particles are introduced through multiple ports at the top of the chamber and heating is produced by an alternating field which eliminates electro-osmosis. The flow is photographed and movable thermistors used to measure the temperature gradients in the fluid so as to determine whether the flow disturbances conform to the hydrodynamic instability suggested by the theory. The results of some of these experiments are in Figs. 3-6. The zero-power case shows rectilinear flow with no disturbances. Measuring temperature at all of the indicated positions gives the local Rayleigh number. As a power is applied, Fig. 4, one sees meandering of the sample streams. The buffer fluid is heated and cooled unevenly as it proceeds into the chamber and the buoyancy instability causes the redistribution shown. Temperature gradients measured internally turned out to be very close to the values predicted by the theory. Taking the velocity profile predicted by stability theory and superimposing this

ORIGINAL PAGE  
BLACK AND WHITE PHOTOGRAPH

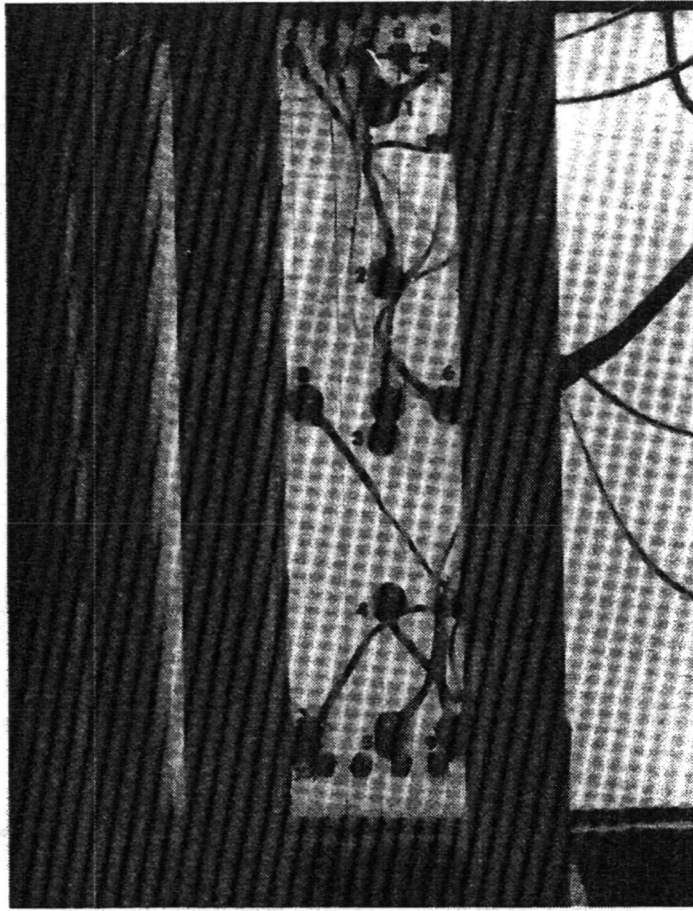


FIGURE 3. Flow at Zero Power Input



FIGURE 4. Flow at Power Input of 6.82 W.

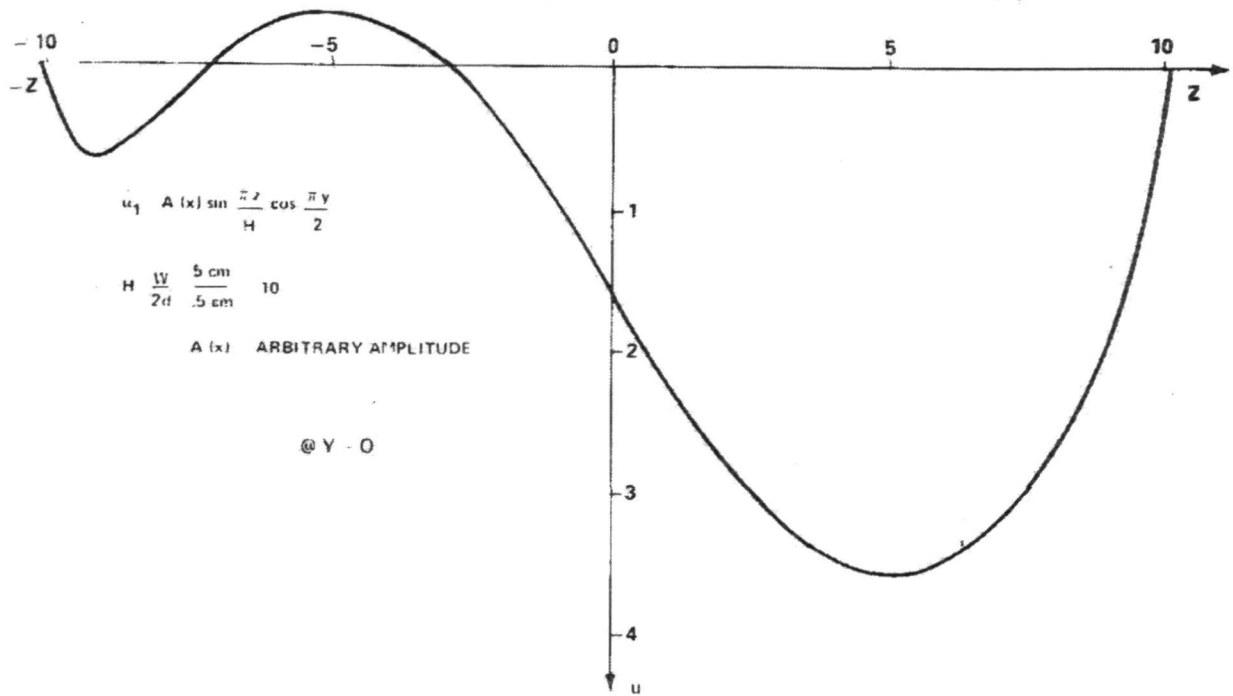


FIGURE 5. Superposition of antisymmetrical flow disturbance on the base flow.



FIGURE 6. Flow at power input of 7.52 W.

on the steady rectilinear flow produces the profile shown in Fig. 5 which displays a structure similar to that shown in the previous photograph. If the power is turned up to an even higher level, to produce a temperature rise of 2-3 °C between the center of the chamber and the wall, patterns shown in Fig. 6 are obtained showing the further development of the flow. We now believe the cause of the meandering phenomenon is a hydrodynamic instability arising from axial temperature gradients that are present because of uneven heating and cooling of one sort or another. Presumably these gradients could be suppressed if the cooling jackets were designed carefully. On the other hand, a microgravity environment reduces the effect of buoyancy and also circumvents the problem.

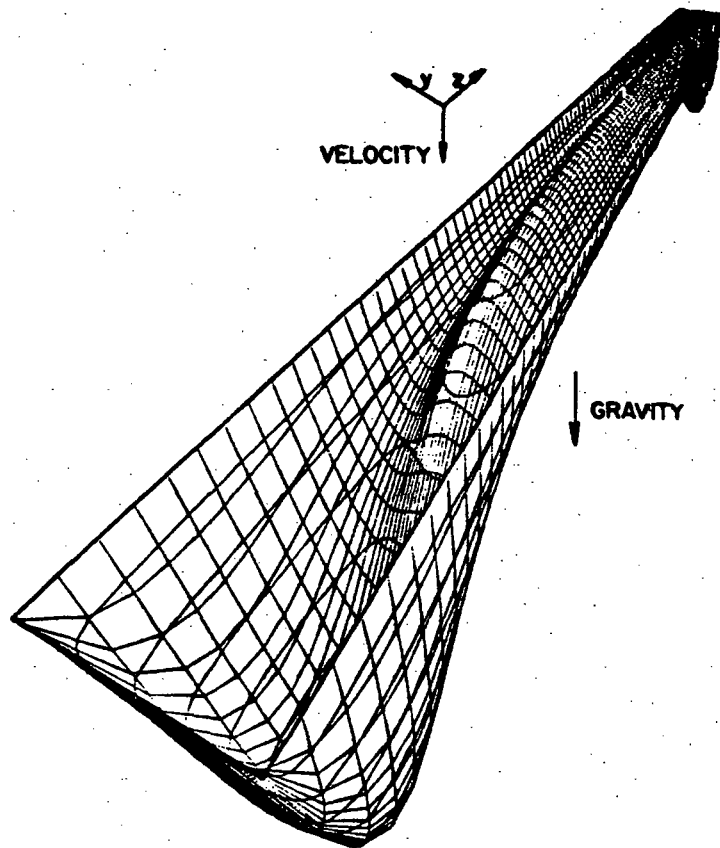


Figure 7. Axial Velocity Field at High Power Levels

ORIGINAL PAGE IS  
OF POOR QUALITY

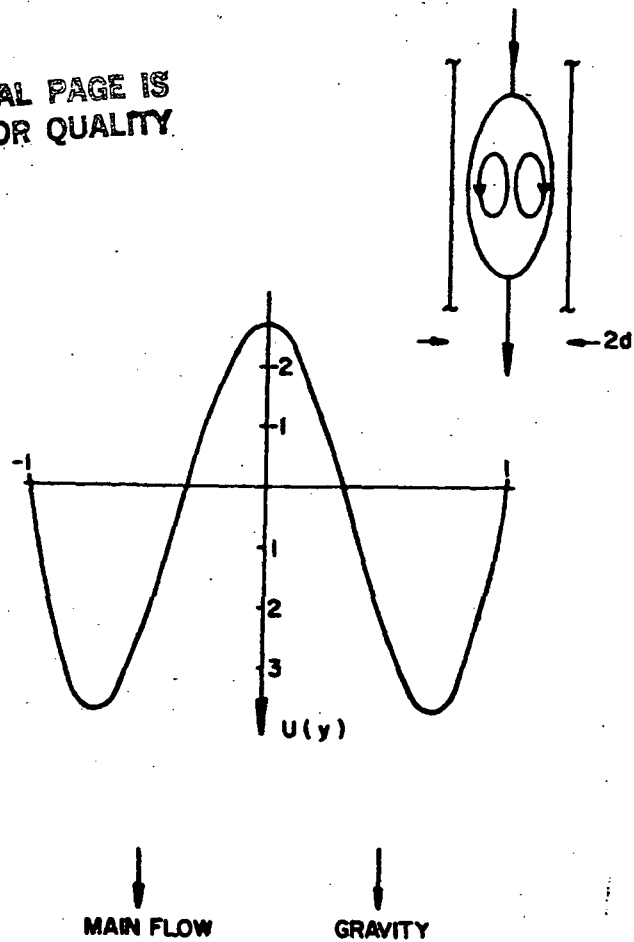


Figure 8. Axial Velocity Profile in Cross-section

Even if the heating problem is overcome the power increased without instability, the buoyancy forces still work against one. Figure 7 shows the velocity field in a cross-section of the chamber at power levels necessary to produce fractionation. Here there is so much Joule heating in the center that the buoyancy forces are large enough to cause a redistribution with downflow along the cold membranes on either side and upflow in the center. For a chamber of finite dimension, this means there is a recirculation. Figure 8 shows the same downflow configuration from the side showing clearly the large trapped eddy. Here any sample would move in and around this trapped eddy giving unsatisfactory results for any separation. In a micro-gravity environment, this recirculation would be absent.

We now understand enough about these instabilities to design an experiment to operate at low power levels in 1-g and at higher power in a micro-gravity environment which would enable us to verify the theory and the scaling laws.

REFERENCES

- [1] D.A. Saville and S. Ostrach, Fluid Mechanics of Continuous Flow Electrophoresis, Final Report on contract NAS-8-31349 Code 361. Prepared for the George C. Marshall Space Flight Center, Marshall Space Flight Center, Alabama.

SECTION D

CRYSTAL GROWTH EXPERIMENTS

N82 32072

21476

CRYSTAL GROWTH BY PRECIPITATION UNDER MICROGRAVITY\*

A.Authier, F. Lefauchaux, M.C. Robert  
Laboratoire de Minéralogie Cristallographie  
associé au CNRS, Université P. et M. Curie, Paris, France

ABSTRACT

After having stressed the importance of understanding the mechanisms associated with defect generation during growth and the influence of gravity, the experiment planned for FSLP is described. The advantages of adapting this experiment to the FES are then discussed. A brief survey of the ground based research under way is given.

\* Supported in part by the Centre National d'Etudes Spatiales, France

# CRYSTAL GROWTH BY PRECIPITATION UNDER MICROGRAVITY

A.Authier, F. Lefauchaux, M.C.Robert  
Laboratoire de Minéralogie Cristallographie  
Associé au CNRS, Université P. et M. Curie, Paris, France

## INTRODUCTION

The influence of growth defects on many physical properties is well known. Semiconductors, piezoelectrical, electrooptical, LASER crystals are good examples. It is therefore very important to learn how defects arise, how to control them and thus how to produce higher quality crystals. These crystals are grown by various methods, from the melt, from the solution or from the vapour phase. The nature of the defects produced during growth depends in general much more on which one of these growth techniques is being used and how far from thermal equilibrium growth is performed than on the actual chemical nature of the crystal. This is particularly true in the case we shall be dealing with in this paper, namely growth from the solution. It is therefore better to perform these studies on model crystals which are easiest and fastest to grow and are best fitted for the study of defects and the derivation of general laws on the generation of defects. It will of course be still better if these crystals have interesting physical properties which could be tested in crystals with different crystalline perfection and on crystals grown on earth and under microgravity conditions.

The major growth defects are growth bands and growth striations, growth sector boundaries, inclusions and dislocations (1),(2). Growth bands are many in nature, ranging from very thin defects nearly one atomic layer in thickness to layers in inclusions and to periodic variations of the lattice parameter associated to corresponding variations in impurity content or vacancy concentration. The origin of these defects is usually attributed among other causes to convectional instabilities associated to temperature gradients or to temperature fluctuations. The main factor for these convection effects is gravity which correlates temperature differences and mass transfers. The various parameters which govern the growth processes and on which the origin of growth defects depends are supersaturation, temperature, pressure, nature and velocity of the solution flux etc ... These parameters are not independent, in particular precisely because of the presence of gravity. In order to understand the influence of these various parameters on the generation of defects it is necessary to be able to vary them independently. A good way to do that is to perform the growth under microgravity conditions so that convection effects should be considerably reduced.

## PREVIOUS STUDIES ON THE RELATIONS BETWEEN GROWTH DEFECTS AND GROWTH CONDITIONS

Many studies have been performed in our laboratory on the characterization of growth defects and on the relations between growth conditions and growth defects. These experiments have been carried out on calcite (3), (4)(5), KDP and KDKP (6,(7), TGS (8), germanates (9), potash alum (10)(11). The various types of growth defects which may arise were identified. In many cases the relation between the growth rate of a face and the screw character of dislocations intersecting this face was clearly demonstrated. Different types of growth defects appear when a perturbation is voluntarily introduced at a given type during growth. Depending on the intensity of the perturbation it may be a very thin growth band or a growth band decorated with inclusions generating or not dislocation bundles. The influence of the solution flux on the generation of defects was established. In particular, it was shown that dislocations are formed on the side of the crystal facing the flux and that liquid inclusions are trapped at the backside which stop dislocation propagation. The development of these defects depends on the values of the supersaturation and of the flux rate and the influence of these parameters was systematically studied. The best quality crystals are obtained when the crystal is stationary with respect to the solution.

### DESIGN OF THE EXPERIMENT TO BE PERFORMED IN FSLP

In order to increase crystalline perfection convections should be avoided and growth performed in a purely diffusional system. It can be shown that growth rates would be extremely long in that case (12) unless a concentration gradient is imposed in some way. One way is to create a temperature gradient between the crystal seed and the solution as proposed by R. LAL (13) for the FES. This may however be the sources of inner stresses within the growing crystal. Another way is that used by D. LIND(14) for the growth of crystals by coprecipitation from the solution in ASTP. We had already used this technique for the study of the habit of calcite crystals depending on the nature of impurities (15).

The principle of the experiment is as follows. Two solutions AB and CD are contained in two compartments 1 and 2 separated by a third one containing a neutral solution N. At the beginning of the experiment compartments 1 and 2 are put in communication with the third one and the solutions AB and CD are allowed to diffuse in it. When they meet, a

reaction takes place of the type :

**ORIGINAL PAGE IS  
OF POOR QUALITY**



BD remains in the solution and AC which is very little soluble precipitates.

D. LIND'S set up in the following :

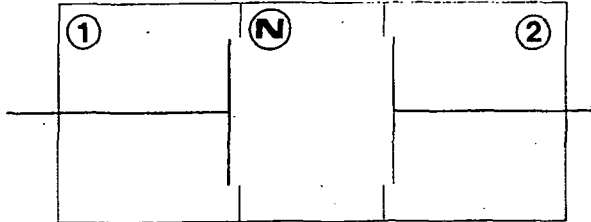


Figure 1

Two pistons are pulled back at the beginning of the experiments thus putting compartments 1 and N, and 2 and N in communication.

In the experiment which we shall perform in FSLP, we shall use a cell of a completely different design in a thermostat where the temperature will be constant to  $\pm 0.1^\circ \text{C}$ . In our design, compartments 1, 2 and N are concentric cylinders, 1 and 2 being annular and on the outside and N an inner cylinder :

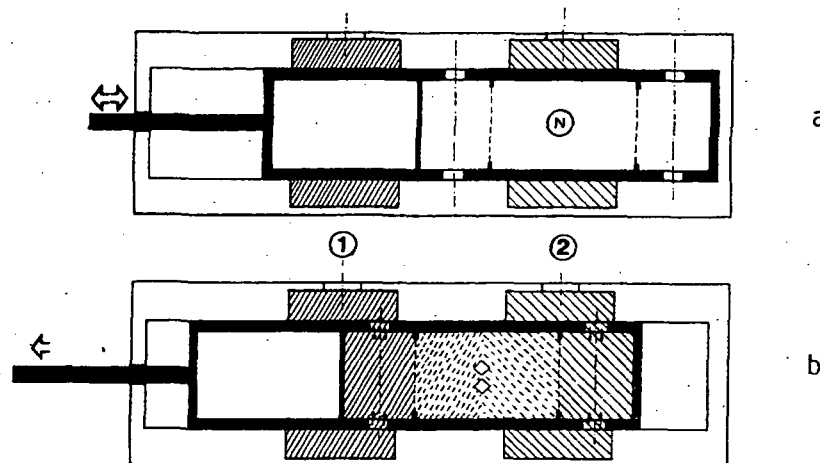
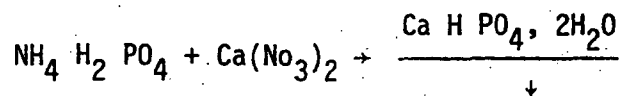


Figure 2

There are openings on the lateral side of the inner cylinder. Before the experiment starts, they do not lie in front of the outer compartments (fig. 2a). By translating the inner cylinder by means of a motor, the openings can be brought in front of compartments 1 and 2 (fig. 2b). Solutions AB and CD then diffuse in the inner compartment. Porous diaphragms on each side of the central reactive cell ensure that the solution flow is laminar. With this set up the compartments are put in communication at constant volume. Furthermore, the movement of the cylinder during the opening will be extremely slow (it will take about half an hour). For all these reasons there will be minimum perturbation of the diffusion flow during the opening process and afterwards. The dimensions of the cell have been determined after calculating the diffusion profiles in order to optimize maximum growth during the time allotted for the experiment (about 90 hours).

The crystals to be grown in the experiment are various phosphates of divalent cations, in particular calcium and lead. They have been chosen on one hand because they grow fast (it is possible to obtain crystal platelets one centimeter across in a few days) and in a shape which allows X-ray topographic studies of the as grown crystal without any cutting to be required, and on the other because they have interesting properties, either physical (lead phosphate is ferroelectric) or biological (calcium phosphate). In the future, other phosphates such as aluminum or lanthanum may also be considered because of their highly interesting physical properties. The type of chemical reaction which will be used will be, for instance in the case of brushite, of the type



#### GROUND BASED EXPERIMENTS

The present ground based research is carried out along two main directions. One is concerned with hydrodynamic studies and calculation of diffusion profiles. The other one is concerned with growth in purely diffusional conditions. A good way to achieve this result on earth is to use gel growth. We are using it for growing both brushite (16)(17) and lead phosphate. It has been checked that purely diffusional conditions have indeed been achieved in our experiments and that FICK's law applies to a very good accuracy, whatever the diameter of the tubes used for the

gel growth or the diffusion lengths. Several types of gels have been tested, with different densities and pH and the crystalline perfection is assessed in each case by X-ray topography. High quality crystals  $10 \times 10 \times 0.5 \text{ mm}^3$  have thus been obtained.

Furthermore, ground tests on the cell to be flown in FSLP are under way.

#### PROPOSED EXPERIMENT IN THE F.E.S.

The experimental set up available in the FES would allow us to perform simultaneously two types of experiments. The first one would be devoted to a continuous observation during the whole length of the experiment of the following growth parameters by means of the holographic system : solution flow and isoconcentration curves to be compared afterwards to calculated ones according to the diffusion theory, nucleation, position, number, growth rate and habit changes of the crystals, isoconcentration gradients around each crystal etc ... On the other hand, it would be extremely interesting to study the influence of a perturbation of the growth conditions on the growth and the generation of defects. This has already been shown in our earlier experiments and in a study by F. Mussard and S. Goldsztaub (18) who have grown sodium chlorate crystals under an interferometric optical microscope. They correlated local perturbations of the concentration gradient observed optically to the generation of dislocation bundles observed afterwards by X-ray topography and to a corresponding dramatic increase of the growth velocity of the face intersected by these dislocations. We therefore propose that the second experiment which could be performed would be study of a perturbation of a single growth parameter. The temperature would be maintained constant and a perturbation in the flow of matter would be introduced at half the time allotted to the experiment by traversing the inner cylinder respective to the outer compartment in order to cut the communication between compartments 1 and 2 and the neutral compartment and then to open it again. By means of the holographic system the perturbation of the solution flow and isoconcentration curves could be measured. X-ray topography of the crystals performed afterwards in the laboratory would show whether defects were generated due to the perturbation and of what nature.

## CONCLUSIONS

Microgravity provides unique conditions for the study of crystal growth and the understanding of the generation of growth defects as well as for the obtention of high perfection crystals. The facility available in FES is very well suited for these types of studies since the holographic system will enable a continuous observation of the growth conditions and any observed change can be correlated afterwards to the defects observed in the crystals by X-ray topography.

## REFERENCES

- [1] A.Authier, *J. Crystal Growth*, 13/14, 34 (1972)
- [2] A.Authier, *Crystal Growth and Materials*, p. 516, Ed. by E.Kaldis and H.J. Scheel, North Holland (1977)
- [3] F.Lefauchaux, M.C. Robert and A.Authier, *J. Cryst. Growth*, 19, 329 (1973)
- [4] N. Yu Ikornikova, F. Lefauchaux and M.C. Robert, *High Temperatures, High Pressures*, 6, 635 (1974)
- [5] F.Lefauchaux and M.C. Robert, *J. Crystal Growth*, 38, 29 (1977)
- [6] C.Belouet, E. Dunia and J.F. Pétroff, *J. Cryst. Growth*, 23, 243 (1974)
- [7] C.Belouet, M.Monnier, E. Dunia and J.F. Pétroff, *Mat. Res. Bull.*, 11, 903 (1976)
- [8] A.Izraël, J.F. Pétroff, A. Authier and Z. Malek, *J. Cryst. Growth*, 16, 131 (1972)
- [9] L.M.Demianetz, N.G. Duderov, A.N. Lobachev, F. Lefauchaux, M.C.Robert and A. Authier, *J. Cryst. Growth*, 44, 570 (1978)
- [10] S. Gits-Léon, F.Lefauchaux et M.C. Robert, *J. Cryst. Growth*, 44, 345 (1978)
- [11] S. Gits-Léon, M.C. Robert and A.Zarka, *Bull.Minér.*, 101, 399 (1978)
- [12] B.Simon, *J. Cryst. Growth*, 43, 640 (1978)
- [13] R. Lal, NASA Technical Memorandum TM 78214 p.25 (1978)
- [14] M.D. Lind, A.S.T.P. Preliminary Report, NASA TM X-58173, p.30-1,(1978)
- [15] F. Lefauchaux, *Bull. Soc. fr. Minér. Crist.*, 94, 2 (1971)
- [16] F. Lefauchaux, M.C. Robert, H. Arend, *J. Cryst. Growth*, 47 (1979)
- [17] F. Lefauchaux, M.C. Robert, E. Manghi, H. Arend, Poster session ECCG 2, Lancaster 1979
- [18] F. Mussard and S. GOLDSZTAUB, *J. Cryst. Growth*, 13/14, 445 (1972)

16  
N82 32073

MORPHOLOGICAL STABILITY OF A CRYSTAL GROWING IN SOLUTION

Dennis Elwell  
Center for Materials Research  
Stanford University  
Stanford, CA 94305

ABSTRACT

A brief outline is given of the problem of the stability of growth of a polyhedral crystal growing in solution in the presence of supersaturation inhomogeneity. An experiment is proposed for a low gravity environment which should provide data for confrontation with the various theoretical approaches to this problem. The validity of this data rests on the assumption that growth occurs in a convection-free environment.

## MORPHOLOGICAL STABILITY OF A CRYSTAL GROWING IN SOLUTION

Dennis Elwell  
Center for Materials Research  
Stanford University  
Stanford, CA 94305

### INTRODUCTION

The importance of satellite experiments in the crystal growth area is primarily that experiments may be performed under conditions where the fluid dynamics is well characterized. In the case of solution growth, the absence of convection is expected to be a handicap in growing large crystals, since the maximum rate of stable growth may be unreasonably low for practical purposes. The most likely method to be used for routine solution growth in low gravity is the isothermal solution reaction technique which seems appropriate for difficult biological and other organic crystals. However, the greatest value of the Space Shuttle for solution growth is more probably for testing models of the growth process and so for improving our understanding of growth mechanisms. Morphological stability is one example of an important area where few detailed and careful experiments have been performed.

### THE PROBLEM IN OUTLINE

Crystals grown from solution are normally polyhedral because of the strong tendency to form low-energy facets. If the resulting polyhedron is to grow in a stable regime its shape will not change with time and the theoretical problem of predicting the conditions for the morphological stability has received considerable attention. If the crystal does not grow in a perfectly stirred solution, the supply of solute varies across any face of the crystal between the face center and the edge, and interferometric measurements such as those of Bunn (1949) indicate that this supersaturation inhomogeneity can be as high as 25 percent. As a result of the higher supersaturation at the edges, crystals tend to develop dendritic forms when grown at high rates or to exhibit terraces stepped from the center to the edges (the so-called "hopper" morphology) when grown under less unstable conditions.

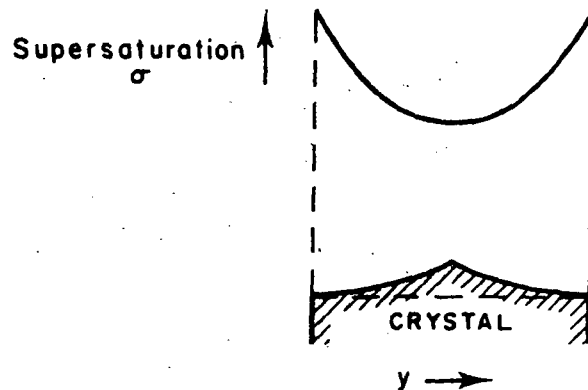


Figure 1: Supersaturation inhomogeneity and compensating change in slope for a crystal face (after Chernov, 1972).

The onset of a terraced growth form limits the rate at which crystals can be grown and so it is important for crystal growers to be able to predict the growth rate at which this instability occurs. Theoretical approaches to solving this problem normally rely on the assumption that solute is transported over the crystal surface only by diffusion in the solution. Cahn (1967) took as his condition for the onset of instability the requirement that the supersaturation should not fall to zero at the face center. He arrived at the following expression for the maximum rate of stable growth:

$$v_{\max} = \frac{D(n_s - n_e)}{\ell\rho} \quad (1)$$

where  $D$  is the solute diffusion coefficient,  $n_s$  the solute concentration in the bulk solution and  $n_e$  the equilibrium value,  $\rho$  the density of the crystal and  $\ell$  the length of the face. For a 1cm crystal,  $D = 10^{-5} \text{ cm}^2 \text{ s}^{-1}$ ,  $n_s - n_e = 5 \times 10^{-2} \text{ g cm}^{-3}$  and  $\rho = 5 \text{ g cm}^{-3}$ , this gives  $v_{\max} \approx 10^{-7} \text{ cm s}^{-1}$  which is lower than experimental values by two orders of magnitude. This discrepancy may be due to convection in the solution or to the stabilizing effect of the interface kinetic mechanism by which the crystal grows.

This latter aspect was considered in more detail by Chernov (1972) who proposed that the supersaturation inhomogeneity may be partially compensated by a variation across the crystal surface in the kinetic coefficient which relates the growth rate to the local value of the supersaturation (see Fig. 1). A higher than average value of the kinetic coefficient is to be expected at the face center because of the tendency of dislocations to propagate from the center of the crystal in a direction normal to the surface.

More recently Wilcox (1977) reviewed the morphological stability of a cube growing in a convection-free solution and gave a careful analysis of the factors governing instability. Numerical calculations were made by Kuroda et al (1977) who presented data in the form of limiting supersaturation for stable growth as a function of crystal size.

#### EXPERIMENTAL TEST

Spacelab presents an ideal opportunity to test these various treatments of morphological instability since it will permit the measurement of the limiting linear growth rate (or supersaturation) for stable growth under diffusion-limited conditions. For this experiment to be valid, it must first be established that the Fluids Experimental System can give convection-free conditions for long periods in orbit. In principle such experiments could be made under convection-free conditions on earth (see the proposed cell of Tiller, 1968) but confirmed success in growing crystals under conditions of pure diffusion is still lacking.

One practical advantage of morphological stability experiments in Spacelab (rather than experiments aimed at the growth of perfect crystals) is that the growth rate is relatively rapid so that the rather short time normally available for experiments is not a serious limitation.

Sodium chlorate  $\text{NaClO}_3$  would appear a suitable choice as the material for this investigation since it grows as crystals of cubic shape and there exist a number of good experimental studies of its growth, including concentration profiles in the solution by an interference method (Mussard and Goldsztaub, 1972). In addition, the most detailed study to date of the role of convection in solution growth (Chen et al, 1979) was made on this material.

A particular aspect which could be investigated in this experiment is the profile of the crystal surface using Tolansky interference microscopy. This technique permits the determination of the slope of the crystal surface to the crystallographic habit plane by the use of monochromatic multiple reflection fringes (Tolansky, 1969). In principle it would be desirable to measure the surface profile during growth, but the optical requirements of such a measurement conflict with those for observation of solute concentration profiles within the liquid. A recent study of yttrium aluminum garnet crystals grown from high temperature solution (Roberts and Elwell, 1979) showed inclinations to the habit plane of 21-54' according to whether the hillocks were of polygonal or elliptical shape and also depending on the crystallographic face considered and the direction within the face. In some cases the slope was found to decrease with distance from the hillock center.

At a later stage of studies in low gravity, it would be desirable to study the morphological stability of a crystal in a unidirectional flow of solution. The measurement of a maximum stable growth rate as the solution is swept across one face of the crystal has become particularly important since Janssen and Bennema (1977) drew attention to the importance of hydrodynamic eddies in inclusion formation.

The practical goal of a sound theory of morphological stability in crystal growth is that it becomes possible to devise optimum programs relating the crystal growth rate to its size as growth proceeds. Temperature programming for solution growth was considered by Scheel and Elwell (1972) using an approximate theory for the maximum stable growth rate but a refined treatment could lead to considerable savings in time and energy if used on a wide scale.

#### REFERENCES

- [1] C. W. Bunn, Disc. Faraday Soc., 5, 132 (1949).
- [2] J. W. Cahn in "Crystal Growth" (Ed. H. S. Peiser) Pergamon, Oxford (1967) p. 681.
- [3] P. S. Chen, P. J. Shlichta, W. R. Wilcox, and R. A. Lefever, J. Crystal Growth 47, 43 (1979).
- [4] A. A. Chernov, Soviet Phys. Crystallog. 16, 734 (1972).
- [5] R. Janssen-van Rosmalen and P. Bennema, J. Crystal Growth 42, 274, (1977).
- [6] T. Kuroda, T. Irisawa, and A. Ookawa, J. Crystal Growth 42, 41 (1977).
- [7] F. Mussard and S. Goldsztaub, J. Crystal Growth 13/14, 445 (1972).
- [8] K. J. Roberts and D. Elwell (1979) to be published.
- [9] H. J. Scheel and D. Elwell, J. Crystal Growth, 12, 153 (1972).
- [10] W. A. Tiller, J. Crystal Growth, 2, 69 (1968).
- [11] S. Tolansky, Metallography, 2, 1 (1969).
- [12] W. R. Wilcox, J. Crystal Growth, 38, 73 (1977).

6  
N82 32074

ANOMALOUS GROWTH OF SINGLE CRYSTALS IN SOLUTION

William N. Gill  
Chemical Engineering Department  
State University of New York at Buffalo  
Amherst, New York 14260

ABSTRACT

It is shown that major discrepancies exist between experiments and theory for ice crystal growth from solution. Accurate data, taken in a microgravity environment, approximate analytical models, and exact (probably numerical) models all are needed to advance our understanding of ice crystal growth phenomena.

A new approximate semi-empirical theory is presented which predicts that a relatively sharp transition from natural convection control to diffusion control for ice growth in pure water occurs at a subcooling of about  $10^{\circ}\text{C}$  (a reduced temperature difference of about 0.125). No reliable data exist to test this prediction. The theory also predicts qualitatively the growth of ice in NaCl solution in which maxima in the growth rates are observed at various levels of subcooling.

For pure water the exponent on the subcooling ( $n$ ) predicted by Equation (11) when cast in the form of Equation (1) is 1.9, which is in reasonable agreement with the experimental value.

## ANOMALOUS GROWTH OF SINGLE ICE CRYSTALS IN SOLUTION

William N. Gill  
Chemical Engineering Department  
State University of New York at Buffalo  
Amherst, New York 14260

The purpose of the proposed single crystal ice growth experiment is to clarify the roles of thermal and concentration driven convection in crystal growth by measuring growth rates, crystal shape, and temperature and concentration fields in the neighborhood of the single crystal, in the microgravity environment of space, by using shadowgraphs, Schlieren and other optical techniques. It is expected that these data, taken in certain critical ranges of the operating parameters, will help to explain the more serious discrepancies which exist among the various theories of crystal growth and the best available data.

Ice crystal growth rates usually are represented by an equation of the form

$$v = a\Delta T^n \quad (1)$$

where  $v$  is the growth velocity and  $\Delta T$  is the subcooling. Ivantsov's theory predicts  $n = 3$  for parabolic platelets. The best experimental values of  $n$  for growth in quiescent water are closer to 2.17. Recent experimental results of Barduhn and Kallungal (1977) have shown ice growth rates to depend on crystal orientation with respect to the gravitational field, and observed rates are an order of magnitude larger than Ivantsov's theory predicts.

Growth rates in the  $a$ -axis direction are controlled by heat and mass transfer; crystal formation kinetics play no part. Observed growth rates depend on the salt concentration of the solution and growth rate maxima are observed with about 1% salt solutions. All of this provides convincing evidence that thermal and concentration driven convection play a major role in the growth of ice crystals despite their small size. However, no adequate theory exists to describe these phenomena.

There are fundamental differences between the best data available on ice and succinonitrile and the theories of crystal growth which have been developed. The data of Barduhn and Kallungal (1977) for ice and those of Glicksman, Shaefer and Ayers (1976) for succinonitrile show that the tip radius,  $R$ , varies as the reciprocal of under cooling so that

$$R = A\Delta T^m \quad (2)$$

where  $m \approx -1$ . However the linear stability theory of Langer and Muller-Krumbhaar (1978) predicts a much larger negative value for  $m$  which is closer to  $-2$ . This is shown in Langer and Muller-Krumbhaar's Figure 4 which, being a log-log plot, tends to make the differences between theory and experiment less obvious. On the other hand the maximum velocity principle predicts  $m = -1$ , which is in accord with experimental data. Unfortunately the maximum velocity assumption significantly underestimates  $A$ .

The Langer-Krumbhaar theory predicts the tip velocity data of Glickman et al. better than the tip radius data with deviations tending to get larger as under cooling increases. This seems to illustrate that linear stability theory often is a useful guide, but seldom is a definitive statement on the quantitative behavior of real systems.

Fernandez and Barduhn (1967), Vlahakis and Barduhn (1974), Simpson et al. (1974), Kallungal and Barduhn (1977) and Huang (1975) have studied various aspects of ice crystal growth in forced convection systems with velocities up to 70 cm/sec. Equation (1) continues to apply here except  $n = 3/2$  as predicted by Fernandez using boundary layer theory (and the maximum velocity principle) and observed experimentally provided the forced velocity is large enough. Equation (2) also applies to forced convection; as before  $m$  is observed and predicted to be  $-1$ . However the maximum velocity principle again predicts values of  $A$  which are too low by a factor of 3 or 4 for ice. The data show conclusively that tip radius is independent of forced flow velocity over six orders of magnitude; it also is independent of crystal orientation.

The data on ice growth in a quiescent ambient fluid clearly are influenced by natural convection as evidenced by their sensitivity to crystal orientation. No adequate theory, which includes thermal convection, has ever been proposed to describe ice crystal growth even in pure water and the situation is complicated markedly when the crystals are grown in saline solution. The difficulty of constructing an exact theory, in the

sense of obtaining exact solutions of the transport equations, is illustrated by the interesting article of Kroeger and Ostrach (1974) on a model which simulates a casting problem and includes forced and natural convection.

Models which include exact solutions of the relevant transport equations are needed and should be worked on. However, in the meantime it may be possible to gain further insight into crystal growth, including thermal convection, by constructing approximate models which perhaps are viewed best as "order of magnitude estimates" of the real phenomena occurring. One such possible approximate approach, which appears to be new, and which includes both thermal convection and the moving boundary effect will be sketched here.

Consider for illustration a crystal growing as a parabolic platelet. A heat balance on the crystal, which will be assumed to be isothermal, gives

$$v = h \frac{T_i - T_\infty}{\rho_c L} = Nu \frac{k(T_i - T_\infty)}{R \rho_c L} \quad (3)$$

where  $Nu = \text{Nusselt number } \left(\frac{hR}{k}\right)$ ,  $k = \text{thermal conductivity of the solution}$ ,  $L = \text{latent heat of fusion}$ ,  $\rho_c = \text{crystal density}$ ,  $T_i$  and  $T_\infty = \text{interfacial and ambient temperatures of the fluid}$ . From the Ivantsov theory, as discussed by Horvay and Cahn (1961), if  $p \ll 1$ , we find

$$p = \frac{vR}{2\alpha} = \left[ \frac{C_p (T_i - T_\infty)}{L \sqrt{\pi}} \right]^2 \quad (4)$$

where  $C_p = \text{heat capacity of the melt}$  and  $\alpha = \text{thermal diffusivity}$ . Thus, if we assume density differences between the crystal and solution are small, Equations (3) and (4) lead to

$$Nu = Nu_{M.B.} = \frac{2}{\pi} \frac{(T_i - T_\infty)}{L/C_p} \quad (5)$$

where the subscript M.B. denotes moving boundary and this Nusselt number reflects two dimensional heat conduction in the melt with the "apparent convection" created by a moving boundary.

Obviously (5) tells only part of the story; it neglects thermal convection entirely. For a parabolic platelet, even with a fixed boundary, it is a formidable job to solve the thermal convection problem with the two dimensional conduction which must be included in the low Rayleigh number ( $Ra$ ) systems encountered in crystal growth. However, some information

can be obtained very easily from the experimental results of Gebhart and Pera (1970) on heat transfer at low Ra from circular cylinders of very small diameter. These data should be relevant to ice growth if heat transfer at the stagnation point of the tip of the parabolic platelet does indeed control the growth process. The correspondence between Fernandez's forced convection theory, which employs the tip radius as the characteristic dimension, and the experimental growth rate data lends considerable credence to this assumption. One can show (for  $Ra < 10^{-4}$ ) from Gebhart and Pera's data that the Nusselt number due to two dimensional conduction and natural convection is

$$Nu_{N.C.} \approx 0.47 Ra^{0.075} \quad (6)$$

where

$$Ra = \frac{\beta g R^3 (T_i - T_\infty)}{\nu \alpha}$$

$\beta$  = thermal conductivity,  $g$  = gravitational constant,  $\nu$  = kinematic viscosity.

Equation (6) is very different from the conventional boundary layer result,  $Nu_{N.C.} \approx 0.5 Ra^{1/4}$ , which grossly underestimates heat transfer rates at very low Ra. If one uses the boundary layer approach, then an arbitrarily enlarged length scale is needed to obtain even qualitative agreement between theory and experiment.

Churchill (1977) in numerous papers has discussed the accuracy of combining rules for finding the Nusselt numbers for "mixed mode convection" among other things. Ruckenstein (1978) has provided a theoretical justification for Churchill's procedure. If we consider natural convection and the moving boundary as two processes competing for dominance, which seems plausible but doesn't seem to have been done before, Churchill's work would suggest that a reasonable approximation can be obtained from

$$Nu^3 = Nu_{M.B.}^3 + Nu_{N.C.}^3$$

or

$$Nu = [Nu_{M.B.}^3 + Nu_{N.C.}^3]^{1/3} \quad (7)$$

Therefore, one obtains using (3), (5), (6), and (7),

$$\nu \approx \left[ \left( \frac{2 \Delta T}{\pi L/C_p} \right)^3 + 0.10 \left( \frac{\beta g R^3 \Delta T}{\nu \alpha} \right)^{0.225} \right]^{1/3} \frac{k \Delta T}{R P_c L} \quad (8)$$

where  $\Delta T = T_i - T_\infty$ . Obviously (8) cannot be viewed at this stage as anything

more than a plausible speculation. However, Equation (8), and other expressions like it which can be derived in a similar fashion, deserve the effort of being compared with experimental data and perhaps modified accordingly.

It is worth noting that if  $Nu_{M.B.} = 2Nu_{N.C.}$ , then  $Nu_{M.B.} = 0.96Nu$ . Even if the factor is 1.25 rather than 2, one gets  $Nu_{M.B.} = 0.87Nu$ . That is, when either of the Nusselt numbers is larger than the other, the mode representing the larger one dominates the process. This can be used to determine the  $\Delta T$  above which natural convection is negligible by setting  $Nu_{M.B.} > Nu_{N.C.}$  and solving for  $\Delta T$  to obtain  $\Delta T \approx 10^\circ C$ . If we had used boundary layer theory, we would have obtained  $\Delta T \approx 0.5^\circ C$  which, on the basis of Kallungal's data, is too small. Unfortunately, reliable data for  $\Delta T$ , equal to 10 or more, do not exist to check this prediction. It also is worth noting that  $Nu_{N.C.}$ , at the very low Ra, is insensitive to the value of Ra. For example,  $Nu_{N.C.}$  changes only by a factor of 2, while Ra changes by  $10^4$ . However, depending on ones purposes, this change may be enough, as noted above, to cause Nu to be dominated by  $Nu_{M.B.}$ .

The forced convection ice crystal growth data for pure water are in good agreement with the theory of Fernandez and Barduhn (1967) if the flow Reynolds number based on tip radius is high enough. However, the experimental values of tip radius are about four times larger than the theory predicts. That is, theory and experiment show that m, in Equation (2), equals minus unity, but the experimental value of  $A = 0.6$ , is about four times the theoretical one; the reasons for this are unknown.

In the subcooling range of  $0^\circ C$  to  $1^\circ C$ , Kallungal and Barduhn (1977) found experimentally that the forced convection growth theory predicts growth rates in pure water down to a Reynolds number, based on tip radius, of  $5 \times 10^{-3}$ . If one examines carefully the data of Gebhart and Pera (1970) on mixed convection heat transfer to fine wire circular cylinders, one finds that natural convection alters forced convection by about 3% when

$$Re = 0.5 Gr^{1/4}$$

The Grashof number, based on experimental values of ice crystal tip radius, is

$$Gr = \frac{0.5 \times 10^{-10}}{\Delta T^2}$$

Thus, for  $0.1 \leq \Delta T \leq 1$ , one gets

$$1.3 \times 10^{-3} \leq Re \leq 4 \times 10^{-3}$$

Consequently, on the basis of mixed convection heat transfer data, one indeed would expect natural convection to influence forced convection ice crystal growth rates in the  $Re$  range where the forced convection theory was found to fail.

The problem of growing ice crystals in saline ( $NaCl$ ) solution is much more complicated and no theories have been proposed which even describe the experimental data qualitatively. The important facts are: growth rates increase substantially up to salt concentrations of about 1%; the tip radius no longer is inversely proportional to  $\Delta T$ ; the location of the density maximum depends on concentration.

Actually, some simple calculations can shed considerable light on the influence of solute concentration on crystal growth rates. Equation (3), together with its counterpart for mass diffusion, yields

$$\frac{C_{\infty}}{C_i} = 1 - \left(\frac{Nu}{Sh}\right) \left(\frac{Sc}{Pr}\right) \frac{C_p (T_i - T_{\infty})}{L} \quad (9)$$

where  $Sh =$  Sherwood number  $\left(\frac{k_d R}{D}\right)$ ,  $Sc =$  Schmidt number  $\left(\frac{\nu}{D}\right)$ ,  $D =$  diffusion coefficient,  $k_d =$  mass transfer coefficient,  $C_i$  and  $C_{\infty} =$  interfacial and ambient concentrations of solute. Equation (9) shows that  $C_i > C_{\infty}$  and that this "concentration polarization" increases with subcooling. Obviously then, the extent of freezing point depression increases with subcooling. If forced convection dominates, to a reasonable approximation  $(Nu/Sh) \approx (Pr/Sc)^{1/3}$  where  $Pr \approx 13.5$ ,  $Sc \approx 2600$  for ice-water- $NaCl$  systems. Since  $T_i$  is the equilibrium freezing temperature, corresponding to  $C_i$  (taking into account the Gibbs-Thompson curvature effect and freezing point depression), Equation (9) completely determines  $C_i$  once  $T_{\infty}$  and  $C_{\infty}$  are specified. Furthermore, the magnitude of  $C_i$  increases, as does the freezing point depression, as  $C_{\infty}$  increases. Thus, with pure forced convection, the only effect of the concentration field is to create a freezing point depression, and one expects the growth rate for a given subcooling to decrease as  $C_{\infty}$  increases (subcooling,  $\Delta T$  is defined as  $T_E - T_{\infty}$ , where  $T_E$  is the freezing point at  $C_{\infty}$ ). In effect, as  $C_{\infty}$  increases a greater fraction of  $\Delta T$  is consumed by the freezing point depression and Gibbs-Thompson curvature and less is left to drive the

crystallization process. This is precisely what Huang (1975) has observed experimentally, and the forced flow velocity necessary for forced convection to dominate was between 10 and 60 cm/sec, which is much higher than those necessary in the absence of salt. Below this velocity, maxima were observed in the plots of growth rates versus  $C_{\infty}$ .

Clearly, the maxima in the growth rates must be due to natural convection induced by concentration differences. Much larger density differences are created by concentration than temperature differences and concentration differences increase with  $C_{\infty}$  for a given subcooling. Also, the Rayleigh number for mass diffusion is about 200 times that for heat transfer if they both are based on the same density difference. All of this means that natural convection created by concentration differences will be very strong and will increase with  $C_{\infty}$ . Consequently, a competition is set up between the freezing point depression effect, which decreases growth rates, and the augmented transfer by natural convection, which increases growth rates. Apparently, natural convection wins at  $C_{\infty}$  less than 1% and freezing point depression prevails about 1% salt by weight.

In the low  $\Delta T$  region, natural convection dominates and this is augmented by concentration differences. To describe this mathematically, first note that

$$T_i - T_{\infty} = (T_E - T_{\infty}) - [K_f (W_{S_i} - W_{S_{\infty}}) + \frac{273.2 \gamma}{\rho L R}] \quad (10)$$

where  $K_f = 31.8$  is the freezing point depression constant,  $W_{S_i}$  and  $W_{S_{\infty}}$  are the mass fractions of solute at the interface and in the bulk solution, and  $\gamma$  is the interfacial tension.

Equations (9) and (10) enable one to calculate  $W_{S_i}$  which then can be used to determine the growth velocity from

$$v = \frac{D}{R} \text{Sh} \left[ 1 - \frac{W_{S_{\infty}}}{W_{S_i}} \right] \quad (11)$$

To use Equations (9), (10), and (11), one must know Nu, Sh, and have a relationship between R and  $\Delta T$ . Realistic theoretical expressions for Nu and Sh are badly needed, but it is a formidable job to obtain them. One can get a rough estimate for these expressions by assuming that the analogy between

heat and mass transfer holds and that Equation (6) applies with the Grashof number given by

$$Gr = \frac{gR^3}{\nu^2} \left( \frac{\rho_i - \rho_\infty}{\rho_\infty} \right) \quad (12)$$

where  $\frac{\rho_i - \rho_\infty}{\rho_\infty}$  reflects both temperature and concentration differences. This leads to  $\frac{\rho_i - \rho_\infty}{\rho_\infty} (Nu/Sh) \approx (Pr/Sc)^{0.075}$ . Thus, all necessary parameters are known once  $T_\infty$  and  $W_S$  are specified.

If one uses (11) with these crude assumptions and the experimental expression for  $R$  in terms of  $\Delta T$ , the results when compared with experimental growth data are encouraging. Equation (11) predicts maxima in the growth versus  $W_S$  curves, as are observed experimentally. Also, the magnitudes of  $v$  predicted are reasonably close to the experimental values. However, the theoretical maxima are not as pronounced as the experimental ones. Predicted rates are somewhat too high near  $W_S = 0$  and somewhat too low at concentrations between 1 and 2 weight percent. When one casts (11) in the form of (1), one finds  $n = 1.9$  for  $W_S = 0$  and  $n = 2.1$  for  $W_S = 0.02$ , which are in reasonable agreement with the experimental values.

It is not clear why  $m = -1.5$  in Equation (2) for the tip radius as observed by Vlahakis and Barduhn (1974) when growth is in a 0.15% NaCl. Hydrodynamic effects do not seem likely to account for this because in pure water  $m = -1$  over a change of 10-fold in  $\Delta T$  and six orders of magnitude for the forced velocity of pure water. This question needs further study.

It is clear that some very important aspects of crystal growth are clouded by thermal and concentration driven convection. Accurate data, taken in a microgravity environment, approximate analytical models, and exact (probably numerical) models all seem to be needed to understand better the important problem of crystal growth.

## REFERENCES

- Churchill, S. W. (1977), AICHE J. 23, 10.
- Fernandez, R. and A. J. Barduhn (1967), Desalination 3, 330.
- Gebhart, B. and L. Pera (1970), J. Fluid Mech. 45, 49.
- Glicksman, M., Shaefer and Ayers (1976), Met. Trans. 7a, 1747.
- Horvay, G. and J. W. Cahn (1961), Acta Met. 9, 695.
- Huang, J. S. (1975), "The Effect of Natural Convection on Ice Crystal Growth in Salt Solutions," Ph.D. Thesis, Chemical Engineering Department, Syracuse University.
- Kallungal, J. and A. J. Barduhn (1977), AICHE J. 23, 294.
- Kroeger, P. G. and S. Ostrach (1974), Int. J. Heat and Mass Trans. 17, 1191.
- Langer, J. S. and H. Muller-Krumbhaar (1978), Acta Met. 26, 1681.
- Ruckenstein, E. (1978), AICHE J. 24, 940.
- Simpson, H. C., et al. (1974, 1975), Desalination 14, 341, and Int. J. Heat and Mass Trans. 18, 615.
- Vlahakis, J. G. and A. J. Barduhn (1974), AICHE J. 20, 581.

## CONVECTIVE FLOW DURING DENDRITIC GROWTH

M. E. Glicksman and S. C. Huang  
Materials Engineering Department  
Rensselaer Polytechnic Institute  
Troy, New York 12181

## ABSTRACT

A review is presented of the major experimental findings obtained from recent ground-based research conducted under the SPAR program. Measurements of dendritic growth at small supercoolings indicate that below approximately 1.5 K a transition occurs from diffusive control to convective control in succinonitrile, a model system chosen for this study. The key theoretical ideas concerning diffusive and convective heat transport during dendritic growth are discussed, and it is shown that a transition in the transport control should occur when the characteristic length for diffusion becomes larger than the characteristic length for convection. The experimental findings and the theoretical ideas discussed suggest that the Fluid Experiment System could provide appropriate experimental diagnostics for flow field visualization and quantification of the fluid dynamical effects presented here.

## CONVECTIVE FLOW DURING DENDRITIC GROWTH

M. E. Glicksman and S. C. Huang  
Materials Engineering Department  
Rensselaer Polytechnic Institute  
Troy, New York 12181

### INTRODUCTION

Accompanying thermal dendritic growth, the latent heat is dissipated from the moving solid-liquid interface through the surrounding supercooled melt. This heat transfer gives rise to a thermal field around the growing dendrite, whereby latent heat flows from solid to liquid along the thermal gradient. The presence of such a gradient alone is responsible for diffusive heat flow. Under terrestrial conditions, however, a pressure gradient develops from the thermal gradient and its associated density gradient. This gradient produces a fluid flow field which changes the thermal distribution near the dendrite, thereby modifying the amount of heat flowing from the interface. The heat flow may be increased or decreased depending on the relative direction between the diffusive flow and the convective flow.

As described above, terrestrial dendritic growth experiments always involve both diffusion and convection. However, the diffusive heat transport process increases rapidly and non-linearly with increased supercooling, whereas the convective heat transport process increases more linearly with supercooling. Thus, at relatively large supercoolings, the diffusive component tends to dominate the heat transfer processes, whereas at small supercoolings, convection must eventually dominate. The diffusion-convection transition in succinonitrile—a material used in a study of diffusion-controlled dendritic growth [1]—occurred at about 1°C. Dendritic growth in succinonitrile at supercoolings smaller than 1°C will thus be controlled

by convection.

In the series of experiments examined in this paper, convection-controlled dendritic growth was the prime subject of study. Experiments reported here include the influence of spatial orientation (from 0-180° relative orientation between the growth direction and the gravity vector) on the dendritic growth of succinonitrile. The description and qualitative explanation of the experimental results were presented in a previous paper [2].

The spatial orientation effect measurements were repeated at several levels of supercooling below 2°C to yield the dependence of the dendritic growth rate on supercooling, in the range where the growth kinetics are controlled by natural convective heat transfer. These results were presented in Refs. [2] and [3]. The discussion of orientation effects on convectively controlled dendritic growth was based originally on a theory proposed by Doherty, Cantor, and Fairs [4]. This theory considers only the case of dendrites growing under counterflow conditions, i.e., where the dendrite tip propagates in opposition to the convective fluid velocity. Moreover, this theory estimates the far-field flow velocity,  $U_{\infty}$  induced by natural convection, by employing a formula developed by Szekely and Themelis [5]. Finally, the convective heat transfer from the dendrite tip can be calculated using a fluid mechanical model originally proposed for forced convection [6]. The supercooling dependence of dendritic growth velocity predicted by this theory is, however, inconsistent with our experimental results [3].

The failure of that theory may be ascribed to the theoretical assumption that the tip region of a growing dendrite is the sole source of heat in the system. Consequently, the convection length scale is linked to the tip dimensions. Actually, in our method of studying solidification, a

dendritic mass consisting of five or six dendrites emerges from the capillary aperture in the bulb (C) - c.f. Fig. 1. Although each dendrite is growing independently, the whole freezing complex acts as a large-scale heat source. The convective current present in our experimental system thus can be expected to flow more rapidly than a fluid current induced by a single dendrite tip acting alone. Hence, the convection length scale should be associated with the multidendrite freezing complex.

In this report, we will first describe a few details of our experimental method and some salient experimental results. We will then present a model intended to explain the supercooling dependence of dendritic growth kinetics under the influence of convective heat transport. Major emphasis is placed on predicting from theory the supercooling level at which the transition from diffusion-controlled to convection-controlled dendritic growth occurs. It should be noted here that preliminary to any analysis of dendritic growth kinetics when under the control of convective heat transport, one must obtain a description of the kinetics when under the control of thermal diffusion alone. Fortunately, a new, and relatively complete, theory of diffusion-controlled dendritic growth was published recently [7]. Furthermore, this theory has been verified in two experiments [8,9] to be correct to at least  $\pm 5\%$ . Thereafter in this report, the supercooling dependence of dendritic growth velocity predicted by this new dendritic growth theory will be used to predict the baseline (diffusional) kinetics to analyze the influence of convection on dendritic growth.

#### EXPERIMENTAL

The present series of experiments was designed to define critically the precise experimental conditions for free dendritic growth with pure

ORIGINAL PAGE IS  
OF POOR QUALITY

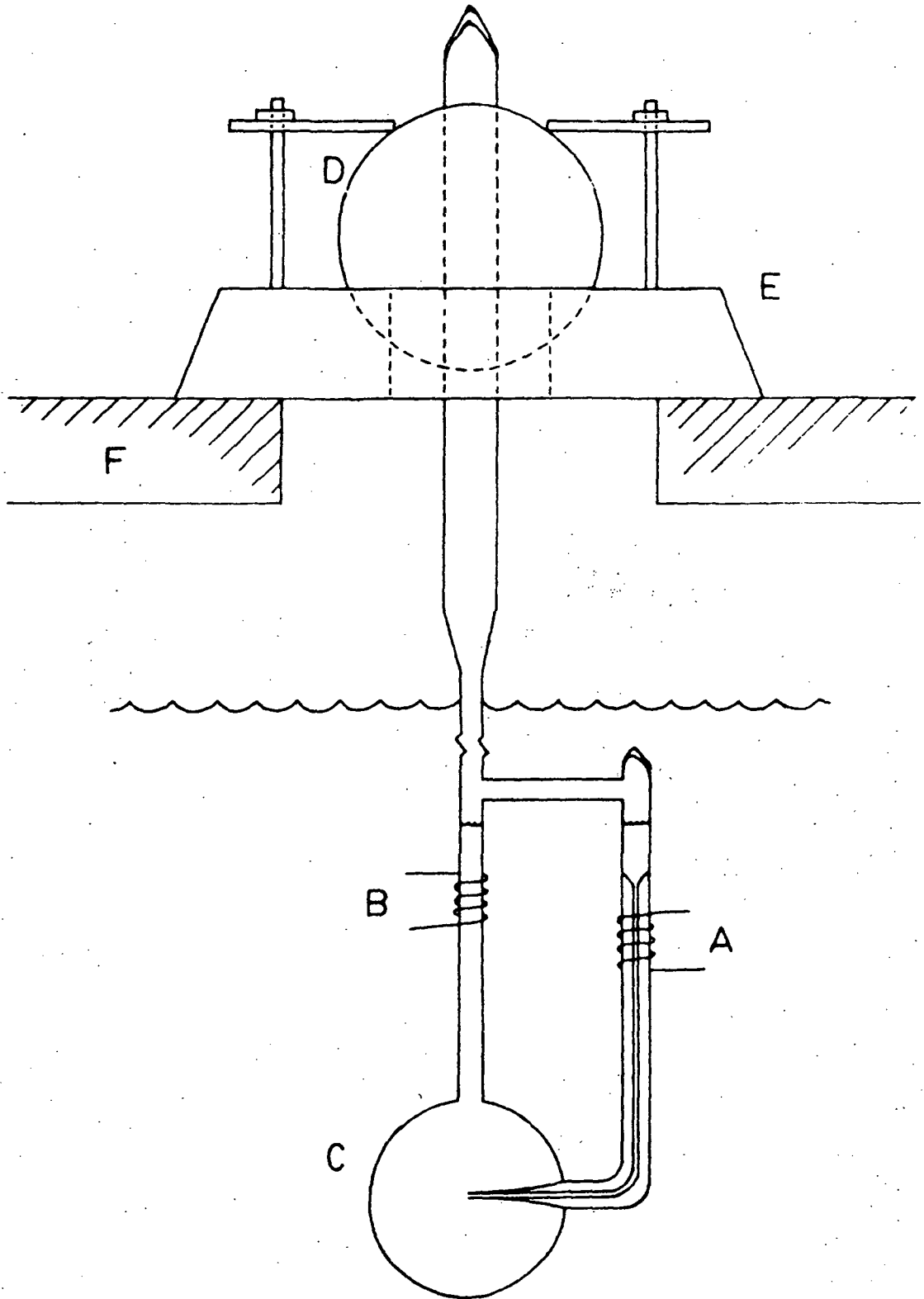


FIGURE 1. Schematic drawing of specimen configuration and support stage. A and B are control heaters; C is the crystal growth chamber; D is the tilting and secondary rotating device; E is the primary rotation and X-Y translation stage; F is the tank cover.

heat transfer (i.e., no solute diffusion). These experiments were designed to permit measurement of pertinent experimental variables, namely: dendritic growth velocity,  $V$ ; dendritic orientation angle with respect to gravity,  $\theta$ ; and supercooling,  $\Delta T \equiv T - T_m$ , where  $T$  is the pre-set temperature of the molten succinonitrile, and  $T_m$  is the equilibrium melting temperature of pure succinonitrile.

Details of specimen purification, specimen characterization, temperature measurements, and temperature control were provided in an earlier paper [2]. The accuracies and measuremental resolution of these factors are compiled in Table 1. As may be shown from Table 1, the uncertainty in measuring the initial supercooling,  $\Delta T$ , is less than  $\pm 0.001^\circ\text{C}$ . Furthermore, our preparing a specimen of succinonitrile with better than 6-9's purity ensures attainment of growth kinetics controlled solely by the flow of latent heat. Solute effects may be safely ignored.

Table 1. Resolution, Control Accuracy, and Purity of Experimental System

Temperature Measurement Resolution	Temperature Measurement Accuracy	Temperature Control Stability	Uncertainty in Melting Temperature	Purity Level in Specimen
0.0004°C	$\pm 0.002^\circ\text{C}$	$\pm 0.0004^\circ\text{C}$	$\pm 0.0004^\circ\text{C}$	> 99.99995%

Dendritic growth studies were carried out in the specimen chamber detailed schematically in Figure 1. Two control heaters, A and B, prevented stray crystals from growing into the chamber C. The succinonitrile could thus be kept liquid in the chamber at any pre-selected temperature established in the thermostatted observation tank. Normally it took about 50 minutes for the entire specimen to achieve a uniform temperature. At that

ORIGINAL PAGE IS  
OF POOR QUALITY

point, control heater A was switched off, and the seed crystal above location A was permitted to propagate into the chamber C through the capillary. The dendrites growing within the chamber were then free of any extraneous interaction with the glass chamber walls until they touched the walls at the end of each run. Furthermore, the outward growing dendrites tended not to interact with one another through overlap of their surrounding thermal fields. Achievement of this unconstrained or free dendritic growth condition is essential to the present kinetics study.

As shown in Fig. 1, the specimen was supported by a special stage which allowed full rotation, a tilt of  $\pm 6^\circ$ , and a two-axis translation of  $\pm 2.5$  cm. The ability to maneuver the growing dendrites into a desired spatial orientation with respect to gravity and the axis of observation was essential to the present study. The growing crystals were observed with a Wild M5A stereomicroscope, equipped with a trinocular assembly and a Wild MKal camera. Photographs were taken through an orange filter using fine-grain Polaroid 105 film (3 1/4" x 4 1/4", ASA 75) with direct, diffused, electronic flash. To minimize optical distortion from the spherical specimen chamber, the observation tank was filled with a mixture of ethylene glycol-17 vol % H<sub>2</sub>O, selected to match the index of refraction of succinonitrile as well as act as the heat transfer medium.

Free dendrites emerged from the tip of the capillary and grew into the spherical chamber in the expected  $\langle 100 \rangle$  cube-edge directions. Although such dendrites were either perpendicular or parallel to each other, they grew in random directions with respect to the direction of observation. To determine the true growth velocity and the true growth orientation with respect to the gravity vector,  $\bar{g}$ , the dendrites were photographed

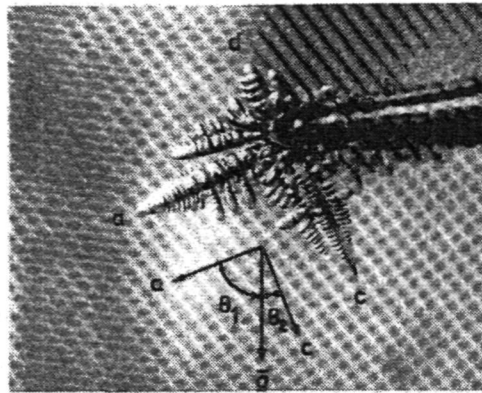
ORIGINAL PAGE IS  
OF POOR QUALITY

from two different directions. Since the microscope was fixed, this required rotation of the specimen chamber.

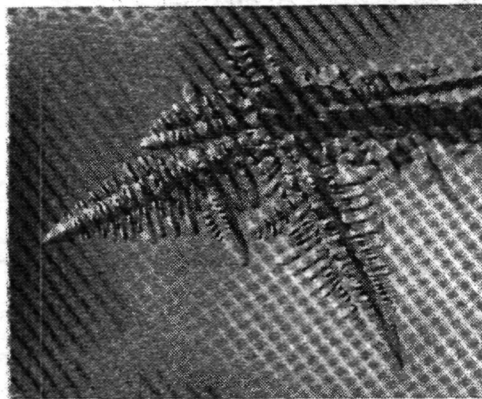
The specimen rotation procedure required to measure true dendritic growth velocities and growth orientations consisted of the following steps:

1) As soon as free dendrites started growing, the specimen chamber was rotated to position a colinear pair of dendrites (e.g., dendrites with axes along  $[100]$  and  $[\bar{1}00]$  in the plane of observation. Figure 2(a) is a photograph taken after completion of this rotation operation. Note that the images of those branches of dendrite c, which were growing perpendicular to the focal plane, appear as a "string of beads". Also, the tips of dendrites a and b were simultaneously rotated into the focal plane. Under this special circumstance, the relative orientation angle of dendrite a from  $\bar{g}$  is expressed by  $\theta_1$ , defined in Fig. 2(a), and that of dendrite b by  $(180-\theta_1)$ . Also, the growth velocity of dendrites a and b can be calculated directly from the tip displacements measured on a series of photographs taken at known time intervals, such as shown in Figs. 2(a) and 2(b).

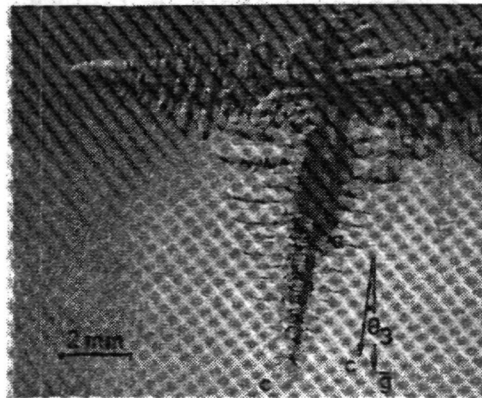
2) The angle  $\theta_2$ , shown in Fig. 2(a), however, might not represent the true deviation angle of dendrite c from  $\bar{g}$ , because dendrite c might be growing at some angle  $\theta_3$  out of the plane of Fig. 2(a). The angle  $\theta_3$  was measured on a photograph taken after the specimen chamber had been rotated  $+90^\circ$  or  $-90^\circ$  about  $\bar{g}$ . This is shown in Fig. 2(c). We note again that the perpendicular branching sheet of dendrite c in Fig. 2(c), was previously observed as the side-branches of dendrite c in Fig. 2(a). Accordingly, the true deviation angle of dendrite c from  $\bar{g}$  should be given by  $\theta_4 = \tan^{-1}[(\tan^2\theta_2 + \tan^2\theta_3)^{1/2}]$  and that of dendrite d by  $(180-\theta_4)$ . Also, the apparent growth velocity of dendrite c, as well as that of dendrite d, must be multiplied by the factor  $(\cos\theta_2 \cdot \sec\theta_4)$ , which accounts for the stereographic corrections discussed above.



(a)



(b)



(c)

FIGURE 2. (a) Dendrite  $\bar{a}$  and  $\bar{b}$  rotated to lie in the focal plane. (b) 4.7 minutes after (a). (c) A sideview of the growing dendrite complex seen in (a) and (b), accomplished by a  $90^\circ$  rotation of the specimen chamber about  $\bar{g}$ .

## RESULTS AND DISCUSSION

Dendritic growth velocities,  $V$ , were measured as a function of growth orientation,  $\theta$ , at seventeen supercoolings ranging from  $0.043^{\circ}\text{C}$  to  $2^{\circ}\text{C}$ . Five typical experimental curves of  $V$  versus  $\theta$  are shown in Fig. 3. As may be noted in Fig. 3, a downward growing succinonitrile dendrite (propagating against the natural convective fluid current) tends to grow faster than an upward-growing dendrite. Detailed discussion of this orientation effect can be found in Ref. [2] and [3]. Also observable in Fig. 3 is that the dependence of the dendritic growth velocity on spatial orientation increases in degree at small supercoolings. The supercooling dependence of growth kinetics for dendrites growing parallel to gravity is summarized in Fig. 4. Also included in Fig. 4 is the theoretical curve of  $V_d$  versus  $\Delta T$  predicted for diffusion-controlled dendritic growth [7-9]. By comparison, the convective flow tends to enhance the growth of downward-growing dendrites below a certain level of supercooling. Fig. 5 is obtained when the measured growth velocities,  $V$ , are normalized to the theoretical diffusive dendritic growth velocities,  $V_d$ . Fig. 5 shows clearly that the diffusion-convection transition occurs rather suddenly at a supercooling of about  $1.5^{\circ}\text{C}$ .

The remainder of this discussion concerns the development of a theory to predict the critical supercooling at which the diffusion-convection transition occurs. To account realistically for the heat transport attendant to the crystal growth method used in this study, we will consider the whole dendritic complex (see again Fig. 2) as the heat emitting source which drives the natural convective fluid flow, Fig. 6. As such, the reference length of the convective flow field,  $l$ , must be chosen as the radius of the dendritic complex ( $l \sim 1 \text{ cm}$ ). This reference length is rela-

ORIGINAL PAGE IS  
OF POOR QUALITY

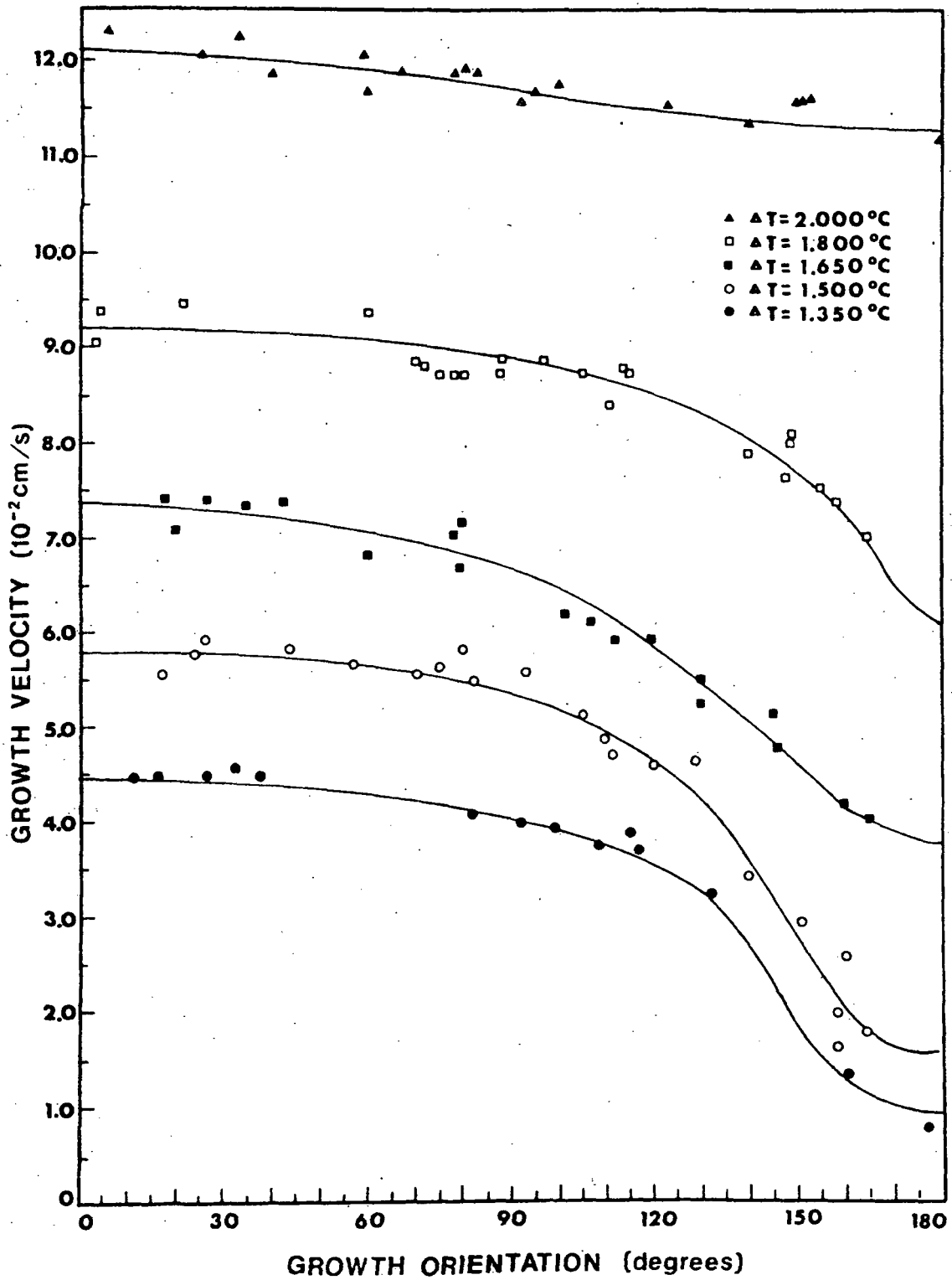


FIGURE 3. Dendritic growth velocity versus growth orientation with respect to gravity at five levels of supercooling.

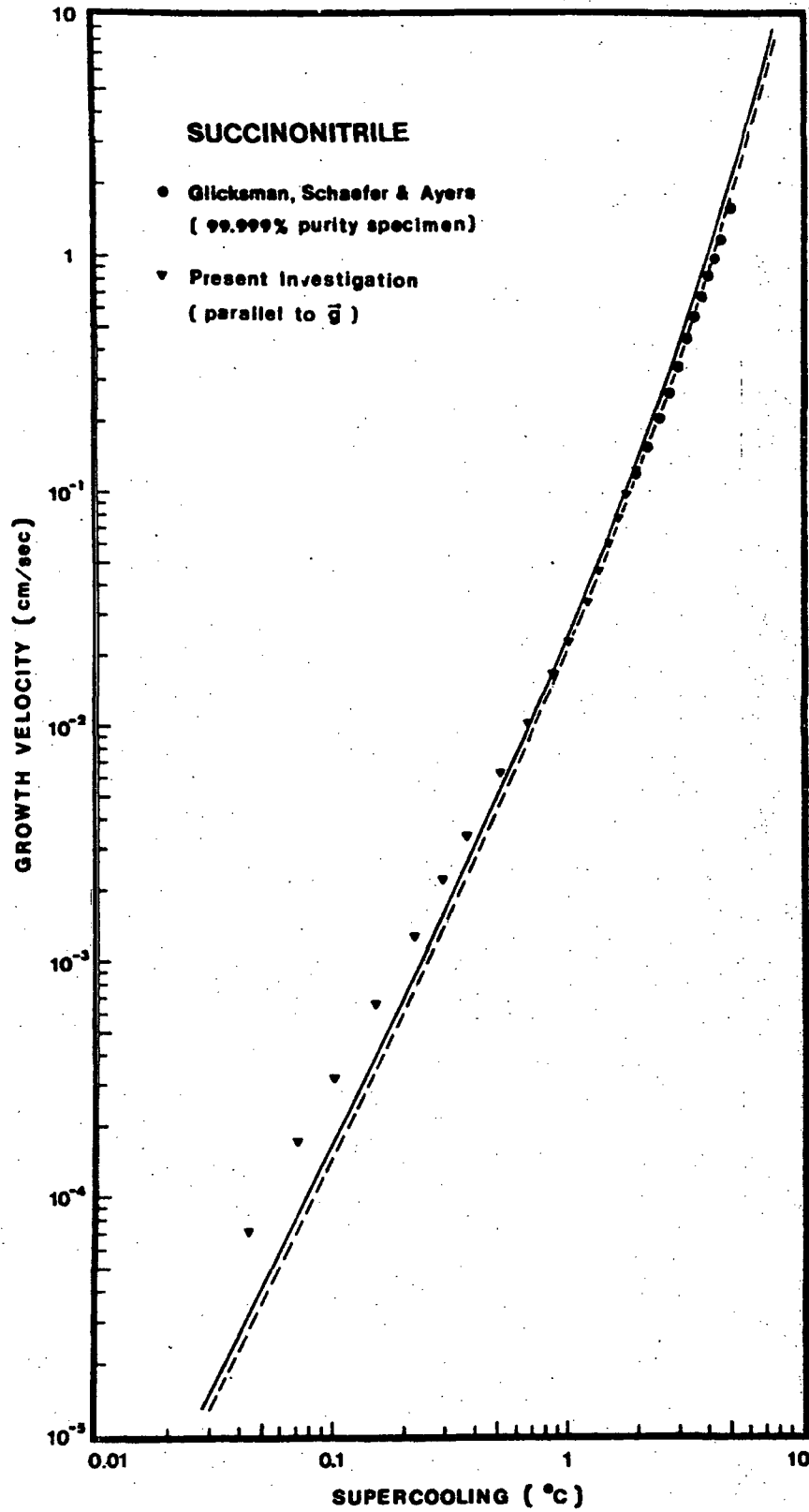


FIGURE 4. Dendritic growth velocity versus supercooling for dendrites growing parallel to gravity.

tively large compared to the dendrite tip radius ( $10^{-4}$  to  $10^{-3}$  cm) which was used as the reference length in the model of Doherty et al. [4]. The velocity  $U_{\infty}$  of the convective flow induced by such a dendritic mass is given by [10]

$$U_{\infty} = A_1 Gr^{1/2} \frac{\nu}{\ell}, \quad (1)$$

where  $A_1$  is a constant approximately equal to unity,  $\nu$  is the kinematic viscosity, and  $Gr$  is the Grashof number defined as

$$Gr = \frac{g\beta\Delta T\ell^3}{\nu^2},$$

where  $g$  is the gravitational acceleration, and  $\beta$  is the volume expansion coefficient. The presence of fluid flow modifies the thermal field surrounding a dendrite, which would be governed by the diffusion of heat were the liquid phase in a quiescent state. The characteristics of heat transfer within a thermal field can be conveniently described by the thickness of the "thermal boundary layer". For the case of convective heat transfer, the thermal boundary layer thickness,  $\delta$ , is given by [11]

$$\delta_T/\ell = A_2 Re^{-1/2} Pr^{-1/3}, \quad (2)$$

where  $A_2$  is a correlation constant approximately equal to 0.5;  $Re$  is the Reynolds number defined as

$$Re = \frac{U_{\infty} \ell}{\nu}; \quad (3)$$

and  $Pr$  is the Prandtl number defined as

$$Pr = \frac{\nu}{\alpha}, \quad (4)$$

where  $\alpha$  is the thermal diffusivity. By combining eq. (1) and (2), the thermal boundary layer thickness can be expressed as

$$\delta_T = A_1^{-1/2} A_2 (g\beta \Delta T)^{-1/4} l^{1/4} \alpha^{1/2} Pr^{1/6} \quad (5)$$

For the case of thermal diffusion at a dendrite tip,  $\delta$  is given by the Stefan boundary layer thickness defined as

$$\delta_s = \frac{2\alpha}{V_d} \quad (6)$$

where  $V_d$  is the diffusion-controlled dendritic growth velocity, which may be described by the power law [1].

$$V_d = \frac{A_3 \alpha \Delta S}{\gamma} \left( \frac{C_p}{L} \right)^{1.5} (\Delta T)^{2.5} \quad (7)$$

Here,  $A_3$  is a constant equal to 0.018,  $\Delta S$  is the entropy of fusion per unit volume,  $\gamma$  is the solid-liquid interfacial energy,  $C_p$  is the heat capacity of the liquid, and  $L$  is the latent heat of fusion. Therefore, the Stefan boundary layer for the pure diffusion case can be expressed as

$$\delta_s = \frac{2\gamma(L/C_p)^{1.5}}{A_3 \cdot \Delta S (\Delta T)^{2.5}} \quad (8)$$

When  $\delta_T = \delta_s$ , a "crossover" can occur in the dominant heat transport mechanism. The "crossover" condition is obtained when the right-hand sides of eq. (5) and (8) are set equal. This procedure yields a critical transition supercooling  $\Delta T^*$ , which when expressed in a dimensionless form  $\Delta\theta^* = \Delta T^* / (L/C_p)$ , is given by

$$\Delta\theta^* = \left[ \left( \frac{g\beta}{l} \right) \left( \frac{A_1}{\alpha} \right)^2 \left( \frac{C_p}{L} \right)^3 \left( \frac{\gamma}{A_2 A_3 \Delta S} \right)^4 \right]^{1/9} Pr^{-2/27} \quad (9)$$

Inserting the pertinent materials parameters (see Ref. [1] and [2]), into eq. 9 yields  $\Delta T^* = 1.23^\circ\text{C}$  for succinonitrile. Comparison of this result to that measured from Fig. 5, indicates that eq. 9 is predictive to within

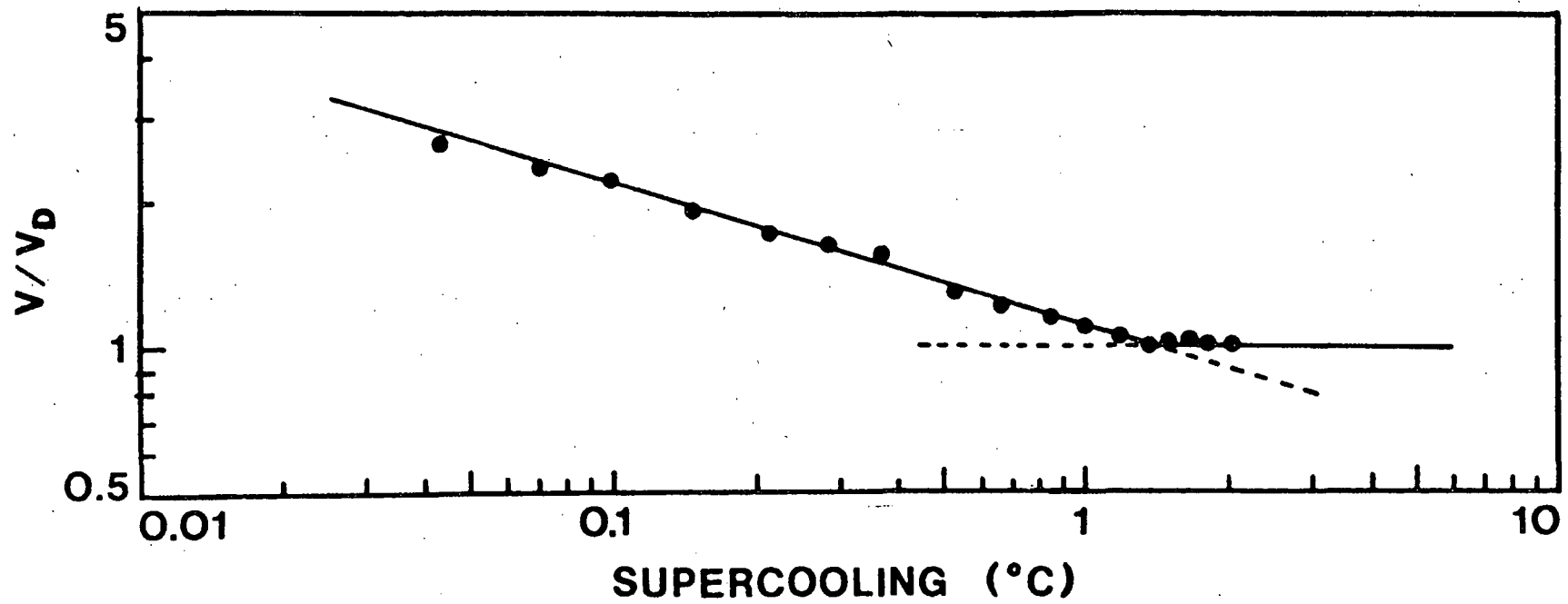


FIGURE 5. Normalized dendritic growth velocity versus supercooling for dendrites growing parallel to gravity.

ORIGINAL PAGE IS  
OF POOR QUALITY

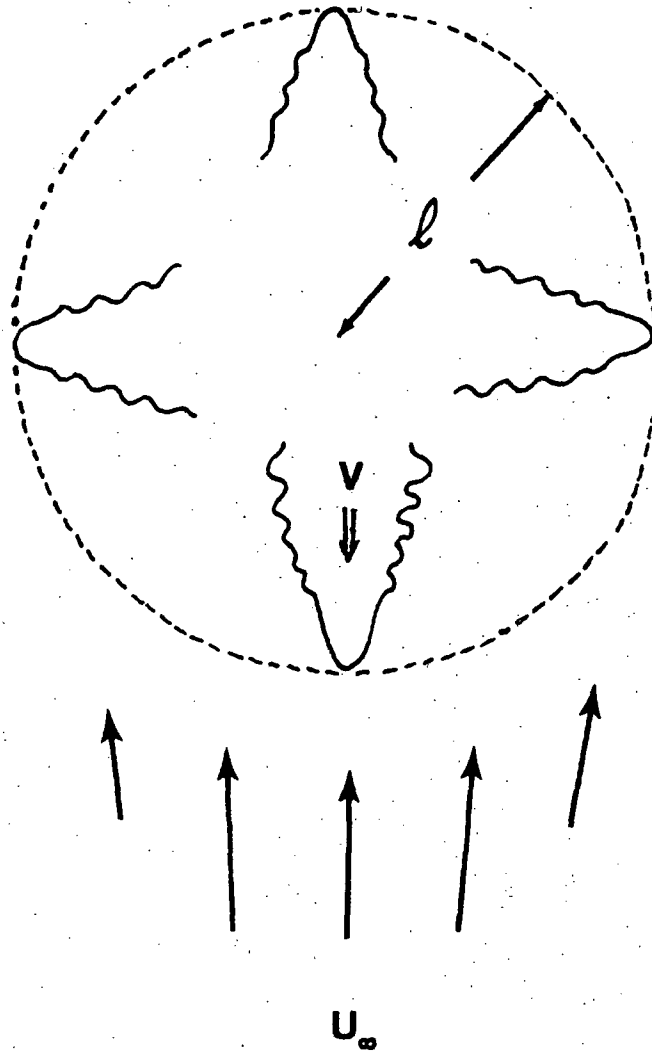


FIGURE 6. Schematic showing the natural convective fluid flow in front of a downward-growing dendrite. The convective flow is induced by heat released by the solidifying dendritic mass.

about 10%, which is the combined level of uncertainty of the parameters.

Normally, viscosity and expansion coefficient are considered important materials parameters in determining the relative ease of natural convection. Equation 9, however, indicates that  $\Delta\theta^*$  varies with  $\beta$  to the 1/9 power, and with  $\nu$  to the -2/27 power. Furthermore, since  $\Delta\theta^*$  is proportional to  $\ell^{-1/9}$ , the manner of choosing the reference scale has relatively little effect on the predicted value of the "crossover" supercooling. The crossover point shows a similarly weak dependence on the gravitational level  $g$ .

#### SUMMARY

1) The kinetics of dendritic growth in pure materials is controlled by the release of latent heat, which is removed from the solid-liquid interface by diffusive and/or convective flow.

2) The diffusion of heat from a dendrite increases rapidly and non-linearly with increasing supercooling, whereas the convection of heat varies in a more linear manner.

3) Significant convection effects in succinonitrile, manifested by the orientation dependence of the growth rate, occur when the supercooling is less than 1.5°C.

4) The crossover between diffusive and convective transport depends on the relative thickness of the Stefan or diffusion length compared with the thermal boundary layer. These lengths become equal at a supercooling which may be calculated from diffusion theory and fluid mechanics.

5) The theoretical expression for the "crossover" supercooling shows that this quantity varies weakly with such factors as the gravitational acceleration, the melt viscosity, and the volumetric expansion coefficient.

ORIGINAL PAGE IS  
OF POOR QUALITY

Ground based experiments have been carried out to measure the influence of melt convection on the growth kinetics of succinonitrile - a model solidification system, which simulates the freezing of metals. Growth velocity measurements will be discussed, with supercooling and spatial orientation with respect to the gravity vector as the two major experimental variables. A distinct transition has been observed near  $1.5^{\circ}\text{C}$  supercooling, where the heat transport mechanism changes from diffusive to convective. The desirability to determine, at least semiquantitatively, the nature of the melt flows will be discussed, along with the requirements which might be imposed by such measurements on the F.E.S.

#### FUTURE DIRECTIONS AND SIGNIFICANCE OF THE FLUID EXPERIMENT SYSTEM

As described in this paper, convective transport can play a major role in dendritic solidification, especially at small supercoolings. A boundary layer analysis developed here suggests, at least in pure systems, that the dominant transport mechanism changes at the "crossover" of the boundary layer thickness. A detailed analysis which characterizes the flow fields surrounding a dendrite has not yet been developed, nor have experiments been performed to elucidate the behavior of these flows. The Fluid Experiment System, (FES), now being developed by NASA for inclusion on Space Lab III, will provide a variety of fluid flow diagnostic techniques. The convective flows during dendritic solidification are generally slow, laminar flows, of three-dimensional character. The use of schlieren, shadowgraphic, or holographic flow visualization techniques could be explored as possible methods to measure the qualitative nature of these flows. More quantitative approaches such as laser doppler or speckle interferometry could be explored for limited, detailed measurements of fluid flow velocities. If the characteristics of the melt convection could be convincingly established at terrestrial gravitational levels, then the effect of reduced gravity under space flight conditions would be justified. Indeed, the elucidation of how convection modifies the kinetics of dendritic growth in different spatial orientations with respect to the gravity vector remains only partially understood. A more quantitative understanding of this complex phenomenon will contribute to better solidification process design—both on earth and in space—and to achieving better materials with controlled chemical distributions and reduced defects. To this end, the FES represents a potentially important opportunity to explore melt convection in far greater detail than has heretofore been possible.

#### ACKNOWLEDGEMENTS

The authors gratefully acknowledge the support provided through the Space Processing and Applications Rocket Program, Marshall Space Flight Center, Huntsville, Alabama, and the Office of Applications, National Aeronautics and Space Administration, Washington, D.C. Also, we thank Professor Dudley Saville, Chemical Engineering Department, Princeton University, for his stimulating comments regarding the boundary layer thickness calculations.

#### REFERENCES

1. M. E. Glicksman, R. J. Schaefer and J. D. Ayers, Met. Trans., 7A, 1747 (1976).
2. M. E. Glicksman and S. C. Huang, "Convective Heat Transfer During Dendritic Solidification," presented at AIAA 16th Aerospace Sciences Meeting, Huntsville, Alabama, January 16-18, 1978.
3. M. E. Glicksman and S. C. Huang, "Convection and Diffusion Effects During Dendritic Solidification," presented at AIAA 17th Aerospace Sciences Meeting, New Orleans, Louisiana, January 15-17, 1979.
4. R. D. Doherty, V. Cantor and S. Fairs, Met. Trans., 9A, 621 (1978).
5. J. Szekely and N. J. Themelis, "Rate Phenomena in Process Metallurgy," p. 18, John Wiley, New York (1971).
6. B. Cantor and A. Vogel, J. Crystal Growth, 41, 109 (1977).
7. J. S. Langer and H. Müller-Krumbhaar, Acta Met., 26, 1681 (1978).
8. T. Fujioka, Ph.D. Thesis, Carnegie-Mellon University, 1977.
9. S. C. Huang and M. E. Glicksman, "Development of Dendritic Tip Structures at Small Supercoolings," presented at the 4th American Conference on Crystal Growth, NBS, Gaithersburg, Maryland, July 16-19, 1978.

10. A. Acrivos, J. Fluid Mech., 12, 337 (1962).
11. S. R. Coriell, D. T. J. Hurle and R. F. Sekerka, J. Crystal Growth,  
32, 1 (1976).

## LOW DIMENSIONAL MAGNETIC SOLIDS AND SINGLE CRYSTAL ELPASOLITES:

## NEED FOR IMPROVED CRYSTAL GROWING TECHNIQUES

Mary L. Good<sup>(a)</sup>

and

Steven Watkins and Robert W. Schwartz<sup>(b)</sup>

A series of  $\alpha$ -amido acid complexes of first row transition metals have been prepared which crystallize as infinite linear chains and exhibit low dimensional magnetic ordering (one or two) at temperatures below 40°K. The synthetic method appears quite general and a variety of materials can be systematically prepared. Correlations of molecular structure and magnetic properties should provide access to design protocols for developing materials with specific properties and sufficient experimental data to evaluate existing and proposed theoretical models for magnetic interactions between localized metal ion sites. To date, most experiments have produced only small crystals which have a tendency to be twinned or to contain imperfections. Crystals suitable for single crystal X-ray diffraction have been grown with difficulty. The need for extensive crystal growing experiments to develop techniques for preparing crystals suitable for magnetic anisotropy measurements and detailed X-ray and neutron diffraction studies is rationalized on the basis of the unique magnetic properties of the materials and their hydrogen bonded structures which have many features in common with metalloenzyme and metalloprotein active sites.

The rare earth complexes which crystallize in the cubic Elpasolite structure ( $\text{Cs}_2\text{NaLnCl}_6$  where Ln is a trivalent lanthanide) provide materials for carrying out detailed and relatively unambiguous investigations of the spectroscopic properties associated with f-f excitations or emissions localized on the lanthanide ions. This crystal system has begun to yield information concerning the energy transfer processes that take place when two different lanthanides are present and certain formulations appear to be possible candidates for microlasers. Single crystals of the single and mixed lanthanide species are prepared by the Bridgeman technique of gradient solidification of molten samples. The effects of crystal imperfections on the optical properties of these materials are an important part of the projected research to be done in this area. Extensive crystal growing studies on the  $\text{Cs}_2\text{NaLnCl}_6$  systems and the analogous  $\text{Cs}_2\text{NaLnF}_6$  systems can be justified in terms of the importance of the fundamental optical studies which are possible on single crystals of these materials and the possible relationship between crystal imperfections and luminescent properties and phase transitions.

---

(a) Division of Engineering Research, Louisiana State University, Baton Rouge

(b) Department of Chemistry, Louisiana State University, Baton Rouge

LOW DIMENSIONAL MAGNETIC SOLIDS AND SINGLE CRYSTAL ELPASOLITES:  
NEED FOR IMPROVED CRYSTAL GROWING TECHNIQUES

INTRODUCTION

At the present time, an interdisciplinary group from the Colleges of Chemistry and Physics and Engineering at Louisiana State University are developing an integrated research program in Material Science. One major component of this research is the synthesis and characterization of new inorganic materials which exhibit unique magnetic and optical properties. The ultimate potential of the research is limited by our ability to grow suitable single crystals and to definitely assess the effects of crystal imperfections. Crystal growth and solidification phenomena have been identified as fundamental areas to be investigated in the NASA program for materials processing in space and this Fluids Experiment System Workshop has included significant discussions on crystal growth experiments. Thus it appears that extensive crystal growth studies are priority activities for this program. The questions to be answered are: What materials will be chosen for study and what measurements and observations will be made? It would appear that the materials to be investigated should have the following characteristics: (1) they must have some intrinsic scientific or technological significance; (2) they must be complex enough that significant new information can be gained; and (3) they should be easily available and not prohibitively expensive since many ground-based experiments will be required. It would appear that two specific problems from the Material Science Group at LSU fit these requirements very well. One is the preparation of good quality single crystals of transition metal complexes with  $\alpha$ -amido acids from aqueous solution and the other is the preparation of single crystals of the highly symmetrical Elpasolites of the general formula,  $Cs_2NaLnX_6$  where Ln is a trivalent lanthanide and X is chloride

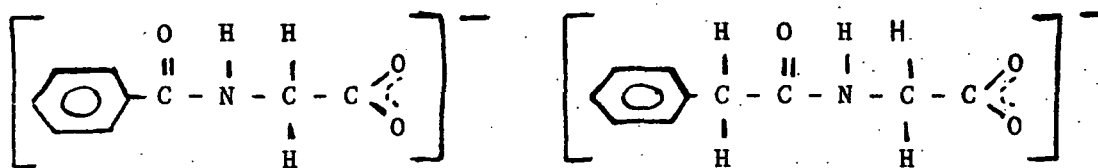
or fluoride. Both of these projects are presently underway [1] and extensive work on sample preparation has been done. However, little detailed research on the crystal growth process itself has been done and present funding does not include resources for such activity. The projects would exemplify two separate crystal growing problems. The low dimensional transition metal materials are prepared from aqueous and mixed aqueous-alcohol solutions of metal ion and ligand and are then recrystallized. The Elpasolites are prepared from high temperature melts of stoichiometric mixtures of the appropriate metal halides. Thus experiments devoted to single crystal growth in these projects should provide fundamental knowledge about the theory of crystal growth from aqueous solution and from high temperature melts. Outlined briefly below are the status of our research in these areas and the proposed ground work we feel needs to be done before space experiments are designed. The ability to provide extensive ground-based data on a variety of specific materials means that any projected space experiments would be clearly defined and adequate ground comparisons would be in place.

#### LOW DIMENSIONAL MAGNETIC MATERIALS

Chemists have routinely examined the magnetic properties of inorganic complexes at high temperatures ( $77^{\circ}\text{K}$  and above) where normal Curie or Curie-Weiss behavior is generally observed. For paramagnetic materials, the assumption has usually been made that they are magnetically dilute and the calculated susceptibility data have been used to determine the magnetic moment of the metal ion and the presence of low symmetry, and to deduce the Boltzmann distribution between the ground electronic state and thermally accessible excited states. Current cryogenic

technology has now progressed to a point where many materials are characterized at very low temperatures,  $4.2^{\circ}\text{K}$  and below. At these temperatures, deviations from Curie and Curie-Weiss behavior are common and new information about cooperative magnetic phenomena can be correlated with molecular and atomic structure. Mathematical models for such interactions have been a long-time interest of theoretical physicists and the determination of structural and magnetic data for a variety of magnetically non-dilute systems provides the necessary focus for the refinement and ultimate utility of such models [2]. We have now prepared and characterized one such set of compounds, a series of first row transition metal complexes of  $\alpha$ -amido acids which crystallize as linear chains and exhibit low-dimensional magnetic properties.

Earlier communications [3,4,5] from our laboratory have reported the structure and magnetic properties for the essentially isostructural cobalt (II), nickel (II) and iron (II) hippurates (hippurate is  $\text{C}_6\text{H}_5\text{CONHCH}_2\text{CO}_2^-$ ; see Figure 1) which have been characterized as canted, linear chain systems and have molecular formulas of  $\text{M}(\text{hipp})_2(\text{H}_2\text{O})_3 \cdot 2\text{H}_2\text{O}$ . The site symmetry of the metal ions was essentially  $\text{C}_{2h}$  (see Figure 2) with two hippurate ions (bonded through a single carboxyl oxygen) and two water molecules in the central plane and two bridging (through the oxygen atom) water molecules in the axial positions. The unit cell (see Figure 3) indicated that the linear chains were arranged in "rows" with interchain hydrogen bonding (see Figure 4 and 5) [6]. The intrachain metal-metal distance was about  $4\text{\AA}$  and the interchain distances were approximately  $7\text{\AA}$  within the "rows" and  $20\text{\AA}$  between "rows". In the Co(II) and Ni(II) cases, antiferromagnetic superexchange was postulated to occur along the chains (c axis) via bridging water molecules.



hippurate anion

phenaceturate anion

Figure 1: Structures of  $\alpha$ -Amido Acid Ligands

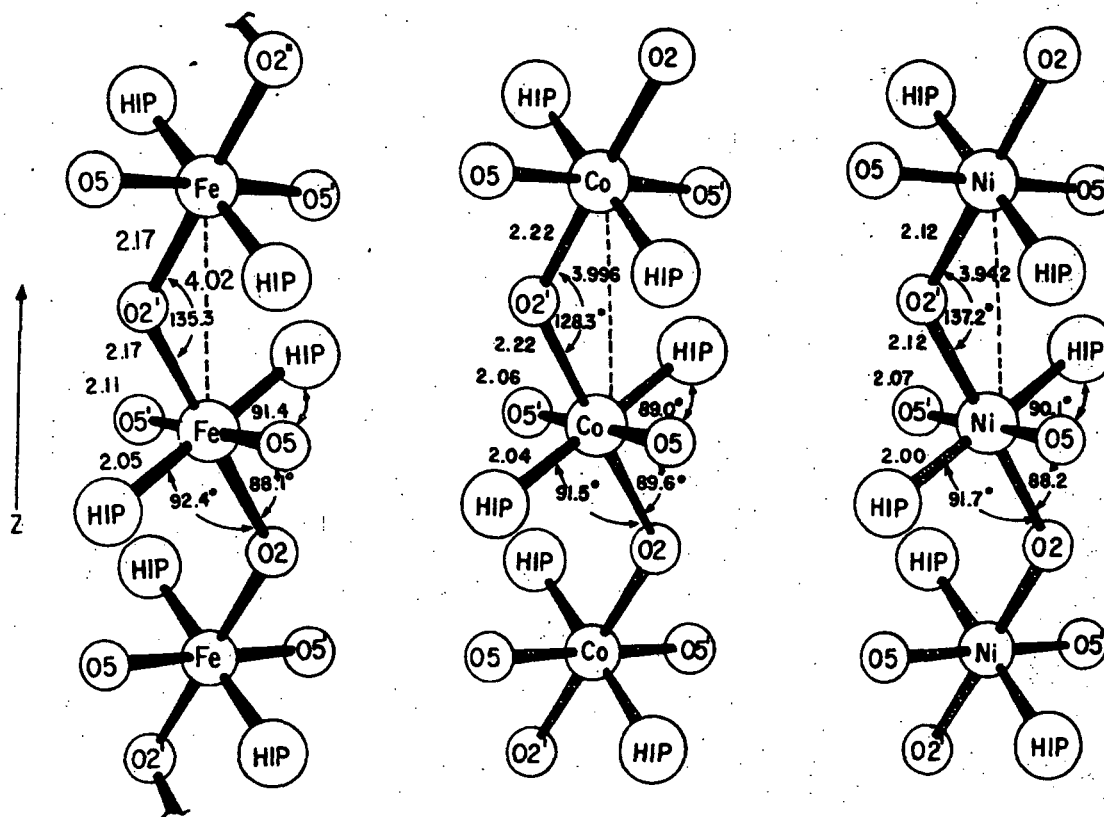


Figure 2: Projection View of the Site Symmetry About the Fe(II), Co(II) and Ni(II) ions in the Hippurate Complexes.

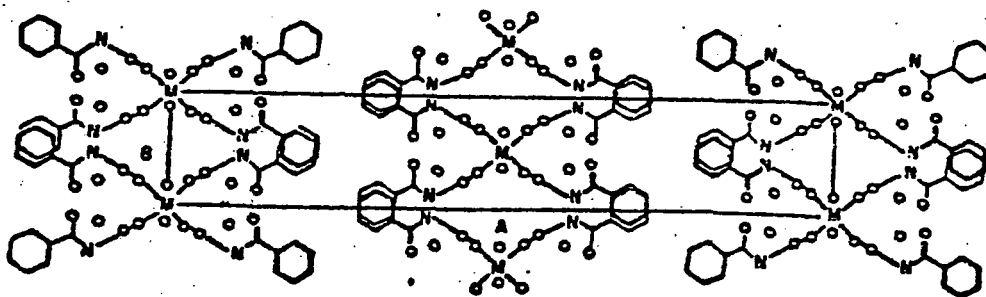


Figure 3: The Unit Cell of the Fe(II), Co(II), and Ni(II) Hippurates as Viewed Down the c Axis lines.

Since alternate spins were canted with respect to one another along the chains, the spin anisotropy of the Ni(II) and Co(II) ions was expected to generate a net spontaneous moment along the chain through the D-M (Dzyaloshinsky-Moriya) interaction [7,8,9]. In addition to this magnetic order along the chains, a low temperature transition was attributed to dipole-dipole interactions between neighboring chains in the "rows" (along the short or b axis) which resulted in the antiferromagnetic coupling of adjacent chains. The stylized model of this two-dimensional system is shown in Figure 6.

The corresponding Fe(II) hippurate was examined by Mössbauer spectra at low temperatures as indicated in Figure 8. A summary of the proposed description of the magnetic and electronic properties of  $\text{Fe(hipp)}_2(\text{H}_2\text{O})_3 \cdot 2\text{H}_2\text{O}$  are as follows: (1) Single ion magnetic moments lie essentially in the x-y plane defined by the coordinate system of the electric field gradient, i.e.  $^5\text{B}_{2g}(\text{d}_{xy})$  electronic ground state; (2) Isotropic superexchange aligns the spins antiparallel along the chain or c axis; (3) Anisotropic superexchange occurs along the chain and results

ORIGINAL PAGE IS  
OF POOR QUALITY

in a weak net spontaneous (D-M) moment directed parallel to the crystallographic a cell axis; (4) A sharp saturation in the superexchange ordering below  $T_c$  indicates the Ising behavior of the Fe(II) ion; and (5) Interchain interactions are not predicted to occur until  $T \rightarrow 0^\circ\text{K}$ . Thus we conclude that the Fe(II) hippurate is a unique example of a one-dimensional Ising chain system.

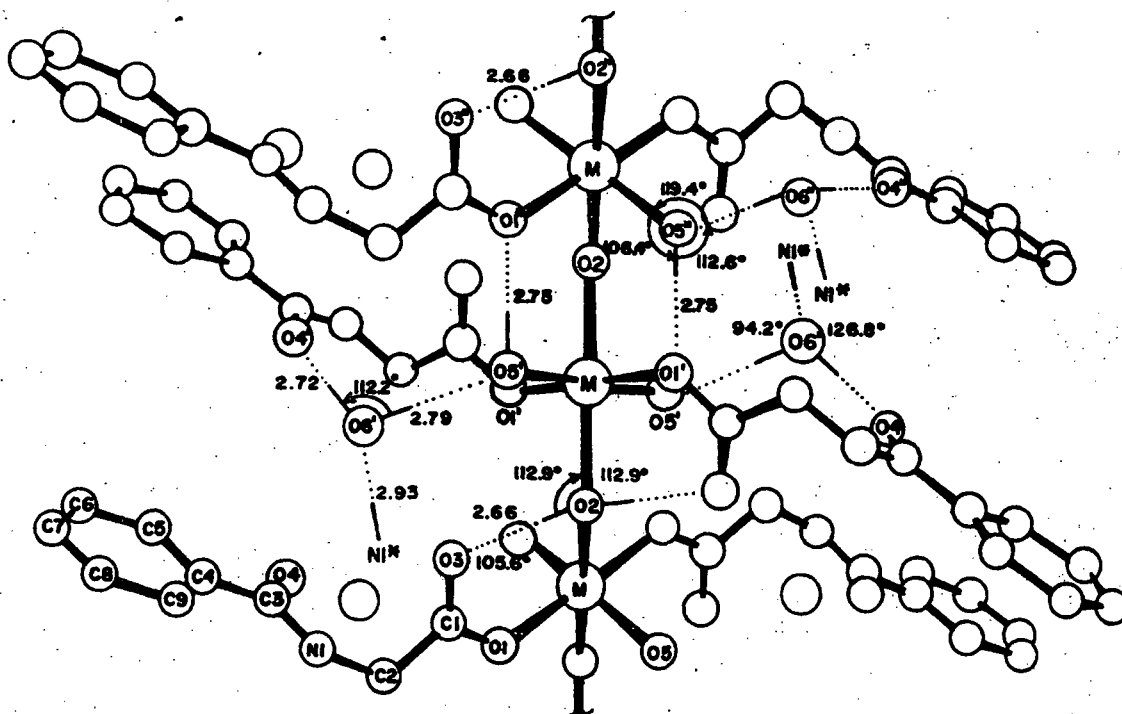


Figure 4: The  $M(\text{hip})_2(\text{H}_2\text{O})_3 \cdot 2\text{H}_2\text{O}$  Molecule. (Hydrogen bonding interactions are shown as dashed lines, while the solid portion of each dashed line represents the position of the hydrogen atoms.)



ORIGINAL PAGE IS  
OF POOR QUALITY

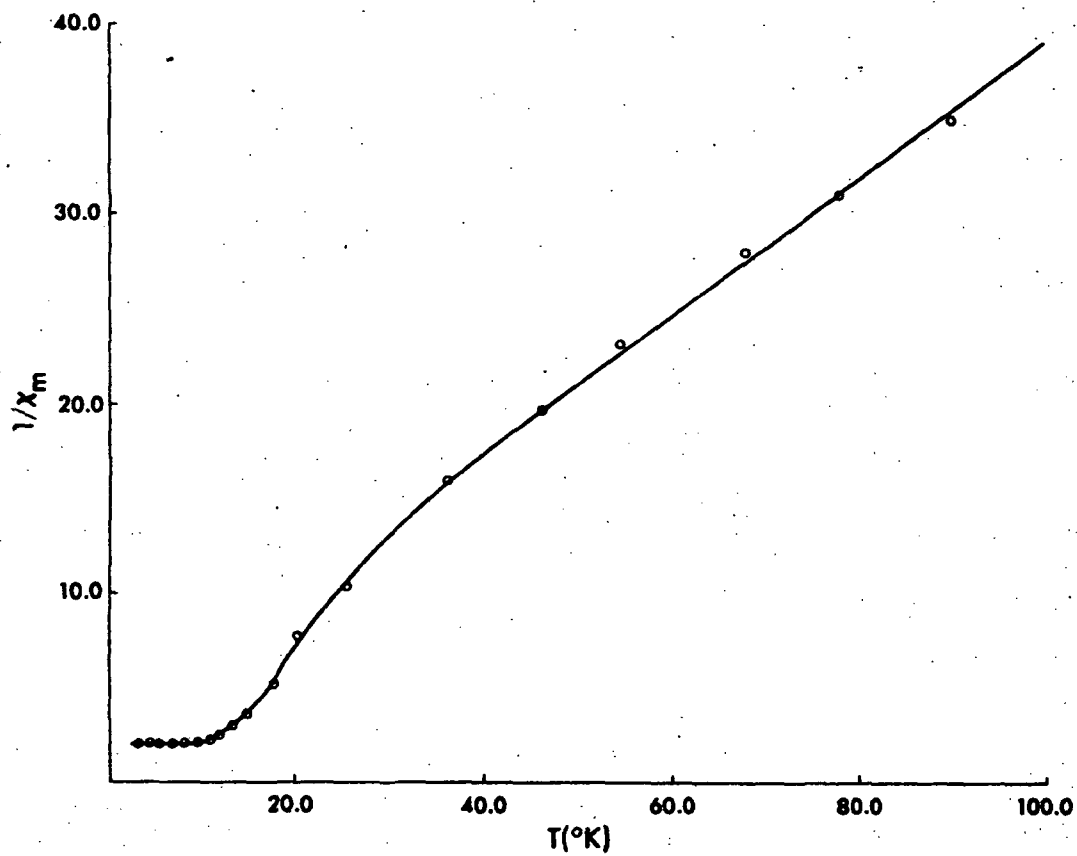
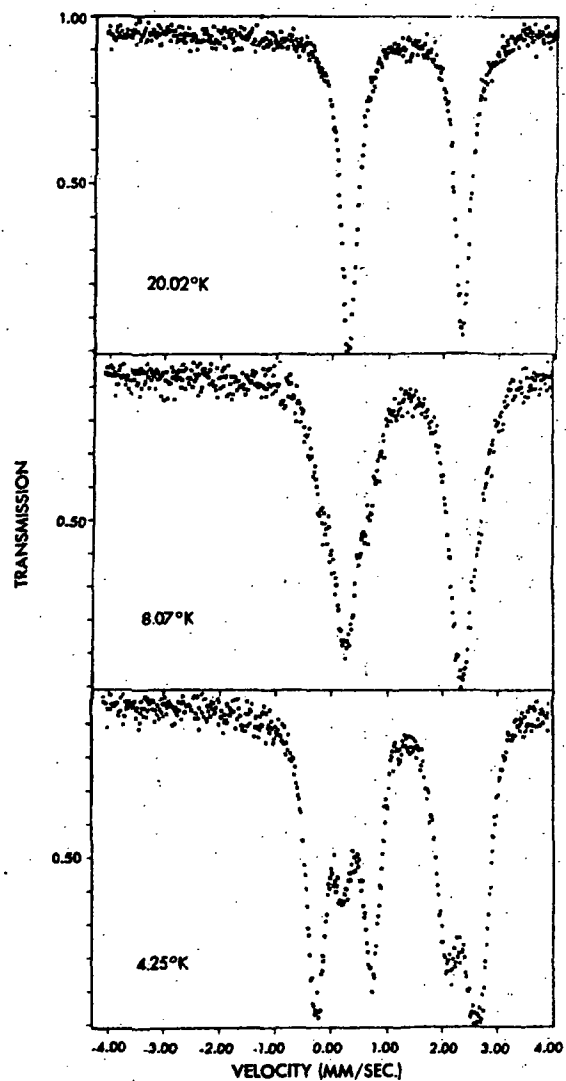


Figure 7: Inverse of the Magnetic Susceptibility vs. Temperature  
for a Powdered Sample of  $\text{Fe}(\text{hipp})_2(\text{H}_2\text{O})_3 \cdot 2\text{H}_2\text{O}$ .

Figure 8: Mössbauer Spectra of  
 $\text{Fe}(\text{hipp})_2(\text{H}_2\text{O})_3 \cdot 2\text{H}_2\text{O}$



MÖSSBAUER SPECTRA OF  $\text{Fe}(\text{hipp})_2(\text{H}_2\text{O})_3 \cdot 2\text{H}_2\text{O}$

In addition to the Co(II), Ni(II) and Fe(II) hippurates, other similar ligands are being used to prepare new materials and other transition metal ions, notably Mn(II), are being investigated. These studies have provided new molecular systems for the evaluation of existing theoretical models and the extension of the work should provide an understanding of the relationship between structure and magnetic

ORIGINAL PAGE IS  
OF POOR QUALITY

properties. Such understanding could ultimately lead to the strategic synthesis of new magnetic systems for practical applications.

ELPASOLITES: LANTHANIDE ION OPTICAL  
SPECTROSCOPY IN SYSTEMS OF HIGH SYMMETRY

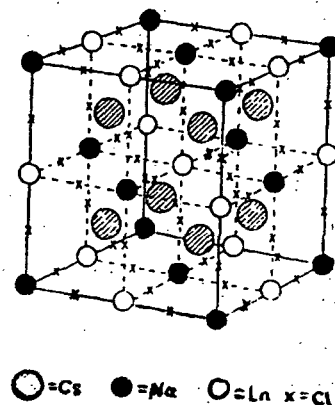
The preparation of materials that are efficient and useful phosphors, lasers, energy transfer or energy up-conversion systems is, to a large extent, still an empirical process. It is not yet possible to predict whether a material will have any of the above mentioned properties; nor is it practical to attempt any large scale design of materials with any of those properties. In certain cases some of the necessary properties are known (for example: in lasers two useful properties are high emission cross-sections and long radiative lifetime) but this is not true in general. The problem is exacerbated by the fact that even when it is known that certain properties are needed it is not always possible to choose in advance materials that have these desired properties.

All of the properties mentioned above are determined by the electronic states of the material and the interactions of these states with structural features. Thus if we are to be able to design materials for any of the above mentioned purposes, it is of prime importance to correlate the electronic structure and its interactions with the properties of interest. This requires materials which have the desired properties and can be studied in detail. The Elpasolite system,  $\text{Cs}_2\text{NaLnCl}_6$  (see Figure 9), with its isomorphs and its extensions, represents such a set of materials.

The bulk of work done to date on trivalent rare earth ions in the solid

state, has utilized crystal systems where the site symmetry of the rare earth ion was low enough to remove all but Kramer's degeneracy. This low symmetry leads to a great deal of crystal field and J-level mixing which makes it essentially meaningless to attach a specific label to a particular state and makes it difficult to obtain accurate metal wavefunctions [10,11]. In addition, in just about all cases which have been studied to date, no account has been taken of the mechanism by which the various transitions acquire intensity. Thus although the past work on rare earth spectroscopy has been voluminous, these two major weaknesses remain. No complete study has been made of trivalent rare earth ions at sites of known, precise, octahedral (6-coordinate) symmetry in the solid state where detailed assignments of existing states can be made and no thorough study of the intensity mechanisms for rare earth f-f transitions has been performed for a large number of these ions with identical, well defined crystal site symmetries. The work underway in Dr. Schwartz's laboratory on the Elpasolites is designed to rectify both of these situations [12-20].

Figure 9: One Unit Cell of  
 $\text{Cs}_2\text{NaLnCl}_6$



The luminescence properties of trivalent lanthanide ions at sites of  $O_h$  symmetry in the cubic crystal system  $Cs_2NaLnCl_6$  ( $Ln = Y^{3+}$  or trivalent lanthanide) are remarkable. Preliminary results indicate that in single crystals of  $Cs_2NaEuCl_6$  doped with  $Tb^{3+}$ , extremely efficient, long-range, energy transfer from  $Tb^{3+}$  to  $Eu^{3+}$  occurs.  $Cs_2NaHoCl_6$  has been observed to be a brilliant red emitter with an extremely high efficiency and  $Nd^{3+}$  in  $Cs_2NaNdCl_6$  and in  $Nd^{3+}: Cs_2NaYCl_6$  shows the longest lifetime of any  $Nd^{3+}$  compound. These three observations indicate that either alone, or in various combinations, lanthanide ions in crystals of this type could prove valuable in such diverse fields as commercial phosphors, laser materials, energy transfer or energy up-conversion systems.

#### CRYSTAL GROWING EXPERIMENTS

As the discussion above indicates, the thrust of our studies is to prepare new materials of high solid state quality (the linear chain magnetic materials) or to prepare well-defined and high quality crystals of rare earth ions in high symmetry environments. In other words we need high quality crystalline materials to study fundamentally important magnetic and optical phenomena. The two projects involve totally different crystal growing techniques. The magnetic materials are grown by mixing solutions of the metal ion and ligands and then recrystallizing from aqueous or mixed aqueous-achohol solutions. The rare earth Elpasolites are grown from the melts of stoichometric mixtures of the metal halides. Inorganic chemists in general have been interested in the properties of the materials synthesized and have had only peripheral interest in the detailed theory and mechanisms of material formation. Their approach to the improvement in crystal quality of their

preparations has been essentially empirical, i.e. try a proposed technique and harvest the resulting crystals. Thus the preparation of high quality crystalline materials has been an art form with success dictated by experience and luck. The two problems outlined here are no different. Recrystallization "recipes" have been used to prepare the small and imperfect linear chain crystals required for X-ray diffraction analysis and known temperature-gradient furnace techniques have been used to prepare the Elpasolites. In both cases, success has depended upon trial and error and experience. No basic information about crystal formation or crystal growing theory has been gained. However both problems rely heavily on the availability of high quality crystals and the low dimensional magnetic material studies have suffered because of the lack of crystals of sufficient size and quality to do single crystal magnetic measurements, heat capacity measurements, precise X-ray diffraction maps where hydrogen atoms can be located, and neutron diffraction experiments where hydrogen atoms can be found and spin structures determined. Thus the motivation for carrying out detailed crystal growing experiments is very high and the results, if successful, will provide materials of scientific and technological significance.

The possibility of carrying out crystal growing experiments in microgravity environments has re-kindled interest in the theory of crystal growing and the delineation of factors involved in single crystal growth. Carruthers [21, 22] has outlined the advantages of low gravity crystal growth and has delineated several ground-based problems which must be solved before full advantage can be taken of space development of new techniques and materials. Areas of concern include characterization and property measurements on materials of significant

technological interest and the definition of processes involved in crystal growth. Older theoretical approaches to crystal growth emphasize the lack of definitive experiments which test theories currently in vogue, particularly in the area of growth from solution [23, 24]. Thus it would appear that extensive crystal growing experiments on the materials of interest in this report would be timely and have high potential for future experiments designed specifically for low-gravity space environments. In both cases the starting materials are readily available and relatively inexpensive. Facilities required are fairly simple and for the most part, they already exist at LSU. A brief overview of the proposed experiments follow.

The linear chain, transition metal complexes of  $\alpha$ -amido acids have fairly complex, hydrogen bonded structures and it is not surprising that material recrystallized under ordinary conditions, with only cursory attention paid to control of growth variables, consisted of badly twinned or extremely small crystals. However, the fact that a more elaborate, re-crystallization growth procedure produced better crystals (although of minimal quality) would lead one to believe that high quality crystals are possible if the growth variables are understood and growth techniques are used which utilize that knowledge. Two approaches are possible: de novo synthesis, with crystallization controlled in part by chemical reaction kinetics and amounts of excess reagents; and controlled recrystallization of the pure compounds. Both approaches have been proposed and preliminary experiments carried out as a prelude to materials processing in space. Weiss and Lind [25, 26] have proposed techniques for growing crystals from the controlled mixing of two solutions containing the insoluble crystal components. Professor Authier

ORIGINAL PAGE IS  
OF POOR QUALITY

of France has also designed a crystallization chamber for carrying out such experiments in space [27]. Lal [28] and Miyagarva [29] have designed experiments for recrystallizing large single crystals under controlled conditions, both with and without seed crystals. We would propose experiments of both types for our linear chain molecules. The gel method of Lind [25] has not been tried for materials of this type and should be investigated. Also variations of Professor Authier's crystallization vessel should be designed and controlled experiments carried out. However, it is anticipated that recrystallization techniques probably have the best chance of producing high quality crystals and our emphasis would be directed toward such studies. The first stage of activity would be to optimize the variables controlling spontaneous nucleation and growth from saturated aqueous solutions. Crystals obtained should be suitable for X-ray diffraction studies and for seeding growth of larger crystals in stage two experiments. These stage two efforts will be directed to the formation of large crystals by controlling precisely the degree of supersaturation and mass transport phenomena. Several different crystallization vessels have been proposed in the literature which could be used for initial design purposes [30, 31]. Crystal growth factors which will be investigated and optimized are: (1) the nature of the solvent; (2) the effects of additives and impurities upon morphology and material properties; and (3) the physical conditions of temperature, evaporation rate, and amount of agitation.

The current technique for preparing the Elpasolites is as follows. A stoichiometric mixture of the respective metal chlorides is evaporated to dryness and placed in a quartz tube having a tapered end (the tapered end facilitates the nucleation of the single crystal). The tube is

vacuum sealed and the single crystals are grown by the Bridgeman technique of gradient solidification of the molten sample. The furnace consists of a tube of alumina wound with nichrome heating wire. The winding of the heating wire is made nonuniform across the length of the tube so as to produce a temperature gradient along the length of the tube and to produce the highest temperatures at the center of the tube. The sample is lowered through the furnace by driving a slow moving motor which has a timer arrangement which can control the rate of travel of the sample. The time required to grow a good single crystal varies from a few days to several weeks. Similar techniques have been proposed (and some experiments carried out in Skylab) for crystal growth experiments from melts in low gravity environments [26, 32-34]. Of special interest is the preparation of single crystals of the fluoroelpasolite,  $A_2^I B^I M^{III} F_6$ . These materials are grown in a manner similar to that outlined above for the chlorospecies except that the fluoride starting materials are placed in a platinum or graphite crucible and melted down in a stream of dry  $N_2$  in a zone melting apparatus. This incongruently melting material is prepared in single crystal form by using a very slow travel rate through the furnace. Many single crystals of these materials will be prepared and their properties monitored by EPR, magnetic circular dichroism and optical spectroscopy. Special attention will be given to the effects of crystal imperfections in luminescent properties and crystalline phase transitions.

#### SUMMARY

We presently have programs of study underway where the ultimate success depends on our ability to prepare large, high quality single

crystals of transition metal and rare earth complexes. Extensive ground-based crystal growing experiments would provide definite data on optimization parameters which could be used to design significant crystal growing experiments in low gravity. The success of the program would be two-fold; new insight into the parameters which control crystal growth would be obtained; and new materials of intrinsic scientific and technological importance would be prepared and characterized.

NOTES AND REFERENCES

1. The  $\alpha$ -amido acid complexes of the first row transition metals are being investigated with NSF funding (Grant No. CHE76-17434, Dr. Good, Principal Investigator) and the Elpasolite research is also presently funded by NSF (Grant No. DMR78-11540, R. Schwartz, Principal Investigator).
2. For a general review of such models and related discussions see: R. L. Carlin and A. J. Van Duyneveldt, "Magnetic Properties of Transition Metal Compounds", Springer-Verlag, New York, 1977.
3. H. Eichelberger, R. Majeste, R. Surgi, L. Trefonas, M. L. Good, and D. Karraker, J. Am. Chem. Soc. 99, 616 (1977).
4. M. M. Morelock, M. L. Good, L. M. Trefonas, L. Maleki, H. R. Eichelberger, R. Majeste, J. Dodge and D. Karraker, J. Am. Chem. Soc., in press (scheduled for August, 1979 issue).
5. M. M. Morelock, M. L. Good, L. M. Trefonas, R. Majeste and D. Karraker, J. Am. Chem. Soc., submitted.
6. Criteria used in postulating the hydrogen bonding are as follows: (1) contact distances should be reasonably short, i.e. less than  $3A^\circ$ ; and (2) assuming that the hydrogen atoms involved in bonding lie very nearly on the line connecting oxygen atoms; H-O-H angles should be comparable to the normal H-O-H angle of  $105^\circ$ .
7. I. Dzyaloshinsky, J. Phys. Chem. Solids, 4, 241 (1958).
8. T. Moriya, Phys. Rev., 120, 91 (1960).
9. T. Moriya, "Magnetism", Vol. 1, G. T. Rado and H. Suhl, Eds., Academic Press, New York, 1963, Chapter 3.
10. H. M. Crosswhite and H. W. Moos, "Optical Properties of Ions in Crystals", Interscience, New York, 1967 and references cited therein.
11. C. H. Dieke, "Spectra and Energy Levels of Rare Earth Ions in Crystals", Interscience, New York, 1968 and references cited therein.
12. "Absorption and Magnetic Circular Dichroism Spectra of Octahedral  $Ce^{3+}$  in  $Cs_2NaYCl_6$ ," R. W. Schwartz and P. N. Schatz, The Physical Review, B8, 3229 (1973).
13. "An EPR Study of  $Ce^{3+}$ ,  $Dy^{3+}$ ,  $Dy^{3+}$  in  $Cs_2NaYCl_6$ . A Crystal with Sites of Perfect Octahedral Symmetry," R. W. Schwartz and N. J. Hill, Journal of the Chemical Society Faraday II, 70, 124 (1974).
14. "The Electronic Structure of  $Cs_2NaEuCl_6$ ," R. W. Schwartz, Molecular Physics, 30, 81 (1975).
15. "Low Temperature Crystalline Phase Transition in Some Elpasolite-Hexachlorides," R. W. Schwartz, S. F. Watkins, C. J. O'Connor, and R. L. Carlin, J. Chem. Soc. Faraday II, 72, 565 (1976).

16. "The Absorption and Magnetic Circular Dichroism Spectra of  $\text{Cs}_2\text{NaPrCl}_6$ ," R. W. Schwartz Molecular Physics, 31, 1909 (1976).
17. "Electron Paramagnetic Resonance Study of  $\text{Er}^{3+}$  and  $\text{Gd}^{3+}$  in  $\text{Cs}_2\text{NaLnCl}_6$ ," C. J. O'Connor, R. L. Carlin, and R. W. Schwartz, J. Chem. Soc. Faraday II, 73, 361 (1977).
18. "Magnetic Circularly Polarized Emission and Magnetic Circular Dichroism Study of the  ${}^7\text{F}_J \rightarrow {}^5\text{D}_4$  Transitions in Crystalline  $\text{Cs}_2\text{NaTbCl}_6$ ," R. W. Schwartz, H. G. Brittain, J. P. Riehl, W. C. Yeakel, and F. S. Richardson, Molecular Physics, 34, 361 (1977).
19. "Emission Spectra of  $\text{Cs}_2\text{NaCl}_6:\text{Tb}^{3+}$ ," L. C. Thompson, O. A. Serra, J. P. Riehl, F. S. Richardson, and R. W. Schwartz, Chemical Physics, 26, 393 (1977).
20. "The Absorption and Magnetic Circular Dichroism Spectra of  $\text{Cs}_2\text{NaTmCl}_6$ ," R. W. Schwartz, T. R. Faulkner, and F. S. Richardson, Molecular Physics, accepted for publication.
21. J. R. Carruthers, Prog. Astronaut. Aeronaut. 1977. 52, (Material Science Space Applications), P. 33-40.
22. J. R. Carruthers, J. Crystal Growth, 42, 379 (1977).
23. P. Bennema, J. Crystal Growth, 24-25, 76 (1974).
24. M. Hayashi and T. Shichiri, J. Crystal Growth, 21, 254 (1974).
25. M. D. Lind, AIAA Journal, 16, 458 (1978).
26. H. Weiss, Proc. R. Soc. London, A., 361, 157 (1978).
27. A. Authier, oral report, Fluids Experiment System Workshop, July 11-12, 1979, NASA, Huntsville, Alabama.
28. R. B. Lal, NASA Report No. AAMU-NAS-002, February, 1977.
29. I. Miyagawa, Prog. Astronaut. Aeronaut., 48, 540 (1976).
30. A. I. Munchaeu, Sov. Phys. Crystallogr., 18, 566 (1974).
31. I. F. Nicolau, Kristall and Technik, 9, 1331 (1974).
32. H. Wiedemeir, NBS Special Publ. (U.S.) 1978 520, p. 25 (1978).
33. H. Walter, Prog. Astronaut. Aeronaut. 48, 463 (1976).
34. A. F. Wilt, H. C. Gatos, M. Lichtensteiger and C. J. Herman, J. Electrochem. Soc., 125, 1832 (1978).

## INFLUENCE OF CONVECTION ON FREE GROWTH OF DENDRITE CRYSTALS FROM SOLUTION

J. Hallett and E. Wedum<sup>(a)</sup>

The free growth of dendrites in a uniformly supercooled solution has been examined using cine photography with a Schlieren optical system. Crystals were grown in the bulk of the solution from a centrally located capillary tube, nucleated at the interface with a liquid nitrogen cooled wire. Crystals propagated along the tube, the slower growing orientations eliminated, and emerged at the tip, usually growing parallel to the tube direction. For both sodium sulfate decahydrate from its solution and ice from sodium chloride solution, growth rate and fineness of dendrites increased with supercooling. In sodium sulfate, upward convection of the less dense depleted solution occurs; downward convection was observed for the rejected, more concentrated sodium chloride solution. In both cases, there was a spatial and temporal delay in the release of the convective plume from the moving dendrite tip. The role of this convection on the growth characteristics and the production of secondary crystals is examined. A proposed low-g experiment will examine differences in growth rate, crystal texture and secondary nucleation in a reduced convective regime where molecular diffusion is the dominant transfer process.

---

<sup>(a)</sup> Atmospheric Sciences Center, Desert Research Institute, Reno, Nevada 89507

INFLUENCE OF CONVECTION ON FREE GROWTH OF DENDRITE CRYSTALS FROM SOLUTION

by

J. Hallett and E. Wedum<sup>(a)</sup>

INTRODUCTION

The growth morphology of a crystal is known to depend in a complex way on the environmental conditions: supersaturation or supercooling, physical properties of the fluid, Prandtl and Sherwood number, and the bulk fluid flow around the crystal. These parameters influence the growth of the crystal through heat and mass transport processes, and, most important from the viewpoint of growth rate and crystal habit, through the kinetic processes taking place at the crystal interface. Plane faces appear when layer growth takes place in low index direction in regions of modest supersaturation, with layers originating either from defects or on crystal edges protruding further into the diffusion field and subject to surface nucleation. Skeletal crystals form when these layers fail to reach the crystal center before nucleation of further layers.

Experimental studies aimed at investigating the nature of these dependencies and the molecular detail of the growth mechanism necessarily aim for an idealization experiment to reduce the number of physical variables. For very small growth rates, an isothermal experiment is a practical idealization; rapid stirring prevents local density differentials. For more rapid growth rates, an adiabatic idealization is practical, with crystals growing freely into an infinite, constant condition environment. This latter case is relevant to more extreme growth conditions with large driving force for growth. In all cases, it is necessary to avoid the presence of extraneous surfaces which give spurious heat transfer or nucleation.

<sup>(a)</sup> Atmospheric Sciences Center, Desert Research Institute, Reno, Nevada 89507

A second feature of crystal growth, especially in the case of these higher driving forces, is the occurrence of secondary crystallization - that is, of the formation of crystals of orientations other than that of an initial single crystal, a phenomenon which gives a differing crystal texture and impurity distribution following complete solidification.

In assessing the role of these different parameters, there are several aspects of the crystal growth to be considered. The habit, the ratio of growth velocity in different low index planes, the absolute growth rate in these directions, the tendency to skeletal growth, and the occurrence of secondary crystals are all important both from the viewpoint of understanding the growth mechanism and from the viewpoint of crystal growth technology.

From the viewpoint of the utility of a low-g environment, there are two aspects of growth selected for study here which are very difficult to investigate in 1-g situations. With dendrites in free growth, the growth rate and dendrite dimension are determined by the ambient supercooling. In 1-g and in an unstirred environment, the release of latent heat and/or depletion of the nearby solution lead to density differences which give rise to local convection. The question arises as to the importance of this self-induced convection on the growth of the dendrite; first, is there an enhancement of dendrite growth because of the motion (it is known that externally imposed motion enhances growth rate), and second is this motion responsible for any secondary crystal nucleation. These questions are relevant for growth in an environment initially at rest with respect to the growing crystal, and not set in motion on the scale of the containing tank. The following experiments were designed to investigate the physical processes occurring in 1-g growth and serve as a basis for assessing the presence of self-induced natural convection by direct comparison with an identical experiment in low-g.

From the viewpoint of ease of study, the crystallization of sodium sulfate decahydrate from supersaturated solution was chosen. A liter of near saturated solution can readily be supercooled as much as 10C; it is transparent and ideal for optical studies in a convenient range of temperatures, the saturated solution crystallizing at 32.5C. Studies were also carried out of ice crystallizing in sea water (approximately 0.4 M NaCl). The solution was contained in a tank with plate glass viewing windows, dimensions 7 in x 7 in high x 1.5 in thick. It was thermostated to  $\pm 0.2C$  with a similar vertical and horizontal uniformity. An L-shaped Teflon capillary tube was located at the side of the tank (Fig. 1). This arrangement allowed crystallization to be initiated in the bulk of the liquid. A liquid nitrogen-cooled wire was inserted into the capillary; nucleation occurred at the cold spot and crystals grew inside the Teflon tube. The slower growing directions were eliminated, and a fast growth dendrite would usually emerge from the open end to grow horizontally into the liquid. The whole system was inserted into a Schlieren optical system, with the results recorded on still or movie film (Fig. 2). This technique is similar to that employed for the studies of sodium chlorate crystals by Chen et al. (1). Sodium sulfate solution crystallizing to decahydrate gave upward convection of diluted solution; sodium chloride solution crystallizing to ice and rejecting the solute gave a denser solution with downward convection (Fig. 3a,b). In both cases, crystallization velocity increased with supercooling. At large supercooling ( $\gtrsim 10C$  for  $Na_2SO_4$  and  $\gtrsim 5C$  for ice) with velocities  $\sim cm\ s^{-1}$ , the crystal growth kept ahead of any convection and no effects were visible. Very low growth velocities ( $R < 0.01\ cm/sec$ ) at  $\Delta T < 3C$  for  $Na_2SO_4$  and  $\Delta T < 0.25C$  for ice, were complicated by thermal interactions with the walls of the tank. This gives a range of supercooling of about 8 C for  $Na_2SO_4$  and 4 C for ice over which data could be obtained where differences

ORIGINAL PAGE IS  
OF POOR QUALITY

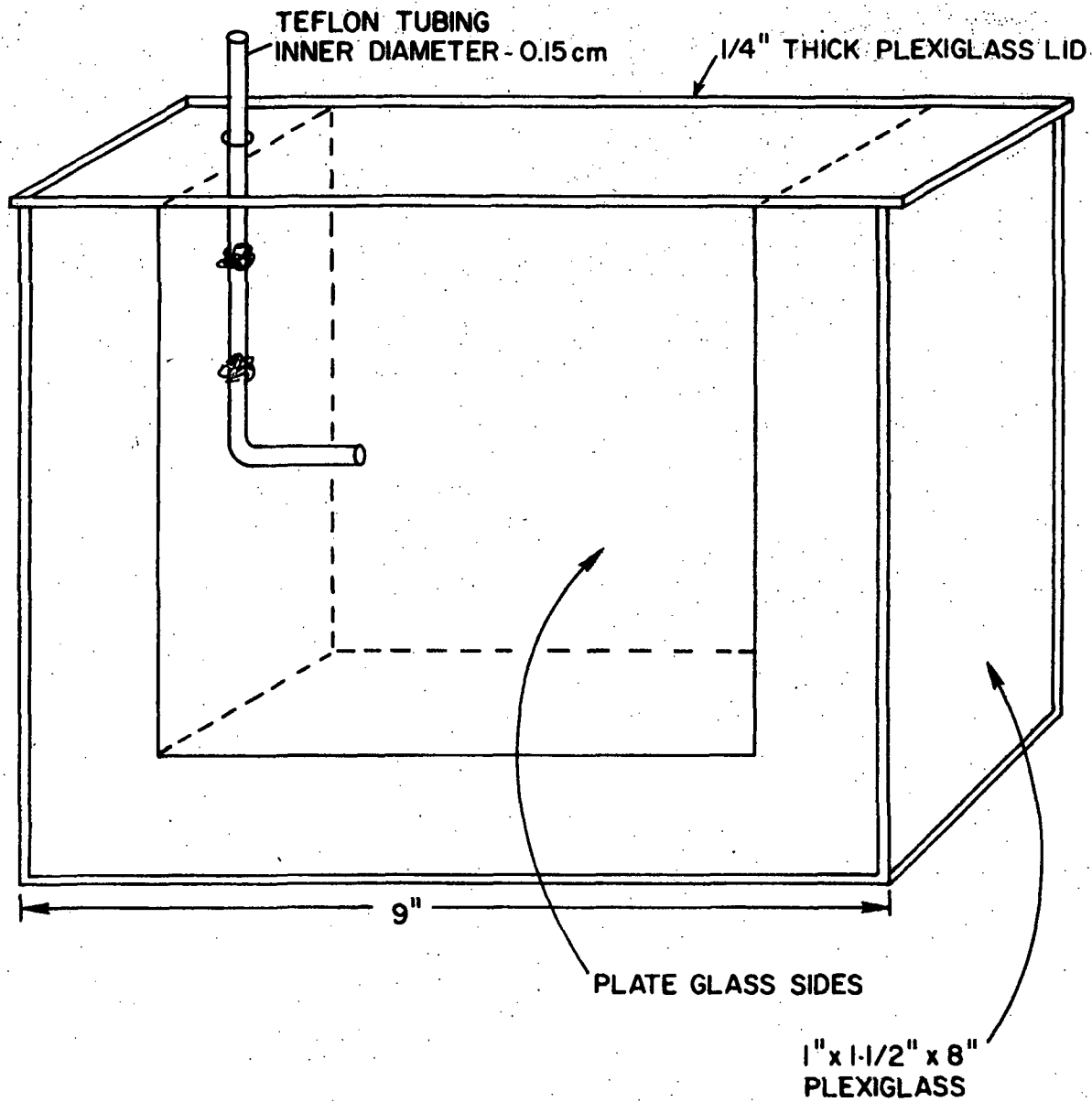


Fig. 1. Tank for initiating crystallization in the bulk of the supercooled liquid. The tip of a stainless steel wire was cooled in liquid N<sub>2</sub> and then inserted into the Teflon tube as far as the bend. Dendrites grew from the tube tip into the liquid.

ORIGINAL PAGE IS  
OF POOR QUALITY

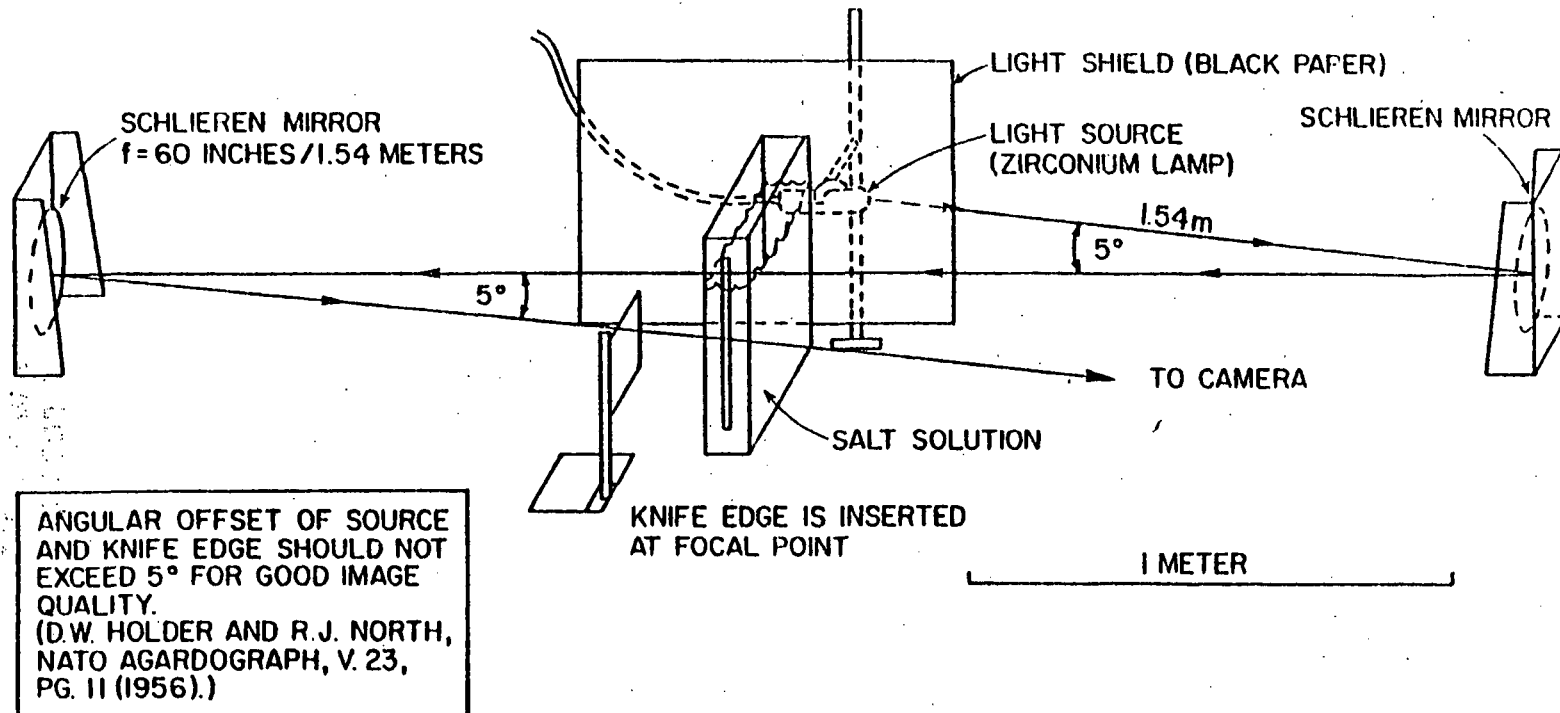
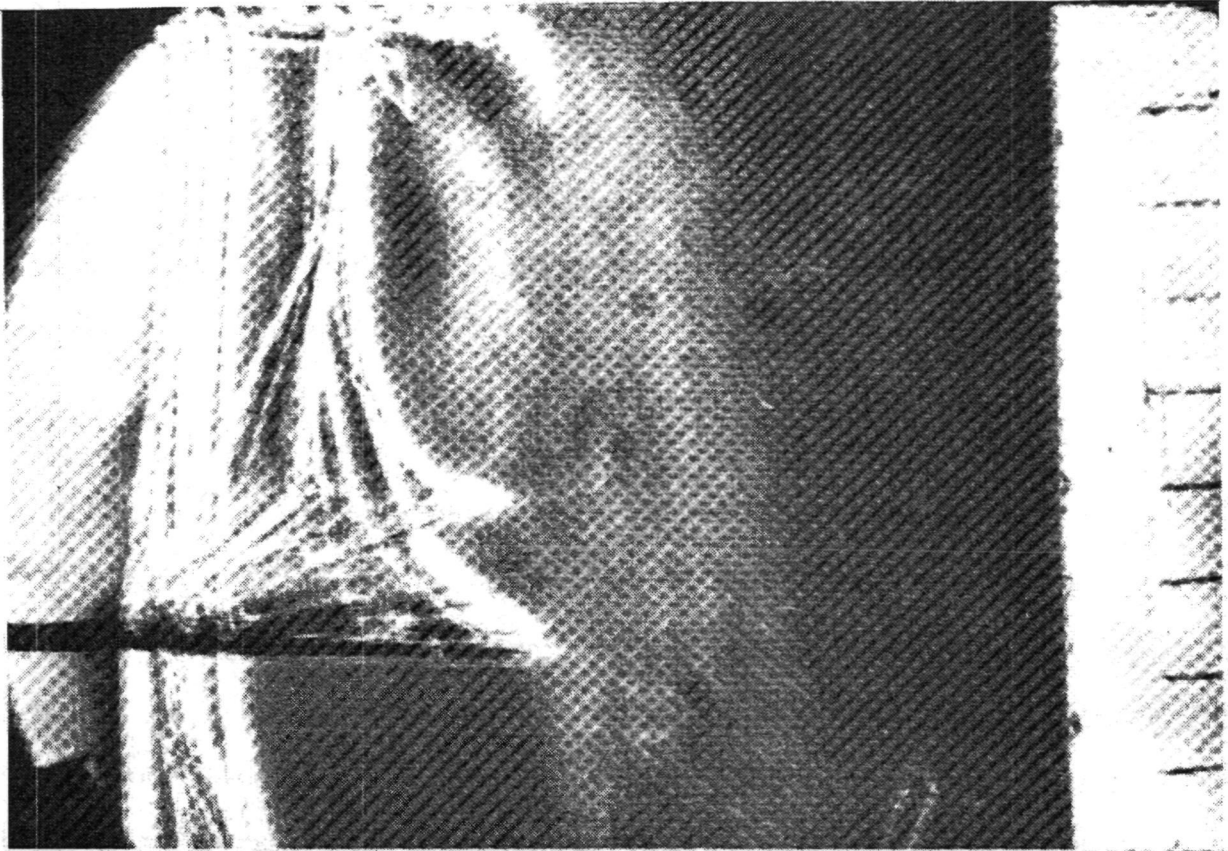


Figure 2. The Schlieren System. The light source is a 10 watt Zirconium arc lamp.

3a



3b

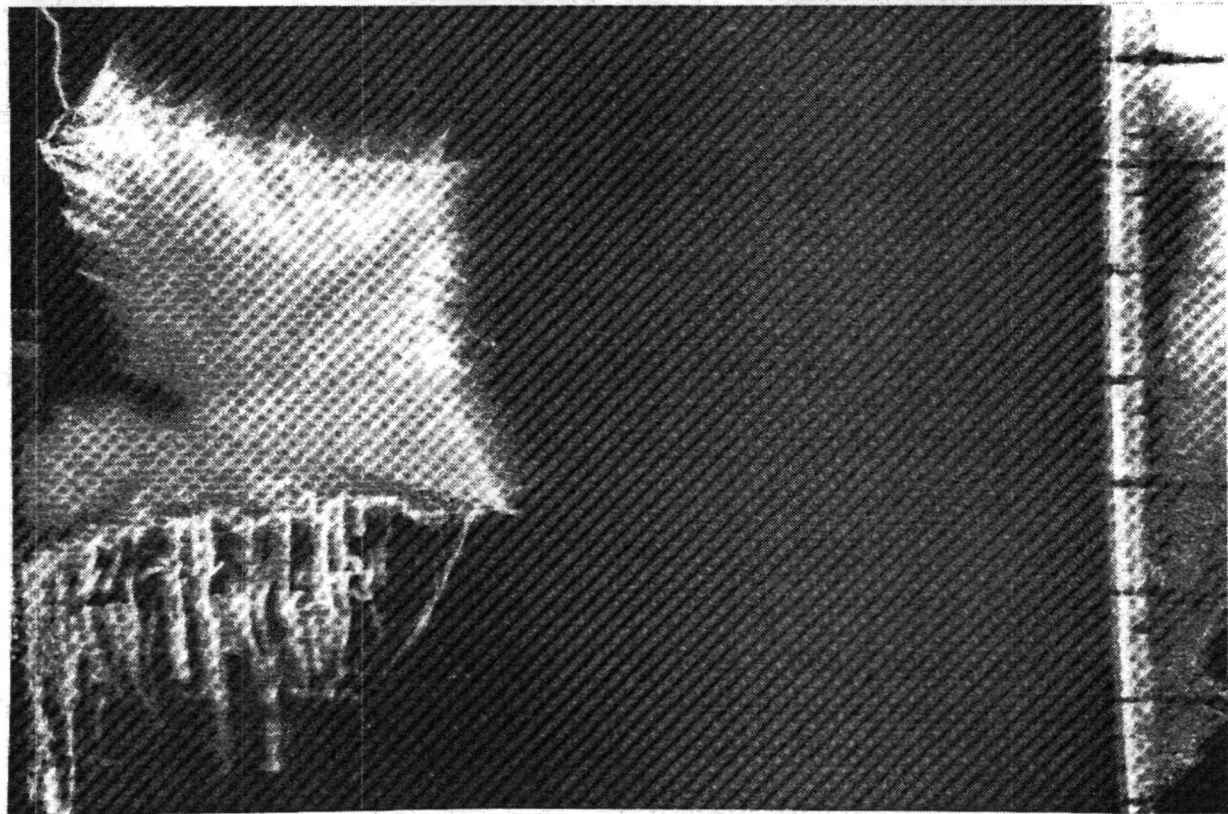


Figure 3. Crystallization of  $\text{Na}_2\text{SO}_4 \cdot 10\text{H}_2\text{O}$  from solution and ice in sea-water. Both pictures were taken with Tr-X film utilizing the tank and Schlieren system shown in Figs. 1 and 2. The plume from growing  $\text{Na}_2\text{SO}_4 \cdot 10\text{H}_2\text{O}$  dendrites (3a) convects upward at  $\sim 0.2 \text{ cm s}^{-1}$  (2.7 M,  $\Delta T = 5.5 \text{ C}$ ). The plume from the ice dendrites (3b) convects downward at  $\sim 0.01 \text{ cm s}^{-1}$  ( $\Delta T = 0.5 \text{ C}$ ). Scale divisions on the right are 1 cm.

are expected because of natural convection. Within this range, it was necessary to examine the growth only during the period that the convection had not set up a general circulation in the tank - some 2 to 30 s.

### RESULTS

For dendrites of both sodium sulfate decahydrate and ice, a convective plume was evident coming from just behind the advancing tip. A starting plume began as growing crystals emerged from the capillary, with velocity  $\sim 0.2 \text{ cm s}^{-1}$  for sodium sulfate and  $0.01 \text{ cm s}^{-1}$  for ice in sea-water (Fig. 4). As this moved away from the tip, the  $\text{Na}_2\text{SO}_4$  plume retained shape similarity with respect to the tip and became approximately parabolic, as can be seen from Fig. 3 for both ice and sodium sulfate. There is a spatial delay in the visible plume detaching from the dendrite, which increases with the crystal growth velocity (Fig. 5). To a first approximation, the time for detachment is independent of the growth velocity and is 10 s for sodium sulfate and 20 s for ice. There is an asymmetry in the growth velocity of dendrites with direction which is a complicated function of both crystal habit and convection velocity. In  $\text{Na}_2\text{SO}_4$  solution (Fig 3a), dendrites will grow more slowly into the disturbed solution with the fastest growing crystal being horizontal, while the ice crystal is distinctly inhibited in the convecting region (3b). Growth of dendrites into undisturbed fluid is aided by convection as can be clearly seen in these figures.

For sodium sulfate, secondary nucleation of crystals occurs for supercoolings between 3 and 6C. These small crystals rise with the buoyant fluid, grow, and produce yet more crystals as they fall out. For ice, larger crystals occasionally break away at supercooling  $>1 \text{ C}$  to give other orientations. Ice, being less dense than the solution, rises - decahydrate being more dense finally sinks relative to the fluid motion. In each case, the crystals move into fresh

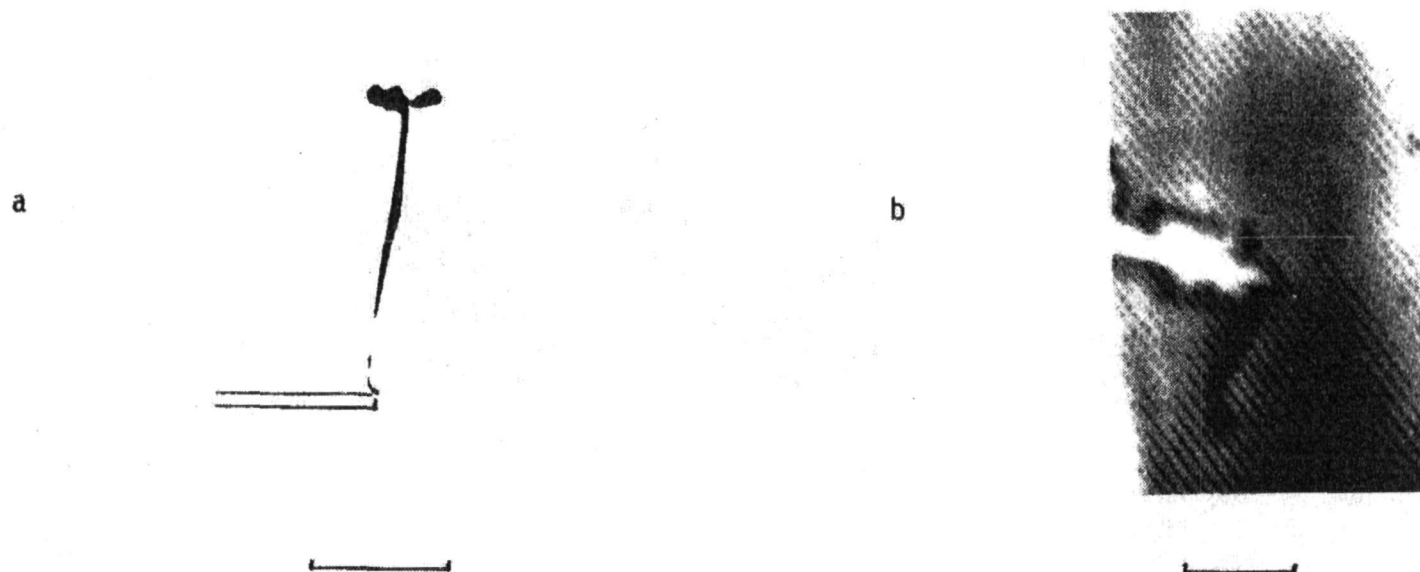


Figure 4. Initial plume from crystal issuing from end of Teflon tube.

a.  $\text{Na}_2\text{SO}_4 \cdot 10\text{H}_2\text{O}$ ; 3.0 M,  $\Delta T = 6.5 \text{ C}$  .

b. Ice in sea-water, 28‰,  $\Delta T = 0.5 \text{ C}$  .

Negative prints from Plus-X Reversal film.

All scales show 1 cm.

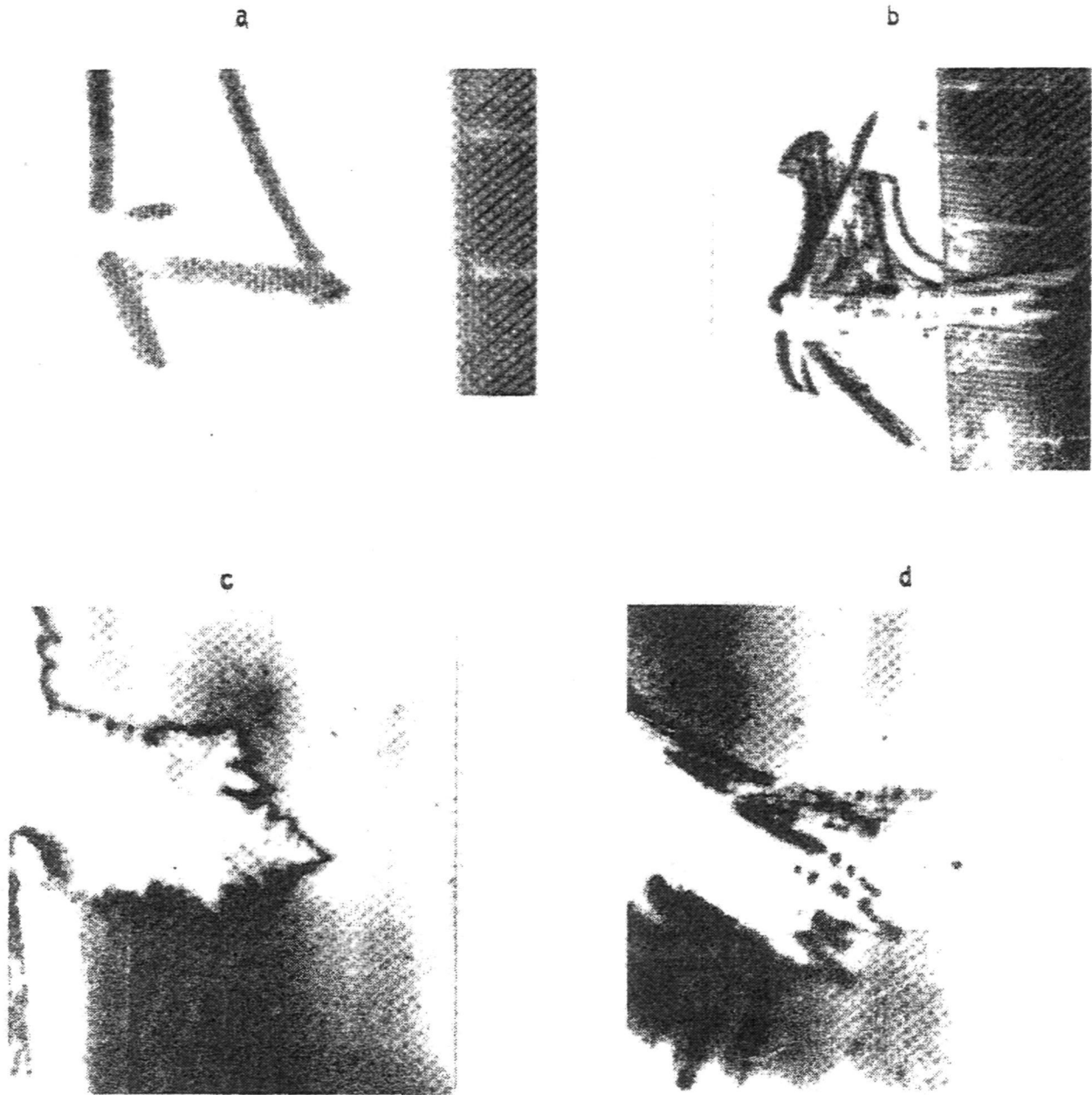


Figure 5. Spatial delay in the separation of the plume from the crystal increases with increased velocity. a and b are 3.0 M  $\text{Na}_2\text{SO}_4 \cdot 10\text{H}_2\text{O}$  dendrites with  $V = 0.02$  cm/sec, spatial delay = 0.16 cm and  $V = 0.2$  cm/sec, delay = 1.7 cm. c and d are 28% salinity sea water dendrites with  $V = 0.008$  cm/sec, delay = 0.16 cm and  $V = 0.025$  cm/sec, delay = 0.5 cm.

environmental fluid. As supercooling is increased, the morphology of the dendrites change, the branches becoming finer and apparently more fragile.

### DISCUSSION

Convective flow is sufficiently slow that the regime is laminar for all situations examined, with  $Re \lesssim 20$ . The convective velocity is consistent with the expected density differences. It increases as  $\Delta\rho^n$  ( $n \sim 1$  to a first approximation). The growth velocity of the dendrites on the other hand increases as  $\Delta\rho^m$  ( $m \sim 2-3$  to a first approximation) so that beyond a critical excess the growth is sufficiently rapid to mitigate any effect of 1-g convection. An estimate of Grashoff number ( $Gr$ ) is difficult, since the dimension to be taken as relevant for convection is not obvious, and the physical properties of the fluids under the experimental conditions are not known very precisely; a crude estimate is in the range 500 to 5000. A reduction of gravity by  $10^4$  would reduce  $Gr$  in proportion, with a corresponding overall reduction in mass heat transfer and velocity.

The role of increasing fineness of dendrites with supercooling is to be assessed in terms of their likelihood of breaking in the local flow or self-induced buoyancy (O'Hara and Tiller) (2). One might expect their strength to increase as  $d^4$  ( $d$  = diameter) with both buoyancy forces and drag force increasing approximately  $d^2$ , so finer dendrites would be more likely to fracture. On the other hand, finer dendrites might be expected to contain fewer defects; there is probably an optimum size for maximum fracture probability.

The lag of convection in detaching from a growing dendrite is to be interpreted in terms of a sufficient dimension being required to enable the buoyant fluid to separate - to be interpreted analytically in terms of a critical Rayleigh number. The possibility exists that there is a convective plume ahead of the visible plume which cannot be detected by the Schlieren technique.

This is limited by the optical path difference caused by the width of the convective plume ( $\sim$  mm), and the refractive index differential ( $\sim 10^{-3}$ ). This gives an order of magnitude refractive index gradient of  $10^{-2} \text{ cm}^{-1}$  overall; the detail of the local gradient is somewhat masked by the nature of the path length integration accomplished by the Schlieren system.

### CONCLUSION

The optical technique used in this experiment gives immediate qualitative information on the nature of the induced fluid flow around free growing dendrites. In the two systems investigated, new crystal orientations appear. In sodium sulfate this occurs only beyond a critical supercooling, and can be hypothesized as being associated with local shear resulting from natural convection. In the case of ice, new orientations apparently result from buoyant displacement of the larger crystals. A better understanding of these physical mechanisms will come from studies over a wider range of environmental conditions than has been attempted so far. In particular, a low-g experiment in which convective velocities are substantially reduced should yield a comparison situation in which no secondary crystals are produced and where growth velocities are uninfluenced by the fluid flow; in this case the optical system should yield detail of the molecular diffusion properties in a stationary environment around the growing dendrite. A candidate material for a study is sodium acetate - a trihydrate with a convenient melting temperature of 58 C.

The comparison study will give a better understanding of the mechanism of dendrite growth and its application in higher velocity crystallization, situations which often occur in metals (3) and solutions.

**ORIGINAL PAGE IS  
OF POOR QUALITY**

### ACKNOWLEDGEMENT

This work was supported in part by NSF Grant #AER75-19601, RANN and NSF Grant #ATM77-07995, Atmospheric Sciences Section of the National Science Foundation, Washington, DC.

## REFERENCES

1. P. S. Chen, P. J. Shlichta, W. R. Wilcox and R. A. Lefever, to appear in J. Crystal Growth, (1979).
2. S. O'Hara and W. A. Tiller, Trans. Metall. Soc. A. S. M. E., 239, 497-501, (1967).
3. P. G. Grodzka and C. S. Griner, AIAA 15th Aerospace Sciences Meeting, Los Angeles, CA, January 24-26, 1977.

**ORIGINAL PAGE IS  
OF POOR QUALITY**

CONVECTIVE AND MORPHOLOGICAL  
INSTABILITY IN VAPOR CRYSTAL GROWTH †

F. Rosenberger  
Department of Physics  
University of Utah  
Salt Lake City, Ut 84112

ABSTRACT

Theoretical and experimental work on the fluid dynamics of physical vapor transport is reported. It is shown that diffusion in viscous interaction with container walls leads to concentration gradients normal to the main transport direction. Consequently any convection threshold is removed. This coupling with convective instabilities makes the theoretical interpretation of earthbound (anisotropic) morphological stability studies on vapor-solid interfaces intractable. Hence low-gravity experiments are suggested that will allow for the establishment of morphological stability criteria under diffusion controlled conditions.

† Research support by the National Science Foundation under grant DMR-7913183 and by the National Aeronautics and Space Administration under grant NSG-1534 is gratefully acknowledged.

## INTRODUCTION

Crystallization from vapors has gained ever increasing importance in materials preparation and solid state device production. Vapor-to-solid processes have various advantages [1] over, say, crystallization from melts. These advantages result mostly from (i) the lower temperatures involved, and (ii) the fact that vapor-solid interfaces, due to their low atomic roughness [2] exhibit considerable morphological (i.e. interfacial shape) stability during growth.

Most solid state devices utilize extensive properties of solids, i.e. properties that have been obtained through the introduction of impurities ("dopants") into the solid, typically during its growth. The performance of devices depends often strongly on the compositional homogeneity and structural perfection of the solid. These, in turn, depend to a large extent upon the mass and heat transfer conditions in the vicinity of the solid-nutrient (vapor) interface during growth. Steady non-uniform, and in particular nonsteady transport [3-5] can result in inhomogeneities that severely limit device performance. Hence a quantitative understanding of the transport mechanisms that prevail in vapor-solid processes under physical and chemical conditions relevant to materials preparation is of great technological importance.

The transport conditions that are characteristic for vapor crystal growth and, hence, the required transport models are unusually complex. The presence of numerous chemical species demands multicomponent concentration diffusion treatments. Displacement flows ("streaming") due to changes in the number of vapor molecules during interfacial reactions must be accounted for. The steep temperature and concentration gradients often employed lead readily to nonsteady, oscillatory convective phenomena. Further complications arise in various semiconductor production processes where vapor (gas) mixtures of components with strongly differing molecular weight are used. Then thermal (Soret) diffusion must be taken into account. Radiative heat transfer is often significant or even dominant. These complex conditions are further aggravated by the complicated geometries and boundary conditions encountered in practice--conditions which have typically not been considered yet in

the fluid dynamics literature. Consequently, with a few exceptions, the current understanding of the transport that prevails in crystal growth from vapors is rather limited and mostly of a qualitative nature.

In order to obtain guidance for advantageous design and control of (vapor-solid) crystal growth processes, three (coupled) questions must be addressed; viz,

- (1) What are the critical (boundary) conditions that lead to time dependent (oscillatory, "turbulent") heat and mass transport?,
- (2) To what extent does the uniformity of (steady) transport depend on practical boundary conditions?,
- (3) What limits the stability of a certain interfacial shape, i.e., how fast can a crystal be grown without developing morphological instabilities--which, in turn, lead to inhomogeneities in the solid even if the transport in the bulk nutrient were steady and uniform--? This question is of particular importance in vapor crystal growth where one encounters often very low growth rates.

The author and his co-workers have begun experimental and theoretical investigations on various simplified model configurations towards the clarification of the first two questions. For a review of these efforts see [1].

In the following we will outline some selected results. Then we will briefly discuss the current state of understanding of morphological stability in vapor growth and point out the necessity for further work in these areas. The selection of topics is oriented on the great potential of a low-gravity environment for the clarification of these fundamentally and practically important questions.

#### DIFFUSIVE-CONVECTIVE TRANSPORT

To date most analyses of transport in closed tube systems have not accounted for the viscous fluid dynamics of the transport flows. One of the reasons is that at the typical flow velocities (Reynolds numbers) neither creeping flow nor boundary layer approximations can yield significant insight. Existing treatments of diffusion-governed mass transport in closed vapor growth systems are exclusively formulated as one-dimensional problems (see summary in [1]).

In order to investigate the effect of viscous interaction of the transport flows with the container walls we have numerically modeled the physical vapor transport of a component A through an inert gas B in vertical cylindrical ampoules. The full fluid dynamic treatment [6-8] shows that the "no-slip condition" (mass average velocity zero on walls) has considerable consequences:

- (1) In contrast to the one-dimensional treatments, where the inert component B is considered stagnant, B is found to recirculate even in the absence of gravity.
- (2) The mere diffusive-advective mass flux (zero gravity) is accompanied by radial concentration gradients. Due to viscous interactions, component A is transported with some preference in the core region, whereas B tends to accumulate at larger radii.
- (3) Convection (buoyancy-driven) fluid motion occurs without threshold due to gravitational interaction with the diffusion-induced (horizontal) density gradients (a new insight into the convective stability of multi-component fluid columns).

Another result that is relevant here stems from our experimental studies of convective instabilities in closed vertical cylinders [9,10]. Measurements of the critical Rayleigh numbers for the onset of various convection modes showed that thermal (Soret) diffusion, in contrast to widespread belief, can play a decisive role in the transport of vapors in ampoules. Drastic convective destabilization and, hence, changes in the concentration distribution was observed in binary gas mixtures.

#### MORPHOLOGICAL STABILITY

The morphological stability of a growing crystal depends on the growth mechanism which in turn is a consequence of the atomic structure of the interface. Rather isotropic growth, i.e., adjustment of the interface to the geometry of the mass and heat transfer field will occur when the interface is atomically rough [2] as in many melt growth systems. Isotropic (one-dimensional) morphological stability theory [11-13] predicts the critical concentration and temperature gradients, normal to a planar interface at which (in practice always present) shape perturbations can grow. Under subcritical conditions all (small amplitude) perturbations in the interface shape decay and the original planar form

is restored. Interfacial breakdown conditions and spatial periodicity of perturbation features observed in crystal growth from melts support isotropic morphological stability rather well. One should mention, however, that few experiments have yet been characterized sufficiently to allow for an evaluation of the "fine-structure" of the various theoretical models. Most recently it has been recognized that in certain parameter regimes there is a strong coupling between morphological and fluid dynamics instabilities [14]. Convective instability (from melt density gradients close to the interface, dominantly due to solute rejection) may considerably lower the critical growth rate predicted from merely diffusive transport.

Solid-vapor interfaces, due to their low atomic roughness, grow dominantly by (anisotropic) layer spreading. Adatoms have to diffuse on the average over distances of many lattice constants before they become incorporated into the lattice. Macroscopically this is reflected in the occurrence of facets. Faceted growth is considerably less responsive to the mass and heat transfer geometry in the fluid than isotropic growth.

In spite of the pronounced kinetics anisotropy, efforts were made to describe morphological stability in vapor growth, in analogy to melt growth, with an isotropic model [15,16]. This constitutional supersaturation concept (CSS) has been employed in various theoretical papers on vapor crystal growth [17,18,19]. However, the only experiment that seemed to verify CSS quantitatively [16] was shown by our group to be in error by one order of magnitude [20]. Other experiments [17,18] agreed with CSS only to within a factor of 2-3. Vapor solid interfaces, are generally found to be more stable than the isotropic CSS predicts.

Anisotropic morphological stability theory [21-23] has been advanced to a point where interfacial breakdown can be predicted in (faceted) solution and vapor growth if (i) certain interfacial kinetics parameters are known and (ii) transport is diffusive from a homogeneous bulk nutrient. The predicted trends [21-23] are well confirmed experimentally. There are, however, no adequately characterized (vapor) growth experiments that allow for a quantitative comparison with anisotropic morphological stability theory.

Much more work on transport dynamics and morphological stability is needed for a better understanding of vapor crystal growth. Much of this work can be performed under 1-g conditions. The investigative possibilities on earth are still far from being fully exploited. However, a low gravity environment offers fascinating possibilities which, even when taking the drastically higher research costs into account, would result in considerable higher efficiency in acquiring the badly needed insights.

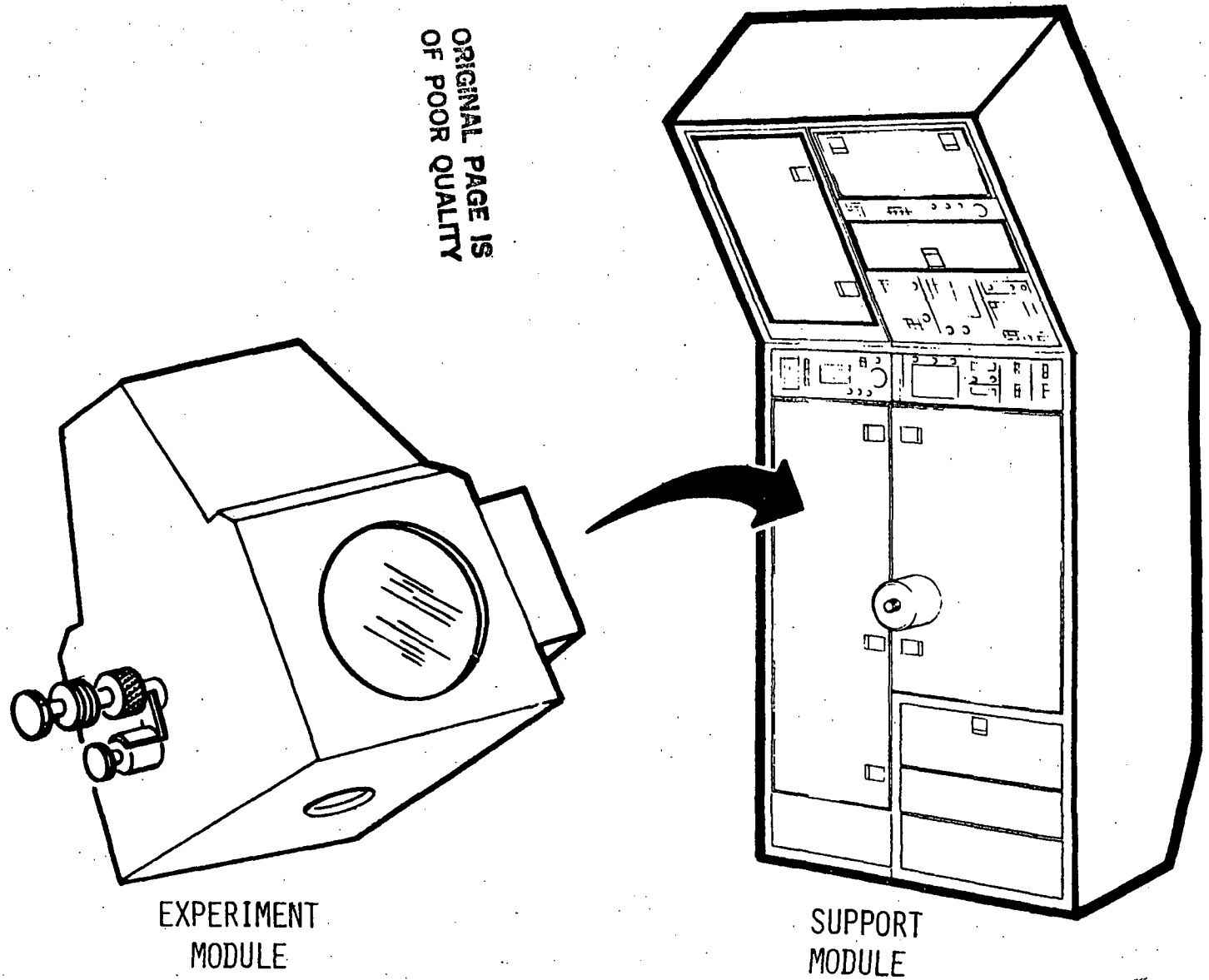
In particular, earthbound vapor-solid morphological stability studies that can be theoretically evaluated will be impractical in the foreseeable future. The anisotropic interface kinetics complicates the problem to an extent where externally imposed temperature and concentration gradients parallel to the interface make a theoretical description mathematically intractable. Meaningful morphological stability studies require relatively large dimensions of the interface (centimeters) in order to observe theoretically expected periodicities in the developing instabilities. Hence, in order to avoid significant diffusion-induced gradients normal to the main transport direction (i.e., radially in an ampoule) walls must be widely spaced from the growing interface. This, however leads to convectively unstable ampoule dimensions and pronounced convection-induced concentration non-uniformities in the (bulk) vapor.

Therefore it is proposed that morphological stability experiments on optimally chosen vapor-solid interfaces (with and without Soret diffusion) be conducted in the Fluid Experiment System. As a "fringe benefit" of these investigations some clarification could be obtained on the concentration profiles which, as our modeling suggests, are introduced by mere diffusion in viscous interaction with container walls, a topic of great general fluid dynamic interest.

REFERENCES

1. F. Rosenberger, Fluid Dynamics in Crystal Growth from Vapors (Levich-Lecture), Int. y. Physico-chemical Hydrodynamics (in press).
2. H. J. Leamy, G. H. Gilmer and K. A. Jackson, Statistical Thermodynamics of Clean Surfaces, Chapter 3 in Surface Physics of Materials, J. M. Blakely, ed. (Academic Press, New York, 1975) Vol. 1, p. 121-188)
3. B. J. Curtis, J. P. Dismukes, Effects of Natural and Forced Convection in Vapor Phase Growth Systems, J. Crystal Growth 17, 128 (1972).
4. J. P. Dismukes, and B. J. Curtis, A Survey of Convective Instabilities in Silicon CVD Systems, Proc. Second Intl. Symp. on Silicon Science and Technology (Electrochem. Soc., Princeton, 1973).
5. F. Rosenberger, Fundamentals of Crystal Growth, Vol. 1: Macroscopic Equilibrium and Transport Concepts, Chapter 6: Segregation (Springer-Verlag, Berlin Heidelberg New York, 1979).
6. D. W. Greenwell, Numerical Studies of Physical Vapor Transport, Ph.D. Thesis, University of Utah (1979).
7. D. W. Greenwell, B. L. Markham and F. Rosenberger, Numerical Modeling of Vapor Transport in Vertical Ampoules (in preparation).
8. B. L. Markham and F. Rosenberger, Velocity and Concentration Distribution in Stefan Diffusion Tubes (in preparation).
9. J. M. Olson and F. Rosenberger, Convective Instabilities in a Closed Vertical Cylinder Heated from Below; Part I: Monocomponent Gases, J. Fluid Mechanics 92, 609 (1979).
10. J. M. Olson and F. Rosenberger, Convective Instabilities in a Closed Vertical Cylinder Heated from Below; Part 2: Binary Gas Mixtures, J. Fluid Mechanics 92, 631 (1979).
11. R. F. Sekerka, Morphological Stability, in Crystal Growth: An Introduction, P. Hartman, ed., (North-Holland, Amsterdam, 1973) p. 403.
12. R. T. Delves, Theory of Interface Stability, in Crystal Growth, B. R. Pamplin, ed., (Pergamon, Oxford, 1975) p. 40.
13. D. K. Wollkind, A Deterministic Continuum Mechanical Approach to Morphological Stability of the Solid-Liquid Interface, in Preparations and Properties of Solid State Materials, Volume 4, W. R. Wilcox, ed. (Marcel Dekker, New York, 1979) p. 111.
14. S. R. Coriell, M. R. Cordes and W. J. Boettinger, Convective and Interfacial Instabilities During Unidirectional Solidification of a Binary Alloy (Submitted to J. Crystal Growth).

ORIGINAL PAGE IS  
OF POOR QUALITY



EXPERIMENT  
MODULE

SUPPORT  
MODULE

Figure 1. Experiment Module and Support Module Exteriors for FES  
(Cell is representative of the Lal Radial Growth Experiment)

## CRYSTAL GROWTH OF SULFIDE MATERIALS FROM ALKALI POLYSULFIDE LIQUIDS

William B. White  
Materials Research Laboratory  
The Pennsylvania State University  
University Park, Pennsylvania 16802

## ABSTRACT

The fluids experiment system has been designed for low temperature solution growth, nominally aqueous solution growth. The alkali polysulfides, compositions in the systems  $\text{Na}_2\text{S-S}$  and  $\text{K}_2\text{S-S}$  form liquids in the temperature range of 190 to 400°C. These can be used as solvents for other important classes of materials such as transition metal and other sulfides which are not soluble in aqueous media. Among these materials are luminescent and electroluminescent crystals whose physical properties are sensitive functions of crystal perfection and which could, therefore, serve as test materials for perfection improvement under microgravity conditions.

# CRYSTAL GROWTH OF SULFIDE MATERIALS FROM ALKALI POLYSULFIDE LIQUIDS

William B. White  
Materials Research Laboratory  
The Pennsylvania State University  
University Park, Pennsylvania 16802

## INTRODUCTION

Crystal growth from solvents has conventionally been divided into three "techniques": solution growth, in which the system pressure is atmospheric or thereabouts and the temperature ranges up to 100°C or a little more; hydrothermal growth, in which the use of confining pressure of 100 or more MPa allows aqueous solutions to be used at temperatures of several hundred degrees centigrade, and flux growth, in which the pressure is again ambient, but the solvent is a fused salt and growth takes place at temperatures above 600 - 800°C. Solution growth and flux growth, although identical in form and process, are regarded as separate crystal growth techniques because of the large gap in temperature between the top of the operating range of water and organic solvents in open systems and the bottom of the flux range dictated by the 600 - 800°C melting points of the fused salts.

The Fluids Experiment System has been devised for experiments with solution growth (among other things) and depends on optical systems to record and transmit information about the crystal growth process. Conventional flux systems are unsuitable not only because of the high temperatures involved but also because thermal emission and the optical opacity of many of the solvents would preclude the optical observations that are at the core of the system design.

The criteria for crystal growth in space should include the following: (i) the crystals should be of technological importance; (ii) the properties that make the crystal important should depend in a sensitive way on crystal perfection. Growth in microgravity conditions is not likely to be a cost-effective way of improving elemental purity, for example. Crystals whose optimum performance demands low dislocation densities, absence of voids and inclusions, absence of segregated impurities on dislocations and grain boundaries, are the ones to which research efforts should be directed. Such properties as dielectric loss, luminescence, domain switching, and electrical conductivity meet these criteria.

The number of materials whose solubility in aqueous or organic solvents is such that solution growth is feasible is somewhat limited. There would be an advantage to extending the range of crystal growth experiments by extending the temperature range and extending the list of useful solvents.

This paper discusses the potential for crystal growth from alkali polysulfide solvents. These are liquids whose composition can be continuously varied by changing alkali-to-sulfur ratios and with liquidus temperatures in the range of 200 - 400°C. Their potential application is to chalcogenide materials, of which those intended for electroluminescent display application might be of immediate interest.

#### ALKALI POLYSULFIDE LIQUIDS

The alkali sulfides  $K_2S$  and  $Na_2S$  have melting points in the range of 900°C and as such could be used as molten salt solvents in normal flux growth although little use seems to have been made of them. They are normally available in hydrated form and the difficulty in eliminating the water may have discouraged their use as fluxes. When sulfur is added to the alkali sulfides, there is a dramatic lowering of the liquidus surface (Figure 1). There is formed a distinct series of polysulfides, some of which melt congruently in the range of 250 to 450°C. As Figure 1 indicates, there is some disagreement about the details of the phase diagram but the existence of  $Na_2S_2$ ,  $Na_2S_3$ ,  $Na_2S_4$ , and  $Na_2S_5$  seems to be certain. Equivalent phases exist in the  $K_2S$ -S system although no phase diagram was found in the literature.

The polysulfides provide a wide range of low-melting liquids of varying properties. By using eutectic compositions, melting points as low as 200°C can be achieved.

The Fluids Experiment System is designed around various optical systems to monitor the growth of crystals and therefore requires the use of transparent solvents. The alkali sulfides are colorless and form transparent liquids. Addition of sulfur to form the polysulfide liquids imparts a yellow color, but the liquids appear to be transparent. More data on this point are needed.

Viscosities have been measured on liquids in the  $Na_2S$ -S system by Cleaver and Davies [3] (Figure 2) as a function of temperature and composition. It can be seen that the viscosity varies by about a factor of four over the temperature range that would be used for crystal growth and that the viscosity

ORIGINAL PAGE IS  
OF POOR QUALITY

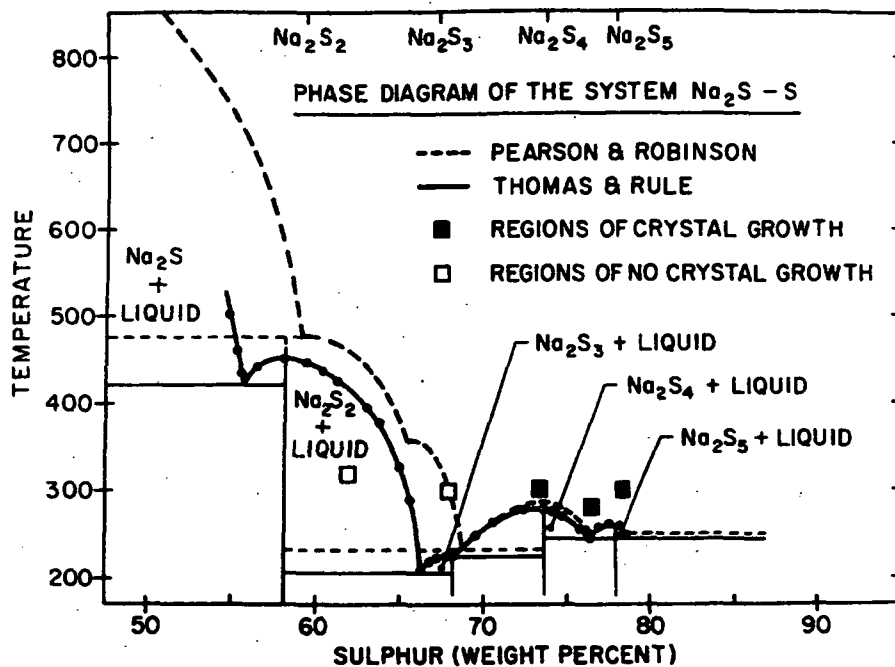


Figure 1. Phase diagram for the system  $\text{Na}_2\text{S}-\text{S}$ . Compiled from data in references [1] and [2].

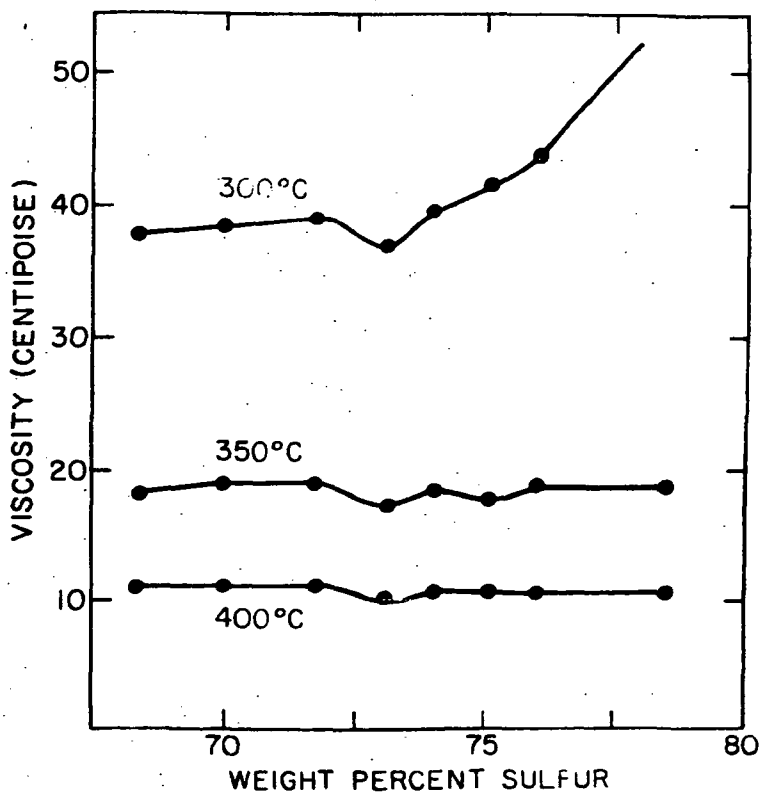


Figure 2. Viscosity of  $\text{Na}_2\text{S}-\text{S}$  melts calculated from [3].

is remarkably independent of composition especially at the higher temperatures. The viscosity data indicate that fluid motion in a growth cell will be qualitatively similar to fluid motion of aqueous solutions at lower temperatures. The electrical conductivity data of Cleaver et al. [4] suggest that these are ionic liquids, not network structures, in spite of the polymerization of the sulfur groups. Further data on liquid structure would also be useful.

### CRYSTAL GROWTH

If the alkali polysulfides are to be used as low temperature fluxes, two criteria must be met: (1) There must be an extensive liquid range between the polysulfide composition and material to be grown. In this range the liquidus should vary smoothly to permit uniform growth by slow cooling, and there should be no compounds formed between the flux liquid and the material to be grown; (2) The liquids should be "good" fluxes. This latter criterion is difficult to state specifically because it is not clear just what properties  $PbO$ ,  $PbF_2$ ,  $Bi_2O_3$ , alkali tetraborates, etc. possess that makes them such universal solvents for flux growth of crystals at higher temperatures. One criterion, perhaps, is that the material to be grown should not form complexes with the liquid. The energy necessary to break up the complexes acts as an additional barrier to crystal growth, raises the necessary supersaturation, and thus increases the possibility of spontaneous nucleation of many small crystals rather than continuous growth of a few large crystals.

Few data are available on the solubilities of materials in the alkali polysulfide liquids. One demonstrated case where crystals can be grown from these liquids is that of mercuric sulfide [5]. The phase relations (Figure 3) show a smooth liquidus curve giving a good range from crystal growth. Mercuric sulfide occurs in two polymorphic forms: cinnabar, a deep red optically active material is stable below  $344^\circ C$ ; metacinnabar, a black semiconductor with the sphalerite structure, is stable at higher temperatures. The phase relations given in Figure 3 show that it is possible to grow the low temperature form over the specified temperature-composition interval without formation of metacinnabar.

The likely candidates for crystal growth from alkali polysulfide liquids are binary and ternary sulfides of various kinds. Figure 4 illustrates some solubility data for four transition metal monosulfides replotted from the

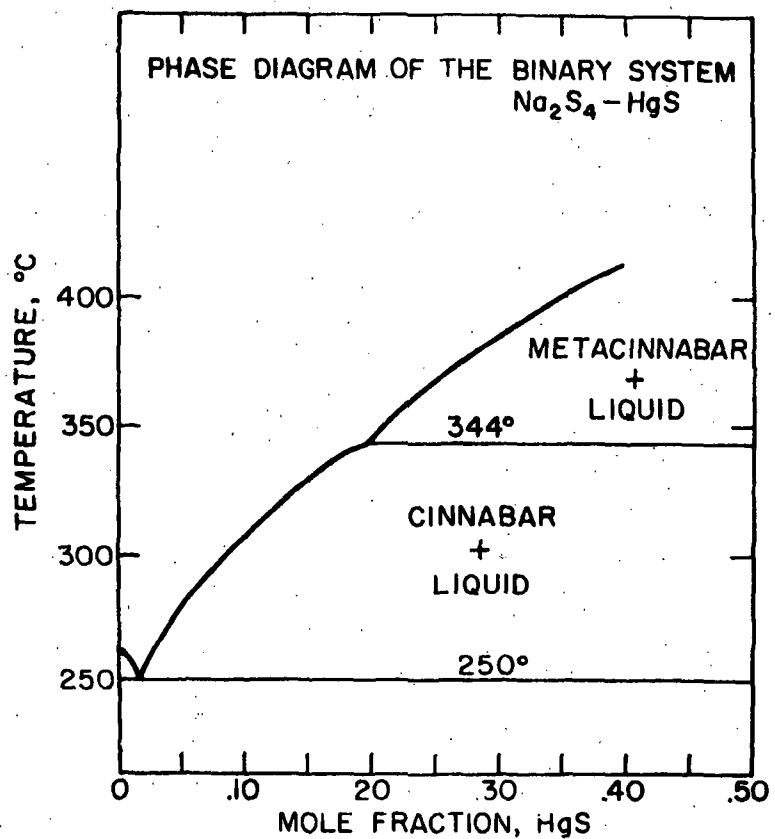


Figure 3. Phase diagram along the join  $\text{Na}_2\text{S}_4\text{-HgS}$  in the ternary system Na-Hg-S. Adapted from [5].

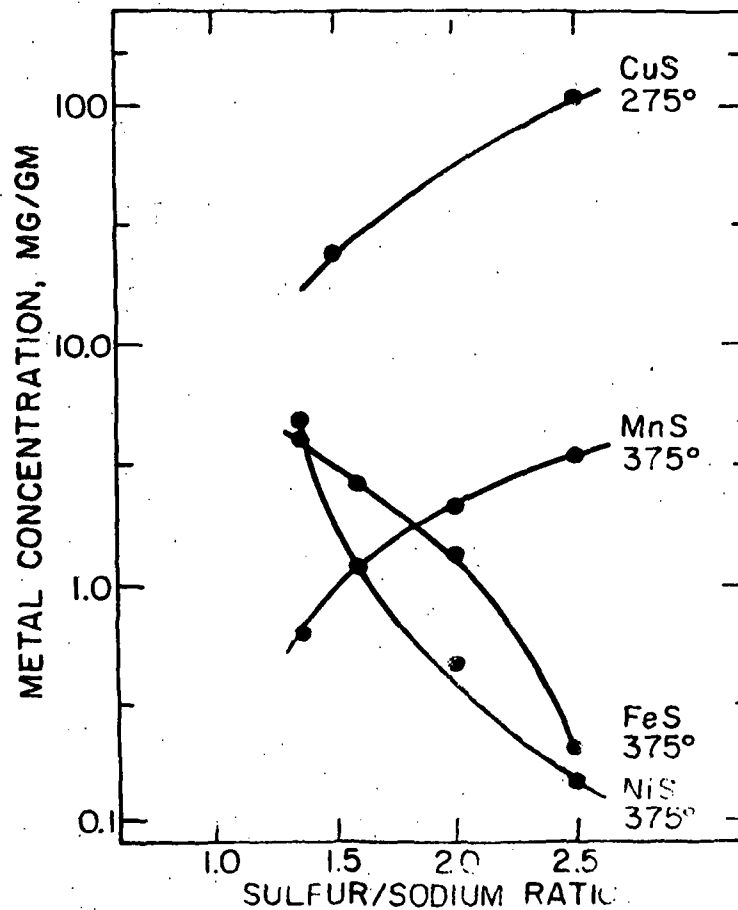


Figure 4. Solubility curves (at temperatures shown) for transition metal sulfides in  $\text{Na}_2\text{S-S}$  melts as a function of melt composition. Adapted from [6].

solubility data of Bailey and Skeaff [6]. Of the four compounds chosen for investigation, two have direct and two have retrograde solubility as a function of the sulfur/sodium ratio in the melt. Melt composition is obviously important and could be chosen to give the greatest solubility. The solubility of CuS is about an order of magnitude higher than the solubility of MnS, FeS, and NiS at the optimum flux composition. Certainly the  $\text{Na}_2\text{S}_5$ -CuS join meets the first criterion for crystal growth.

#### DEVELOPMENT OF SULFIDE GROWTH EXPERIMENTS

Let us return now to the statement made in the introduction. The number of substances that are suitable for growth from low temperature aqueous solutions and at the same time are of strong technological interest is quite limited. The overall design concept for the Fluids Experiment System suggests 400 to 500°C as an absolute upper limit beyond which optical systems could not be used because of the thermal radiation background. This paper suggests that there is at least one family of solvents from which crystals could be grown in the intermediate temperature range. However, knowledge of these systems is very primitive and two categories of research and development would be required before such growth experiments in microgravity could be contemplated.

The present Fluids Experiment System was designed to operate only to 100°C with a possible extension to 200°C. It would be necessary to review the FES design to determine whether it could be adapted for operation at higher temperatures without complete redesign of the system.

The case for the alkali polysulfide melts as growth media is predicated on the idea that these liquids could be used to grow complex sulfides among which are important luminescent and electrooptic materials for which a high degree of crystal perfection would be desired. Research necessary before prototype growth experiments could be designed include

1. Determination of phase equilibria in the  $\text{K}_2\text{S}$ -S system where lower melting liquids might be expected.
2. Determination of the optical properties of the liquids, particularly absorption in the visible regions.
3. Determination of solubility curves for selected binary and ternary sulfides as a function of temperature and polysulfide liquid composition.

4. Experiments to determine cooling regimes necessary to produce single crystals of selected materials.
5. Optimization of crystal growth conditions in ground-based experiments.
6. Determination of the crystal perfection of materials obtained from solution growth as compared with alternative preparation techniques such as melt growth or chemical vapor deposition.

Only after these steps have been taken could a final materials selection be made and a growth-in-space experiment designed.

#### REFERENCES

- [1] J.S. Thomas and A. Rule, J. Chem. Soc. 105, 1063 (1914).
- [2] T.G. Pearson and P.L. Robinson, J. Chem. Soc. 1930, 1473 (1930).
- [3] B. Cleaver and A.J. Davies, Electrochim. Acta 18, 727 (1973).
- [4] B. Cleaver, A.J. Davies and M.D. Hames, Electrochim. Acta 18, 719 (1973).
- [5] R.W. Garner and W.B. White, J. Crystal Growth 7, 343 (1970).
- [6] R.A. Bailey and J.M. Skeaff, J. Chem. Eng. Data 24, 126 (1979).

FLUID EXPERIMENT SYSTEM (FES) - OUTLINE OF CAPABILITIES

JACK KROPP  
MPS/SL PROJECT  
TRW DSSG - REDONDO BEACH, CA

Introduction

The NASA MPS/SL Project currently includes Shuttle Attached Payload systems for the Spacelab-3 (SL-3) mission and a Pallet payload mission. One of the SL-3 payload experiments is the Fluids Experiment System (FES). The Fluids Experiment System will be designed to be a multi-purpose facility that can be used by different experiments on several Spacelab flights beyond SL-3.

A significant portion of the MPS/SL project includes the design, development, fabrication, test, integration and operation of the FES facility. The project is managed by W.R. Adams at Marshall Space Flight Center, Alabama. TRW Defense and Space Systems Group is the prime contractor on the MPS/SL hardware project. Currently, the FES is in a conceptual design phase. This paper presents the capabilities of the FES as they are currently designed and explains the operation of the facility. The experiment currently approved for flight on FES is the Radial Growth Experiment of R.V. Lal (Alabama A&M University) and R. Kroes (MSFC). This experiment is used as an example in this paper where specifics are discussed.

FES Concept Description

The FES is designed to be a multi-flight facility and will provide the capability for conducting fluid phenomena investigation using optical observation techniques in the near-weightless environment of earth orbit. The facility will be designed to accommodate several types of fluid experiments during the Spacelab flight program.

The FES is contained in a double Spacelab rack. The major portion of this double rack is designed as the support module. Each experiment-unique part is contained in an experiment module. The description of these two modules is given below and Figure 1 gives a representation of the support and experiment modules.

ORIGINAL PAGE IS  
OF POOR QUALITY

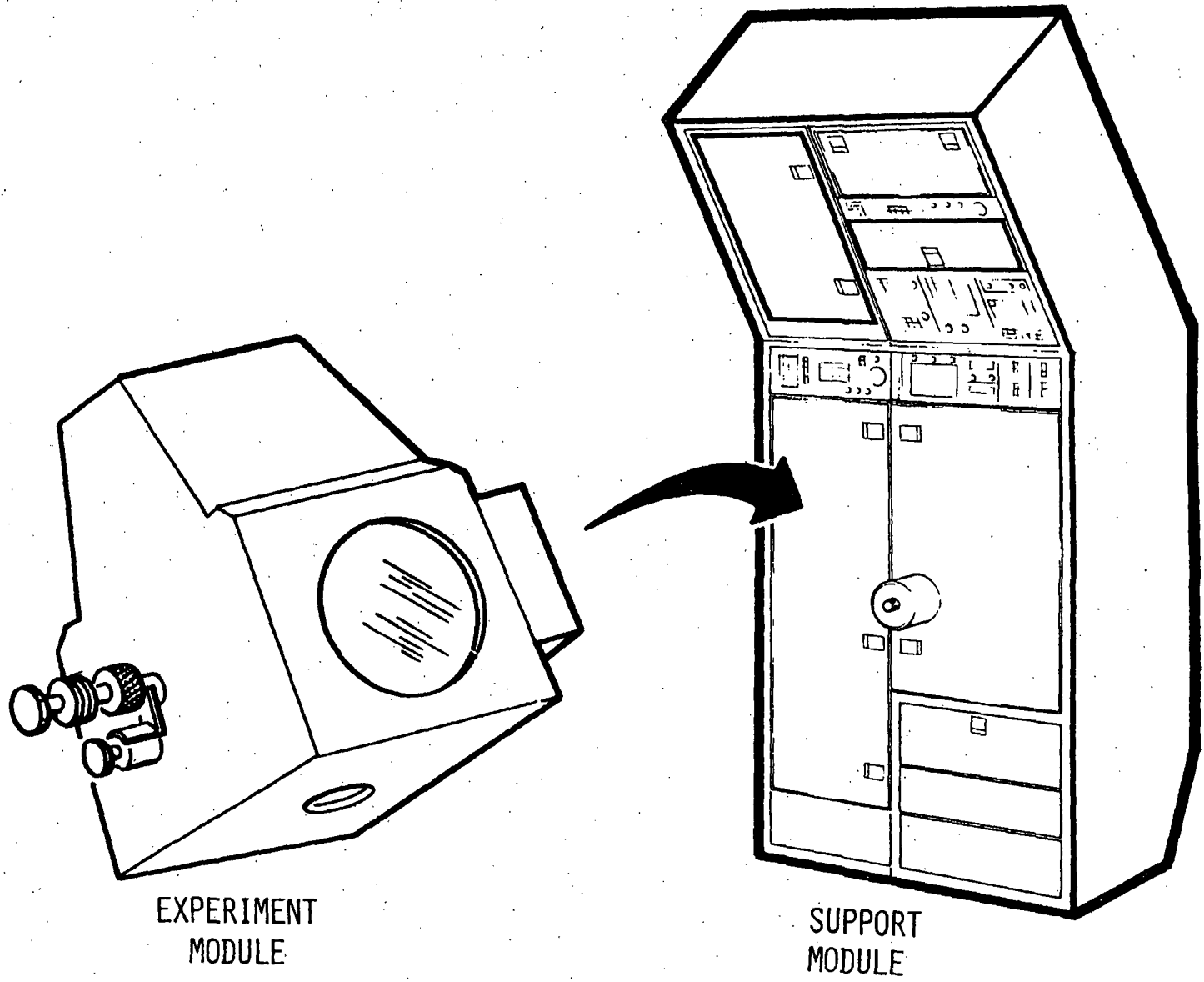


Figure 1. Experiment Module and Support Module Exteriors for FES  
(Cell is representative of the La1 Radial Growth Experiment)

The support module includes those functions common to all FES experiments:

- The optical system which generates holograms during the experiment and real-time flow visualization of the experiment zone.
- Thermal control of the experiment module and of the optics.
- Command and data control for facility functions.
- Electrical power for the optical assembly, experiment module, thermal cooling and other functions.
- An experiment enclosure to house the experiment module.
- Storage for experiment modules not in use.
- Common diagnostics (currently an accelerometer and temperature probes).
- Vidicon for on-board viewing and downlinked display of the flow field.
- Two film transport mechanisms for recording up to 150 holograms each per experiment cycle.

While the support module will be designed to have general functions, the experiment module is individually tailored to the particular FES experiment. It provides the following functions:

- Heat exchange interface; stirring, thermal isolation; thermal gradient, etc.
- Mechanism for experiment initiation, i.e., injection mechanism; mixing; sting, etc.
- Interfaces to support module electrical and thermal controls.

The size and volume of the experiment cell is defined by the volume available in the support module. Each experiment module must be constructed with interfaces compatible with those of the support module.

The experiment sequences on FES are conceived to be automated sequences where the sequence is chosen by the Payload Specialist. The operating characteristics of an experiment are as follows. An individual experiment cell is inserted for each experiment. The cell is loaded and the FES operated by the

Payload Specialist. Each experiment will entail unique sequences of thermal conditioning, sample injection, and optical observation and recording for each cell. The primary data record will be the resultant holograms. Up to eight experiment modules (of one or more experiments) can be stored per flight. Vidicon viewing of the flow fluid will be provided to the Payload Specialist and can be downlinked. A typical FES experiment sequence is shown in Figure 2. This experiment sequence is based upon the current timeline of the Radial Growth experiment.

### Optical System

A diagram of the Optical Bench is given in Figure 3. This diagram shows the essential elements in the system. The laser light source is a 25 MW helium-neon laser emitting at 632.8 NM. The light beam is split into an illuminating beam and into a reference beam. The reference beam is further split into reference beams to the forward and the transverse film transports. The beam entering the test cell illuminates a 10 x 10 cm area. The cell area viewed by the forward hologram is 70mm x 100mm. The transverse window is 5 cm in diameter and scattered light from the object is recorded on a hologram with film area of 70 x 100mm.

The parameters of the optical system are optimized so that the forward hologram has  $20\mu$  resolution. A  $20\mu$  change in the crystal boundary will be detected. The fringes on the holograms can be translated into changes in the index of refraction of the fluid. The index of refraction change can be measured to 2 parts in  $10^5$  in a gradient of  $5 \times 10^{-4}/\text{mm}$  or less.

The film transport and light intensity control the optical parameters such as exposure time and frame rate. Each film transport will accept cassettes containing film for 100-150 holograms. This number is the upper limit on the frames per transport per experiment since the interchange of film cassettes will seriously disturb the microgravity environment. The exposure time for each hologram can be varied from 0.1 sec to a 10 sec exposure. The time to access a new frame is 30 seconds. This time is limited by the transport mechanism (designed to maintain the low gravity conditions); and the seating of the film on the vacuum platen to obtain the required resolutions.

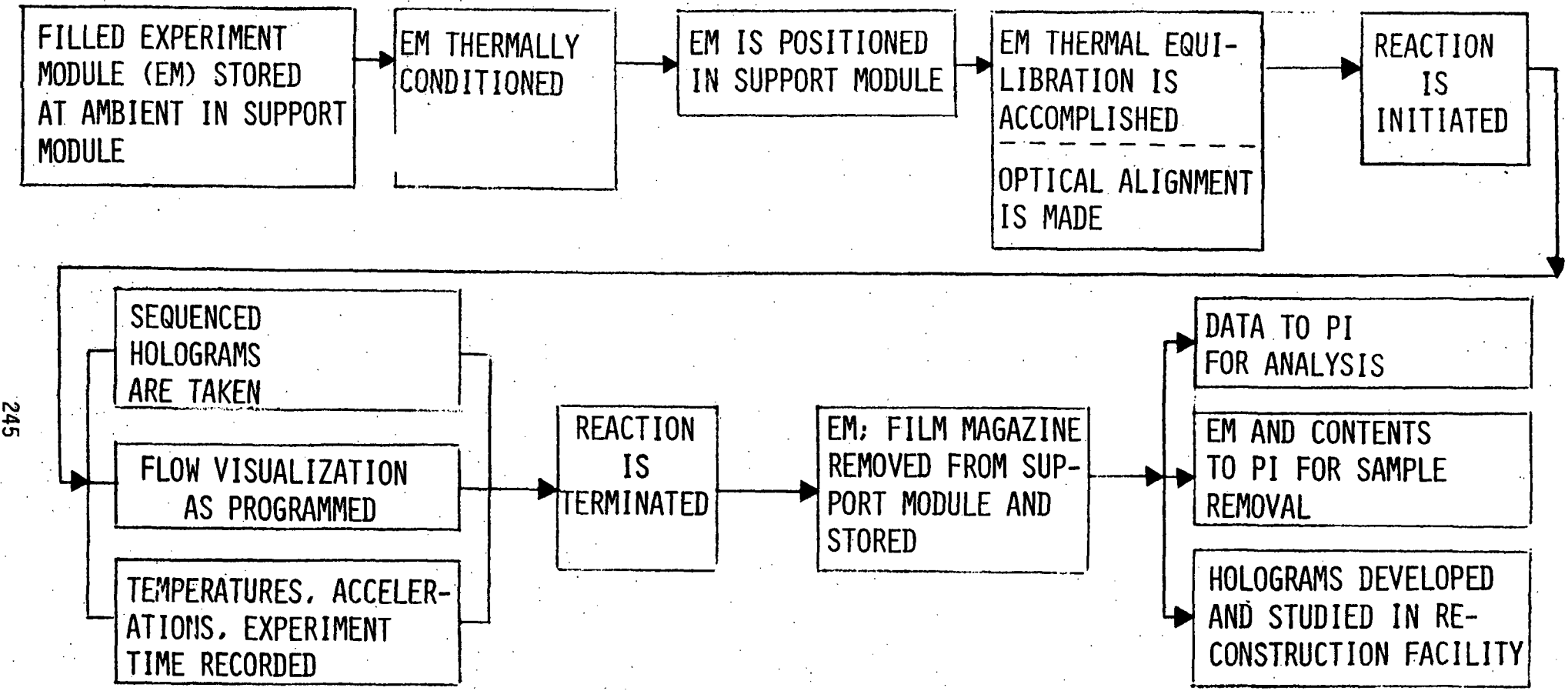
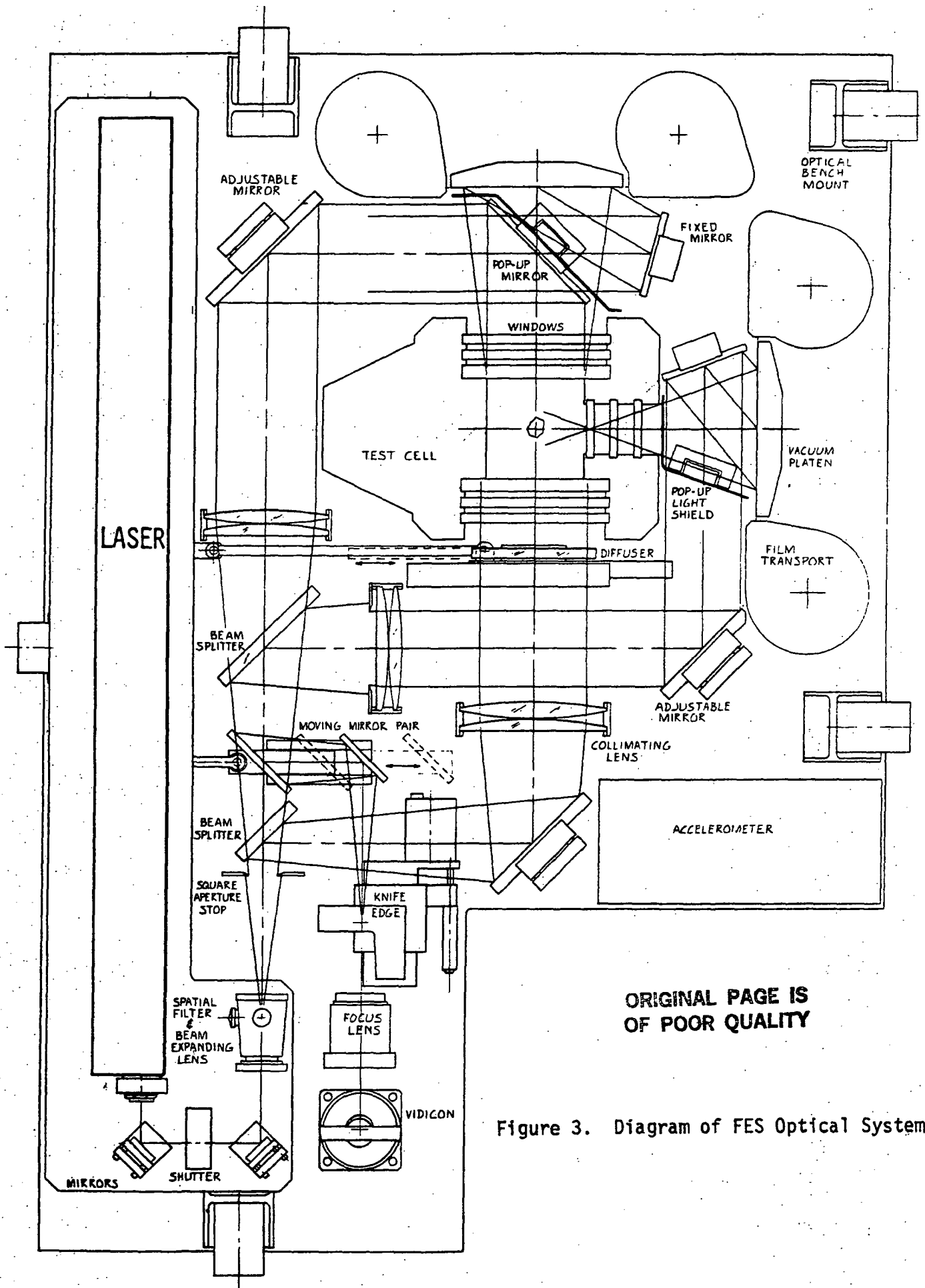


Figure 2. Typical FES Experiment Sequence

ORIGINAL PAGE IS OF POOR QUALITY

245



ORIGINAL PAGE IS  
OF POOR QUALITY

Figure 3. Diagram of FES Optical System

The flow visualization method in the present concept utilizes Schlieren optics to view the entire 10 x 10 cm area. To obtain the flow visualization, a series of movable and pop-up mirrors are used to block the reference beam and to direct the main beam after it has passed through the cell back to focus at a knife edge and then image it on the vidicon screen. The flow visualization is designed to measure small changes in  $\Delta n$  over the cell. The method of obtaining flow visualization involves the movement of mirrors and the blocking of the film plane, therefore, hologram recording and flow visualization cannot be obtained simultaneously. The change time from flow visualization to holographic recording mode is of the order of 1 minute.

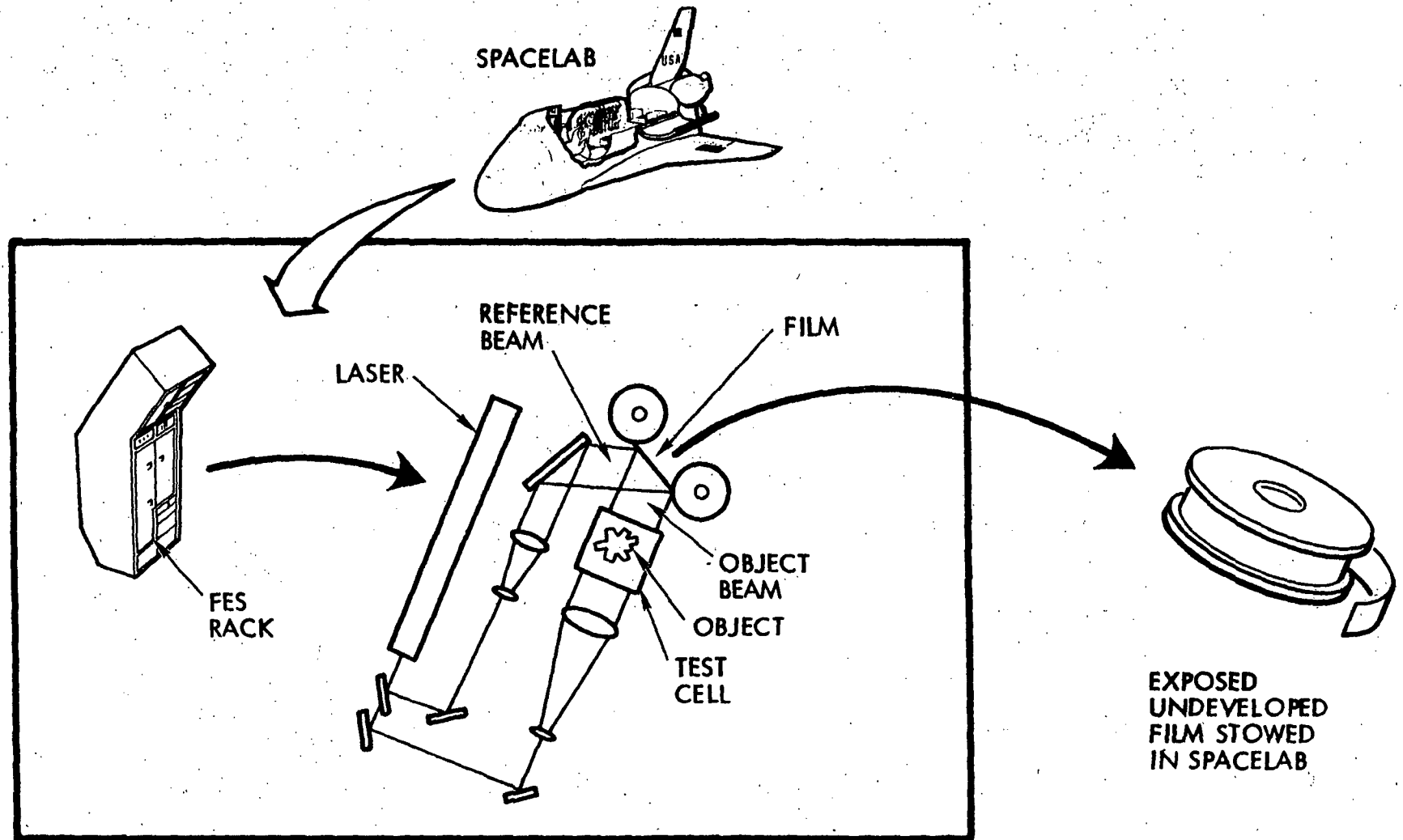
#### Holographic Capability

The recording of holograms in-flight for the analysis of the Spacelab experiment results allows the study of the in-flight image in a ground based analysis situation.

Figure 4 shows the essentials of the holographic system. The laser light is split into an object beam and a reference beam. The object beam illuminates the scene and then impinges on the film plane. The reference beam is a pure light beam that has the same path length as the object beam. The two beams interfere at the film plane. The interference pattern contains all of the information that is in the object beam. There are two film transport locations. The total object beam falls on the forward film transport. Light scattered from the object falls on the transverse film. Both films will contain the information regarding the object (i.e., crystal) such as changes in morphology, size, etc.

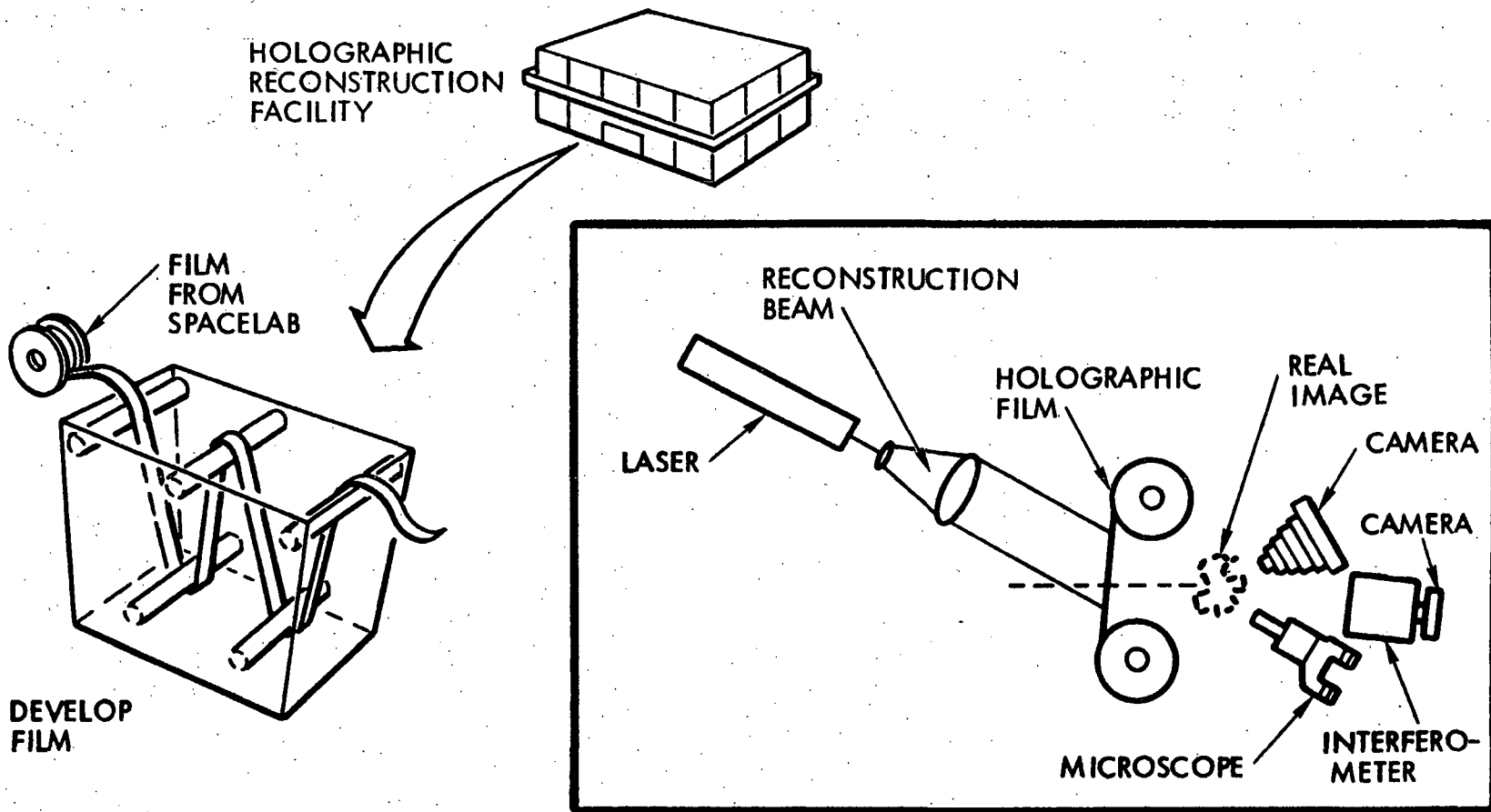
All holograms made during a flight are stored in cassettes on board until landing.

Figure 5 illustrates the post flight analysis method. The film cassettes are first developed using care to preserve all of the holographic detail. Then each frame will be analyzed individually in a holographic reconstruction facility. This facility will allow the experimenter to view the real image



- LASER LIGHT IS SPLIT INTO TWO BEAMS:  
1) REFERENCE BEAM, 2) OBJECT BEAM
- OBJECT BEAM ILLUMINATES OBJECT AND SCATTERED LIGHT FALLS ONTO THE FILM
- REFERENCE BEAM CONSTRUCTIVELY AND DESTRUCTIVELY INTERFERES WITH THE OBJECT BEAM AND THE FILM RECORDS THIS LIGHT AND DARK PATTERN

Figure 4. Concept to Generate Holograms in FES



● LASER RECONSTRUCTS HOLOGRAM INTO REAL IMAGE PROJECTION

DATA OUTPUT

- FLOW PATTERNS
- TEMPERATURE GRADIENTS
- INDEX OF REFRACTION CHANGE
- BUBBLE DYNAMICS
- MICROSCOPE ANALYSIS
- CRYSTAL GROWTH PATTERNS
- DROPLET GROWTH PATTERNS
- PARTICLE FORMATION
- PHOTOGRAPHIC REPRODUCTION

ORIGINAL PAGE IS OF POOR QUALITY

Figure 5. Post-Flight Analysis Sequence

of the object and to make measurements of that scene. Index of refraction changes can be obtained by interferometric measurements; these data can, in turn, be related to temperature and concentration gradients. A microscope can be used to view changes in the object from hologram to hologram. The hologram presents the entire experiment scene and three dimensional viewing will allow the analyst to focus upon various areas of the scene. Various optical tools can be brought to the reconstruction facility as the analysis requirements demand.

#### Other Support Module Data

##### Power.

The FES can accommodate up to 2 kW power. However, the power available to the FES on a given mission may be less than 2 kW. For example, on SL-3, the first mission that will carry FES, the power budget forecast allows FES 1 kW average power. The FES experiments for this mission, the radial growth experiment, must conform to this power budget.

##### Accelerometer.

A tri-axial accelerometer will be mounted on the optical bench. This will have the capability of measuring G levels in the range  $1 \times 10^{-6} G$  to  $1 \times 10^{-2} G$  with vibrations measured over a 0 to 50 Hz bandwidth. The error in the measurement is  $5 \times 10^{-5} G$  at 50 Hz.

##### Temperature Range.

The FES was originally designed to accommodate experiment temperatures from ambient to 200°C. Higher temperatures may be accommodated by a smaller experiment cell volume and greater insulation, provided power requirements and heat rejection requirements for Spacelab are met. The accommodation must be considered on an individual experiment basis. The accommodation of experiments requiring lower temperatures again depends upon the power required to achieve the temperature desired.

#### Experiment Cell

The experiment cell is unique to each experiment flown on FES. The current radial growth cell accommodates a volume of liquid of 2.5 liters. A three dimensional representation of the cell is shown in Figure 6. All experiment cells must be configured to fit into the space 29 cm x 35 cm x 21 cm.

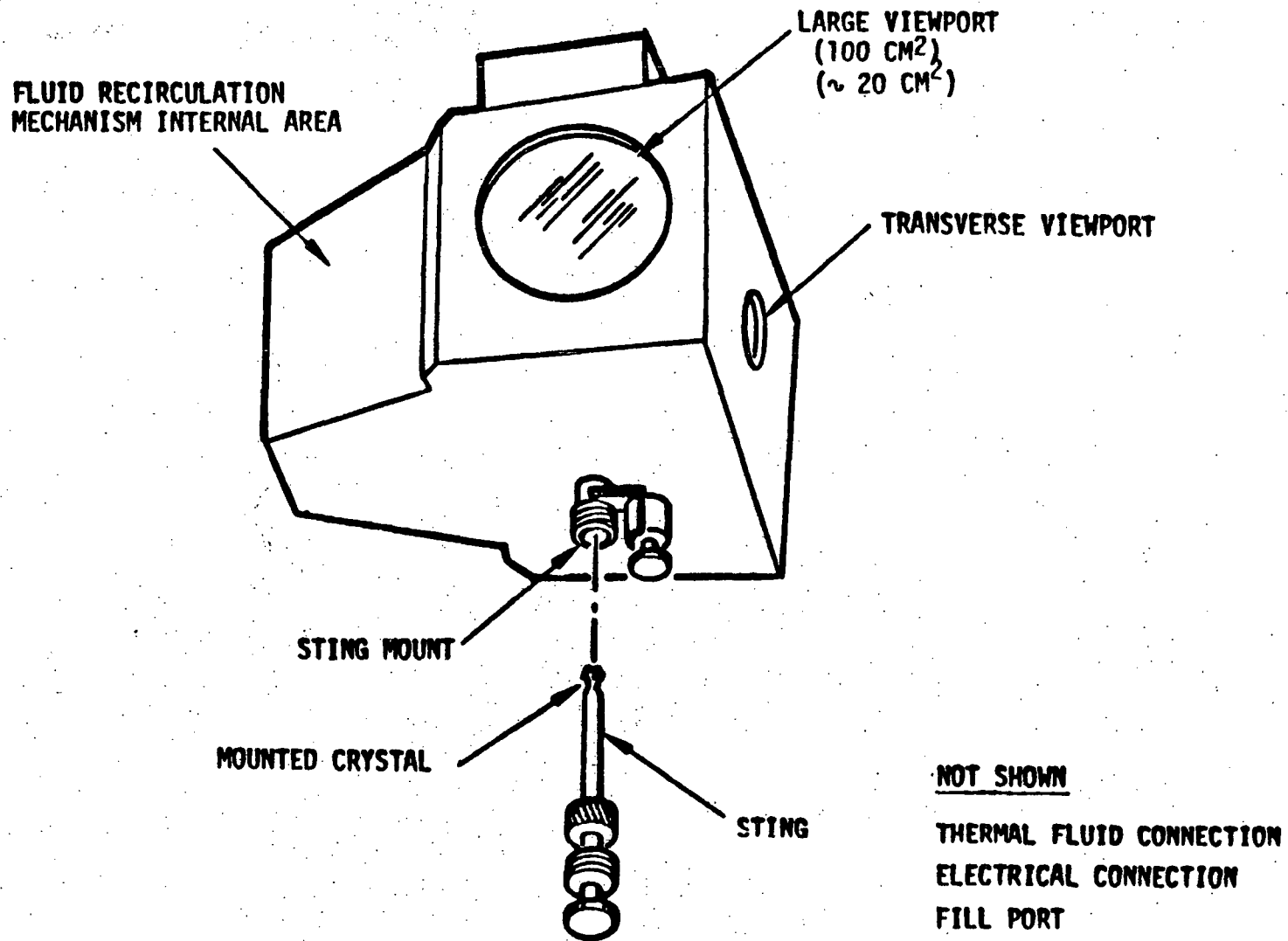


Figure 6. Current External View of Radial Growth Cell for FES

ORIGINAL PAGE IS  
OF POOR QUALITY

The cell will be configured to include all of the functions that are unique to the particular experiment. For example, the experiment cell will include the stirring mechanism; heaters or coolers to regulate the thermal environment; heat exchangers if required for fluid temperature cycling; and view ports that are compatible with the optical system. Provisions for the reaction initiation must also be included in the experiment cell. In the case of the Lal experiment, this is a seed crystal contained on a sting. In other experiments, this could include also injection capabilities of bubbles or dyes or an immiscible liquid for example.

The experiment cell will interface to the support module for thermal, power and data interfaces. It will also be designed in each case to utilize the FES optical system.

#### Conclusion

The FES system is designed to accommodate several types of fluid experiments in Spacelab. The system is based upon an optical observation of the experiment scene via holograms recorded during flight. The analysis is then accomplished through the studies of the holograms that are generated. Real time flow visualization is available to the experimenter. Data given here may change in particulars during the design phase but overall capabilities will generally remain as described.

**ORIGINAL PAGE IS  
OF POOR QUALITY**

A P P E N D I X A

PARTICIPANT LIST FOR FES WORKSHOP

Dr. Charles Alcock  
Dept. of Metallurgy & Materials Science  
University of Toronto  
Toronto, Canada

Dr. Andre Authier  
Laboratoire Mineralogie-Cristallographie  
Tour 16  
Universite P. et M. Curie  
4 Place-Jussieu  
75230 Paris CEDEX 05  
France

Dr. Donald Brooks  
Dept. of Pathology  
Univ. of British Columbia  
Vancouver, British Columbia V6T1W5

Dr. Frederick S. Brown  
TRW D-5SG 100-1168  
One Space Park  
Redondo Beach, CA 90278

Mr. Tom Cochran  
501-7  
NASA-Lewis Research Center  
Cleveland, OH 44135

Dr. Giles Cokelet  
Box RBB  
University of Rochester Medical Center  
601 Elmwood Ave.  
Rochester, NY 14642

Dr. Dennis Elwell  
Center for Materials Research  
Stanford University  
Stanford, CA 94305

Dr. Steve Flannagan  
City of Hope National Medical Center  
1500 East Duarte Road  
Duarte, CA 91010

Dr. Stanley Gelles  
S. H. Gelles Associates  
2836 Fisher Road  
Columbus, OH 53204

Dr. William Gill  
Dept. of Chemistry  
State University of New York  
Amherst, NY 14260

ORIGINAL PAGE IS  
OF POOR QUALITY

Dr. Marty Glickman  
Rensselaer Polytechnic Institute  
Troy, NY 12181

Dr. Mary Good  
Div. of Engineering Research  
3418 CEBA  
Louisiana State University  
Baton Rouge, LA 70803

Dr. John Hallett  
Atmospheric Science Center  
D.R.I. P.O. 60220  
Reno, NV 89506

Dr. G. C. Kuczynski  
Dept. of Metallurgical Engineering & Materials Science  
University of Notre Dame  
Notre Dame, IN 46556

Dr. Irvin Krieger  
Dept. of Chemistry  
Case Western Reserve University  
Cleveland, OH 44106

Dr. J. Adin Mann, Jr.  
Dept. of Chemical Engineering  
Case Western Reserve University  
Cleveland, OH 44106

Dr. Ed Meehan  
% Dr. Charles E. Brigg  
Univ. of Alabama in Birmingham  
Institute of Dental Research  
Birmingham, AL 35233

Dr. H. Meiselman  
Dept. of Physiology & Biophysics  
Univ. of Southern California School of Medicine  
2025 Donal Ave.  
Los Angeles, CA 901133

Dr. Simon Ostrach  
Dept. of Mechanical & Aerospace Engineering  
Case Western Reserve University  
Cleveland, OH 44106

Dr. Franz Rosenberger  
University of Utah  
312 N. Physics Bldg.  
Salt Lake City, UT 84112

Dr. Sidney Ross  
Cogswell Lab, Rm 314  
Rensselaer Polytechnic Institute  
Troy, NY 12181

Dr. Ronald Sapiieszko  
Dept. of Chemistry  
Clarkson College of Technology  
Potsdam, NY 13676

Dr. Dudley Saville  
Dept. of Chemical Engineering  
Princeton University  
Princeton, NJ 08540

Dr. Anthony Schwartz  
2260 Glenmore  
Rockville, MD 20850

Dr. R. Shankar Subramanian  
157/316  
Jet Propulsion Laboratory  
4800 Oak Drove Drive  
Pasadena, CA 91103

Dr. John W. Vanderhoff  
Sinclair Laboratory #7  
Lehigh University  
Bethlehem, PA 18015

Dr. William White  
Materials Research Laboratory  
Pennsylvania State University  
University Park, PA 16802

Dr. Charles Whitehurst  
College of Engineering  
Louisiana State University  
Baton Rouge, LA 70803

Dr. William Wilcox  
Peyton Hall  
Clarkson College of Technology  
Potsdam, NY 13676

ORIGINAL PAGE IS  
OF POOR QUALITY

Dr. John B. Hendricks  
Physics Dept., UAH  
Box 1247  
Huntsville, AL 35807

Dr. Jack Kropp  
TRW Onc.  
One Space Park  
Redondo Beach, CA 90278

Dr. John Carruthers  
EM-7  
NASA Headquarters  
Washington, DC 20546

Dr. Milton Harris  
Dept. of Chemistry  
Univ. of Alabama in Huntsville  
Huntsville, AL 35807

Dr. Clyde Riley  
Dept. of Chemistry  
Univ. of Alabama in Huntsville  
Huntsville, AL 35807

Mr. Tom Cochran  
501-7  
NASA/LRC  
Cleveland, OH 44135

Dr. Daniel Fitzjarrald  
% Dr. George Fichtl  
NASA/MSFC  
MSFC, AL 35812

Dr. Edwin Rush  
Dept. of Physics  
Univ. of Alabama in Huntsville  
Huntsville, AL 35807

Dr. R.B. Lal  
A&M University  
Huntsville, AL 35811

Dr. Mike Weinberg  
Jet Propulsion Laboratory  
California Institute of Technology  
4800 Oak Grove Dr.  
Pasadena, CA 91103

ORIGINAL PAGE IS  
OF POOR QUALITY

All persons listed below are at the following address:

NASA/MSFC  
George C. Marshall Space Flight Center  
Huntsville, AL 35812

Mr. John Williams, LA01  
Mr. Warren Campbell, ES82  
Dr. Robert Naumann, ES71  
Dr. Lewis Lacy, ES74  
Dr. Robert Snyder, ES73  
Dr. Gary Nishioka, ES74  
Dr. Neil Ivory, ES73  
Ms. Alice Maurer, ES73  
Mr. Ruddy Ruff, ES74  
Ms. Barbara Askins, ES52  
Dr. Roger Kroes, ES74  
Mr. Bob Adams, PF11  
Mr. Vaughn H. Yost, EE05



FLUIDS EXPERIMENT SYSTEM WORKSHOP

July 11  
(cont.)

11:00 a.m. Discussion - Led by R. Naumann

12:15 p.m. Lunch - Noojin House

SESSION B - CHEMICAL PROCESSES

1:15 p.m. B1 - G. Kuczynski (Notre Dame) and C. Alcock  
(Univ. of Toronto) - "Ostwald Ripening in  
Microgravity"

1:30 p.m. B2 - E. Matijevic and R. Sapiieszko (Clarkson  
College) - "Formation of Metallic and  
Metal Hydrus Oxide Dispersions"

1:45 p.m. B3 - J. Vanderhoff (Lehigh) - "Flocculation of  
Colloidal Sols and Flocculation by Poly-  
meric Flocculants"

2:00 p.m. Discussion - Led by R. Naumann

2:30 p.m. Coffee Break

SESSION C - BIOLOGICAL PROCESSES

2:45 p.m. C1 - D. Brooks (Univ. of British Columbia)  
"Cell Partion in Two Phase Polymer System"

3:00 p.m. C2 - G. Cokelet (Univ. of Rochester Medical  
Center), H. Meiselman (Univ. of Southern  
California School of Medicine) and  
H. Goldsmith (Univ. Medical Clinic, Montreal  
Quebec, Canada) - "Some Potential Blood  
Flow Experiments for Space"

3:15 p.m. C3 - S. Flannagan (City of Hope National Medical  
Center) - "Geometrical Consideration in the  
Separation of Biological Particles by  
Affinity Partitioning"

3:30 p.m. C4 - E. Meehan (Univ. of AL in Huntsville) -  
"Crystallization of Biological Macro-  
molecules in Reduced Gravity Environment"

3:45 p.m. C5 - D. Saville (Princeton), P. Rhodes and  
R. Snyder (NASA/MSFC) - "Fluid Mechanics  
of Continuous Flow Electrophoresis"

4:00 p.m. Discussion - Led by R. Naumann

4:30-5:30 p.m. Cocktail Hour at the Noojin House

5:30 p.m. Bus leaves the Noojin House for the Space and  
Rocket Center

FLUIDS EXPERIMENT SYSTEM WORKSHOP

July 11 (cont.)	6-7 p.m.	Tour Space and Rocket Center - Advise that you see Lunar Odyssey first as it closes at 7:00 p.m.
	7:00 p.m.	Barbecue at the Space and Rocket Center
	8-8:30 p.m.	Return to Hilton Hotel
July 12	8-8:10 a.m.	Vans leave from Hilton Hotel for Noojin House
	8:15 a.m.	Continental breakfast - Noojin House
	8:40 a.m.	Announcements - J. Hendricks

SESSION D - CRYSTAL GROWTH EXPERIMENTS

8:45 a.m.	D1 - A. Authier (Universite P et M Curie, Paris, France) - "Crystal Growth from Solution by Coprecipitation in Microgravity Conditions"
9:00 a.m.	D2 - D. Elwell (Stanford) - "Solution Growth Experiments in Low Gravity"
	D3 - W. Gill - (SUNY- Buffalo) - "Anomalous Growth of Single Ice Crystals"
	D4 - M. Glicksman (Rensselaer) - "Convective Flow During Dendritic Growth"
9:45 a.m.	Coffee Break
10:00 a.m.	D5 - M. Good and C. Whitehurst (Louisiana State) - "Crystal Growing Experiments in Microgravity"
10:15 a.m.	D6 - J. Hallett and E. Wedum ( Univ. of Nevada) - "Influence of Convections on the Growth of Dendrite Crystals in Solutions"
10:30 a.m.	D7 - F. Rosenberger (Univ. of Utah) - "Fluid Dynamics of Vapor Transport"
10:45 a.m.	D8 - W. White (Pennsylvania State) - "Crystal Growth from Low Temperature Fluxes"
11:00 a.m.	Discussion - Led by J. Carruthers
12:00 a.m.	Introduction to Holography exhibit - W. Witherow
12:15 p.m.	Lunch at the Noojin House
1:15 p.m.	Talk by J. Carruthers - "NASA Research Opportunities"

FLUIDS EXPERIMENT SYSTEM WORKSHOP

ORIGINAL PAGE IS  
OF POOR QUALITY

July 12 (cont.)	2:00 p.m.	Presentation on the FES facility - J. Kropp - TRW
	2:30 p.m.	Discussion of FES facility
	3:30 p.m.	Adjourn

NOTE: From 12:30 to 4:00 a holography demonstration will be available.